School of Civil and Mechanical Engineering
Faculty of Science and Engineering

Structural Response of Precast Segmental Concrete Beams Prestressed with Unbonded Steel/CFRP Tendons

Duy Tan Le

0000-0002-7214-0833

This thesis is presented for the Degree of

Doctor of Philosophy

of

Curtin University

December 2019

DECLARATION

To the best of my knowledge and belief this thesis contains no material previously published by any other person except where due acknowledgment has been made.

This thesis contains no material which has been accepted for the award of any other degree or diploma in any university.

Signature: _____

Date: 12/12/2019

To my grandparents
my parents
my wife, my daughter and
my younger brother

For their unending love and encouragement

ABSTRACT

Precast segmental prestressed concrete beams (PSBs) have been increasingly used in many bridge construction projects around the world. The use of unbonded tendons and dry joints are preferred for the construction of new segmental concrete beams as they enable fast installation and easier replacement in cases of deterioration. However, corrosion problem of the steel tendons at segment joints is a great concern of PSBs, in particular when the structure is exposed to harsh environmental conditions. In extreme cases, corrosion might lead to the structure collapse as reported in the literature. In addition, due to the lack of bonding between the tendons and surrounding concrete, strain compatibility at critical sections is no longer valid. This behaviour presents a real challenge in predicting the flexural response of the structure even though extensive efforts have been paid to the investigation of PSBs with unbonded tendons.

This thesis presents research results on the performance of segmental concrete beams prestressed with unbonded steel/CFRP tendons. The primary aim of the study is to investigate the possible use of carbon fibre-reinforced polymer (CFRP) tendons as an alternative solution for PSBs to tackle the corrosion issue. CFRP tendons are corrosion-free and possess a high tensile strength that even exceeds steel tendons. They are lighter than steel, which allow easier handling and reduce dead load of the structure. To the author's best knowledge, the application of FRP tendons on PSBs has not been reported in the open literature. Another main objective is to provide closer examinations on PSBs prestressed with unbonded steel tendons. With the growing use of this type of structure, better understanding the performance of PSBs with unbonded tendons are required to develop more reliable analysis and design of the structure.

In total, nine large-scale segmental concrete beams were built and tested in this study to investigate the use of CFRP tendons on PSBs. All the beams had T-shaped cross-section of 400 mm height and 3.9 m length. Each beam consisted of four reinforced concrete segments, which were connected together using post-tensioning technique. Different testing parameters including tendon materials (steel/CFRP), tendon profiles (internal/external), tendon bonding conditions (unbonded/bonded) and type of joints (dry/epoxied) were considered. All the beams were tested under four-point cyclic loadings up to failure. The test results indicated that CFRP tendons can be well used in segmental concrete beams. All the tested beams with CFRP tendons exhibited

excellent load-carrying and deflection capacities compared to their counterparts with steel tendons, indicating they could be used to replace steel tendons for better corrosion resistance. Bonding conditions and tendon profile greatly affected the failure mode, strength and ductility of the beams while the type of joints showed insignificant effects on the overall performance of the structure.

All the design procedures from codes examined in this study predict well the tendon stress at the ultimate stage, thus the load-carrying capacity of the tested beams with bonded tendons, however, the accuracy significantly reduces when the unbonded tendons are used in the beams. Modifications are then made for the strain reduction coefficient, Ω_u, for better prediction of the stress increment in the unbonded steel/CFRP tendons. Similarly, the examined design procedures do not well estimate the deformation capacity of the beams with unbonded tendons. An analytical procedure to predict the load-deflection curve of segmental concrete beams with unbonded steel/CFRP tendons is therefore developed. Its accuracy is confirmed with the experimental and numerical results. In addition, an empirical equation, for the first time, to estimate the balanced reinforcement ratio of PSBs with unbonded steel/CFRP tendons is also proposed. The equation is validated with detailed numerical predictions and the testing results.

This study also presents a numerical approach to predict the flexural behaviour of PSBs with unbonded steel/CFRP tendons. This is the first time a three-dimensional numerical model is built and successfully validated against experimental results of PSBs in the literature. The verified numerical model is used to conduct intensive simulations of PSBs with different parameters for tension-controlled, compression-controlled and balanced sections. The effects of various parameters such as the effective prestress, prestressing steel reinforcement ratio, and span length-to-tendon depth ratio, concrete strength, type of load and number of joints on the failure modes, joint opening, stress increment in the tendon and the stress transfer mechanism of PSBs are fully discussed. The numerical results are compared with those from the existing models for predicting the strength of PSBs and are used to validate analytical predictions proposed in this study.

The results in this study demonstrated that CFRP tendons can be used in segmental concrete beams to replace conventional steel tendons with excellent performances in all indices. The corresponding design analysis procedures were also developed in the study for applications of CFRP tendons in PSBs in construction practice for corrosion control to reduce the lifecycle maintenance costs of structures.

ACKNOWLEDGEMENT

First and foremost, I would like to express my deepest gratitude to my supervisor Professor Hong Hao for his valuable advice, enlightening guidance, patience and kindness throughout my PhD course. It was my honour to work with him on this topic. I would also like to express my sincere thanks to my co-supervisor Dr. Thong Pham for his assistance, guidance and encouragement during my study. His generous support and invaluable comments helped to improve this thesis.

I am grateful to the Curtin Strategic International Research Scholarship (CSIRS) for providing me the full PhD scholarship and Centre for Infrastructural Monitoring and Protection, School of Civil and Mechanical Engineering, Curtin University and the Australian Research Council Laureate Fellowships FL180100196 for financial support during my research.

I would also like to thank very much all staffs at the Civil Engineering laboratory, Curtin University, especially Mark Whittaker, Darren Isaac, Mick Elliss, Luke English, Ashley Hughes, Arne Bredin, Rob Walker, Gary Woodward, and Kevin Reilly for giving me generous help during my experimental programs. I would like to acknowledge Prof. Yifei Hao for helping to purchase CFRP tendons and post-tensioning fixtures. Without this help, it would have been much more difficult for the procurement and to complete the experimental works on time. Many thanks are also expressed to Han Li, Jaxier Koa and Xyrus Dangazo, especially Cheng Yuan for their great help in the experimental works. My sincere thanks also go to Tin Van Do, Tung Thanh Tran, Tuan Tang Ngo and research colleagues in Prof. Hao's research group for their great friendship and help during my study course.

I would like to thank all my friends and family, of which there are too many to mention by name, for their support and understanding over the past three years.

Last but not least, I would like to express my profound gratitude to my grandparents, my parents and my young brother, to whom this thesis is dedicated. My heartfelt thanks and love are for my wife Mrs Thi Kim Chang Nguyen and my daughter Miss Nguyen Lam Anh Le whose love, understanding, encouragement and joy made this thesis possible.

LIST OF PUBLISHED WORK AND WORK PREPARED FOR PUBLICATIONS

The list of published paper and work prepared for publications, with the full bibliographic citations in the order they appear in the thesis, are listed below.

Chapter 2:

Le, T. D., Pham, T. M., Hao, H., and Hao, Y. (2018). Flexural behaviour of precast segmental concrete beams internally prestressed with unbonded CFRP tendons under four-point loading. *Engineering Structures*, 168(2018), 371-383.

Chapter 3:

Le, T. D., Pham, T. M., Hao, H., and Yuan, C. (2019). Performance of precast segmental concrete beams posttensioned with carbon fiber-reinforced polymer (CFRP) tendons. *Composite Structures*, 208, 56-69.

Chapter 4:

Le, T. D., Pham, T. M., and Hao, H. (2019). Behavior of Precast Segmental Concrete Beams Prestressed with External Steel/Carbon Fiber-Reinforced Polymer (CFRP) Tendons. (Revision submitted).

Chapter 5:

Le, T. D., Pham, T. M., and Hao, H. (2020). Numerical study on the Flexural Performance of Precast Segmental Concrete Beams with Unbonded Internal Steel Tendons. *Building and Construction Materials*, 248: 118362.

Chapter 6:

Le, T. D., Pham, T. M., and Hao, H. (2019). Analytical Investigation of the Performance of Precast Segmental Concrete Beams Internally Prestressed with Unbonded Steel Tendons. (Under review).

LIST OF RELEVANT ADDITIONAL PUBLICATIONS

The list of additional publications relevant to the thesis, with the full bibliographic citations, is given below.

Le, T. D., Pham, T. M., and Hao, H. (2018). Application of Carbon Fiber-Reinforced Polymer (CFRP) Tendons on Precast Segmental Prestressed Concrete Beams. *26th Annual International Conference on Composites or Nano Engineering, ICCE-26 July 15-21, 2018 in Paris, France*.

Pham, T. M., **Le, T. D**., and Hao, H. (2018). Behaviour of Precast Segmental Concrete Beams Prestressed with CFRP Tendons. *Proc., 9th International Conference on Fibre-Reinforced Polymer (FRP) Composites in Civil Engineering (CICE 2018)*, 945-953.

Pham, T. M., **Le, T. D.**, and Hao, H. (2019). Flexural Performance of Precast Segmental Concrete Beams Prestressed with CFRP Tendons. *The 16th East Asia-Pacific Conference on Structural Engineering & Construction (EASEC16), 3-6 December 2019 – Brisbane, Queensland, Australia (Accepted)*.

STATEMENT OF CONTRIBUTION OF OTHERS

The works presented in this thesis were primarily carried out by the first author, which mainly include but not limited to reviewing the literature, conducting experimental tests, implementing analytical analyses, developing numerical models, and writing manuscripts. Contributions of the co-authors are described below:

Chapter 2:

Dr. Thong Pham helped in suggesting the scope, method and analysis of experimental tests. Prof. Hong Hao approved and provided further instructions on testing and research methodologies. Prof. Yifei Hao helped purchase testing materials and fixtures. In addition, Dr. Thong Pham and Prof. Hong Hao had thoroughly revised and edited draft manuscript prepared by the first author. The financial support for the experimental tests was from Curtin Strategic International Research Scholarship (CSIRS) and Centre for Infrastructural Monitoring and Protection, School of Civil and Mechanical Engineering, Curtin University.

Chapter 3 and Chapter 4:

Dr. Thong Pham helped in suggesting the scope, method of experimental tests. Prof. Hong Hao approved and provided further suggestions on testing and analysing test results. Mr. Cheng Yuan and Ms. Han Li provided great helps to the experimental tests. The first author prepared the manuscript and had been thoroughly revised and edited by Dr. Thong Pham and Prof. Hong Hao.

Chapter 5 and Chapter 6:

Dr. Thong and Prof. Hong Hao helped in suggesting analysis method. The first author prepared the manuscript and had been thoroughly revised and edited by Dr. Thong Pham and Prof. Hong Hao. The financial support from the Australian Research Council Laureate Fellowships FL180100196 is acknowledged.

TABLE OF CONTENTS

LIST OF FIGURES

LIST OF TABLES

NOTATION

A	=	distance from centre of support to loading point
A_{ct}	=	area of a portion of cross-section between flexural tension face and centroid of gross section
A_g	=	gross area of concrete section
A_{ps}	=	area of prestressing tendons
$A_{s,min}$	=	minimum area of longitudinal reinforcement
A_u	=	area under load-deflection curve at ultimate deflection
A_y	=	area under load-deflection curve at yielding of steel
B	=	width of the cross-section
b_c	=	constant factor to determine plastic strain in compression in CDP model
b_t	=	constant factor plastic strain in tension in CDP model
b_w	=	width of the cross-section's web
C	=	neutral axis depth of the section
c_u	=	neutral axis depth of the section at the ultimate stage
d_c	=	compressive damage parameter
d, d_{ps}	=	distance from extreme top fibre to centroid of prestressing steel
d_t	=	tensile damage parameter
E_c	=	modulus of elasticity of concrete
E_p	=	modulus of elasticity of FRP tendon
E_{ps}	=	modulus of elasticity of prestressing steel
E_s	=	modulus of elasticity of conventional steel
E	=	flow potential eccentricity in CDP model
e_m	=	tendon eccentricity at the midspan
e_{ps}	=	eccentricity of prestressing steel to the neutral axis

e_s	=	tendon eccentricity at the support
f'_c	=	compressive concrete strength
f_{cYP}	=	stress in the concrete in the extremely tensile fibre corresponding to f_{psYP}
f_{ct}	=	cracking strength of concrete in tension
f_{cu}	=	cube strength of concrete
f_{expt}	=	experimental value of tendon stress at ultimate stage
f_{pe}	=	effective stress in the prestressing steel after transfer
f_{ps}	=	stress in prestressing steel
f_{psYP}	=	stress in prestressing steel at yield point
f_{pu}	=	ultimate tensile strength of prestressing steel
f_{py}	=	yield strength of prestressing steel
f_s	=	conventional steel stress
H	=	depth of cross-section
h_f	=	depth of flange of cross-section
K	=	deflection coefficient that depends on the loading type and support conditions
K_c	=	ratio of the second stress invariant on the tensile meridian to the compressive meridian
K	=	ratio of the neutral axis depth to the FRP tendon depth
I	=	moment of inertia of the beam section
I_1, I_2	=	moment of inertia of the section corresponding to loading stages
I_{cr}	=	moment of inertia of a cracked section
I_e	=	effective moment of inertia
I_g	=	gross moment of inertia of the concrete section
L	=	span length

l_e	=	$l_i/(1+[N/2])$
l_i	=	length of the tendon between anchorages
M	=	applied moment
M_a	=	maximum moment in the member at which the deflection is being computed
M_{cr}	=	cracking moment
M_{SW}	=	moment due to self-weight
N	=	number of support hinges crossed by the tendons
N	=	modulus ratio
P, P_1, P_2	=	applied loads
P_{cr}	=	cracking load
P_{expt}	=	experimental value of applied load at ultimate stage
P_{pe}	=	prestressing force in the tendons due to f_{pe}
P_{theo}	=	theoretical value of applied load at ultimate stage
P_u	=	applied load at ultimate stage
P_y	=	applied load at yield point
S_b	=	section modulus, $S_b = I_g/y_{cb}$
W	=	unit weight of the beam
y_{bps}	=	distance from centroid of prestressing steel to neutral axis of beam's gross section
y_{cb}	=	distance from extremely bottom fibre to the neutral axis of the concrete section
$y_{t,cr}$	=	distance from the extreme top fibre to the neutral axis of the cracked section
β	=	material parameter
β_1	=	concrete compression stress-block reduction factor

β_d	=	softening factor
Δ_1, Δ_1, Δ_2	=	beam deflections
Δ_{expt}	=	experimental value of beam deflection at ultimate stage
$\Delta_{J,cr}$	=	joint opening at cracking
$\Delta_{J,u}$	=	joint opening at ultimate stage
$\Delta_{J,y}$	=	joint opening at ultimate stage
Δ_u	=	midspan deflection of a beam at ultimate
Δ_y	=	midspan deflection of a beam at yielding of tension steel
$\Delta\varepsilon_{ps}^{bonded}$	=	strain increment in bonded prestressing steel
$\Delta\varepsilon_{py}^{bonded}$	=	strain increment in the bonded tendon from effective prestress strain to yield strain
$\Delta\varepsilon_{u}^{bonded}$	=	strain increment in bonded prestressing steel at the ultimate stage
$\Delta\varepsilon_{u}^{unbonded}$	=	strain increment in unbonded prestressing steel at the ultimate stage
Δf_{ps}^{bonded}	=	stress increment in bonded prestressing steel
$\Delta f_{ps}^{unbonded}$	=	stress increment in unbonded prestressing steel
$\delta_{mid,cr}$	=	midspan deflection at cracking
$\delta_{mid,u}$		midspan deflection at ultimate stage
$\delta_{mid,y}$		midspan deflection at yield point
ε'_c	=	concrete strain corresponding to f_c'
ε_c	=	concrete strain in compression
ε_{ce}	=	strain in concrete at level of prestressing steel due to f_{pe}
ε_{ct}	=	concrete strain corresponding to f_{ct}
ε_{cu}	=	concrete compressive strain at ultimate stage

ε_{cSW}^{bot}	=	strain in the concrete at the bottom fibre due to self-weight of the beam
ε_{cSW}^{top}	=	compressive strain in the concrete at the extreme top fibre due to self-weight
ε_{pe}	=	effective strain in the prestressing steel
ε_{ps}	=	strain of prestressing steel
ε_{psSW}	=	strain of prestressing steel due to self-weight
ε_{pu}	=	ultimate tensile strain of prestressing steel
ε_{py}	=	strain of prestressing steel at yielding
ε_t	=	concrete strain in tension
$\dot{\varepsilon}_c^{in}$	=	concrete inelastic strain in compression defined in CDP model
ε_{oc}^{el}	=	concrete elastic strain in compression defined in CDP model
ε_{ot}^{el}	=	concrete elastic strain in tension defined in CDP model
ε_c^{pl}	=	concrete plastic strain in compression defined in CDP model
$\dot{\varepsilon}_t^{ck}$	=	concrete cracking strain in tension defined in CDP model
λ	=	ratio of plastic hinge length to the neutral axis depth
μ	=	viscosity parameter in CDP model
ρ_b	=	balanced reinforcement ratio
ρ_{ps}	=	prestressing steel reinforcement ratio
ρ_b^u	=	balanced reinforcement ratio of a beam with unbonded tendons
ρ_b^b	=	balanced reinforcement ratio of a beam with bonded tendons
σ_{b0}/σ_{c0}	=	ratio of initial equibiaxial compressive yield stress to initial uniaxial compressive yield stress in CDP model
σ_c	=	concrete stress in compression

σ_{cSW}^{bot}	=	stress in the concrete at the bottom fibre at the level of prestressing steel due to self-weight
σ_{cfpe}^{bot}	=	stress in the concrete in the bottom fibre due to prestressing
σ_t	=	concrete stress in tension
ϕ_w	=	reduction factor which accounts for the behaviour of thin components
ψ	=	dilation angle in CDP model
Ω	=	strain reduction coefficient in pre-cracking stage
Ω_{cr}	=	strain reduction coefficient in post-cracking stage
Ω_u	=	strain reduction coefficient
ω_{ps}	=	reinforcement index

CHAPTER 1 INTRODUCTION

1.1 Background

Precast segmental prestressed concrete beams (PSBs) have been increasingly used in many bridge construction projects around the world. Time-saving and economic benefits are among the advantages that made the PSBs very well suitable for the construction of medium to moderate long-span bridges (Hindi et al. 1995). To date, steel tendons are used as the only prestressing material to join individual segments to form completed bridge spans. Steel tendons have been designed as internal, external or a combination of internal and external tendons. Corrosion problem of the steel tendons at segment joints, however, is a great concern of the application of PSBs, particularly in places with highly aggressive environmental conditions. Inappropriate design choices and poor-quality construction of the corrosion protection systems are the main factors that have been contributing to the corrosion-induced damages, which greatly increase lifecycle costs of the structures. In extreme cases, the whole structure might even completely collapse as reported in previous studies (Woodward and Williams 1988; Wouters et al. 1999; Concrete Society Technical Report 2002).

The primary aim of this study is to investigate the possible use of fibre-reinforced polymer (FRP) tendons in segmental concrete beams for possible replacement of steel tendons in construction to mitigate the corrosion problems. FRP tendons are typically made from one of the three popular fibres, which include aramid, carbon, and glass. Of these, Aramid FRP (AFRP) and carbon FRP (CFRP) are typically recommended for prestressing applications. Glass fibres have poor resistance to creep under sustained loads and are more susceptible to alkaline degradation than carbon and aramid fibres, therefore, are mostly employed as conventional reinforcing bars (ACI 440.4R 2004). This study focuses on the use of CFRP tendons as internal and external prestressing material in precast segmental concrete beams.

Carbon Fibre-reinforced polymer (FRP) tendons are corrosion-free and possess a high tensile strength that even exceeds steel tendons. In addition, they are lighter than steel, which allow easier handling and reduce dead load of the structure. These characteristics make CFRP tendons a potential use for segmental concrete beams. To the authors' best knowledge, CFRP tendons have been only applied for monolithic concrete beams and this is the first study that uses CFRP tendons for prestressing

segmental concrete beams. While CFRP tendons have many superior material properties, many problems need to be solved before their practical applications on segmental concrete beams. Firstly, CFRP tendons show a linear stress-strain relationship up to failure, which differs from that of the steel tendons (ACI 440.4R 2004). This behaviour may cause a beam with FRP tendons to fail in a brittle and explosive manner when the CFRP tendons rupture. A beam with steel tendons fails in a more ductile manner as it shows a plastic behaviour after the yielding of steel tendons. Secondly, CFRP tendons used in the infrastructure industry generally have lower elastic modulus than steel tendons and their transverse modulus are significantly smaller than their longitudinal modulus. The longitudinal and transverse modulus of the prestressing steel tendons are similar and are taken as 195 GPa while those of CFRP tendons are different. The longitudinal modulus of CFRP tendons ranges from 142 GPa to 150 GPa while their shear modulus is around 7.2 GPa and the longitudinal modulus of Aramid fibre reinforced polymer (AFRP) tendons ranges from 65 GPa to 70 GPa while their transverse modulus is about 2.2 GPa (ACI 440.4R 2004). The low elastic modulus potentially causes the beam to undergo larger deflections under the same applied loads. The asymmetry of transverse and longitudinal mechanical properties leads to the inefficiency and failure of the anchor. A number of mechanical or bonded type anchor systems were designed and developed for CFRP tendons, but there has not yet a reliable anchor system for CFRP tendons (Schmidt et al. 2012). The design of an anchor system for CFRP tendons, however, is not considered in this study.

The relatively low transverse strength of CFRP tendons also leads to another concern that needs due care, especially when the external tendons are used, namely the so-called harping effect. When FRP tendons are deviated, stress concentration in the tendons due to harping effect may cause a strength reduction in the tendons. Previous studies showed that deviator curvature, harping angle, and tendon size are the main factors affecting the stress increment in tendons owing to the harping effect. Grace and Abdel-Sayed (1998) reported 19% and 34% reductions in breaking forces for carbon fibre composite cable (CFCC) tendons draped at 3^o angle and 5^o angles when using 50.8 mm diameter deviators, respectively. When 508 mm diameter deviators were used, those reductions were 12% and 26% at draping angles of 5^o and 10^o, respectively. Quayle (2005) reported reductions ranging between 13% and 50% in the tensile strength of the CFRP tendons when the tendons were draped at 2^o to 15^o using

deviators of the radius of 50 mm to 1000 mm, respectively.

Another issue that may impede the popular use of FRP tendons is the unfavourable fire resistance. Even though carbon fibres may be heat resistant to 1000°C, the resins are generally sensitive to heat (ACI 440.4R 2004). The decomposition of epoxy resin at high temperatures causes the CFRP tendons to fail. Wang and Kodur (2005) found that FRPs maintain a linear stress-strain response at both ambient and elevated temperature. However, the mechanical properties of FRP reinforcements degrade quickly at higher temperatures and CFRP tendons retain approximately 50% of their original strength at 250^{o}C while that for steel tendon is 580^{o}C. Test results by Yu and Kodur (2014) showed that CFRP tendons could retain most of the tensile strength and modulus up to around 200^{o}C but decline rapidly for temperature over 300^{o}C. Regarding moisture resistance, studies showed that CFRP tendons demonstrate excellent resistance to moisture penetration while GFRP tendons are susceptible to moisture attack (Hollaway 2010), which again restricts the use of GFRP tendons in prestressed members.

Nevertheless, as the resin performance continuously increases, a variety of high-performance epoxy resin can be used in composites. It was found in the previous study (Han et al. 2015) that the high-temperature resistant and toughened epoxy resin can significantly improve the transverse mechanical properties and fire-resistance of CFRP tendons. The transverse compressive strength of the new CFRP tendons of 5 mm diameter developed by Han et al. (2015) was 2.3 times that of the corresponding value of commercial CFRP tendons. The shear strength of the new CFRP tendons improved by 30% to 40% for larger diameters.

Since of high fibre and resin costs, bridges using FRPs are likely to have higher initial costs than traditional reinforced concrete bridges. The material cost of the FRP tendons is roughly two to ten times that of conventional steel tendons (Wang and Wu 2010). However, provided that the life-cycle cost of the structure is considered, using FRPs has the potential to be a cost-effective design alternative to traditional steel tendons. Eamon et al. (2012) found that the CFRP alternative becomes the least expensive option over the lifetime of the structure and this starts at year 23-77 after initial construction, with a 95% probability depending on the bridge case considered. Yang et al. (2020) also found that the life-cycle cost of FRP cables for long-span cable

supported bridges is superior to that of traditional steel cables due to their excellent anti-fatigue and corrosion-resistant properties.

It is shown that there are a number of factors that need to be investigated before applying CFRP tendons to PSBs. Such factors are largely due to the different mechanical properties of the CFRP tendons compared to the traditional steel tendons, including the linear behaviour up to failure, substantially low transverse strength compared to the longitudinal strength, and low fire resistance. This study, therefore, investigates the behaviour of PSBs prestressed with CFRP tendons, in which it will focus on the effects of the linear behaviour of CFRP tendon and its low transverse strength to the performance of the structure under normal working environments, while not considering the performance of the structure at elevated temperature or moisture conditions.

The use of unbonded tendons on the segmental concrete beams is another focus of this study. Unbonded tendons enable fast installation and ease replacement in cases of deterioration or damage. As such, they are favourable to new segmental concrete bridge constructions. However, due to the lack of bonding between tendons and surrounding concrete, it is still a real challenge in predicting the structural response of segmental beams with unbonded tendons. Extensive studies have been conducted on the prediction of the load-carrying capacity of PSBs with unbonded tendons while very few studies have addressed prediction of the deflection of the structure. Existing codes (PCI 2004; AASHTO LRFD 2012; ACI 318 2015) only recommend methods to compute the instantaneous deflections of beams with bonded tendons while guidance for the calculation of deflections of the beams with unbonded tendons has not been provided. Harajli and Kanj (1992) presented several approaches, which were reported in the literature for computing the deflections of bonded or partially bonded prestressed members and modifications were made for the application in the beams with unbonded tendons. The critical point is the computation of the moment of inertia of cracked section, I_{cr}. In order to determine I_{cr}, they assumed the effective area of the unbonded prestressing tendons to be $\Omega_{cr}A_{ps}$, where Ω_{cr} is a bond reduction coefficient in the elastic cracked state proposed by Naaman (1990). However, the estimation of an exact value of Ω_{cr} for different types of loading and tendon profiles is an extremely difficult task. After a careful analysis, they assumed Ω_{cr} is equal to Ω, where Ω is a bond reduction coefficient in the pre-cracking stage, which can be determined when the

loading type and tendon profiles are known. However, it is unknown that whether this method is applicable for PSBs with unbonded CFRP tendons since the use of CFRP tendons may lead to a different value of Ω_{cr}. Au et al. (2005) extended the use of coefficient λ proposed by Pannell (1969), which is the ratio of plastic hinge length to the neutral axis depth *c* at critical sections, to the cracked section analysis of unbonded partially prestressed concrete beams. However, the calculation procedure is tedious, and it is inconvenient for practical use to compute the deflections of partially unbonded prestressed concrete beams. Du et al. (2016) proposed a method to estimate the deflection of partially unbonded prestressed continuous beams. The method proposed by Du et al. (2016) yields satisfactory predictions of deflection until the yielding of non-prestressed steel while the deflection afterwards till the ultimate stage was not considered in their model. In PSBs with unbonded tendons, there is almost no contribution of the conventional steel to the beam's strength capacity since the steel is cut-off at the segment joints. This method, therefore, cannot be applied for PSBs with unbonded tendons.

Meanwhile, the balanced reinforcement ratio of a PSB with unbonded tendons is another factor, which requires further investigations. To the author's best knowledge, an estimation of the balanced reinforcement ratio for beams with unbonded tendons, $\rho_b{}^u$, has not been reported in the open literature except the work recently done by Lee et al. (2017). Due to the absence of bonding between the prestressing tendons and the surrounding concrete as mentioned previously, the stress increment in the tendons depends on the deformation of the entire member rather than the analysis of a single section. As a result, the determination of $\rho_b{}^u$ becomes more challenging for beams with unbonded tendons. Lee et al. (2017) developed an analytical model based on three equivalent curved blocks for simply supported monolithic beams internally prestressed with unbonded carbon fibre reinforced polymer (CFRP) tendons and then conducted parametric studies to evaluate the effects of various parameters on $\rho_b{}^u$. It was found that $\rho_b{}^u$ is always smaller than that of a beam with bonded tendons, $\rho_b{}^b$ and the ratio of $\rho_b{}^u/\rho_b{}^b$ were shown to be between 0.43 and 0.83. However, the computation procedure for $\rho_b{}^u$ is tedious and it is inconvenient for practical engineers to get the first estimation of the minimum amount of reinforcement required. In addition, this proposed procedure is applicable for monolithic beams only while there has been no such study for precast segmental beams.

The accuracy in the prediction of the stress increment in the unbonded tendons is still questionable (Yuan et al. 2014). Yuan et al. (2014) found that all methods including Naaman and Alkhairi (1991), Harajli (2006), ACI 318 (2008) and AASHTO (1999) encounter considerable scatter in the prediction of the stress increment for PSBs with unbonded tendons. As such, with the increase in the application of PSBs with unbonded tendons, closer examinations in the analysis and design of this type of structures are necessary. Therefore, this study further investigates the flexural behaviour of PSBs prestressed with unbonded tendons under bending, in which the predictions of the load-carrying capacity and displacement at the ultimate stage are discussed. The determination of the balanced reinforcement ratio of precast segmental concrete beams with unbonded tendons is also a research question to be addressed.

1.2 Research objectives

The primary aim of the study is to investigate the possible use of carbon fibre-reinforced polymer (CFRP) tendons as an alternative solution for PSBs to mitigate the corrosion issue. This is done through a series of experimental tests on large-scaled segmental concrete beams, in which both internal and external steel/CFRP tendons are used for prestressing the specimens. Both analytical analysis and numerical studies are then carried out to investigate the flexural behaviour of the PSBs with unbonded steel/CFRP tendons. The specific objectives of this study are as follows:

Experimental studies:

- To answer the questions: Can CFRP tendons be applied for precast segmental concrete beams? Are they good for PSBs in regards to the strength, ductility, stiffness and the ductile failure modes?
- To investigate the flexural response of PSBs with CFRP tendons in comparison with the beams with steel tendons. Do they show similar or different flexural behaviours?
- To investigate the effects of different types of joints (dry/epoxied), bonding conditions of the tendons (bonded/unbonded), tendon profiles (internal/external) and tendon materials (steel/CFRP tendons) on the flexural behaviour of PSBs.

Analytical studies:

- To examine the accuracy in the prediction of the flexural behaviour of PSBs with unbonded tendons by existing models.
- To predict the load-carrying capacity of PSBs with unbonded tendons at the ultimate stage.
- To develop a new procedure in predicting the load-deflection curves of PSBs with unbonded tendons.
- To develop a new guide to estimate the balanced reinforcement ratio of PSBs with unbonded tendons.

Numerical studies:

- To enhance the understanding of the flexural response of PSBs with unbonded tendons.
- To conduct parametric studies for which the effects of different factors on the flexural behaviour of PSBs with unbonded tendons are investigated including the effective prestress, the prestressing reinforcement ratio, the span length to tendon depth ratio, the strength of concrete, the type of load, and the number of joints.
- To validate the analytical prediction results and investigate some factors and measures which could not be achieved from the experimental studies, i.e. stress flow of concrete and shear stress in CFRP tendons.

1.3 Research outline

This thesis is written based on journal papers prepared by the candidate during his PhD studies that are either published, accepted or under review. These papers form individual chapters and therefore can be read independently, however, each chapter may have similar minor parts due to the description of the experimental studies. The contents of each chapter are briefly described below:

Chapter 1 presents the introduction which includes a background of the research topic, research gaps and objectives of the research.

Chapter 2 presents an experimental study on the use of internal unbonded CFRP tendons on precast segmental concrete beams. The flexural responses of the beams under four-point loading are investigated in which the effects of different types of

joints (dry/epoxied) and tendon materials (steel/CFRP tendons) on the structural behaviour are highlighted. The accuracy of existing standards in predicting the load-carrying capacity of PSBs with unbonded CFRP tendons is also examined. Based on experimental results, a modified strain reduction coefficient is proposed for better prediction of stress in the unbonded CFRP tendons at the ultimate stage, thus better prediction of the load-carrying capacity of the structure.

Chapter 3 investigates the effect of bonding condition of CFRP tendons on the structural response of PSBs for which both unbonded and bonded CFRP tendons are used in the specimens. In addition, this chapter examines the accuracy of existing codes in the prediction of the deflection of PSBs with unbonded CFRP tendons, of which they showed large differences. As such, modifications are made in the calculation of cracking moment of inertia of PSBs with unbonded CFRP tendons for better deflection predictions of the structure at the ultimate stage.

Chapter 4 investigates the use of external CFRP tendons for prestressing PSBs. The effects of tendon materials (steel/CFRP tendons) and tendon profiles (internal/external) on the failure modes, joint opening, and stress development in the external tendons are investigated. This chapter also examines the predictions of stress in the external tendons at the ultimate stage by existing codes. The adequacy of the current code predictions are examined and discussed, and improvements are suggested.

Chapter 5 presents a numerical investigation of the flexural performance of PSBs with unbonded tendons. This is the first three-dimensional numerical model successfully validated against experimental results of segmental concrete beams in the literature. Based on the verified numerical model, intensive simulations are carried out in terms of performances of segmental beams with different parameters and various conditions, i.e. tension-controlled, compression-controlled and balanced sections. A parametric study is also conducted to investigate the effects of main factors that are supposed to strongly affect the flexural response of PSBs with unbonded tendons.

Chapter 6 presents analytical approaches for the prediction of the flexural response of PSBs with unbonded tendons. Three main subjects are presented in this chapter. Firstly, a new analytical procedure which is based on the bilinear method to predict the load-deflection curves of PSBs with unbonded tendons is proposed. This

calculation procedure accurately predicts the load-deflection curves of PSBs with unbonded steel tendons. Secondly, an empirical equation for the first time is developed to estimate the balanced reinforcement ratio of PSBs with unbonded tendons. This empirical equation can be applied for both the PSBs with unbonded steel and CFRP tendons. Its accuracy is verified against the numerical results. Finally, based on regression analysis, a new strain reduction coefficient, Ω_u, is proposed for the application on PSBs with unbonded steel tendons to gain better predictions of stress increment in the unbonded tendons at the ultimate stage.

Chapter 7 summarizes the outcomes of this study and also outlines recommendations for future studies.

1.4 References

AASHTO (1999). *Guide Specifications for Design and Construction of Segmental Concrete Bridges: 2nd Ed with 2003 Interim Revis*, American Association of State Highway and Transportation Officials, Washington, DC.

AASHTO LRFD (2012). "Bridge Construction Specifications, 6th Edition, U.S. Units." American Association of State Highway and Transportation Officials, Washington, DC.

ACI 318 (2008). *Building code requirements for structural concrete and commentary*, ACI 318-08, American Concrete Institute, Farmington Hills, MI.

ACI 318 (2015). "Building code requirements for structural concrete and commentary (ACI 318-14)." American Concrete Institute, Farmington Hills, MI.

ACI 440.4R (2004). "Prestressing concrete structures with FRP tendons (Reapproved 2011)." American Concrete Institute, Farmington Hills, USA.

Au, F., Du, J., and Cheung, Y. (2005). Service load analysis of unbonded partially prestressed concrete members. *Magazine of Concrete Research*, 57(4), 199-209.

Concrete Society Technical Report (2002). Durable post-tensioned concrete structures. *TR 72*,.

Du, J., Au, F. T., Chan, E. K., and Liu, L. (2016). Deflection of unbonded partially prestressed concrete continuous beams. *Engineering Structures*, 118(2016), 89-96.

Eamon, C. D., Jensen, E. A., Grace, N. F., and Shi, X. (2012). Life-cycle cost analysis of alternative reinforcement materials for bridge superstructures considering cost and maintenance uncertainties. *Journal of Materials in Civil Engineering*, 24(4), 373-380.

Grace, N. F., and Abdel-Sayed, G. (1998). Behavior of externally draped CFRP tendons in prestressed concrete bridges. *PCI Journal*, 43(5), 88-101.

Han, Q., Wang, L., and Xu, J. (2015). Experimental research on mechanical properties of transverse enhanced and high-temperature-resistant CFRP tendons for prestressed structure. *Construction and Building Materials*, 98, 864-874.

Harajli, M. H. (2006). On the stress in unbonded tendons at ultimate: Critical assessment and proposed changes. *ACI Structural Journal*, 103(6), 803.

Harajli, M. H., and Kanj, M. Y. (1992). Service Load Behavior of Concrete Members Prestressed with Unbonded Tendons. *Journal of Structural Engineering*, 118(9), 2569-2589.

Hindi, A., MacGregor, R., Kreger, M. E., and Breen, J. E. (1995). Enhancing strength and ductility of post-tensioned segmental box girder bridges. *ACI Structural Journal*, 92(1), 33-44.

Hollaway, L. (2010). A review of the present and future utilisation of FRP composites in the civil infrastructure with reference to their important in-service properties. *Construction and Building Materials*, 24(12), 2419-2445.

Lee, C., Shin, S., and Lee, H. (2017). Balanced Ratio of Concrete Beams Internally Prestressed with Unbonded CFRP Tendons. *International Journal of Concrete Structures and Materials*, 11(1), 1-16.

Naaman, A. E. (1990). New methodology for the analysis of beams prestressed with external or unbonded tendons. *Special Publication*, 120(1990), 339-354.

Naaman, A. E., and Alkhairi, F. (1991). Stress at ultimate in unbonded prestressing tendons: Part 2—Proposed Methodology. *ACI Structural Journal*, 88(6), 683-692.

Pannell, F. (1969). The ultimate moment of resistance of unbonded prestressed concrete beams. *Magazine of Concrete Research*, 21(66), 43-54.

PCI (2004). *Design Handbook*, 6th ed., Precast/Prestressed Concrete Institute, Chicago, IL.

Quayle, T. G. (2005). Tensile-flexural Behaviour of Carbon-fibre Reinforced Polymer (CFRP) Prestressing Tendons Subjected to Harped Profiles. MS thesis. Univ. Waterloo.

Schmidt, J. W., Bennitz, A., Täljsten, B., Goltermann, P., and Pedersen, H. (2012). Mechanical anchorage of FRP tendons – A literature review. *Construction and Building Materials*, 32, 110-121.

Wang, X., and Wu, Z. (2010). Evaluation of FRP and hybrid FRP cables for super long-span cable-stayed bridges. *Composite Structures*, 92(10), 2582-2590.

Wang, Y. C., and Kodur, V. (2005). Variation of strength and stiffness of fibre reinforced polymer reinforcing bars with temperature. *Cement and Concrete Composites*, 27(9-10), 864-874.

Woodward, R., and Williams, F. (1988). Collapse of YNS-Y-GWAS Bridge,

Glamorgan. *Proceedings of the Institution of Civil Engineers*, 84(4), 635-669.

Wouters, J., Kesner, K., and Poston, R. (1999). Tendon corrosion in precast segmental bridges. *Transportation Research Record: Journal of the Transportation Research Board*(1654), 128-132.

Yang, Y., Wang, X., and Wu, Z. "Life cycle cost analysis of FRP cables for long-span cable supported bridges." *Proc., Structures*, Elsevier, 24-34.

Yu, B., and Kodur, V. (2014). Effect of temperature on strength and stiffness properties of near-surface mounted FRP reinforcement. *Composites Part B: Engineering*, 58, 510-517.

Yuan, A., He, Y., Dai, H., and Cheng, L. (2014). Experimental Study of Precast Segmental Bridge Box Girders with External Unbonded and Internal Bonded Posttensioning under Monotonic Vertical Loading. *Journal of Bridge Engineering*, 20(4), 04014075.

CHAPTER 2 FLEXURAL BEHAVIOUR OF PRECAST SEGMENTAL CONCRETE BEAMS PRESTRESSED WITH INTERNAL UNBONDED CFRP TENDONS[1]

Abstract

This chapter investigates the use of carbon fibre reinforced polymer (CFRP) tendons on precast segmental beams (PSBs) to tackle the corrosion problems which are likely to occur at joint locations of PSBs prestressed with steel tendons. Up to date, the use of CFRP tendons was extensively documented for monolithic beams while their application on PSBs has not been reported yet. Three precast segmental T-section beams including two beams with unbonded CFRP and one with steel tendons were built and tested under four-point loads in this chapter. The test results showed that CFRP tendons can be well used to replace the steel tendons on PSBs. The beams with CFRP tendons demonstrated both high strength and high ductility as compared to the beam with steel tendons. However, the stresses in the unbonded CFRP tendons at the ultimate loading conditions of the tested beams were low, ranging from only about 66% to 72% of the nominal breaking tensile strength. The type of joints i.e. dry and epoxied, greatly affects the initial stiffness of the beams but has no effect on the opening of joints at the ultimate loading stage. Moreover, a comprehensive examination on four existing code equations to predict the stress in the unbonded tendons showed that the four examined codes predicted well the stress at the ultimate loading condition of the unbonded steel tendons, however, they significantly under-predicted those in the CFRP tendons. A modification in the strain reduction coefficient used by ACI 440.4R (2004) for predicting the stress increment in unbonded CFRP tendons of monolithic beams is therefore proposed for PSBs based on the experimental results.

[1] This chapter is compiled from the following paper which was published in Engineering Structures:
Le, T. D., Pham, T. M., Hao, H., and Hao, Y. (2018). Flexural behaviour of precast segmental concrete beams internally prestressed with unbonded CFRP tendons under four-point loading. *Engineering Structures*, 168(2018), 371-383.

2.1 Introduction

Since its first application for concrete bridges in the 1950's, precast segmental prestressed concrete girder bridges have gained rapid acceptance as they not only allow speeding up the construction process but also improve the quality control. So far, steel tendons have been used as the only prestressing solution to connect individual beam segments to form the completed bridge spans. The steel tendons can be bonded or unbonded to the concrete and placed inside or outside of the beam cross-section, known as internally or externally prestressing techniques. Corrosion of steel tendons at joint locations, however, causes deterioration or even total collapse of the whole structures (Woodward and Williams 1988; Wouters et al. 1999; Concrete Society Technical Report 2002) .

Fibre-reinforced polymer (FRP) tendons have been used for the prestressing technique as a promising solution to replace steel tendons to deal with the corrosion issue. The term "FRP tendons" denotes the use of one of the various types of fibres, i.e. aramid (AFRP), carbon (CFRP) or glass (GFRP). In the literature, the use of FRP tendons has only been applied to monolithic concrete beams (ACI 440.4R 2004). When tendons are internally bonded to the concrete, FRP and steel prestressed beams behave differently after concrete cracked (Maissen and de Smet 1998; Dolan and Swanson 2002; ACI 440.4R 2004). In the first stage, both beams with FRP and steel tendons will deform elastically until cracking of concrete. After cracking, beams prestressed with steel tendons exhibits nonlinear load-deflection behaviour until the beams fail by crushing of concrete or rupture of tendons. In contrast, beams prestressed with FRP tendons will continue to deform in an approximately linear manner with the increase in the applied load until the tendons rupture or the concrete reaches its ultimate compressive strain. Furthermore, Maissen and de Smet (1998) reported that the moment redistribution mechanism in the beams prestressed with CFRP tendons differed from that of the beams with steel tendons because CFRP tendons did not exhibit elastoplastic deformation characteristics. Zou (2003) pointed out that the conventional ductility index for concrete beams prestressed with steel tendons was not suitable for beams with FRP tendons since FRP did not have a yield point. As such, a new deformability index counting for both deflection and strength factors was proposed and it applied to beams with either FRP tendons or steel tendons. It is noted that this proposed deformability index was based on the analysis of monolithic beams

prestressed with carbon fibre reinforced polymer (CFRP) tendons or steel tendons.

In cases of unbonded tendons, on the other hand, beams with FRP and steel tendons behave very similarly (Pisani 1998; Tan and Tjandra 2007; Lou et al. 2012). The only difference is FRP tendons showed linear behaviour up to the ultimate load and have lower elastic modulus as compared to steel tendons. Pisani (1998) numerically analysed simply supported beams prestressed with unbonded GFRP or steel tendons and stated that the beams with unbonded GFRP tendons showed non-linear load-deflection behaviour up to the ultimate load, which was very similar to that of the unbonded steel tendons beams. The ductility of the GFRP beams was even better, although their ultimate strength was lower than beams reinforced with steel tendons. Similar observations were also reported by Lou et al. (2012) for beams externally prestressed with FRP tendons. Tan and Tjandra (2007) tested continuous beams and concluded that the use of external CFRP tendons did not lead to significant differences in the ultimate loads, tendon stresses, and deflections as compared to conventional steel tendons.

When FRP tendons are used for prestressing, stress concentration in the tendon due to harping effect is an important factor that needs due care. The localized curvature generated by the deviation will cause a high-stress concentration in the tendons which adversely prevents the tendons to fully achieve its breaking capacity. The effects of the deviator curvature, harped angle, and tendon size are found to be the main factors impacting the stress increment in the CFRP tendons accounting for the harping effect (Mutsuyoshi and Machida 1993; Grace and Abdel-Sayed 1998; Quayle 2005; Wang et al. 2015). Mutsuyoshi and Machida (1993) found that CFRP tendons deviated at an angle of 11.3^{o} ruptured at approximately 80% of their breaking load when 400-mm diameter steel deviators were used. Grace and Abdel-Sayed (1998) reported 19% and 34% reductions in breaking forces for carbon fibre composite cable (CFCC) tendons draped at 3^{o} angle and 5^{o} angles when using 50.8 mm diameter deviators. When 508 mm diameter deviators were used, those reductions were 12% and 26% at draping angles of 5^{o} and 10^{o}, respectively. Quayle (2005) found reductions ranging between 13% and 50% in the tensile strength of the CFRP tendons when the tendons were draped at 2^{o} to 15^{o} with 50 mm to 1000 mm radii deviators, respectively. Based on finite element analysis on Basalt FRP tendons, Wang et al. (2015) recommended a bending angle less than 3° to avoid the strength reduction percentage exceeding 10%.

Joints between segments are the most critical part of PSBs as they permit the shear transfer and integrity of the whole structure. The joints can be epoxied or dry, flat or keyed, and having single or multiple shear keys and are made of plain concrete or reinforced concrete. The behaviour of joints under direct shear were extensively studied in the literature (Turmo et al. 2006a; Li et al. 2013b; Jiang et al. 2015). From experimental tests on panels, Turmo et al. (2006a) concluded that the use of steel fibre reinforced concrete (SFRC) did not increase the shear capacity of the panel joints. In addition, the formulation recommended by AASHTO (1999) yielded the best prediction for the shear capacity of the joints as concluded by the authors.

This different feature between a segmental and a monolithic beam may cause further concern to the PSBs as the opening of joint and sliding of segments may cause stress concentration in the tendon and change the loading distributions in the beam. This, in turn, raises up a question, is FRP tendon a good solution for prestressing PSBs despite owning excellent mechanical properties? In other words, can the FRP tendon fully achieve its breaking capacity or will it suffer from premature failure due to stress concentration at joint locations? Since FRP tendon is made of anisotropic material, it has very low transverse modulus and strength as compared to those in the longitudinal direction.

This chapter, therefore, focuses on investigating the behaviour of PSBs prestressed with unbonded CFRP tendons. As far as the authors are aware, this is the first time CFRP tendons are applied to post-tensioning segmental concrete beams. The effect of tendon types and joint types on the structural behaviour of segmental concrete beams will be discussed.

2.2 Experimental program

To evaluate the use of CFRP tendons on PSBs, three large scale segmental concrete beams including two beams post-tensioned with CFRP tendons and one beam with unbonded steel tendons which served as a reference specimen were built and tested in the Civil Engineering Laboratory, Curtin University. Two types of dry or epoxied multiple shear-keyed joints were used in the beams. All the beams were then tested under four-point loading test up to failure. The details of specimen design and test set up are described in the subsequent sections.

2.2.1 Design of specimens

All the specimens were made of reinforced concrete and were designed according to the requirements of AASHTO (1999) for segmental concrete beams and ACI 440.4R (2004) for beams prestressed with FRP tendons. The total length of a beam is 3.9 m with T-shaped cross-section of 400 mm height. Each beam consisted of four individual segments which were connected together by two steel or CFRP tendons using the post-tensioning technique. For convenience, each specimen was labelled as given in Table 2-1, in which Beam BS1 was prestressed with two steel tendons and had dry joints while Beams BC1 and BC2 was prestressed with CFRP tendons with different joint types, i.e., dry or epoxied. Figure 2-1 shows the design details and dimensions of the tested beams.

Table 2-1: Configuration of specimens.

Specimen	Tendon type	Joint type	Concrete strength	Effective tendon stress		Tendon force
			f_c' (MPa)	f_{pe} (MPa)	f_{pe}/f_{pu}	F_{pe} (kN)
BS1	2 steel tendons	Dry	44	1280	0.64	119
BC1	2 CFRP tendons	Dry	44	818	0.35	108
BC2	2 CFRP tendons	Epoxied	44	661	0.27	83

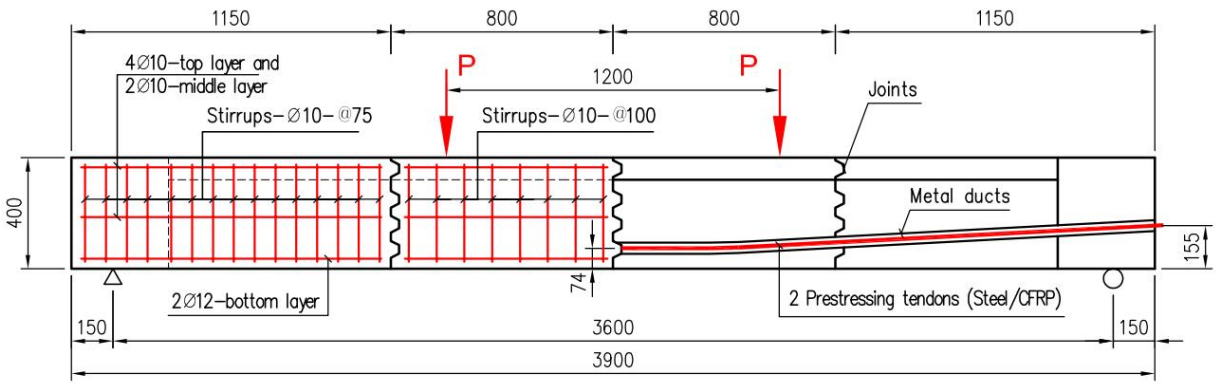

Figure 2-1: Detailed dimensions of the tested beams

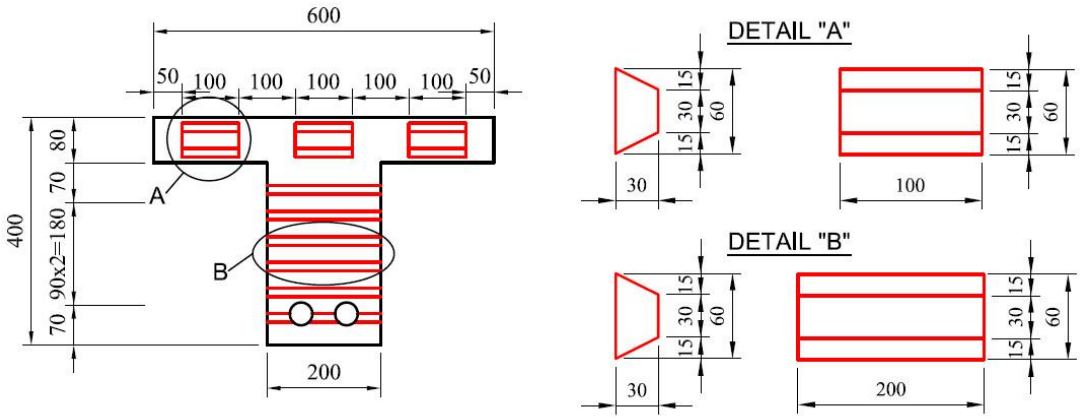

Figure 2-2: Multiple shear-keyed joints

Previous studies showed that the shear stress distribution in the multiple shear-keyed joints, which are widely used in practice, is more uniform than in the single keyed joints (Zhou et al. 2005; Li et al. 2013b; Jiang et al. 2015). As such, multiple shear-keyed joints were adopted in the present study. The size of the multiple shear keys was selected based on the joint design suggested in Article 24.4 of AASTHO (1999). The Guide recommends a ratio of the key depth to the key width approximately 1:2 (h:d = 1:2), and the key depth is not less than twice the maximum size aggregate diameter. Concrete with aggregate of 10 mm maximum size was used, therefore, keys with a depth of 30 mm and a width of 60 mm were used in this study. These shear keys had the same cross-section size but different lengths on the flange and on the web of the specimens as shown in Figure 2-2.

Each segment of the beams was reinforced with the minimum amount of non-prestressed reinforcement at the top and bottom of the segment. This minimum amount reinforcement was in accordance with the requirements of ACI 318 (2015) for beams with unbonded tendons. The minimum area of the longitudinal reinforcement was computed as: $A_{s,min} = 0.004A_{ct}$, where A_{ct} is the area of that part of the cross-section between the flexural tension face and the centroid of the gross section. Two 12 mm diameter deformed bars were used for the bottom longitudinal reinforcement and four 10 mm diameter deformed bars were used for the top layer. These steel bars were cut off leading to the discontinuity of the longitudinal steel reinforcement at each joint location. 10 mm diameter deformed bars were also used for transverse reinforcements which were placed at 100 mm spacing for the two middle segments and at 75 mm spacing for the two end segments to strengthen beams in shear (Figure 2-1).

All the beams were under-reinforced according to strength design (AASHTO 1999). Beam BS1 has an unbonded prestressing reinforcement ratio of $0.112\rho_b$, while those of Beams BC1 and BC2 are $0.53\rho_b$ and $0.58\rho_b$, respectively. It is noted that ρ_b is the balanced prestressing reinforcement ratio for an counterpart beam with bonded tendons, which was given by ACI 440.4R (2004) and presented in Eq. 2.1:

$$\rho_b = 0.85\beta_1 \frac{f_c^{'}}{f_{pu}} \frac{\varepsilon_{cu}}{\varepsilon_{cu} + \varepsilon_{pu} - \varepsilon_{pe}} \tag{2.1}$$

where f'_c is the compressive concrete strength, ε_{cu} is the ultimate compressive strain of concrete and taken as 0.003, f_{pu} and ε_{pu} are the design ultimate tensile strength and the corresponding strain of CFRP tendon, respectively, and ε_{pe} is the effective strain in the CFRP tendon caused by initial effective stress f_{pe}. It is noted that f_{pu} and ε_{pu} are replaced by the yield strength and the corresponding strain of steel tendons when calculating the balanced reinforcement ratio for Beam BS1.

2.2.2 Materials

Pre-mixed concrete was used in this experiment and was supplied by a local supplier. Determination of concrete properties was conducted according to the Australian Standards AS 1012.8.1 (2014) and AS 1012.9 (2014) for concrete cylinders. The cylinders were of 100 mm diameter and 200 mm height. The average compressive strength of three concrete cylinders on the testing day was 44 MPa with a standard deviation of 1.47. Conventional steel bars of 12-mm and 10-mm diameters were used for longitudinal and transverse steel reinforcements, respectively. The ultimate tensile strength of 12-mm deformed bars N12 and 10-mm deformed bars N10 were 587 MPa and 538 MPa, respectively, as provided by the manufacturer. 7-wire 12.7-mm diameter steel tendons and single strand 12.9-mm diameter CFRP tendons were used in the specimens. The CFRP tendons were supplied by Dextra Building Products (GuangDong) CO., LTD (Dextra Group). The mechanical properties of the CFRP tendons were reported by the manufacturer after testing 16 CFRP coupons. Detailed properties of the materials used in the specimens were given in Table 2.

Table 2-2: Properties of materials

Type	Diameter (mm)	Area (mm^2)	Yield strength (MPa)	Ultimate strength (MPa)	Elastic modulus (GPa)
12-mm steel bars N12	12.0	113.0	534	587	200
10-mm steel bars N10	10.0	78.5	489	538	200
Steel tendon	12.7	100.0	1674	1860	195
CFRP tendon	12.9	126.7	N/A	2450	145

2.2.3 Casting of specimens

Steel cages of each segment of all beams were prepared and placed in a timber formwork. Corrugated metal duct of 40-mm diameter which was cut in designed length was also installed into the steel cages to create holes for placing tendons later. To separate each segment during pouring concrete, T-shaped timber plates having the same dimension as beam's cross-section were cut and placed in the formwork at intended locations as separation plates. Foam blocks were attached to the separation plates to form the shear keys as shown in Figure 2-3.

All segments were cast using match-casting method, i.e. the first and third segments were cast in the first concrete batch, and then they were used as a formwork in the second batch to make the second and fourth segments. By this way, it ensured the male and female keys perfectly fit between two adjacent segments. Cylinders (100 mm diameter and 200 mm height) were also cast to determine the concrete properties.

Figure 2-3: Casting of specimens

After casting, all the segments were cured in a moist condition in which wet hessian rags were placed on top of the segments and were watered twice a day to keep them moist. The formwork was removed after 7 days of casting, then the segments were left for continuous curing at least 28 days before post-tensioning and testing. Figure 2-3 shows a typical segment at completion.

2.2.4 Post-tensioning and epoxy

Figure 2-4 shows a photo of typical set up of post-tensioning. One end of CFRP tendons was connected to a steel tendon via steel couplers as shown in Figure 2-5. By this way, the prestressing procedure for the CFRP tendons was done similarly to the steel tendons. It is noted that this anchor design was made to ensure the tendon failure not to occur at the anchor region which was therefore not a concern of this study. Also, the stress concentration at joint locations is critical for the CFRP tendons since the transverse modulus of CFRP tendons is significantly smaller than their longitudinal modulus. The concrete surfaces of the holes formed by the steel ducts, therefore, were carefully ground and treated for smooth stress transfer of the tendons to the concrete during stressing or from the concrete to the tendons during loading.

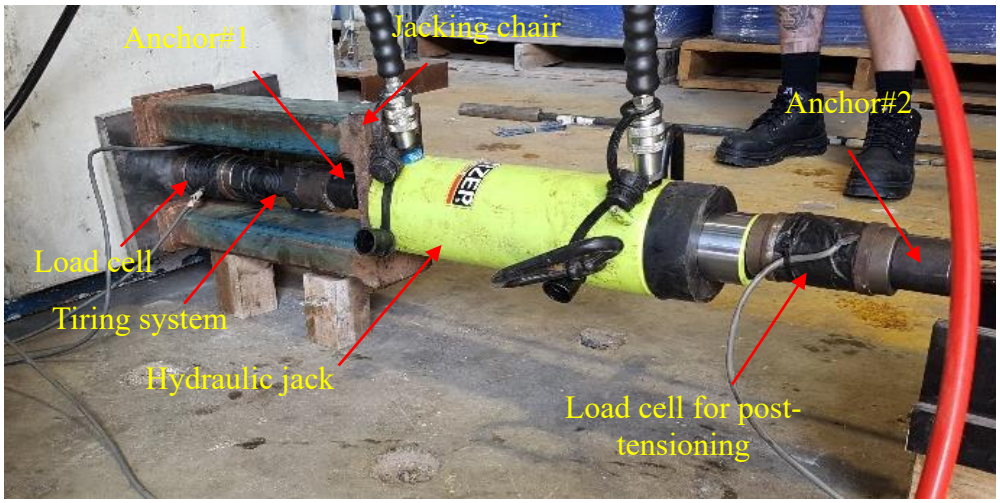

Figure 2-4: Typical set up for post-tensioning

The stressing force was generated by a monostrand hydraulic jack of 30 tons that seated onto a jacking chair. Two sets of wedges and barrel anchors were used in the stressing end, in which one was placed after the hydraulic jack called post-tensioning anchor #2 and another one was placed before the jack called working anchor #1. Hollow bolts and nuts (tightening system) were placed inside the jacking chair just before the working anchor for tightening and releasing the force later. 20-ton capacity

load cells were used to measure the tensioning force generated by the hydraulic jack and the force in the tendon during the test.

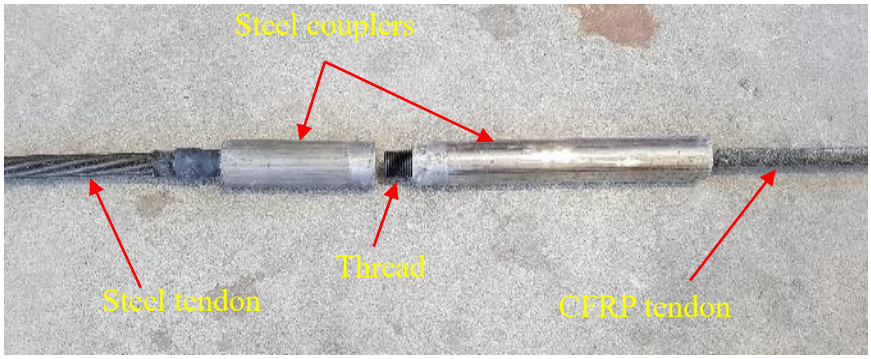

Figure 2-5: CFRP tendon with steel couplers

For Beam BC2 with epoxied joints, the concrete surfaces of the shear keys were thoroughly cleaned using a steel brush and an air gun to make sure the surface in a good condition and free from dust. The concrete surfaces were then thoroughly watered and left to dry for at least 2 hours before applying the adhesive. A thin layer of Sikadur-30 epoxy adhesive (Sika Australia) was applied to the joint surfaces of the segments using a trowel. After post-tensioning, the epoxied beam was left for curing of the adhesive for 3 days.

The stressing procedure was done as follows. In the first step, the tendons were stressed an initial force of approximately 10% of the total stressing force, F_s, to close the gaps between segments and to remove the slack. F_s was computed from the control stress in the tendons, which were taken as 0.75 f_{pu} for steel tendons (AASHTO 1999) and 0.4 f_{pu} for CFRP tendons (ACI 440.4R 2004). Then each tendon was stressed in three load levels at 20%, 60% and 100% of the total stressing force until completion. Load cells and strain gauges attached to the tendons were used to monitor and measure the stresses in the tendons during the post-tensioning process. The effective tendon stresses and the corresponding force in the tendons immediately following transfer are listed in Table 2-1.

2.2.5 Measurements, test set up and loading

Measurements recorded during the tests include the applied load, vertical displacement, opening of joints, strain in prestressing tendons and non-prestressing rebars. The applied load was monitored by load cells attached to the hydraulic jacks. The load cells were calibrated to have less than 1% error at the maximum loading

capacity of 40 tons, and the error was smaller at lower range, usually 0.5% to 1%. Linear variable differential transformers (LVDTs) of 100 mm measurement range were used for tracking the vertical displacement and opening of joints. The accuracy of the LVDTs was around 0.5% to 1% over 100 mm span. Strain in the rebars and prestressing tendons were measured by strain gauges and load cells attached at the end of the beams as shown in Figure 2-6. FLA-2 series of strain gauges supplied by Bestech Company were used in the tests.

The applied load was exerted by two vertical hydraulic jacks of 55 tons each placed equally at one-third span. Two horizontal I steel beams were used to uniformly transfer the vertical loads from the jacks to the beams. All the beams were tested under monotonic loads progressively up to failure and the progressive loading pattern is shown in Figure 2-7. Two load cycles were performed at each loading level. The load increment in each loading level was 20 kN. In each cycle, the applied load was gradually increased to the designated value of that loading level and then was reduced to around 5 kN before starting the next cycles, except the first loading cycle when the applied load started from 0. All the tests were carried out under load control at a rate of 3 to 5 kN/min.

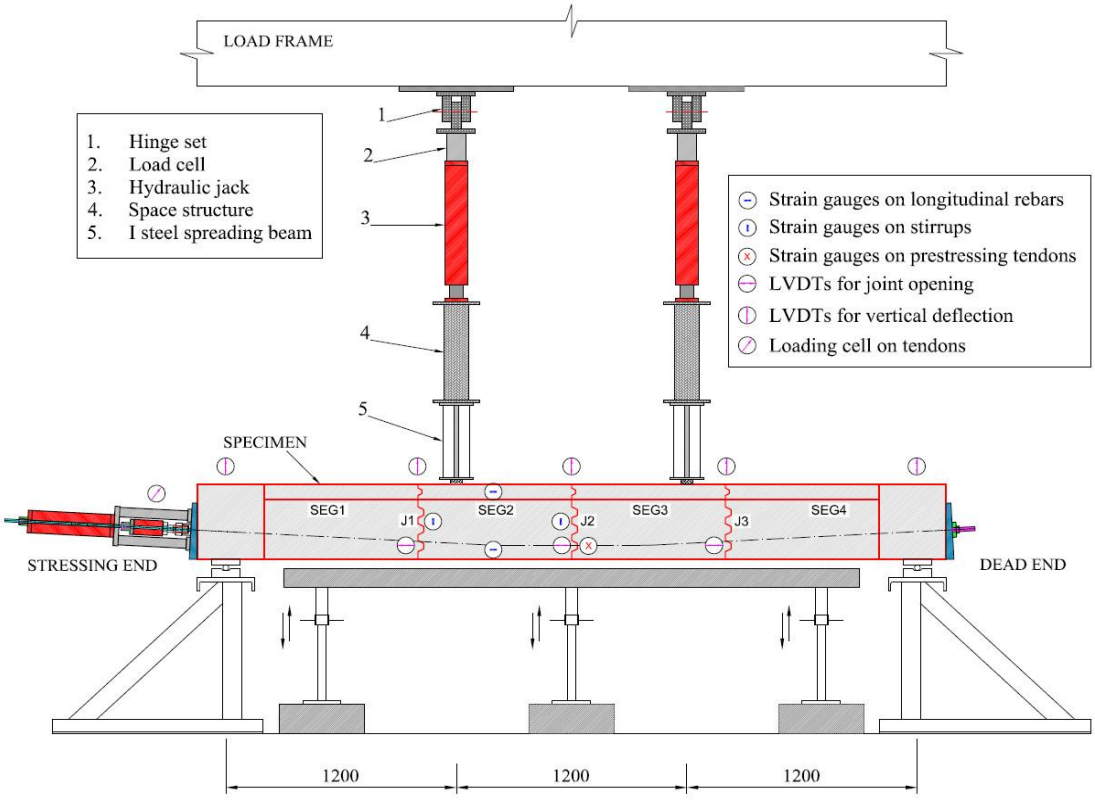

Figure 2-6: Typical test set up

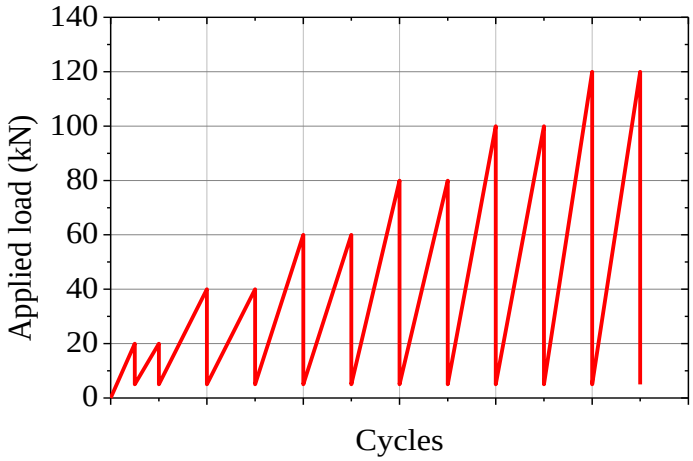

Figure 2-7: Progressive loading cycles

2.3 Experimental results

2.3.1 Failure modes

The tested results of all the specimens are shown in Table 2-3, in which P_y, P_u, $\delta_{mid,y}$, $\delta_{mid,u}$, $\Delta_{J,y}$, $\Delta_{J,u}$ are the applied loads, midspan deflections, and openings of the middle joint of the specimens at yield point and at ultimate condition, respectively. The definition of the yield point is given in Figure 2-11.

The failure of all the tested beams is shown in Figure 2-8. The failure started by concrete crushing on the top fibre followed by yielding of the steel tendons for Beam BS1 or rupturing of CFRP tendons for beams prestressed with CFRP tendons. The crushing of concrete and rupture of tendons occurred at the middle joint located at the midspan for all the beams. All the beams in this study were under-reinforced in regards to a counterpart beam with bonded tendons, therefore the failure mode would theoretically be tension controlled since $c/d < 0.42$ by AASHTO LRFD (2012), where c is the depth of the neutral axis, d is the distance from the extreme top fibre to the centroid of tension force. However, the test results show concrete crushing failure. In fact, unbonded tendons shifted the failure mode of the under-reinforced counterparts from tension controlled to compression controlled. This phenomenon may be attributed to the fact that the strain in the unbonded tendons does not depend on the section analysis but the whole beam behaviour (Naaman and Alkhairi 1991), which allows the beam to achieve larger deflection leading to the higher compression strain in the concrete on the top fibre. As a result, the calculation of the balanced reinforcement ratio for beams with unbonded tendons requires further consideration.

Lee et al. (2017) found that the balanced reinforcement ratio of a beam with unbonded tendons (ρ_b^U) was always smaller than that of a beam with bonded tendons (ρ_b^B) and the ratio of ρ_b^U / ρ_b^B varied in a range between 0.43 and 0.83 for specimens considered in their study.

Table 2-3: Experimental testing results

Specimen	Applied load (kN)		Midspan deflection (mm)		Joint opening (mm)		Failure mode
	P_y	P_u	$\delta_{mid,y}$	$\delta_{mid,u}$	$\Delta_{J,y}$	$\Delta_{J,u}$	
BS1	51.2	96	5.4	89.4	0.20	30.44	Compression failure and yielding of tendons
BC1	53.4	113	8.4	94.7	0.55	27.70	Compression failure and rupture of CFRP tendons
BC2	54.1	123	2.3	101.1	0.07	30.02	Compression failure and rupture of CFRP tendons

a) Beam BS1

b) Beam BC1

c) Beam BC2

Figure 2-8: Failure modes of the tested specimens

2.3.2 Load-deflection curves

The load-deflection curves for all the specimens under four-point loading at different

loading levels are shown in Figure 2-9. The envelop curves of these relations are plotted in Figure 2-10. As shown, Beam BC1 with unbonded CFRP tendons behaved very similar to Beam BS1 with steel tendons. In both cases, the load-deflection curves were divided into two stages by a transition zone. In the first stage, both beams had high stiffness and showed a linear relationship between the applied load and deflection. In the second stage, the beams' stiffness sharply reduced and the beams deformed in a non-linear manner up to failure. The transition from the first stage to the second stage is related to the opening of the middle joint J2 under the applied loads. The middle joint J2 in Beams BS1 and BC1 started to open at the applied loads of approximately 43.3 kN and 40.1 kN, respectively. At the same time, the stiffness of the beams started to reduce dramatically. The only difference between the two beams was that Beam BS1 had a higher initial stiffness than Beam BC1. However, after cracking Beam BS1 showed a lower tangent stiffness because of its lower reinforcement index, $\omega_{ps} = \frac{f_c^{'}}{f_{pu}} \rho_{ps}$ where ρ_{ps} is the reinforcement ratio. This behaviour is similar to segmental beams prestressed with external steel tendons reported in previous studies (Li et al. 2013b; Saibabu et al. 2013).

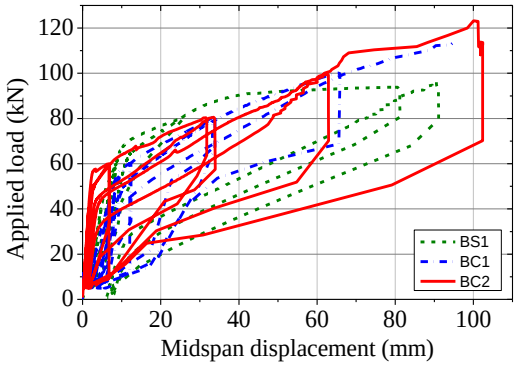

Figure 2-9: Load vs deflection curves

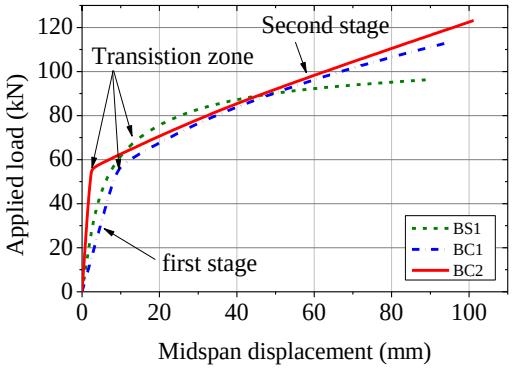

Figure 2-10: Envelop curves of load vs deflection

Similarly, the load-deflection curve of Beam BC2 with epoxied joints also exhibited two stages. However, in the second stage, the beam still deformed almost linearly with the applied load up to failure by rupture of the tendons. It is worth noting that the

transition zone in the curve is the result of concrete cracking in tension at bottom fibre at a load of approximately 44.7 kN. The tensile crack was formed by one vertical crack cutting off all the shear-key bases of joint J2 located at midspan of the beam when the tensile stress generated by the applied load exceeded the tensile strength of the concrete (Figure 2-8c). Further details on this type of cracking are discussed in the next section.

Type of joints also affected on the initial stiffness of the beams. As shown in Figure 2-10, Beam BC1 with dry joints had a lower initial stiffness as compared to Beam BC2 with epoxied joints. This difference was resulted from the distinguished moment of inertia of the two beams in which Beam BC1 with dry joint had the moment of inertia much smaller than that of Beam BC2 associated with epoxied joints.

Previous studies (Tao and Du 1985; Lou and Xiang 2007) showed that the response of monolithic beams with completely unbonded tendons (without any ordinary tension reinforcement) is quite different from that of beams with additional ordinary tension reinforcement as it behaves as a shallow tied arch after cracking rather than a flexural member. Beam BS1 in this study may be considered as a beam without any tension reinforcement as all the tension reinforcements were discontinued at joint locations, however, the load-deflection curve had a good performance as it showed an ascending branch after cracking. This is an additional benefit of segmental beams as compared to monolithic ones associated with internal unbonded tendons.

2.3.3 Ductility

It is seen in Figure 2-9 and Figure 2-10 that all the specimens achieved large deflection before complete failure. The maximum midspan displacement of Beam BS1 reached 89.4 mm which was equal to 1/40 of the span length, L. The maximum midspan displacements of Beams BC1 and BC2 were 94.7 and 101.1 mm, corresponding to 1/38L and 1/35L, respectively. It is noted that the maximum allowable midspan displacement of these beams is L/800 according to AASHTO LRFD (2012). These deflection capacities ensure to give engineers warnings before failure or total collapse of the structures.

To reflect the physical behaviour of the tested beams in terms of ductility indices, two calculation methods for the ductility of the beams, namely displacement ductility and

energy ductility were adopted in this study: Method 1, $\mu = \frac{\Delta_u}{\Delta_y}$ and Method 2, $\mu = \frac{A_u}{A_y}$, where Δ_u is the ultimate midspan deflection; Δ_y is the midspan deflection of the beam at yielding of tension steel; A_u is the area under the load-deflection curve at ultimate deflection, and A_y is the area under the load-deflection curve at yielding of steel. The definition of yield point proposed by Park (1989) was adopted in this study and was illustrated in Figure 2-11. The yielding of the structure was due to the joint opening in cases of beams BS1 and BC1 and the concrete cracking in the tension zone at beam's soffit in the case of Beam BC2. The ductility of the beams is presented in Table 2-4.

It is seen from Table 2-4 that both the displacement ductility and energy ductility of Beam BS1 are higher than those of Beam BC1 although Beam BC1 achieved the maximum displacement at 94.7 mm which was even larger than that of Beam BS1. The ductility of Beam BC2 is approximately 3 times higher than that of Beam BS1. It can be noted that both the beams with CFRP tendons have higher displacement capacity, and the ductility is governed by the yielding displacement. This observation has proven that CFRP tendons can be used to replace steel tendons to achieve the required strength and possibly even better ductility for segmental beams.

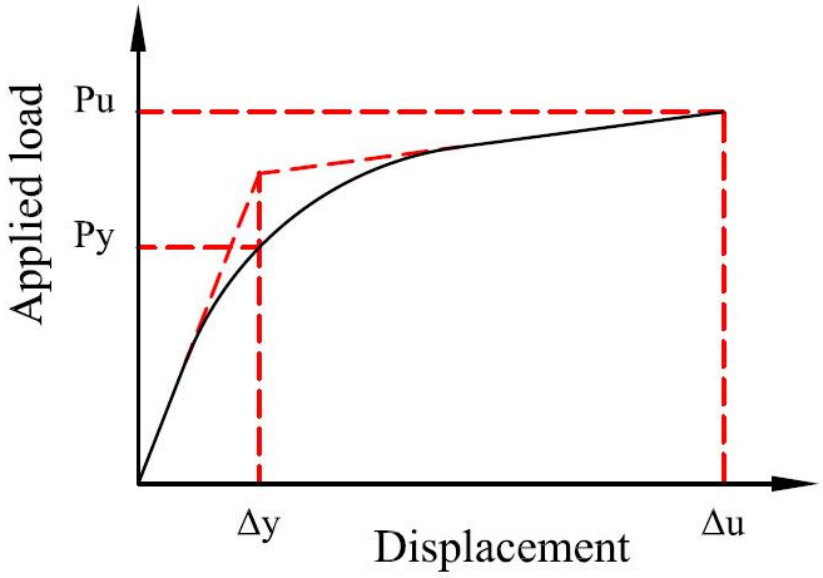

Figure 2-11: Definition of yield point

Table 2-4: Ductility of the specimens

Specimen	Method 1			Method 2		
	Δ_y	Δ_u	Δ_u/Δ_y	A_y	A_u	A_u/A_y
BS1	5.4	89.4	16.6	201	7298	36.3
BC1	8.4	94.7	11.2	336	7853	23.4
BC2	2.3	101.1	44.0	67	9154	136.6

Interestingly, Beam BC2 had a ductility approximately 4 times higher than that of Beam BC1 as given in Table 2-4. However, it can be observed from Figure 2-10, Beam BC1 showed similar strength and deflection capacities as beam BC2. The reason for this big difference is due to the variation in the value of the equivalent displacement at the yield point. As shown, Beams BC1 and BC2 had relatively similar maximum displacements and strengths but their yield points were different leading to the 4 times difference in ductility. It means that the ductility of these beams is significantly governed by the displacement at the yield point which can only be approximately obtained from the testing data. The definition and calculation of ductility of PSB beams prestressed with CFRP tendons with dry or epoxied joints need further verification.

2.4 Discussions

2.4.1 Joint openings

Figure 2-12 shows the opening of all joints along beam's axis at the ultimate state. It can be seen from the curves that in all the beams only the middle joints (J2) opened while the other joints (J1 and J3) almost remained closed under the ultimate loads and the magnitude of the opening at the ultimate load was nearly equal regardless of the types of joint used. This observation confirms the assumption that the beam develops one major crack at the midspan at the ultimate stage, which can be used to calculate the plastic hinge length and the stress in the unbonded tendons in several models (Lee et al. 1999; Roberts-Wollmann et al. 2005; Harajli 2006). These models assumed that the tendon elongation occurred only at the opening hinge at the midspan of the beam. The opening of the middle joint at the ultimate state for Beams BS1, BC1 and BC2 was 30.44 mm, 27.70 mm and 30.02 mm, respectively.

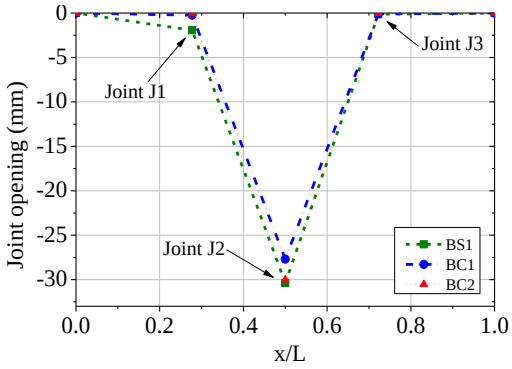

Figure 2-12: Opening of joints along beam's axis

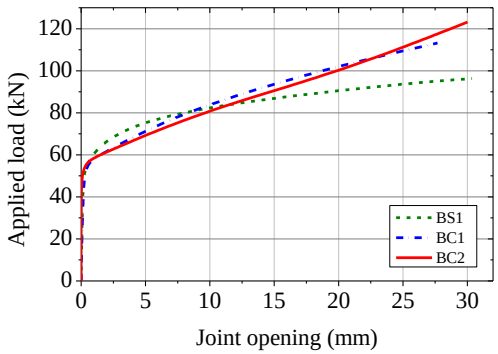

Figure 2-13: Applied load vs joint opening

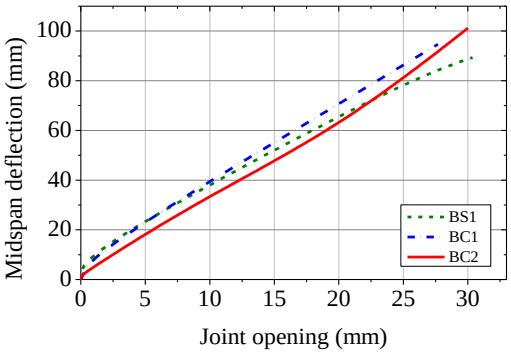

Figure 2-14: Relationship between joint opening vs midspan deflection

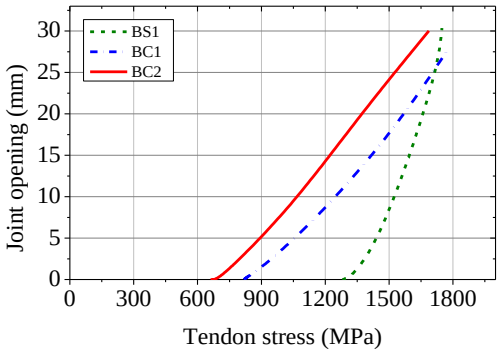

Figure 2-15: Tendon stress vs joint opening

The joint opening with respects to the applied loads for all the beams was plotted in Figure 2-13. It can be seen from the figure that the shapes of the applied load-joint opening curves are very similar to the curves of the applied load and deflection for all the beams as shown in Figure 2-10. At the beginning, the joint still remained closed by the time it reached the opening load or cracking load as discussed previously. After that, the joint started to open at a much larger rate leading to the sudden reduction in the stiffness of the beams.

It is worth mentioning that the opening of joint J2 in Beam BC2, in fact, was the development of a flexural vertical crack cutting off all shear-keyed bases as shown in Figure 2-8c. The flexural crack started from the bottom and quickly propagated to a certain height of the joint. This phenomenon is because the tensile strength of the adhesive was much higher than the tensile strength of concrete (20 MPa vs ~4 MPa) and there was no ordinary steel rebars through the joint. After cracking, the middle joint in the epoxied beam behaved similarly to those in dry joint specimens as seen in Figure 2-12. It is noted that all joints completely closed when the load was released at

the end of each load level as the effect of prestressing.

The relationships between the joint opening and midspan deflection for specimens are plotted in Figure 2-14. It can be clearly seen from the figure that for all the specimens the joint showed an almost linear relationship with the midspan deflection. Therefore, it can be stated that the width of the vertical crack in case of the epoxied beam developed linearly with the midspan deflection under the applied load. The joint opening was also plotted against the tendon stress in Figure 2-15. It is seen from the figures that in Beams BC1 and BC2, the stress in the CFRP tendons increased approximately linearly with the joint opening up to ultimate stage. Meanwhile, Beam BS1 showed a non-linear relationship between the tendon stress and the joint opening. This observation suggests the calculation of stress in the unbonded tendons of a segmental beam based on the deflection of the beam by assuming the elongation of the tendon is equal to the opening of the joint.

2.4.2 Stress development in the tendon under applied load

Figure 2-16 shows the evolution of the prestressing tendon stress under four-point loading. The corresponding envelop curves are plotted in Figure 2-17. The effective stresses in the tendon at the beginning of the loading process for beams BS1, BC1, and BC2 were 1280 MPa, 818 MPa and 661 MPa, respectively. It is seen from the figure that the tendon stress in all the beams started to increase from the beginning of the test. The increase in the tendon stress was due to the deflection of the beam under applied loads as such the applied load and tendon stress curves are very similar to the curves of the applied load and deflection. From the figure, it can be seen that the applied load vs tendon stress of the beams with CFRP tendons showed a bilinear relationship but not for the beam with steel tendons. The one with steel tendon showed a highly non-linear behaviour. It means the stress in the CFRP tendons increased nearly linearly to the applied load, but with different increase rate before and after joint opening.

The tendon stress at the ultimate load in Beam BS1 was 1748 MPa, which was equal to 94% of the nominal tensile strength of the prestressing steel tendons (1860 MPa). It is worth mentioning that the test for Beam BS1 was stopped for the safety reason when large physical damage was observed in the concrete on the top fibre (Figure 2-8a). At that time, the prestressing steel tendons already yielded but had not ruptured yet. After releasing the applied load, the beam still recovered a certain deformation due to the

retraction of steel tendons. In both Beams BC1 and BC2, the CFRP tendons ruptured at the ultimate load. The tendon stresses at rupture were 1774 MPa and 1687 MPa for Beams BC1 and BC2, respectively. It is worth noting that these stress values were far below the nominal breaking strength of the CFRP tendon as they were only equal to 72% and 69% of the breaking strength which was 2450 MPa as reported by the manufacturer after carrying out 16 coupon tensile tests. This reduction in the tensile strength of the CFRP tendons was affected by the loading type (bending loading), harping effect, and the joint opening. Harped angle greatly prevents the increase in the tendon stress as shown in previous studies (Quayle 2005; Wang et al. 2015). In this study, a harping angle of 3° was used to avoid the strength reduction exceeding 10% as recommended by Wang et al. (2015). Therefore, the joint opening was responsible for low stress increment in CFRP tendons which requires further investigation.

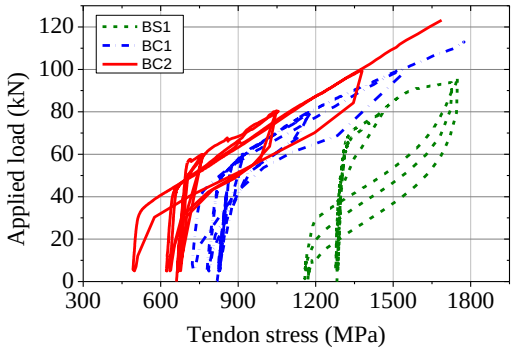

Figure 2-16: Applied load vs tendon stress

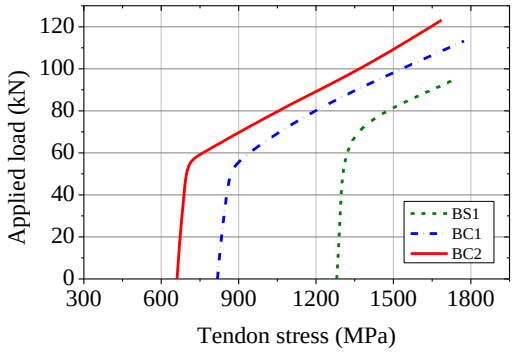

Figure 2-17: Envelop curves of applied load vs tendon stress

After joint opening, the beams deformed at a much faster rate under the applied load so that the increase in the tendon stress was much larger than that in the first stage when the beams were still in the elastic region (Figure 2-18). The total tendon stress increment in Beam BS1 was 468 MPa, which equals $0.25f_{pu}$ and those in Beams BC1 and BC2 were 956 MPa and 1026 MPa, which equal $0.33f_{pu}$ and $0.27f_{pu}$, respectively (Table 2-5).

2.4.3 Tendon stress increment versus midspan deflection

Figure 2-19 shows the relationship between the tendon stress and vertical displacement of the beams. It is seen from the curves that in all the beams, the tendon stress increment exhibited an approximately linear relation to the midspan deflection up to the ultimate load regardless of the type of tendons used. Even though, there was a

slight variation in the curves of beams BS1 and BC1 after joint opening. This observation is similar to previous studies conducted on monolithic beams prestressed with unbonded tendons. Experimental tests by Tao and Du (1985) showed that there exists such linear relationship for moderately reinforced partially prestressed concrete beams with unbonded steel tendons. Lou and Xiang (2007) confirmed this observation based on their numerical analysis. Wang et al. (2015) also found this linear relationship between tendon stress increment and midspan deflection when conducting tests on beams externally prestressed with BFRP tendons. As such, this observation confirms the calculation procedure for stress increment in the PSB prestressed with unbonded CFRP tendons based on midspan deflection which have been used for monolithic beams (Harajili and Kanj 1992; He and Liu 2010).

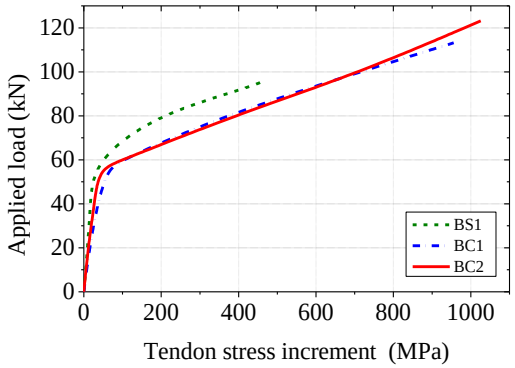

Figure 2-18: Applied load vs tendon stress increment

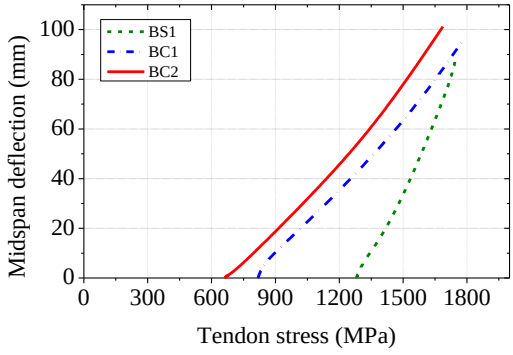

Figure 2-19: Tendon stress vs midspan deflection

2.4.4 Strain in rebars

Since all the beams showed similar behaviour regarding the strain evolution in the ordinary steel rebars under the applied loads, only the experimental results of Beam BS1 was given in Figure 2-20 for brevity, where R1 and R2 are the strains in the bottom and top longitudinal rebars; R3, R4 and R5 and R6 are the strains in the stirrups of segment No.2 near middle joint J2, and joint J3 as shown in Figure 2-6, respectively.

At the beginning, the strain in the top bars (R2) was almost zero, while the bottom longitudinal bars were in compression with a strain of around -300 μm/m resulted from prestressing. When loads were applied, the top bars started to be compressed, however, the strain developed in the bars at the ultimate stage was very small since the strain gauge was attached in the middle of the segment which was far from the failure position. Meanwhile, the stress in the bottom bars gradually changed from

compression to tension at cracking. The strain in the bottom bars was also very small at the ultimate load at around 100 μm/m, which is far below the yielding point. This indicates that there is very small contribution of longitudinal reinforcement bars to the loading capacity of segmental beams. Yuan et al. (2013) and Jiang et al. (2016) reached the same conclusion in their studies on segmental beams prestressed with steel tendons.

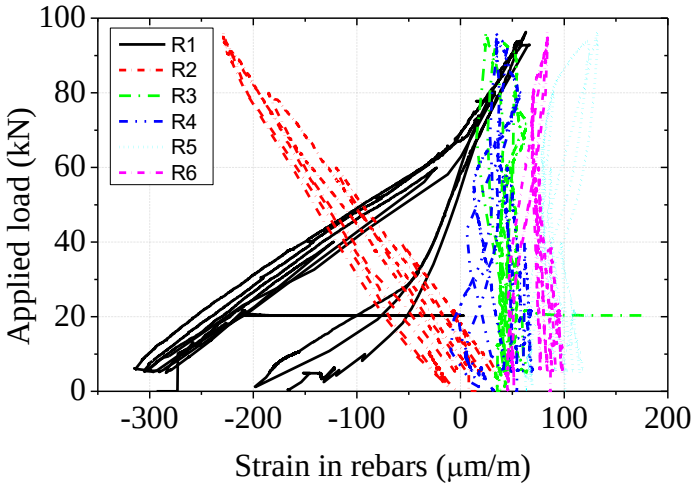

Figure 2-20: Strain in rebars in Beam BS1

Steel stirrups near joint J2 developed a very small strain since J2 was in the pure bending region under loading. The strain in the stirrups near J1 was also very small, even though J1 was in the region with combined shear and bending. This indicates that the stirrups contributed little to resisting the shear force at the joint locations as was also reported in the previous study (Li et al. 2013b).

2.4.5 Residual displacement

Figure 2-21 shows the residual displacement at the end of each loading level of the specimens. It can be seen from the figure that at the end of the load level just onset of the failure, the beams prestressed with CFRP tendons underwent lesser residual displacement than the beam with steel tendons.

Beam BS1 underwent 8.06 mm residual displacement (0.22% *L*), while those for Beams BC1 and BC2 were 5.47 mm (0.15% *L*) and 1.61 mm (0.04% *L*), respectively. However, before opening of the joints, Beam BS1 had better performance than Beam BC1 as it showed a smaller residual displacement after each load level. After joint opening, the residual displacement sharply increased at the end of each load level in

Beam BS1. Meanwhile, the residual displacement in beam BC1 approximately increased linearly from the first to the last loading level. As can be seen that replacing steel tendons by CFRP tendons resulted in a better self-centring capacity of a PSB in which the beam could recover close to its original position after excessive loading, for example from overloaded trucks.

Moreover, the epoxied joints greatly affect the behaviour of the beams with regards to the residual deflection. It can be seen from the figure that beam BC2 underwent much lesser residual deflection than Beam BC1. The experimental results have shown that the epoxied joints can be used to achieve better self-centring capacity.

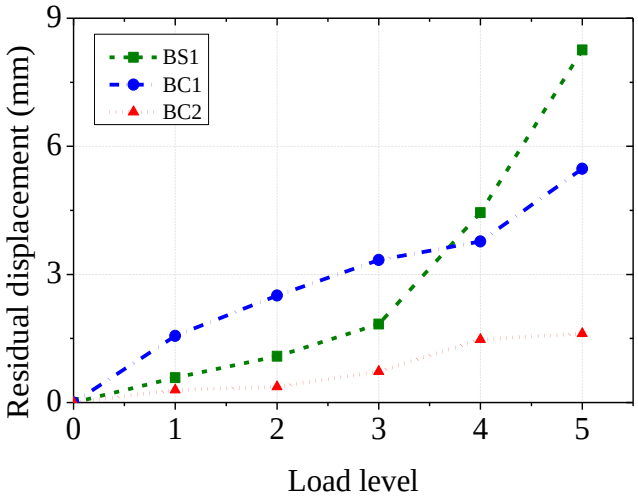

Figure 2-21: Residual displacement of specimens

2.5 Analytical calculations

In this section, the accuracy of the current design procedures and equations recommended for the calculation of the unbonded tendon stress at the ultimate load is evaluated. The examined codes include AASHTO (1999) , ACI 440.4R (2004), ACI 318 (2015) and BS 8110 (1997). However, it is noted that except AASHTO (1999), the equations for calculating tendon stress, f_{ps}, recommended by these codes are developed for the analysis of monolithic concrete beams, no equation is provided in these codes to address segmental beams prestressed with unbonded CFRP tendons. The design procedure presented in AASHTO (1999) is used for segmental beams prestressed with steel tendons. ACI 440.4R (2004)'s equations are developed for monolithic beams with CFRP tendons. ACI 318 (2015) and BS 8110 (1997) are for

monolicthic beams with steel tendons. In brief, there is no specific design guide yet for segmental beams prestressed with CFRP tendons.

For convenience, symbolic for the same parameter in different codes is modified to be identical.

AASHTO (1999) adopted the following equation to predict the average stress in the unbonded tendons in precast segmental concrete beams:

$$f_{ps} = f_{pe} + 6200\left(\frac{d_{ps} - c}{l_e}\right), MPa \tag{2.2}$$

where f_{ps} is the effective tendon stress, d_{ps} is the distance from extreme top fibre to centroid of prestressing tendons, $l_e = l_i/(1+[N/2])$, in which l_i is the length of the tendon between anchorages, and N is the number of support hinges required to form a mechanism crossed by the tendon. The formula is based on the work of McGregor's research (Roberts-Wollmann et al. 2005). Up to date, there has been no recommendation by AASHTO (1999) for FRP tendons in PSBs.

ACI 440.4R (2004) recommended the following equation to predict the stress in CFRP tendons based on the work of Naaman et al. (2002):

$$f_{ps} = f_{pe} + \Omega_u E_{ps} \varepsilon_{cu}\left(\frac{d_{ps}}{c_u} - 1\right) \tag{2.3}$$

where E_{ps} is the tendon modulus of elasticity; ε_{cu} is the ultimate concrete compression strain which was taken as 0.003; c_u is the neutral axis depth at ultimate loading; and Ω_u is a strain reduction coefficient defined as $\Omega_u = 1.5/(L/d_{ps})$ for one-point midspan loading and $\Omega_u = 3/(L/d_{ps})$ for uniform or third-point loading, in which L is the span length. It is noted that Eq. 2.3 was also used to calculate the stress in the unbonded steel tendons as it was originally developed for beams with steel tendons (ACI 440.4R 2004). A limitation of 0.94 f_{py} was recommended in Eq. 2.3 by Naaman and Alkhairi (1991) based on the observation of experimental results, where f_{py} is the yield strength of steel tendons.

ACI 318 (2015) suggested the following equation which is based on the research performed by Mattock et al. (1971):

$$f_{ps} = f_{pe} + 69 + \frac{f_c^{'}}{100\rho_{ps}}, MPa \tag{2.4}$$

where ρ_{ps} is the prestressing reinforcement ratio. This equation is applicable to beams with $L/d_{ps} \leq 35$.

BS 8110 (1997) recommended the following equation:

$$f_{ps} = f_{pe} + \frac{7000}{\frac{L}{d_{ps}}}\left(1 - 1.7\frac{f_{pu}A_{ps}}{f_{cu}bd_{ps}}\right), MPa \tag{2.5}$$

where A_{ps} is the area of prestressing tendons and f_{pu} is the nominal tensile stress at ultimate loading of the tendon, b is the width of the cross-section, and f_{cu} is the cube strength of concrete taken as $f'_c/0.8$.

The analytical and experimental results of the tendon stress and load capacity at ultimate condition for all the specimens are listed in Table 2-5. The accuracy comparison of analytical prediction of all code equations is shown in Figure 2-22 and Figure 2-23. As can be seen from Figure 2-22, all the code equations predicted well the ultimate stress for Beam BS1 with unbonded steel tendons. It is worth mentioning that the result from Eq. 2.3 was taken as 0.94 f_{py} as recommend by Naaman and Alkhairi (1991) because the stress value from Eq. 2.3 was higher than 0.94 f_{py}. This value from Eq. 2.3 was, however, too conservative since in the test the steel tendons in Beam BS1 already yielded. Results from AASHTO (1999), ACI 318 (2015), and BS 8110 (1997) equations are a bit larger than the experimental result for Beam BS1 since the test was stopped for safety reason as mentioned previously.

The accuracy of the design equations in these codes considerably reduced in cases of the beams with CFRP tendons as these codes are not specified for segmental beams with CFRP tendons. AASHTO (1999) and BS 8110 (1997) equations underestimated f_{ps} by about 22% for Beam BC1 with dry joints and 28% for Beam BC2 with epoxied joint as compared with the experimental results. ACI 318 (2015) yielded the most conservative predictions at 31% and 36% lower than the experimental results for Beams BC1 and BC2, respectively. Again, ACI 440.4R (2004)'s equation overestimated f_{ps} for both Beams BC1 and BC2 (Figure 2-22). This is not common for a code equation since a code normally yields conservative results. The reason for this

substantial difference may lie on the ratio L/d_{ps}. ACI 440.4R (2004) limits the application of Eq. 2.3 for beams with CFRP tendons having an unbonded length greater than 15 times the depth of the beam. In this study, the ratio of unbonded tendon length to beam depth was equal to 9.

Table 2-5: Theoretical calculation of the four codes

Specimen	f_{pe} (MPa)	Δf_{ps} (MPa)			f_{ps} (MPa)				P_u (kN)		
		Theo.	Expt.	Theo/ Expt	Theo.	Expt.	Theo/ Expt	f_{expt}/f_u	Theo.	Expt.	Theo/ Expt
AASHTO (1999)											
BS1	1280	531	468	1.13	1811	1748	1.04	0.94	97	96	1.01
BC1	818	539	956	0.56	1357	1774	0.76	0.72	93	113	0.82
BC2	661	543	1026	0.53	1204	1687	0.71	0.69	83	123	0.67
ACI 318 (2015)											
BS1	1280	505	468	1.08	1785	1748	1.02	0.94	96	96	0.99
BC1	818	413	956	0.43	1231	1774	0.69	0.72	84	113	0.74
BC2	661	413	1026	0.40	1074	1687	0.64	0.69	74	123	0.60
ACI 440.4R (2004)											
BS1	1280	294	468	0.63	1574	1748	0.90	0.94	84	96	0.88
BC1	818	1276	956	1.33	2094	1774	1.18	0.72	141	113	1.25
BC2	661	1345	1026	1.31	2006	1687	1.19	0.69	136	123	1.10
BS 8110 (1997)											
BS1	1280	604	468	1.29	1884	1748	1.08	0.94	101	96	1.05
BC1	818	579	956	0.61	1397	1774	0.79	0.72	95	113	0.84
BC2	661	579	1026	0.56	1241	1687	0.74	0.69	85	123	0.69

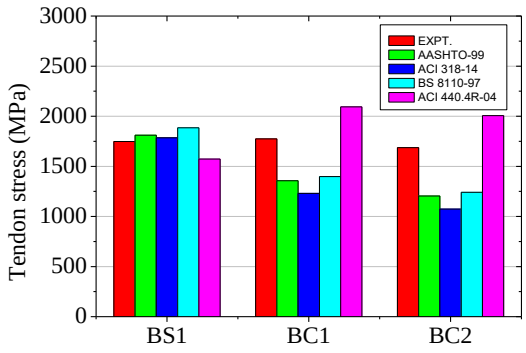

Figure 2-22: Comparison of calculation of f_{ps}

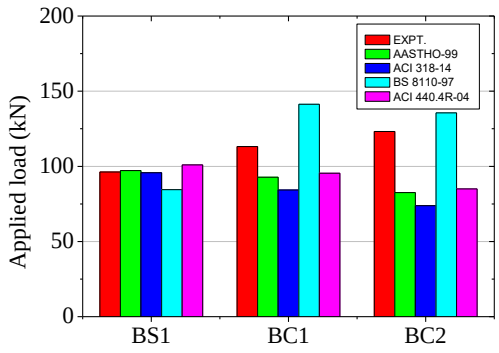

Figure 2-23: Comparison of calculation of P_u

Similarly, except ACI 440.4R (2004), all code equations predicted well P_u for beams with steel tendons but less accurate when CFRP tendons were used. P_u predicted by AASHTO (1999) and BS 8110 (1997) equations were respectively 18% and 16% lower than the experimental results for the beams with dry joints, while those for the beams with epoxied joints were worse at 33% and 31%, respectively. ACI 318 (2015) underestimated P_u by 26% in the case of dry joint and 40% in the case of epoxied

joints, respectively. ACI 440.4R (2004) highly overestimated P_u due to the fact that the L/d_{ps} used in this study was lower than the code's recommendation.

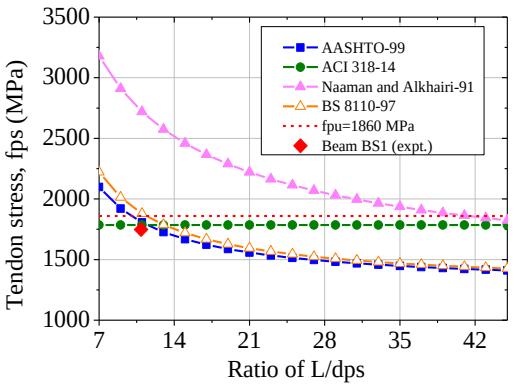

Figure 2-24: Relationship between f_{ps} and L/d_{ps} ratio for beams with steel tendons

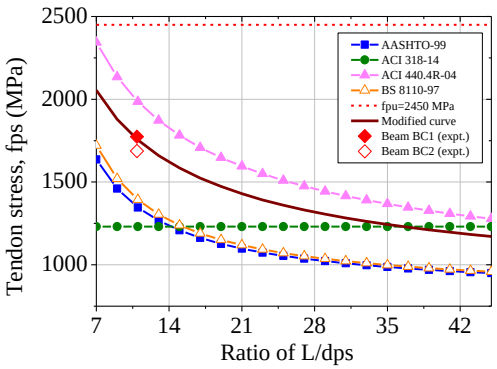

Figure 2-25: Relationship between f_{ps} and L/d_{ps} ratio for beams with CFRP tendons

In order to verify the sensitivity of L/d_{ps} to the increase in the tendon stress of the tested beams against the code equations, an analysis was made by plotting the tendon stresses computed by the code equations against L/d_{ps} for all specimens. Only L/d_{ps} ratio was assumed to vary between 7 and 45 while the other characteristics of the tested beams were kept constant. The curves are shown in Figure 2-24 for the case of beams with steel tendons and in Figure 2-25 for beams with CFRP tendons.

It can be seen from Figure 2-24 that the change in the tendon stress is considerly influenced by the ratio of L/d_{ps} in all codes, except ACI 318 (2015) where the tendon stress at ultimate loading only depends on f_{pe}, f'_c and ρ_{ps} as seen in Eq. 2.4. The increase in L/d_{ps} leads to the decrease in the f_{ps}. As discussed previously, all codes predicted closely to the experimental results of Beam BS1, except the prediction by Eq. 2.3. As such, the limitation of 0.94 f_{py} was used in the calculation.

From Figure 2-25, similar trend is observed between f_{ps} and L/d_{ps} for beams with CFRP tendons by all codes. AASHTO (1999), BS 8110 (1997), and ACI 318 (2015) underestimated the stress in the tendon at ultimate condition. In which AASHTO (1999) and BS 8110 (1997) yielded similar predictions, while ACI 318 (2015) returned the least conservative result. ACI 440.4R (2004) overestimated f_{ps} at ultimate loading, however, both code prediction and experimental results were far below the nominal breaking strength of the tendons. Therefore, the strain reduction coefficient used by ACI 440.4R (2004) in Eq. 2.3 is modified to $\Omega_u = 2.1 / (L/d_{ps})$ based on the experimental results conducted in this study for segmental beams prestressed with CFRP tendons.

The curve of the modified Eq. 2.3 is also shown in Figure 2-25.

2.6 Conclusion

An experimental study was conducted to evaluate the application of CFRP tendons on precast segmental concrete beams. Three T-section segmental beams with either unbonded CFRP tendons or steel tendons were built and tested under cyclic loads. Assessment of the four code equations to predict the stress increment in the unbonded tendons was also presented. The main findings are summarized as follows:

- CFRP tendons can be well in replacement of steel tendons for segmental concrete beams. They can assure the beams to achieve both good strength and ductility capacity.
- The CFRP prestressed beam with dry joints performed similarly as the beam with unbonded steel tendons in terms of overall load and deflection curve. They both showed non-linear load and displacement relations after cracking. However, CFRP prestressed beams with epoxied joints showed a linear load and displacement relation up to failure.
- Unbonded CFRP tendons shifted the failure mode of under-reinforced beams from tension controlled to compression controlled. This transition in the failure modes may prevent the beams from a brittle failure manner when sudden rupture of the CFRP tendons in tension occurs.
- Epoxied or dry joints greatly affected the initial stiffness of the beams but had no effect on the joint opening under the applied loads after cracking.
- The average stress in the unbonded CFRP tendons for the beams with dry joints and epoxied joints was only 72 % and 69% of the nominal tensile strength, respectively. The reduction in the tendon stress at ultimate loading might be governed by the loading type, harping effect and the joint opening which requires further investigation.
- All the examined codes in this paper predicted well the unbonded steel tendon stress at ultimate condition, however, the accuracy significantly reduced when CFRP tendons were used. AASHTO (1999) and BS 8110 (1997) equations yielded better prediction among others, but underestimated f_{ps} by approximately 22% for

Beam BC1 with dry joints and 28% for Beam BC2 with epoxied joint compared to the experimental results. A modification of ACI 440.4R (2004) code equation was suggested for segmental beams prestressed with unbonded CFRP tendons to predict the stress in the tendon at ultimate loading.

- Even though all the beams achieved similar deflection at the ultimate loading, the ductility calculation showed large difference among these specimens. The reason might be due to the sensitivity in determining the equivalent yielding point.

2.7 References

AASHTO (1999). *Guide Specifications for Design and Construction of Segmental Concrete Bridges: 2nd Ed with 2003 Interim Revis*, American Association of State Highway and Transportation Officials, Washington, DC.

AASHTO LRFD (2012). *Bridge Construction Specifications, 6th Edition, U.S. Units*, American Association of State Highway and Transportation Officials, Washington, DC.

ACI 318 (2015). *Building code requirements for structural concrete and commentary*, ACI 318-14, American Concrete Institute, Farmington Hills, MI.

ACI 440.4R (2004). *Prestressing concrete structures with FRP tendons (Reapproved 2011)*, American Concrete Institute, Farmington Hills, USA.

AS 1012.8.1 (2014). Methods of testing concrete - Method 8.1: Method for making and curing concrete—Compression and indirect tensile test specimens. *Standards Australia International Ltd., NSW*.

AS 1012.9 (2014). Methods of testing concrete - Method 9: Compressive strength tests— Concrete, mortar and grout specimens. *Standards Australia International Ltd., NSW*.

Bestech Company https://www.bestech.com.au/.

BS 8110 (1997). *Structural use of concrete*, British Standards Institution, London.

Concrete Society Technical Report (2002). Durable post-tensioned concrete structures. *TR 72,*.

Dextra Group. "CFRP tendons." https://www.dextragroup.com/offices/dextra-building-products-limited.

Dolan, C. W., and Swanson, D. (2002). Development of flexural capacity of a FRP prestressed beam with vertically distributed tendons. *Composites Part B: Engineering*, 33(1), 1-6.

Grace, N. F., and Abdel-Sayed, G. (1998). Behavior of externally draped CFRP tendons in prestressed concrete bridges. *PCI Journal*, 43(5), 88-101.

Harajili, M., and Kanj, M. (1992). Ultimate flexural strength of concrete members prestressed with unbonded tendons. *Structural Journal*, 88(6), 663-674.

Harajli, M. H. (2006). On the stress in unbonded tendons at ultimate: Critical assessment and proposed changes. *ACI Structural Journal*, 103(6), 803.

He, Z., and Liu, Z. (2010). Stresses in External and Internal Unbonded Tendons: Unified Methodology and Design Equations. *Journal of Structural Engineering*, 136(9), 1055-1065.

Jiang, H., Chen, L., Ma, Z. J., and Feng, W. (2015). Shear Behavior of Dry Joints with Castellated Keys in Precast Concrete Segmental Bridges. *Journal of Bridge Engineering*, 20(2), 04014062.

Jiang, H., Cao, Q., Liu, A., Wang, T., and Qiu, Y. (2016). Flexural behavior of precast concrete segmental beams with hybrid tendons and dry joints. *Construction and Building Materials*, 110, 1-7.

Lee, C., Shin, S., and Lee, H. (2017). Balanced Ratio of Concrete Beams Internally Prestressed with Unbonded CFRP Tendons. *International Journal of Concrete Structures and Materials*, 11(1), 1-16.

Lee, L.-H., Moon, J.-H., and Lim, J.-H. (1999). Proposed methodology for computing of unbonded tendon stress at flexural failure. *Structural Journal*, 96(6), 1040-1048.

Li, G., Yang, D., and Lei, Y. (2013). Combined shear and bending behavior of joints in precast concrete segmental beams with external tendons. *Journal of Bridge Engineering*, 18(10), 1042-1052.

Lou, T., and Xiang, Y. (2007). Effects of ordinary tension reinforcement on the response of beams with unbonded tendons. *Advances in Structural Engineering*, 10(1), 95-109.

Lou, T., Lopes, S. M. R., and Lopes, A. V. (2012). Numerical analysis of behaviour of concrete beams with external FRP tendons. *Construction and Building Materials*, 35, 970-978.

Maissen, A., and de Smet, C. A. (1998). Prestressed concrete using carbon fibre reinforced plastic (CFRP) strands. *Materials and Structures*, 31(3), 175-177.

Mattock, A. H., Yamazaki, J., and Kattula, B. T. (1971). Comparative study of prestressed concrete beams, with and without bond. *Journal Proceedings*, 68(2), 116-125.

Mutsuyoshi, H., and Machida, A. (1993). Behavior of Prestressed Concrete Beams Using FRP as External Cable. *Special Publication*, 138, 401-418.

Naaman, A. E., and Alkhairi, F. (1991). Stress at ultimate in unbonded prestressing tendons: Part 2—Proposed Methodology. *ACI Structural Journal*, 88(6), 683-692.

Naaman, A. E., Burns, N., French, C., Gamble, W. L., and Mattock, A. H. (2002). Stresses in unbonded prestressing tendons at ultimate: Recommendation. *Structural Journal*, 99(4), 518-529.

Park, R. (1989). Evaluation of ductility of structures and structural assemblages from laboratory testing. *Bulletin of the New Zealand national society for earthquake engineering*, 22(3), 155-166.

Pisani, M. A. (1998). A numerical survey on the behaviour of beams pre-stressed with FRP cables. *Construction and Building Materials*, 12(4), 221-232.

Quayle, T. G. (2005). Tensile-flexural Behaviour of Carbon-fibre Reinforced Polymer (CFRP) Prestressing Tendons Subjected to Harped Profiles. MS thesis. Univ. Waterloo.

Roberts-Wollmann, C. L., Kreger, M. E., Rogowsky, D. M., and Breen, J. E. (2005). Stresses in external tendons at ultimate. *ACI Structural Journal*, 102(2), 206.

Saibabu, S., Srinivas, V., Sasmal, S., Lakshmanan, N., and Iyer, N. R. (2013). Performance evaluation of dry and epoxy jointed segmental prestressed box girders under monotonic and cyclic loading. *Construction and Building Materials*, 38, 931-940.

Sika Australia Sikadur-30. *https://aus.sika.com/*.

Tan, K. H., and Tjandra, R. A. (2007). Strengthening of RC continuous beams by external prestressing. *Journal of Structural Engineering*, 133(2), 195-204.

Tao, X., and Du, G. (1985). Ultimate stress of unbonded tendons in partially prestressed concrete beams. *PCI Journal*, 30(6), 72-91.

Turmo, J., Ramos, G., and Aparicio, A. C. (2006). Shear strength of dry joints of concrete panels with and without steel fibres. Application to precast segmental bridges. *Engineering Structures*, 28(1), 23-33.

Wang, X., Shi, J., Wu, G., Yang, L., and Wu, Z. (2015). Effectiveness of basalt FRP tendons for strengthening of RC beams through the external prestressing technique. *Engineering Structures*, 101, 34-44.

Woodward, R., and Williams, F. (1988). Collapse of YNS-Y-GWAS Bridge, Glamorgan. *Proceedings of the Institution of Civil Engineers*, 84(4), 635-669.

Wouters, J., Kesner, K., and Poston, R. (1999). Tendon corrosion in precast segmental bridges. *Transportation Research Record: Journal of the Transportation Research Board*(1654), 128-132.

Yuan, A., Dai, H., Sun, D., and Cai, J. (2013). Behaviors of segmental concrete box beams with internal tendons and external tendons under bending. *Engineering Structures*, 48, 623-634.

Zhou, X., Mickleborough, N., and Li, Z. (2005). Shear strength of joints in precast concrete segmental bridges. *ACI Structural Journal*, 102(1), 3.

Zou, P. X. W. (2003). Flexural Behavior and Deformability of Fiber Reinforced Polymer Prestressed Concrete Beams. *Journal of Composites for Construction*, 7(4), 275-284.

CHAPTER 3 FLEXURAL BEHAVIOUR OF PRECAST SEGMENTAL CONCRETE BEAMS PRESTRESSED WITH UNBONDED AND BONDED CFRP TENDONS[2]

Abstract

Precast segmental prestressed concrete beams (PSBs) have been widely used in many elevated highway bridge projects around the world. Steel tendons at joint locations, however, are vulnerable to corrosion damages, which cause deteriorations and in extreme cases lead to the collapse of the whole structures. This chapter experimentally investigates the use of carbon fibre-reinforced polymer (CFRP) tendons as an alternative solution for the PSBs to tackle the corrosion issue. Four large-scale segmental T-shaped concrete beams with internal bonded or unbonded tendons and dry or epoxied joints were built and tested under four-point loading. The test results indicated that CFRP tendons showed satisfactory performances therefore could replace steel tendons for the use in PSBs. All the tested beams exhibited excellent load-carrying capacity and ductility. Tendon bonding condition greatly affected the flexural performance of the segmental beams. Joint type had only a slight effect on the load-carrying capacity and ductility of the beams, but significantly affected the beams' initial stiffness. Unbonded tendons experienced an evident reduction in the tendon strength at the ultimate stage as a consequence of the loading type, harping effect and joint opening. Both AASHTO (1999) and ACI 440.4R (2004) predicted well the tendon stress, thus the load-carrying capacity of the beams with bonded tendons, however, the accuracy significantly reduced for the cases with unbonded tendons. Similarly, the codes did not well estimate the deformation capacity of the prestressed beams with unbonded tendons. An empirical formula is proposed to predict the deflections of beams with unbonded tendons, which yields very close predictions to the experimental results.

[2] This chapter is compiled from the following paper which was published in Composite Structures:
Le, T. D., Pham, T. M., Hao, H., and Yuan, C. (2019d). Performance of precast segmental concrete beams posttensioned with carbon fiber-reinforced polymer (CFRP) tendons. *Composite Structures*, 208, 56-69.

3.1 Introduction

Precast segmental prestressed concrete beams (PSBs) have been widely used in many bridges around the world, especially in the United States, France, Spain and China over the past four decades. Time-saving and economic benefits are among the advantages that made the PSBs very well suited to the construction of the medium to moderate long-span bridges (Hindi et al. 1995). To date, steel tendons are used as the only prestressing material to join individual segments to form completed bridge spans. The tendons have been designed using internal tendons, external tendons or a combination of internal and external tendons. Corrosion problems of the steel tendons at segment joints, however, are a great concern of the application of PSBs, particularly in the places with highly aggressive environmental conditions. Inappropriate design choices and poor quality construction of the corrosion protection systems are the main factors that have been contributing to the corrosion-induced damages, which greatly increase and lifetime maintenance costs of such bridges. In extreme cases, the whole structure might even completely collapse as reported in previous studies (Woodward and Williams 1988; Wouters et al. 1999; Concrete Society Technical Report 2002).

Fibre-reinforced polymer (FRP) tendons are corrosion free and possess a high tensile strength that even exceeds steel tendons. Furthermore, they are lighter than steel, which allow easier handling and reduce dead load of the structure. As such, FRP tendons are likely to be a potential alternative to steel tendons for the precast segmental concrete beams to dealing with the corrosion issues. In the literature, the use of FRP tendons has only been applied to monolithic concrete beams while their application on PSBs has not been reported yet. It is noted that unlike steel tendons, FRP tendons show linear stress-strain relationship up to failure, lower elastic modulus and are weak in shear. These properties can possibly lead to higher deflections of the structure and premature failure of the tendons at the segment joints due to the stress concentration. It is therefore important to investigate the behaviour of PSBs prestressed with FRP tendons before its possible practical applications. This study performs experimental tests to investigate the structural performance and ductility of segmental concrete beams strengthened with FRP for possible use in PSBs.

3.2 Literature reviews

A large number of studies has been performed over the last four decades to investigate

the structural behaviour of precast segmental structures. An extensive literature review on segmental concrete beams prestressed with steel tendons either internal bonded/unbonded or external unbonded can be found elsewhere (Li et al. 2013b; Yuan et al. 2013; Jiang et al. 2016). Key findings can be summarized as follows. Up to date, steel tendons have been the only prestressing solution to connect individual beam segments, forming the final bridge spans. Internal bonded tendons and epoxied joints are normally used in the first PSBs generations. This type of tendon is shown to be the most effective prestressing method for PSBs as it better mobilizes tendon strength at the ultimate, thus increases the beam's strength capacity, better maintains tendon eccentricity and allows the beam to achieve greater ductility under loads. However, it is difficult to monitor and check the bond quality between the tendon and concrete during grouting and during service life, and almost impossible to replace the tendon in the case of corrosion or other types of damage and deterioration.

External unbonded steel tendons are then introduced to the next PSBs generations. The use of external tendons along with dry joints is considered the fastest way to construct the precast segmental beams. Corrosion problems are also greatly improved since external tendons are easier to handle, monitor and replace when necessary. Detailed discussions of advantages and disadvantages of the external unbonded tendons are given in previous studies (MacGregor 1989; Hindi et al. 1995; Aparicio et al. 2002). However, a reduction in the capacity of the externally unbonded prestressed PSBs in both strength and ductility is evident. Breakdown of deviators or anchorage systems can cause catastrophic failure due to the sudden loss of the prestressing force, which is a concern of using the external unbonded system.

PSBs with a mixture of external and internal tendons were recently studied by researchers. This combination takes advantage of both types of tendons, i.e. the internal tendons can improve the ductility of the beam, and the external tendons are convenient for maintenance. Yuan et al. (2013) and Yuan et al. (2014) conducted a series of tests to investigate the behaviour of PSBs with hybrid tendons and epoxied joints. The specimens were designed with different ratios of the external and internal tendons and were then tested under monotonic vertical loading. The test results indicated that the ratio of the hybrid tendons significantly affected the strength capacity and ductility of the segmental beams. The more internal bonded tendons were used, the higher were the load-carrying capacity and better ductility. As such, the ratio of

internal to external tendons not less than 1:1 was recommended. Jiang et al. (2016) investigated the flexural behaviour of PSBs with hybrid tendons and dry joints. The beams had T-shaped cross-section and were post-tensioned with either external tendons or hybrid tendons, which were all unbonded to the concrete. It was found that the use of hybrid tendons enhanced the flexural behaviour of the segmental beams and increased both the ultimate bending capacity and ductility compared to beams with solely external tendons. Furthermore, there was no significant difference between the stress increments of the internal and external tendons as a result of the bond absence between the internal tendons and surrounding concrete.

Joints between segments are the most critical part of PSBs as they ensure the shear transfer and integrity of the whole structure. The joints can be epoxied or dry, flat or keyed, and single or multiple shear keys made of plain concrete or reinforced concrete. Extensive studies on the behaviour of joints under direct shear are available in the literature, which was reviewed elsewhere (Shamass et al. 2014; Jiang et al. 2015). Meanwhile, little research has been carried out on the behaviour of joints under combined shear and bending (Li et al. 2013b). For brevity, only some recent studies on the flexural behaviour of PSBs that focus on the joint performance are reviewed here. Saibabu et al. (2013) conducted an experimental program to evaluate the performance of dry and epoxied joints in precast segmental box girders under monotonic and cyclic loading. It was found that the applied load at the maximum and at the failure of the beams with dry joints were less than those with the epoxied joints because of the high concentration of rotation and deflection at individual dry joints of the beams. Although the dry joints opened at a lower load compared to the epoxied joints, both the beams achieved almost the same deflection at failure. In addition, both joint types underwent significant repeated openings and closures during cyclic loading tests without failure. Li et al. (2013b) studied the behaviour of joints when they were subjected to the combined shear and bending. Both dry and epoxied joints were used in the specimens. The authors concluded that when a precast segmental beam subjected to vertical loads located at the immediate vicinity of the joint, the failure of the beam was different from the traditional bending failures and shear failures, and the failure of epoxied joints was also different from that of dry joints. In the case of the epoxied joints, the failure cracks propagated vertically in the concrete adjacent to the segment interface but did not develop toward the loading point. In contrast, the failure of the

dry joints occurred in the segment interface. Also, join position had a significant effect on the joint strength when the applied loads were in the immediate vicinity of the joints. When the joint was close to the midspan, the joint strength was reduced.

In the literature, the use of FRP tendons has only been applied to monolithic concrete beams. A lot of research work has been done to investigate the flexural behaviour of the monolithic beams prestressed with FRP tendons. Extensive literature review on the matter can be found elsewhere (Heo et al. 2013; Forouzannia et al. 2016). Here, only studies to address the differences in the structural behaviour of a beam prestressed with FRP tendons and the one with steel tendons are briefly reviewed. For an FRP prestressed beam, when the tendon is internally bonded to the concrete, it shows different behaviour to the steel prestressed beam after concrete cracking (Dolan and Swanson 2002; ACI 440.4R 2004; Lou et al. 2015). Both the beams exhibit a linear relationship between the applied load and midspan deflection in the first stage. However, after cracking the steel prestressed beam deforms nonlinearly up to the failure. Whereas, FRP prestressed beam continues to deform in an approximately linear manner with the applied load until failure.

In contrast, in the cases of unbonded tendons, both FRP and steel prestressed beams show similar behaviour under the applied load up to the ultimate stage (Pisani 1998; Tan and Tjandra 2007; Lou et al. 2016). Pisani (1998) conducted a numerical investigation on beams prestressed with FRP tendons. Prestressing types including bonded/unbonded internal, external, and the tendon types including steel and GFRP were studied. It was observed that the structural behaviour of beams prestressed with unbonded FRP tendon was similar to beams with unbonded steel tendons. However, the low creep rupture limitation of the GFRP tendons, normally less than 30%f_u, greatly restricted its high efficiency in prestressing application. Similar behaviours were reported by Lou et al. (2016) on beams internally prestressed with unbonded CFRP and steel tendons. The type of unbonded tendons had limited influence on the cracking mode, deformation capacity, stress increments in the unbonded tendon and in the non-prestressed steel, and had practically no influence on the development of moment redistribution. Tan and Tjandra (2007) tested continuous beams and concluded that the use of external CFRP tendons did not lead to significant differences in terms of the ultimate load, tendon stress, and deflection as compared to beams with steel tendons.

When FRP tendons are deviated, stress concentration in the tendons due to harping effect is an issue that needs due care. This stress concentration phenomenon adversely prevents the increase in the tendon stress because FRP tendon is made of an anisotropic material, it has very low transverse strength as compared to its tensile strength. The deviator curvature, harping angle, and tendon size are observed to be the main factors impacting the stress increments in the tendon regarding the harping effect. Mutsuyoshi and Machida (1993) found that CFRP tendons with 400 mm diameter steel deviators ruptured at 77% and 80% of their breaking load when deviated at angles of 7.1^{o} and 11.3^{o}, respectively. Grace and Abdel-Sayed (1998) reported 19% and 34% reductions in breaking forces for carbon fibre composite cable (CFCC) tendons draped at 3^{o} angle and 5^{o} angles when using 50.8 mm diameter deviators, respectively. When 508 mm diameter deviators were used, those reductions were 12% and 26% at draping angles of 5^{o} and 10^{o}, respectively. Wang et al. (2015) recommended the harping angle should be less than 3^{o} to avoid the strength reduction percentage exceeding 10%. Quayle (2005) reported reductions ranging between 13% and 50% in the tensile strength of the CFRP tendons when the tendons were draped at 2^{o} to 15^{o} using deviators of the radius of 50 mm to 1000 mm, respectively.

Many efforts have been paid to overcome the corrosion problems of the steel tendons that, however, are still a great concern of PSBs. FRP tendons have been widely used for monolithic beams as a promising solution to replace steel tendons owning to its excellent properties such as high corrosion resistance, and high strength-to-weight ratio. The use of FRP tendons on precast segmental structures has not been reported yet. As such, the possible use of FRP tendons for post-tensioning PSBs is investigated in the present study.

3.3 Experimental program

Four large-scale precast segmental concrete T-shaped beams were built and tested in this section to investigate the flexural behaviour of PSBs prestressed with CFRP tendons. Both internal bonded and unbonded CFRP tendons, together with two types of joints, i.e., dry and epoxied multiple shear-keyed joints were used in the beams. It is noted that all the beams in this chapter had the same dimensions and conventional reinforcements as those given in Section 2.2 of Chapter 2. Similar materials, post-tensioning and testing procedure were used. As such, these parts are not presented here but referred to when appropriate for the sake of brevity.

Table 3-1 gives the detailed configuration of the specimens, in which Beams C1 and C2 contained bonded tendons but different joint types, and Beams C3 and C4 had unbonded tendons and different joint types. Details of beams' dimensions, material properties can be found in Figure 2-1 and 2-2 and Table 2-2 in Section 2.2 of the previous chapter.

Table 3-1: Configuration of specimens.

Beam	Bonding type	Joint type	f'_c (MPa)	f_{pe} (MPa)	f_{pe}/f_{pu}	P_{pe} (kN)
C1	Bonded	Dry	44	917	0.37	116
C2	Bonded	Epoxied	44	942	0.38	119
C3	Unbonded	Dry	44	818	0.33	104
C4	Unbonded	Epoxied	44	661	0.27	84

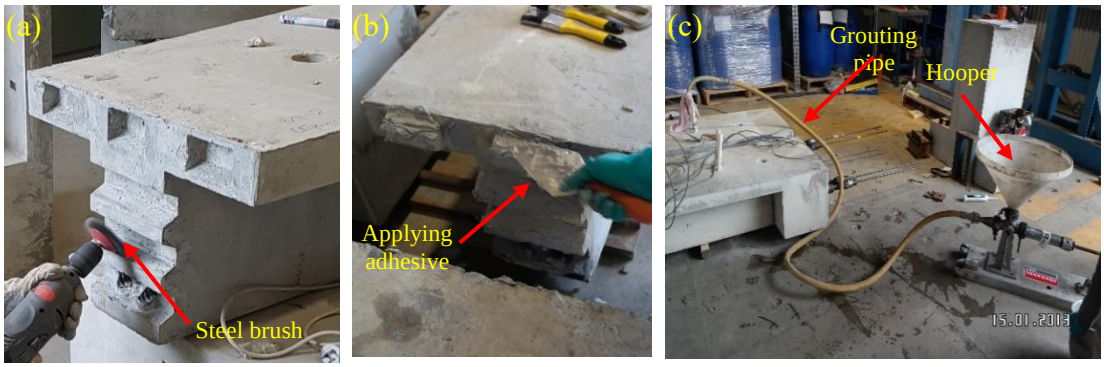

Figure 3-1: Epoxy and grouting

The specimens' fabrication and post-tensioning are presented in Section 2.2 of the previous chapter. For the beams with epoxied joints, the key surfaces were thoroughly cleaned using a steel brush and an air gun to make sure the surfaces in a good condition and free from dust (Figure 3-1a). The concrete surfaces were then thoroughly watered and left to dry for at least 2 hours before applying the adhesive. A thin layer of Sikadur-30 (Sika Australia) was applied to the joint surfaces of the segments using a painting brush and a trowel. After post-tensioning, the epoxied beam was left for curing of the adhesive for 3 days (Figure 3-1b).

For the beams with bonded tendons, grouting was done after the completion of post-tensioning. The metal duct was carefully cleaned using a high-pressure air gun to ensure the ducts free of dirt and debris before placing and stressing the tendons. SikaGrout-300PT was used in the specimens, which was mixed by a grout mixer (Sika Australia). The grout was then injected into the ducts via the PVC pipes at one end

using a manual grout pump until it came out from the other end. The beams were left for 7 days for curing of the grout (Figure 3-1c). All the beams were cyclically tested under four-point loading test up to failure. Further details on testing set up and measurements were presented in Section 2.2 of Chapter 2.

3.4 Experimental results and discussions

3.4.1 Summary of tested results

The test results for all the specimens are given in Table 3-2, in which P_{cr}, $\delta_{mid,cr}$, $\Delta_{J,cr}$ and P_u, $\delta_{mid,u}$ and $\Delta_{J,u}$ are the applied load, midspan deflection, and opening of the middle joint of the specimens at cracking and at the ultimate stage, respectively. It is noted that the applied load, corresponding midspan deflection and joint opening of Beams C1 and C3 at the cracking are taken as yielding values as defined by Park (1989) and is illustrated in Figure 2-11 in Chapter 2.

Photos of the specimens' failures are presented in Figure 3-2(a-d), which clearly show different failure modes of the tested beams. Beams C1 and C2 with bonded tendons failed by rupture of CFRP tendons without any concrete spalling on the top while Beams C3 and C4 failed by concrete spalling on the compressive side and CFRP tendons rupturing at the bottom. The concrete crushing or the rupture of tendons occurred at the middle joint at the midspan for all the specimens.

The load-deflection curves of the specimens and their corresponding envelops are plotted in Figure 3-3 and Figure 3-4. It is observed that the beams with bonded tendons showed much higher strengths but lower ductility compared to the beams with unbonded tendons. The ultimate strengths of Beams C1 and C2 were an average of 167 kN which was 41.5% higher than those of Beams C3 and C4 at an average of 118 kN. In contrast, Beams C1 and C2 only experienced 47.2 mm deflection on average at the ultimate stage which was about half of the maximum deflection observed in Beams C3 and C4, which was 97.9 mm on average. It is worth noting that even though the ultimate deflection of Beams C1 and C2 was much smaller than that of Beams C3 and C4, these values well satisfied the maximum allowable midspan deflection specified by AASHTO LRFD (2012). AASHTO LRFD (2012) limits the maximum deflection to 1/800 of the beam's span length while Beams C1/C3 and C2/C4 in this study underwent deflections of approximately 1/75 and 1/37 of the beam's span lengths at the ultimate stage, respectively.

Table 3-2: Testing results.

Beam	Cracking			Ultimate		
	P_{cr}	$\delta_{mid,cr}$	$\Delta_{J,cr}$	P_u	$\delta_{mid,u}$	$\Delta_{J,u}$
C1	54.5	6.9	0.26	164	47.8	4.73
C2	56.4	2.9	0.04	169	46.6	3.51
C3	53.4	8.4	0.55	113	94.7	27.70
C4	54.1	2.3	0.07	123	101.1	30.02

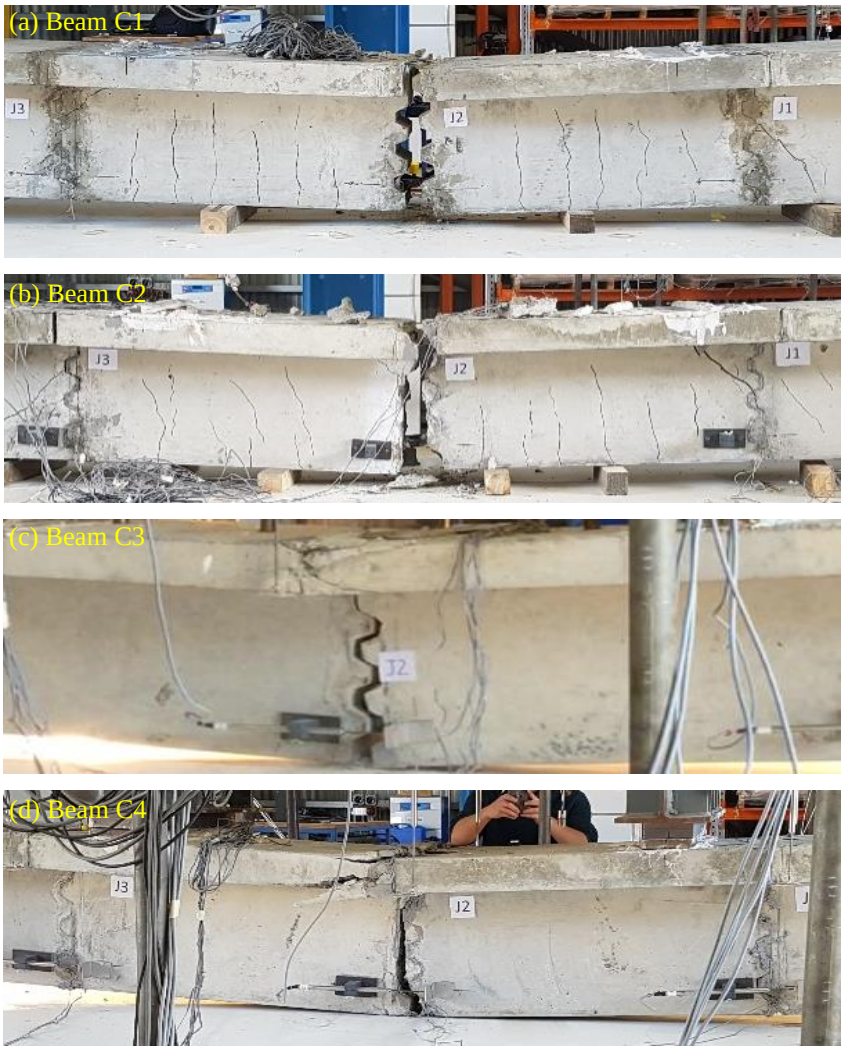

Figure 3-2: Failure modes of the tested beams

In addition, the experimental results from the previous studies (Le et al. 2018; Pham et al. 2018) on both segmental beams with unbonded steel tendons and CFRP tendons showed that the beams with unbonded CFRP tendons even achieved larger deflections at the ultimate stage compared to the beam with unbonded steel tendons. The ultimate deflection of the beam with unbonded steel tendons was equal to approximately 1/40

(89.4 mm) of the beam's span length. Further analyses and discussions regarding the flexural behaviour of PSBs with unbonded steel and CFRP tendons can be found in the previous studies (Le et al. 2018; Pham et al. 2018). CFRP tendons could, therefore, well replace the steel tendons for the use in the precast segmental concrete beams to overcome the possible corrosion-induced damage frequently observed in this type of structures.

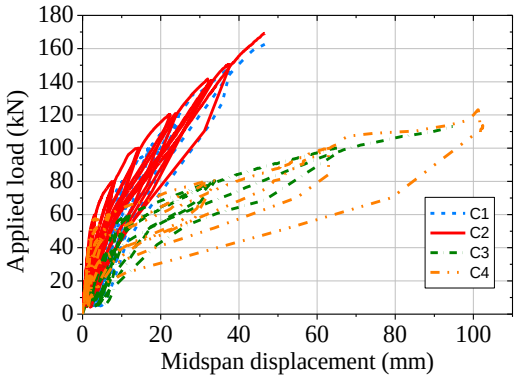

Figure 3-3: Load vs deflection curves

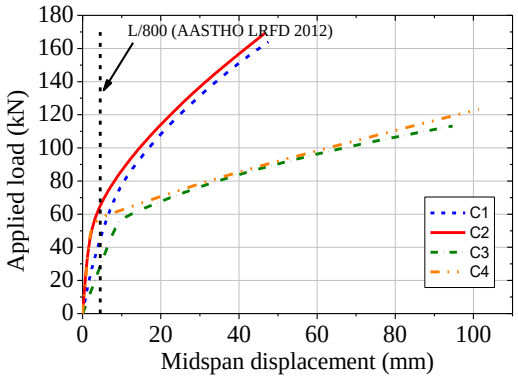

Figure 3-4: Envelop curves of load vs deflection

Two stages can be identified for the load-deflection curve of each specimen with one inflection point representing the cracking of concrete at the bottom fibre for the beams C2 and C4 with epoxied joints or the opening of the middle joint for the beams C1 and C3 with dry joints, which are similar to the behaviour observed on segmental beams with external steel tendons reported in the previous studies (Li et al. 2013b; Saibabu et al. 2013). This observation is different from the cases of monolithic beams with unbonded tendons, where the load-deflection curves exhibited almost three distinct stages due to the presence of reinforcing steel, which exhibits a further inflection point when the reinforcing steel yields (Tao and Du 1985; Wang et al. 2015).

3.4.2 Effect of bonding condition on structural behaviour

Bonding condition between the tendon and concrete strongly affected the flexural behaviour of the beams. The use of bonded tendons significantly increased the strength of the precast segmental beams as observed in Beams C1 and C2 while the use of unbonded tendons greatly improved the ductility of Beams C3 and C4. This can be explained by a well-known fact that the change in the tendon strain of a bonded tendon is sectional dependent while that in an unbonded tendon is member dependent (Mattock et al. 1971; Naaman and Alkhairi 1991). As a result, at the same level of

concrete strain in the compressive top fibre of the section, the beam with bonded tendons more effectively mobilizes the strain in the tendon, and hence the tendon strength as observed later in Figure 3-10, leading to the higher load carrying capacity. Meanwhile, the strain change in the unbonded tendons is relatively uniformly distributed to the whole length of the tendons, rather than concentrated at a single section, which allows the beam to achieve larger deflection. As such, the selection of bonded or unbonded tendons depends on the actual design requirement.

Bonding condition of the tendons also affected the stiffness of the beams. By comparing the load-deflection curves of Beams C1 and C3 (Figure 3-4), it can be observed that Beam C1 exhibited higher stiffness than Beam C3 and the difference in the beams' stiffness became considerable when the applied load reached about 54 kN as the middle joint started to open highly. In the meantime, Beam C3 substantially lost its stiffness while Beam C1 still showed high stiffness. This is because the use of the bonded tendons in Beam C1 helped restrain the detachment of the two adjacent segments preventing the reduction in the beam's section height.

In contrast, the bonding type had no effect on the initial stiffness of the epoxied joints beams. This is reasonable since both the beams with epoxied joints behaved like monolithic beams before cracking, thus no changes in the section geometry leading to the same initial stiffness as observed in Figure 3-4. After cracking, Beam C2 still showed high stiffness while Beam C4 substantially lost its stiffness, which again clearly demonstrates the effectiveness of the bonded tendons regarding the strength enhancement of the beams.

The failure modes of the beams were also affected by the bonding condition of the tendons. All the beams in this study were under-reinforced, consequently, the failure mode would theoretically be controlled by tension since $c/d < 0.42$ by AASHTO LRFD (2012) as observed in Beams C1 and C2. However, the use of unbonded tendons shifted the failure mode of Beams C3 and C4 from tension controlled to compression controlled as they showed severe concrete crushing on the top fibre before the rupture of the tendons at the ultimate stage. This phenomenon is attributed to the member dependence of the unbonded tendons as discussed above. The failure in Beams C3 and C4 occurred gradually and less explosive than that in the Beams C1 and C2 with bonded tendons. Effects of the tendon bonding condition on the beam's crack pattern,

joint opening, and the strains in the tendon and steel reinforcements will be discussed in subsequent sections.

3.4.3 Effect of joint types on structural behaviour

By comparing the load-deflection curves of Beams C1 versus C2 and Beams C3 versus C4, it can be observed that regardless of the tendon bonding condition, the type of joints had only a slight effect on the load-carrying capacity and ductility of the beams, but significantly affect the beams' initial stiffness. Both Beams C1 and C2 had similar strength and deflection at the ultimate stage as mentioned previously, and that was also true for the cases of Beams C3 and C4, although both Beams C2 and C4 with epoxied joints showed a bit higher ultimate strength than those of their counterparts with dry joints, Beams C1 and C3, by 3.1% and 8.8%, respectively.

Both Beams C2 and C4 had an initial stiffness of approximately 22.5 kN/mm, which were about 2.8 and 3.5 times those of the counterparts with dry joints C1 and C3, respectively. This means that at the same load levels in the elastic region, a beam with dry joints and bonded tendons will experience deformations 2.8 times that of the equivalent beam with epoxied joints and that deformation is even higher at 3.5 times when the unbonded tendons were used, which once again demonstrates the effect of bonding condition of the tendons on the structural behaviour of the beams. This observation needs to be taken into account in the design of a bridge structure since main components of the structure are designed to be working in the elastic limit, especially in the service limit stage when the elastic deformations of the structure are checked.

3.4.4 Crack patterns

Cracking patterns of the tested beams are greatly affected by the bonding condition of the tendons. When bonded tendons were used, the beams could develop both flexural and shear cracks regardless of the joint type used as clearly observed in Figure 3-2 (a,b). Both Beams C1 and C2 exhibited similar crack patterns regarding the crack width, crack length and uniformly distributed along the beams' axis, which was similar to the crack pattern of a traditional monolithic prestressed concrete (PC) beam. The crack propagation of Beam C2 was noted as follows. When the applied load was about 54 kN, one vertical crack appeared at the middle joint at the midspan with cracking sounds that vertically cut off all the shear-keyed bases of the joint as seen in Figure

3-2b. The crack was at a certain height of the section at the beginning and then gradually developed vertically to the top under the increase in the applied load. Soon after, vertical cracks were also formed at Joints J1 and J3 (refers to Figure 3-2 for joints' locations) that also cut off all the shear-keyed bases of the joints. When the applied load reached about 85 kN to 90 kN, flexural and shear cracks were observed at bottom of the beam. These cracks were symmetrically developed on each side of the beam until the beam failed by the rupture of the tendons, which occurred at the middle joint at the midspan. The crack propagation of Beam C1 was very similar to that of Beam C2. The only difference was that the vertical cracks at the joints J1 to J3 already existed since dry joints were used. It is worth noting that, although the crack pattern of Beams C1 and C2 was very similar to that of a PC beam, the crack propagation was different. In the segmental beams, flexural cracks occurred at joint locations first and then the flexural cracks within the segments appeared due to the contribution of reinforcing steel of the segments, which did not exist at joint locations. Meanwhile, in a PC beam, the flexural cracks normally develop at the midspan and then spreads gradually to the ends under the increases of the applied load. The crack propagation of a segmental beam, however, should be analysed together with the effects of the number of segment and the segment length in practical situations.

Conversely, due to the lack of restriction of the unbonded tendons, no cracks were observed in the cases of Beams C3 and C4. Although Beam C4 developed a vertical crack at the middle joint J2, the crack was, in fact, the opening of the epoxied joint when the applied load exceeded the cracking load. Therefore, the contribution of the normal reinforcing steel to the flexural capacity of the segmental beams should be considered depending on the bonding condition of the prestressing tendons.

3.4.5 Joint openings

The openings of all the joints along the beams' axis at the ultimate stage are plotted in Figure 3-5. It is observed that the opening of the joints was greatly affected by the bonding conditions of the tendons regardless of the joint type. All the joints of the beams with bonded tendons opened at the ultimate load and the opening of the joints proportionally distributed along the beams' axis. In contrast, in the cases of the beams with unbonded tendons, only the middle joint opened while the others almost remained closed. In the cases the tendons were bonded to the concrete within the segments, the separation of the two adjacent segments, thus the opening of the joints was equal to

the extension of the tendon between the joints. As such, the joint opening distribution in Beams C1 and C2 would be comparable to the tendon strain distribution along the beams' axis, as observed in Figure 3-5. The lack of bonding between the concrete and the tendons in Beams C3 and C4 caused large opening of the middle joint under the applied load. The opening of the middle joint might be the factor to restrain the other joints. This observation supports the assumption that the beam with unbonded tendons develops one major crack at the midspan at the ultimate stage, which is used to calculate the plastic hinge length, thus the stress in the unbonded tendons in several models (Lee et al. 1999; Roberts-Wollmann et al. 2005; Harajli 2006).

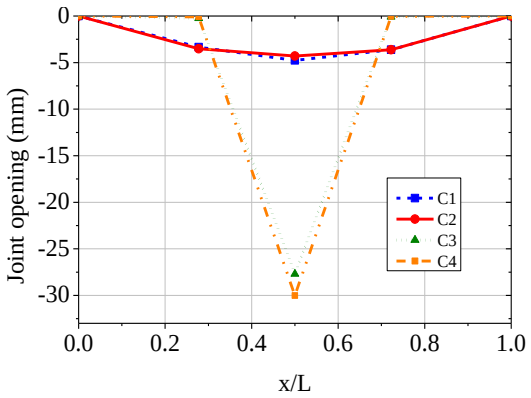

Figure 3-5: Joint openings along the beam's axis

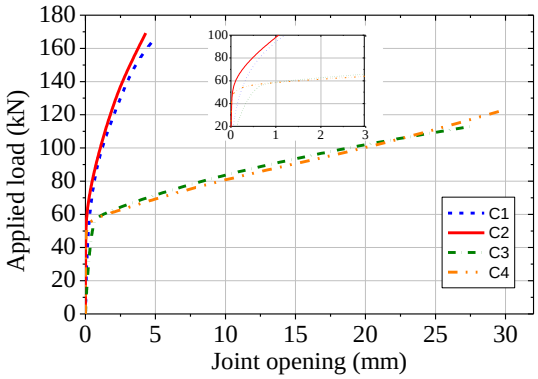

Figure 3-6: Load vs opening of the middle joint

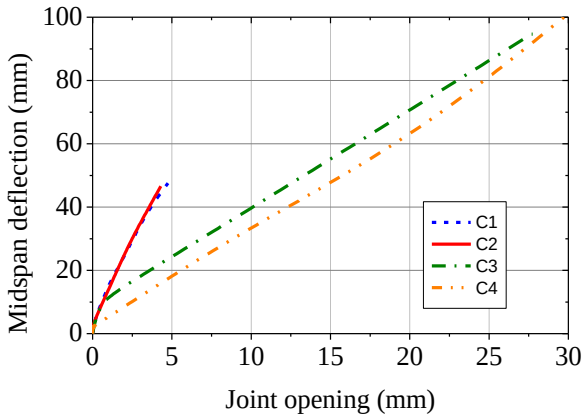

Figure 3-7: Joint opening vs midspan deflection

The opening of the middle joint with respect to the applied load for the specimens are given in Figure 3-6. It is observed that the middle joint in Beams C1 and C3 started to open soon after the load was applied since dry joints were used in these beams. The gradual opening of the joint leads to the smoother change in the beam's stiffness compared to the corresponding beams with epoxied joints as observed in Figure 3-4. Meanwhile, the middle joints in Beams C2 and C4 still remained closed until cracking

load was reached. At the ultimate load, the middle joint of Beams C1 and C2 exhibited almost equal openings at 4.73 mm and 4.30 mm, which were much smaller than those of Beams C3 and C4 at 27.7 mm and 30.02 mm, respectively, which again demonstrates the effect of bonding the tendon in construction.

The opening of the middle joint with respect to the midspan deflection is also plotted in Figure 3-7. It can be seen clearly that the opening of the joint showed an approximately linear relation with the midspan deflection of the beam under the applied loads. In the cases of the epoxied joints beams, it can be stated that the width of the vertical crack developed linearly with the midspan deflection of the beam under the loads. However, it is worth noting that this linear relationship is only valid when the applied load went beyond the cracking load. Before that load value, the epoxied joints still remained closed.

3.4.6 Load-strain relationships

Figure 3-8 shows the load-strain relationships of the conventional longitudinal steel rebars and CFRP tendons in Beams C3 and C4. It is observed that after the opening of the joint, the strain in the CFRP tendons in the two beams started to increase significantly that were approximately linear to the applied load, while the strain in the steel rebars almost maintained constant at a very small value of around 100 μm/mm. This result indicates that the tension force was mainly contributed by the CFRP tendons and almost no any contribution of the steel rebars because they are discontinuous at the joints. The strain in the steel rebars also explained why no flexural crack was observed at the bottom of the segments in Beams C3 and C4 as discussed above. The ultimate strain of the CFRP tendons in Beams C3 and C4 were 1.22% and 1.16%, which were only equal to 72% and 69% of the nominal tensile strain of the tendon.

In contrast, the steel rebars in the beams with the bonded tendons yielded as shown in Figure 3-9, leading to the flexural cracks observed at the segment bottom of Beams C1 and C2 as shown in Figure 3-2(a,b). CFRP tendons showed a greater strain increments compared to the steel rebars since only CFRP tendons contributed to the tension force at the joint locations and the strain measurement of the steel rebars was taken at the middle of the segment, which was not at the middle joint at the midspan as in the case of CFRP tendons. Similar to the cases of Beams C3 and C4, Beams C1 and C2 also

exhibited an approximately linear relationship between the tendon strain, thus the tendon stress and the applied load after the opening of the joints. The tendon strains at the ultimate stage reached about 93% of the nominal tensile strain on average in the cases of Beams C1 and C2 with bonded tendons.

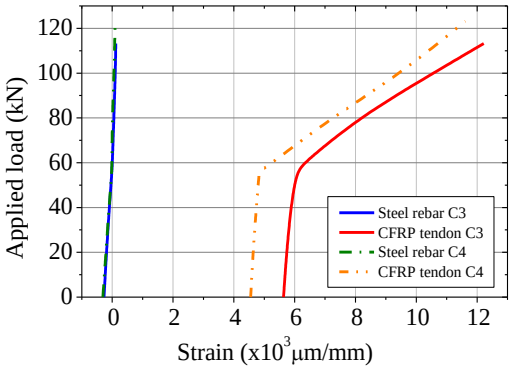

Figure 3-8: Load vs strain of Beams C3 and C4

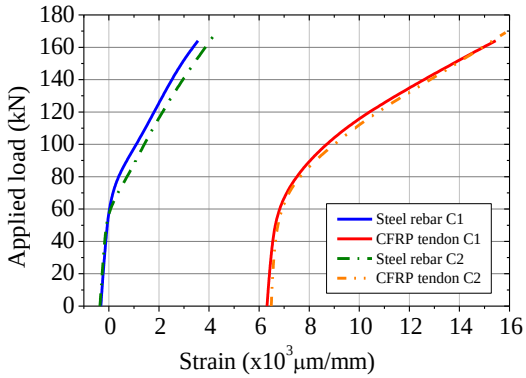

Figure 3-9: Load vs strain of Beams C1 and C2

3.4.7 Stress increment in the CFRP tendons

Figure 3-10 shows the tendon stress increment with respect to the applied load for the specimens. It is observed from the figure that the tendon stress in all the beams started to increase from the beginning of the test. However, the increment rate in the tendon stress just prior to the cracking of concrete or opening of the joint (before the inflection point) was very small showing approximately 6% to 8%. The tendon stress increment was due to the beam's deflection under the applied load. All the beams exhibited an approximate bilinear relationship between the applied load and tendon stress increment.

By comparing the stress increment curves of Beams C1 versus C2 and Beams C3 versus C4, it is observed that the curves of the two beams with bonded tendons or the two with unbonded tendons exhibited almost similar trends (Figure 3-10). This indicated that the type of joints had only a slight effect on the increase in the tendon stress. The stress increment in the beams with bonded tendons was approximately 54% of the nominal tensile strength of the CFRP tendons, f_{pu}, while that was of 40% f_{pu} in the cases of the beams with unbonded tendons.

The relationships between the stress increment and the midspan deflection for the beams are also plotted in Figure 3-11. It is observed that the change in the tendon stress exhibited an approximately linear manner with the midspan deflection for all the

beams regardless of the tendon bonding condition and the joint type. This observation is similar to the previous studies conducted on monolithic beams prestressed with unbonded tendons (Tao and Du 1985; Lou and Xiang 2007; Wang et al. 2015). As such, it supports the calculation of the stress increment in the CFRP prestressed PSB beams based on the midspan deflection as in the cases of monolithic beams (Harajili and Kanj 1992; He and Liu 2010). Since the opening of the joints represents the elongation of the tendon as a whole, approximately linear relationships were also observed between the stress increment and the joint opening in all the specimens as shown in Figure 3-12.

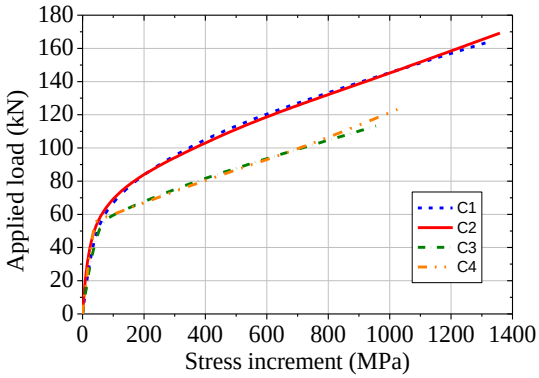

Figure 3-10: Stress increment in the tendons

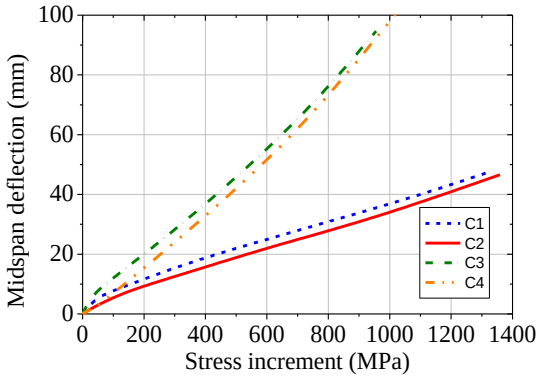

Figure 3-11: Stress increment vs midspan deflection

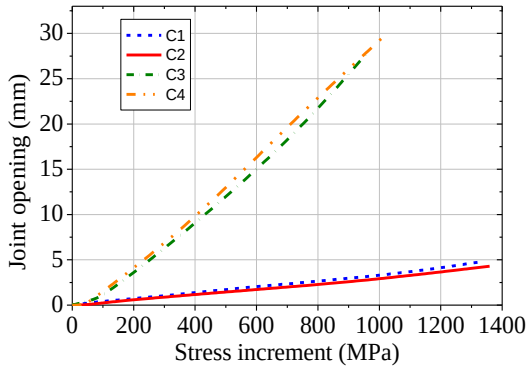

Figure 3-12: Stress increment vs joint opening

3.5 Theoretical considerations

3.5.1 Beams' strength

The strength capacity of the beams were calculated in accordance with the design procedure recommend by AASHTO (1999) and ACI 440.4R (2004). However, it is noted that none of these equations addresses precast segmental beams with CFRP tendons. The design equations presented in AASHTO (1999) are used for segmental

beams prestressed with steel tendons while those in ACI 440.4R (2004) are for monolithic beams with FRP tendons. AASHTO (1999) adopted the following expressions to compute the stress in the tendons. For bonded tendons AASHTO LRFD (2012):

$$f_{ps} = f_{pu}\left(1 - k\frac{c}{d_{ps}}\right) \tag{3.1}$$

in which $k = 2\left(1.04 - f_{py} / f_{pu}\right)$; f_{pu} is the nominal tensile strength of the tendon; f_{py} is the yield strength which is taken as f_{pu} since CFRP is a linear elastic material; c is the neutral axis depth at the ultimate stage, d_{ps} is the distance from the extreme compression fibre to the centroid of the tendons. For unbonded tendons:

$$f_{ps} = f_{pe} + 6200\left(\frac{d_{ps} - c}{l_e}\right), MPa \tag{3.2}$$

where f_{pe} is the effective tensile stress of the tendons, $l_e = l_i/(1+[N/2])$, in which l_i is the length of the tendon between anchorages, and N is the number of support hinges required to form a mechanism crossed by the tendon.

ACI 440.4R (2004) recommended Eq. 3.3 to predict the stress in the unbonded FRP tendons at the ultimate. The nominal tensile strength f_{pu} is used in the case of beams with bonded tendons.

$$f_{ps} = f_{pe} + \Omega_u E_{ps} \varepsilon_{cu}\left(\frac{d_{ps}}{c_u} - 1\right) \tag{3.3}$$

where E_{ps} is the tendon modulus of elasticity; ε_{cu} is the ultimate concrete compression strain which was taken as 0.003; and Ω_u is a strain reduction coefficient which is defined as $\Omega_u = 1.5/(L/d_{ps})$ for one-point midspan loading and $\Omega_u = 3/(L/d_{ps})$ for uniform or third-point loading, where L is the span length.

Strain compatibility analysis was then used for computating the flexural resistance of the specimens. The computed results are given in Table 3-3 and Table 3-4. It is seen from the tables that both the codes predicted well the stress and corresponding flexural capacity of the beams, although the experimental stress values were a bit smaller than those of theoretical calculations. Both the codes showed only 1% to 5% differences in the prediction of the load bearing capacity of the bonded tendons beams.

In the cases of beams with unbonded tendons, the accuracy of the code equations significantly reduced. AASHTO (1999) underestimated the stress in the unbonded tendons, in which the predicted stress values were of only 76% and 71% of the experimental results for the tendons in Beams C3 and C4, respectively. As a result, the load bearing capacities of the two beams predicted by this code were also lesser than the experimental results, which were of approximately 82% and 67%, respectively. In contrast, ACI 440.4R (2004) highly overestimated the stress in the tendons, thus the load carrying capacity of the two beams at the ultimate stage. The tendon stresses predicted by this code was approximately 20% higher than the experimental values. The reason for this substantial difference may lie on the length-to-beam's depth ratio *L/h*. ACI 440.4R (2004) limits the application of Eq. 3.3 for beams prestressed with CFRP tendons having the unbonded length greater than 15 times the depth of the beam. In this study, the unbonded length tendon-to-the beam's depth was equal to 9 as presented in the previous chapter.

Table 3-3: Theoretical calculations of tendon stress, f_{ps}.

Beam	f_{expt}. (MPa)	f_{ps} (MPa)		f_{ps}/f_{expt}		f_{expt}/f_{pu}
		AASTHO 1999	ACI 440.4R	AASTHO 1999	ACI 440.4R	
C1	2243	2428	2450	1.08	1.09	0.91
C2	2301	2428	2450	1.05	1.06	0.94
C3	1774	1357	2094	0.76	1.18	0.72
C4	1687	1204	2006	0.71	1.19	0.69

Table 3-4: Theoretical calculations of applied load, P_u.

Beam	P_{expt}. (kN)	P_{theo} (kN)		P_{theo}/P_{expt}	
		AASTHO 1999	ACI 440.4R	AASTHO 1999	ACI 440.4R
C1	164	162	164	0.99	1.00
C2	169	162	164	0.96	0.97
C3	113	93	141	0.82	1.25
C4	123	83	136	0.67	1.10

3.5.2 Deflection calculation for beams with bonded tendons

The short-term deflection of the tested beams with bonded tendons was calculated using two methods, bilinear approach and effective moment of inertia, which were recommended by PCI (2004), AASHTO LRFD (2012) and ACI 440.4R (2004). In the bilinear approach, the total deflection of the beam, Δ, is the sum of deflections Δ_1 due

to the load leading to cracking based on the gross moment of inertia of the concrete section, I_g, and Δ_2 due to the increment of load from cracking to the ultimate using the moment of inertia of a cracked section, I_{cr}. PCI (2004) suggested the following expression to calculate I_{cr}:

$$I_{cr} = nA_{ps}d_{ps}^2\left(1-1.6\sqrt{n\rho_{ps}}\right) \tag{3.4}$$

where n is the modulus ratio between the prestressing tendon and concrete, A_{ps} is the area of the prestressing tendon, and ρ_{ps} is the reinforcement ratio.

In the second method, an effective moment of inertia, I_e, is firstly determined and the deflection is then calculated for the total load by substituting I_e for I_g. The effective moment of inertia is recommended by AASHTO LRFD (2012) as follows:

$$I_e = \left(\frac{M_{cr}}{M_a}\right)^3 I_g + \left(1-\left(\frac{M_{cr}}{M_a}\right)^3\right) I_{cr} \le I_g \tag{3.5}$$

in which M_{cr} is the cracking moment and M_a is the is the maximum moment in the member at which the deflection is being computed; I_g is the moment of inertia of the gross concrete section about the centroid axis. ACI 440.4R (2004) adopted the following equation to calculate I_e, which accounts for the reduced tension stiffening in FRP-reinforced members:

$$I_e = \left(\frac{M_{cr}}{M_a}\right)^3 \beta_d I_g + \left(1-\left(\frac{M_{cr}}{M_a}\right)^3\right) I_{cr} \le I_g \tag{3.6}$$

in which β_d is the softening factor given by:

$$\beta_d = 0.5\left[\frac{E_p}{E_s}+1\right] \tag{3.7}$$

and

$$I_{cr} = \frac{b(kd)^3}{3} + nA_{ps}\left(d-kd\right)^2 \tag{3.8}$$

where E_p is the modulus of elasticity of FRP tendon, E_s is the modulus of elasticity

of steel, *b* is the width of the section, *d* is the distance from the extreme compression fibre to the centroid of prestressing steel, and *k* is ratio of the neutral axis depth to the FRP tendon depth.

3.5.3 Deflection calculation of beams with unbonded tendons: proposed changes

The deflection calculation of a beam with unbonded tendons is more complex than for bonded tendons, since the strain compatibility at critical sections is not maintained. Therefore, the strain reduction factor, Ω, developed by Naaman and Alkhairi (1991) is employed in this study to convert the strain behaviour of a unbonded tendon into an equivalent behaviour of a bonded tendon, then bilinear approach suggested by PCI (2004) as mentioned previously is used to calculate the total deflection of the beams. The closed-form equation for computation of deflections can be expressed as follows Branson (1977):

$$\Delta = KM\,L^2 / E_c I \tag{3.9}$$

then,

$$\Delta = \Delta_1 + \Delta_2 \tag{3.10}$$

where,

$$\Delta_1 = KM_1 L^2 / E_c I_1 \tag{3.11}$$

$$\Delta_2 = KM_2 L^2 / E_c I_2 \tag{3.12}$$

in which, *K* is a deflection coefficient that depends on the loading type and support conditions, for the two third-point loading test and two harped-point tendon profile for the beams in this study, $K = 23/216$ (2004); *M*, *M1* and *M2* are the applied moments; *L* is the span length; E_c is the concrete modulus of elasticity; and I_1 and I_2 are the moment of inertia of the section corresponding to loading stages.

In the first stage of loading, when the beam is still in the elastic uncracked state, I_1 is taken as I_g, which is the moment of inertia of the gross concrete section about the centroid axis. After cracking, I_2 is taken as I_{cr}, which is calculated herein based on the cracked section analysis (Figure 3-13).

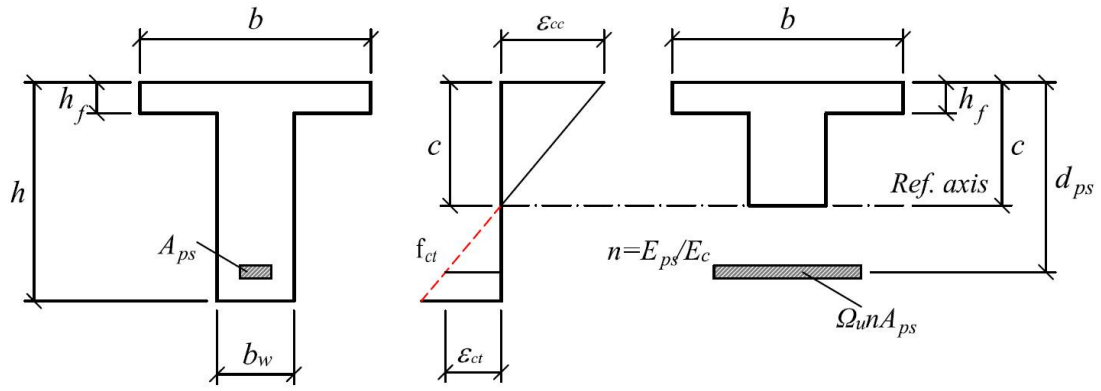

Figure 3-13: Transformed concrete section

From the cracked section analysis of a reinforced concrete beam, one important relation between the steel stress, f_s and the concrete stress at the location of steel, f_{ct} is found as $f_s / f_{ct} = n$, where n is the modulus ratio. Applying this observation to the prestressed concrete, neglecting the depression strain of concrete due to prestressing since it is very small (ACI 440.4R 2004), the following relations are obtained:

For a bonded tendon:

$$n = \frac{E_{ps}}{E_c} = \frac{E_{ps}\varepsilon_{ct}}{E_c\varepsilon_{ct}} = \frac{E_{ps}\Delta\varepsilon_{ps}^{bonded}}{E_c\varepsilon_{ct}} = \frac{\Delta f_{ps}^{bonded}}{f_{ct}} \tag{3.13}$$

For an unbonded tendon, n_{unb} is defined as follows:

$$n_{unb} = \frac{\Delta f_{ps}^{unbonded}}{f_{ct}} = \frac{\Omega_u \Delta f_{ps}^{bonded}}{f_{ct}} = \Omega_u n = \Omega_u \frac{E_{ps}}{E_c} \tag{3.14}$$

Then, to find the moment of inertia of the cracked section, it is assumed that the amount of prestressing tendons is replaced by an equivalent amount of concrete, which is proposed to be equal to $\Omega_u n A_{ps}$. Taking the first moment of inertia of the cracked section area with respect to the reference axis, the neutral axis c can be determined from the following quadratic equation for T-sections:

$$\frac{1}{2}b_w c^2 + \left[(b-b_w)h_f + \Omega_u n A_{ps}\right]c - \left[\frac{1}{2}(b-b_w)h_f^2 + \Omega_u n A_{ps} d_{ps}\right] = 0 \tag{3.15}$$

$$c = \frac{\sqrt{D} - (b - b_w)h_f - \Omega_u n A_{ps}}{b_w} \tag{3.16}$$

where

$$D = (b - b_w)h_f \left[bh_f + 2\Omega_u n A_{ps} \right] + 2\Omega_u n A_{ps} b_w d_{ps} + {\Omega_u}^2 n^2 A_{ps}^2 \tag{3.17}$$

and

$$I_{cr} = \frac{1}{12}(b - b_w)h_f^3 + (b - b_w)h_f \left(c - h_f \right)^2 + \frac{1}{3} b_w c^3 + \Omega_u n A_{ps} \left(d_{ps} - c \right)^2 \tag{3.18}$$

For rectangular sections, substitute $b = b_w$, and $\rho_{ps} = \frac{A_{ps}}{b d_{ps}}$ leading to:

$$D = {\Omega_u}^2 n^2 \rho_{ps}^2 + 2\Omega_u n \rho_{ps} \tag{3.19}$$

$$c = \left(\sqrt{D} - \Omega_u n \rho_{ps} \right) d_{ps} = k_1 d_{ps} \tag{3.20}$$

$$I_{cr} = \frac{1}{3} b \left(k_1 d_{ps} \right)^3 + \Omega_u n A_{ps} \left(1 - k_1 \right)^2 d_{ps}^2 \tag{3.21}$$

where $k_1 = \sqrt{D} - \Omega_u n \rho_{ps}$.

3.5.4 Verification of the proposed method

The calculated deflection of the beams are given in

Table 3-5. The theoretical calculations are also plotted against the experimental results, which are shown from Figure 3-14 to Figure 3-17. As seen from these tables and figures, all the code equations returned very good outcomes for predicting the ultimate deflection of the beams with bonded tendons, in which the bilinear approach suggested by PCI (2004) yielded the closest predictions. The maximum deflections calculated by PCI (2004) for Beams C1 and C2 were 48.6 mm and 48.4 mm, which were almost equal to the experimental results of the two beams of 47.8 mm and 46.6 mm, respectively. ACI 440.4R (2004) overestimated the deflections by approximately 13.4% on average compared to the experimental results while AASHTO LRFD (2012) underestimated the deflection by approximately 12.3%. AASHTO LRFD (2012) used factors to account for the variability in the flexural cracking strength of concrete and bonding types of prestressing tendons for computing the cracking moment. This might

be the reason for the smaller deflections given by AASHTO LRFD (2012).

In contrast, all the code equations did not predict well the deflections of Beams C3 and C4 when unbonded tendons were used. Modifications were made as presented in Section 3.5.3 and the predicted deflections showed very good agreements with the experimental results as shown in Figure 3-16. It, however, overestimated the ultimate deflection of Beam C4 by approximately 15% compared to the experimental results (Figure 3-17).

Table 3-5: Deformation calculations

Beam	$I_g \times 10^6$ (mm^4)	Bilinear method			Effective method				Δ_{expt} (mm)
		PCI 2004			AASTHO LRFD		ACI 440.4R		
		$I_1 \times 10^6$ (mm^4)	$I_2 \times 10^6$ (mm^4)	Δ_1 (Proposed) (mm)	$I_{e1} \times 10^6$ (mm^4)	Δ_2 (mm)	$I_{e2} \times 10^6$ (mm^4)	Δ_3 (mm)	
C1	1669	625	105	48.6 (51.8)	199	40.5	166	52.5	47.8
C2	1669	1669	105	48.4 (N/A)	196	42.4	164	54.6	46.6
C3	1669	366	31	25.8 (89.9)	–	–	–	–	94.7
C4	1669	1669	31	35.4 (109.6)	–	–	–	–	101.1

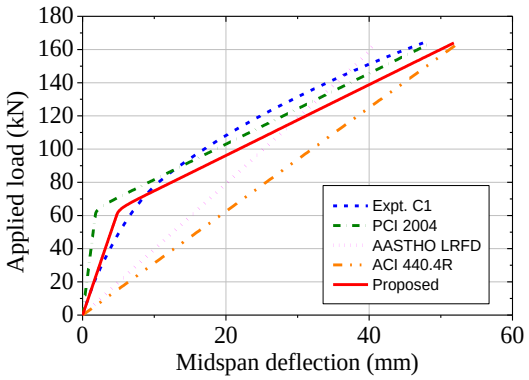

Figure 3-14: Comparison of load vs deflection curves of Beam C1

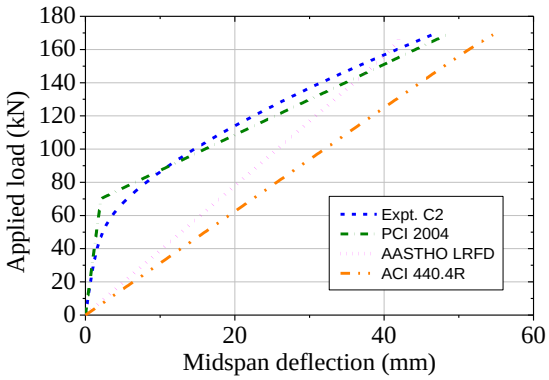

Figure 3-15: Comparison of load vs deflection curves of Beam C2

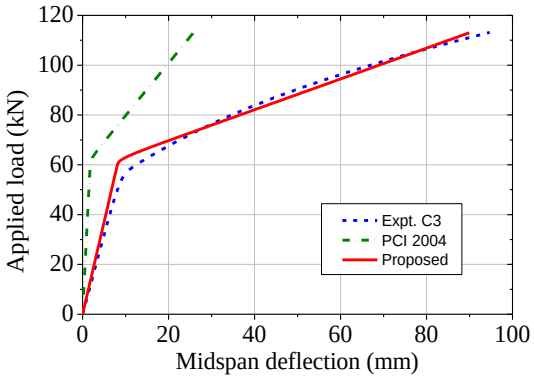

Figure 3-16: Comparison of load vs deflection curves of Beam C3

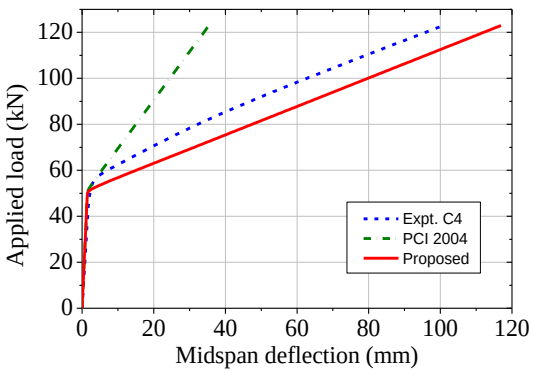

Figure 3-17: Comparison of load vs deflection curves of Beam C4

It is worth noting that substituting n by $\Omega_u n$ in Eqs. 3.4 and 3.8 will return approximately similar results as that by Eq. 3.21 for the computation of I_{cr}. As such, bilinear approach is recommended for calculating the deflection of the PSBs prestressed with CFRP tendons. In the first elastic stage, moment of inertia of the section, I_1, is taken as I_g. In the second stage, I_2 is used which is taken as the moment of inertia of the cracked section, I_{cr}, which is calculated using Eq. 3.18 for T-section or Eq. 3.21 for rectangular-section.

3.6 Conclusion

This chapter investigates the use of CFRP tendons as a prestressing material on the precast segmental concrete beams. Four large-scale segmental T-shaped concrete beams with either internal bonded and unbonded tendons and with dry or epoxied joints were built and tested under four-point loading. Main findings from the study are summarized as follows:

- CFRP tendons can be used to replace the steel tendons for the use in the precast segmental concrete beams to overcome the possible corrosion-induced damage. All the tested beams with CFRP tendons exhibited excellent load-carrying capacity and ductility.

- Tendon bonding condition greatly affected the flexural behaviour of the segmental beams. Beams with bonded tendons showed higher strength and stiffness and larger crack mobilization while the use of unbonded tendons allowed the beams to achieve much greater ductility and less explosive failure at the ultimate stage.

- The joint type had only a slight effect on the loading capacity and ductility of the beams, but significantly affected the initial stiffness. When the joint opened, it showed an approximately linear relation with the midspan deflection of the beam under the applied loads.

- Bonded tendons almost reached its nominal tensile strength at the ultimate stage but this was not true for the cases of unbonded tendons; the unbonded tendons only achieved about 70% of the nominal tensile strength on average at the ultimate stage.

- AASHTO (1999) and ACI 440.4R (2004) predicted well the tendon stress, thus the load-carrying capacity at the ultimate stage of the beams with bonded tendons. However, the accuracy significantly reduced for the cases of the beams with unbonded tendons, which requires further investigation.

- Similarly, PCI (2004), AASHTO LRFD (2012) and ACI 440.4R (2004) predicted well the deflection capacities of the beams with bonded tendons, but the prediction accuracy largely varied for the beams with unbonded tendons.

- The proposed method for estimating the beam deflections took consideration of the stiffness reduction of the beam for dry joints and unboned tendons, and the estimated results showed very good agreement with the experimental results.

3.7 References

AASHTO (1999). *Guide Specifications for Design and Construction of Segmental Concrete Bridges: 2nd Ed with 2003 Interim Revis*, American Association of State Highway and Transportation Officials, Washington, DC.

AASHTO LRFD (2012). *Bridge Construction Specifications, 6th Edition, U.S. Units*, American Association of State Highway and Transportation Officials, Washington, DC.

ACI 318 (2015). *Building code requirements for structural concrete and commentary*, ACI 318-14, American Concrete Institute, Farmington Hills, MI.

ACI 440.4R (2004). *Prestressing concrete structures with FRP tendons (Reapproved 2011)*, American Concrete Institute, Farmington Hills, USA.

Aparicio, A. C., Ramos, G., and Casas, J. R. (2002). Testing of externally prestressed concrete beams. *Engineering Structures*, 24(1), 73-84.

Branson, D. E. (1977). *Deformation of concrete structures*, McGraw-Hill Companies.

Concrete Society Technical Report (2002). Durable post-tensioned concrete structures. *TR 72*,.

Dextra Group. "CFRP tendons." https://www.dextragroup.com/offices/dextra-building-products-limited.

Dolan, C. W., and Swanson, D. (2002). Development of flexural capacity of a FRP prestressed beam with vertically distributed tendons. *Composites Part B: Engineering*, 33(1), 1-6.

Forouzannia, F., Gencturk, B., Dawood, M., and Belarbi, A. (2016). Calibration of Flexural Resistance Factors for Load and Resistance Factor Design of Concrete Bridge Girders Prestressed with Carbon Fiber–Reinforced Polymers. *Journal of Composites*

for Construction, 20(2), 04015050.

Grace, N. F., and Abdel-Sayed, G. (1998). Behavior of externally draped CFRP tendons in prestressed concrete bridges. *PCI Journal*, 43(5), 88-101.

Harajili, M., and Kanj, M. (1992). Ultimate flexural strength of concrete members prestressed with unbonded tendons. *Structural Journal*, 88(6), 663-674.

Harajli, M. H. (2006). On the stress in unbonded tendons at ultimate: Critical assessment and proposed changes. *ACI Structural Journal*, 103(6), 803.

He, Z., and Liu, Z. (2010). Stresses in External and Internal Unbonded Tendons: Unified Methodology and Design Equations. *Journal of Structural Engineering*, 136(9), 1055-1065.

Heo, S., Shin, S., and Lee, C. (2013). Flexural Behavior of Concrete Beams Internally Prestressed with Unbonded Carbon-Fiber-Reinforced Polymer Tendons. *Journal of Composites for Construction*, 17(2), 167-175.

Hindi, A., MacGregor, R., Kreger, M. E., and Breen, J. E. (1995). Enhancing strength and ductility of post-tensioned segmental box girder bridges. *ACI Structural Journal*, 92(1), 33-44.

Jiang, H., Chen, L., Ma, Z. J., and Feng, W. (2015). Shear Behavior of Dry Joints with Castellated Keys in Precast Concrete Segmental Bridges. *Journal of Bridge Engineering*, 20(2), 04014062.

Jiang, H., Cao, Q., Liu, A., Wang, T., and Qiu, Y. (2016). Flexural behavior of precast concrete segmental beams with hybrid tendons and dry joints. *Construction and Building Materials*, 110, 1-7.

Le, T. D., Pham, T. M., Hao, H., and Hao, Y. (2018). Flexural behaviour of precast segmental concrete beams internally prestressed with unbonded CFRP tendons under four-point loading. *Engineering Structures*, 168(2018), 371-383.

Lee, L.-H., Moon, J.-H., and Lim, J.-H. (1999). Proposed methodology for computing of unbonded tendon stress at flexural failure. *Structural Journal*, 96(6), 1040-1048.

Li, G., Yang, D., and Lei, Y. (2013). Combined shear and bending behavior of joints in precast concrete segmental beams with external tendons. *Journal of Bridge Engineering*, 18(10), 1042-1052.

Lou, T., and Xiang, Y. (2007). Effects of ordinary tension reinforcement on the response of beams with unbonded tendons. *Advances in Structural Engineering*, 10(1), 95-109.

Lou, T., Lopes, S. M. R., and Lopes, A. V. (2015). A comparative study of continuous beams prestressed with bonded FRP and steel tendons. *Composite Structures*, 124, 100-110.

Lou, T., Lopes, S. M., and Lopes, A. V. (2016). Response of continuous concrete

beams internally prestressed with unbonded FRP and steel tendons. *Composite Structures*, 154(2016), 92-105.

MacGregor, R. J. G. (1989). Evaluation of strength and ductility of a three-span externally post-tensioned box girder bridge model. University of Texas at Austin.

Mattock, A. H., Yamazaki, J., and Kattula, B. T. (1971). Comparative study of prestressed concrete beams, with and without bond. *Journal Proceedings*, 68(2), 116-125.

Mutsuyoshi, H., and Machida, A. (1993). Behavior of Prestressed Concrete Beams Using FRP as External Cable. *Special Publication*, 138, 401-418.

Naaman, A. E. (2004). *Prestressed Concrete Analysis and Design: Fundamentals*, New York: McGraw-Hill.

Naaman, A. E., and Alkhairi, F. (1991). Stress at ultimate in unbonded prestressing tendons: Part 2—Proposed Methodology. *ACI Structural Journal*, 88(6), 683-692.

Park, R. (1989). Evaluation of ductility of structures and structural assemblages from laboratory testing. *Bulletin of the New Zealand national society for earthquake engineering*, 22(3), 155-166.

PCI (2004). *Design Handbook*, 6th ed., Precast/Prestressed Concrete Institute, Chicago, IL.

Pham, T. M., Le, T. D., and Hao, H. (2018). Behaviour of Precast Segmental Concrete Beams Prestressed with CFRP Tendons. *Proc., 9th International Conference on Fibre-Reinforced Polymer (FRP) Composites in Civil Engineering (CICE 2018)*, 945-953.

Pisani, M. A. (1998). A numerical survey on the behaviour of beams pre-stressed with FRP cables. *Construction and Building Materials*, 12(4), 221-232.

Quayle, T. G. (2005). Tensile-flexural Behaviour of Carbon-fibre Reinforced Polymer (CFRP) Prestressing Tendons Subjected to Harped Profiles. MS thesis. Univ. Waterloo.

Roberts-Wollmann, C. L., Kreger, M. E., Rogowsky, D. M., and Breen, J. E. (2005). Stresses in external tendons at ultimate. *ACI Structural Journal*, 102(2), 206.

Saibabu, S., Srinivas, V., Sasmal, S., Lakshmanan, N., and Iyer, N. R. (2013). Performance evaluation of dry and epoxy jointed segmental prestressed box girders under monotonic and cyclic loading. *Construction and Building Materials*, 38, 931-940.

Shamass, R., Zhou, X., and Alfano, G. (2014). Finite-Element Analysis of Shear-Off Failure of Keyed Dry Joints in Precast Concrete Segmental Bridges. *Journal of Bridge Engineering*, 20(6), 04014084.

Sika Australia Sikadur-30. *https://aus.sika.com/*.

Sika Australia SikaGrout-300PT. *https://aus.sika.com/*.

Tan, K. H., and Tjandra, R. A. (2007). Strengthening of RC continuous beams by external prestressing. *Journal of Structural Engineering*, 133(2), 195-204.

Tao, X., and Du, G. (1985). Ultimate stress of unbonded tendons in partially prestressed concrete beams. *PCI Journal*, 30(6), 72-91.

Wang, X., Shi, J., Wu, G., Yang, L., and Wu, Z. (2015). Effectiveness of basalt FRP tendons for strengthening of RC beams through the external prestressing technique. *Engineering Structures*, 101, 34-44.

Woodward, R., and Williams, F. (1988). Collapse of YNS-Y-GWAS Bridge, Glamorgan. *Proceedings of the Institution of Civil Engineers*, 84(4), 635-669.

Wouters, J., Kesner, K., and Poston, R. (1999). Tendon corrosion in precast segmental bridges. *Transportation Research Record: Journal of the Transportation Research Board*(1654), 128-132.

Yuan, A., Dai, H., Sun, D., and Cai, J. (2013). Behaviors of segmental concrete box beams with internal tendons and external tendons under bending. *Engineering Structures*, 48, 623-634.

Yuan, A., He, Y., Dai, H., and Cheng, L. (2014). Experimental Study of Precast Segmental Bridge Box Girders with External Unbonded and Internal Bonded Posttensioning under Monotonic Vertical Loading. *Journal of Bridge Engineering*, 20(4), 04014075.

Zhou, X., Mickleborough, N., and Li, Z. (2005). Shear strength of joints in precast concrete segmental bridges. *ACI Structural Journal*, 102(1), 3.

CHAPTER 4 FLEXURAL BEHAVIOUR OF PRECAST SEGMENTAL CONCRETE BEAMS PRESTRESSED WITH EXTERNAL STEEL/CFRP TENDONS[3]

Abstract

Precast segmental concrete beams (PSBs) prestressed with external tendons have become increasingly popular. This type of structure takes advantages of both the segmental construction method and external prestressing technique. However, corrosion of steel tendons is still a great concern, which may increase the lifecycle costs of the structure. This chapter presents an experimental investigation on the use of carbon fibre-reinforced polymer (CFRP) tendons as an alternative to steel tendons for segmental concrete beams to mitigate the corrosion problems. To the authors' best knowledge, this is the first study of using CFRP tendons to externally prestressing segmental concrete beams. Four large-scale segmental T-shaped concrete beams with different types of joints and tendon materials (steel/CFRP tendons) were built and tested under four-point cyclic loadings. The test results showed that CFRP tendons can well replace steel tendons in segmental concrete beams as an external prestressing material. All the tested beams showed good performances regarding the load-carrying capacity and ductility. The type of joints had an insignificant effect on the overall flexural behaviour of the beams. After joints opened, the beams with epoxied joints behaved similarly as the beams with dry joints. The beams with CFRP tendons also exhibited non-linear behaviour after the opening of joints, however, the level of non-linearity was much less than that of the beams with steel tendons. Steel tendons achieved very high stress at the ultimate stage, which were about 94% to 95% of their ultimate tensile strength. Meanwhile, CFRP tendons ruptured at quite low stress, which were approximately 78% of its nominal breaking strength. Finally, all the codes examined in this study predicted well the tendon stress and the ultimate load of the beams with steel tendons but encounter large scatter for the predictions of the tendons' stress and strength of the beams with CFRP tendons.

[3] This chapter is compiled from the following paper which is under review:
Le, T. D., Pham, T. M., and Hao, H. (2019). Behavior of Precast Segmental Concrete Beams Prestressed with External Steel/Carbon Fiber-Reinforced Polymer (CFRP) Tendons. *Journal of Composites for Construction*, (Revision submitted).

4.1 Introduction

External prestressing technology has been used for prestressed concrete girder bridges over the last four decades. Compared to internal prestressing technique, construction and replacement of external tendons are convenient. In addition, the thickness of the web of the cross-section can be reduced since the tendons and ducts are placed outside of the concrete section, which results in a possible reduction in dead load. The use of external tendons particularly benefits the segmental construction since it eliminates the misalignment of ducts at joints, which is a common problem to internally prestressed segmental construction. Combining the advantages of external prestressing technology and the segmental construction method, precast segmental concrete beams prestressed with external tendons have become increasingly popular.

To date, steel tendons have been the only material for prestressing segmental concrete beams. In order to protect the tendons against corrosion, the exposed parts of the tendons between deviators are usually grouted/oiled and enclosed in sheathing. However, due to the natural rust properties of steel, corrosion problem of steel tendons is always a great concern for the service life of the structure. Inappropriate design choices and failure in construction of the corrosion protection system may cause corrosion-induced damages, which greatly increase lifecycle maintenance costs. As such, this study investigates the use of carbon fibre-reinforced polymer (CFRP) tendons on PSBs in replacement of steel tendons to tackle the corrosion problems. With the authors' best knowledge, this is the first study that external CFRP tendons are used in segmental concrete beams. CFRP tendons are corrosion-free, therefore, they can extend the useful life of the structure and reduce the maintenance cost. Moreover, CFRP tendons possess a high tensile strength that even exceeds steel tendons and are lighter than steel. This helps reduce the dead load of the structure and facilitates handling. However, CFRP tendons show a linear stress-strain relationship up to failure, which may cause a structure to fail in a brittle manner compared to the ductile behaviour of the beams with steel tendons. In addition, CFRP tendons show lower elastic modulus and are week in shear. These properties can result in higher deflections of the beam and premature failure of the CFRP tendons at deviators due to stress concentration. It is therefore important to investigate the performance of PSBs externally prestressed with FRP tendons before its possible practical applications.

In the literature, the use of FRP tendons on PSBs has not been reported yet, except for

the works recently done by Le et al. (2018) and Le et al. (2019) on PSBs internally prestressed with CFRP tendons. Le et al. (2018) conducted an experiment on segmental concrete beams prestressed with internal unbonded tendons. Both steel/CFRP tendons and dry/epoxied joints were used in the specimens. All the beams were cyclically tested under four-point loading up to failure. The tested results showed that all the tested beams with CFRP tendons exhibited excellent load-carrying capacity and ductility, therefore, could replace steel tendons for the use in PSBs. However, stress in the CFRP tendons at rupture was low, which corresponded to about 70% of the nominal breaking strength on average. This premature failure was due to the shear stress concentrated at the middle joints exceeding the tendons' shear strength, which was later confirmed by the numerical results (Le et al. 2020). This behaviour requires attention on the design of ducts for the internal CFRP tendons at the joints to ensure a relatively uniform stress transfer in the tendons at the joints' locations.

Le et al. (2018) also presented a comparison of segmental beams with CFRP tendons and the corresponding ones with steel tendons. It is found that the beam with internal unbonded CFRP tendons performed similarly to the beam with internal unbonded steel tendons. Both the beams showed non-linear load-deflection responses after joints opened up to failure. However, the rupture of CFRP tendons caused a sudden loss in the applied load at the ultimate stage compared to a ductile failure manner of the beam with steel tendons. Similar conclusions were also made in the case of monolithic beams prestressed with steel/FRP tendons (Pisani 1998; Tan and Tjandra 2007; Lou et al. 2016). Pisani (1998) conducted a numerical investigation and found that the structural behaviour of beams prestressed with internal/external unbonded glass fibre-reinforced polymer (GFRP) tendons was similar to beams with unbonded steel tendons. However, the low creep rupture limitation of the GFRP tendons, normally less than 30%f_u, greatly restricted its high efficiency in prestressing applications. Lou et al. (2016) investigated concrete beams with internal tendons and concluded that the type of unbonded tendons (steel or CFRP tendons) had insignificant influence on the cracking mode, deformation capacity, stress increments. Tan and Tjandra (2007) tested continuous beams and concluded that the use of external CFRP tendons did not lead to significant differences for the ultimate load, tendon stress, and deflection compared to the beams with steel tendons.

Le et al. (2019) found that bonding condition of the tendons to the concrete

significantly affected the flexural behaviour of PSBs with CFRP tendons. The use of bonded tendons greatly increased the strength of the beams while decreased the beams' ductility. Bonding condition led to different behaviour of the beams after joints opening or cracking. After joints opening/cracking, the beams with bonded tendons continued to deform in an approximately linear manner with the applied load up to failure while the beams with unbonded tendons showed non-linear behaviour between the deflection and the applied load. Bonding condition also affected the failure modes of the beams. All the beams in Le et al. (2019) were under-reinforced and would fail in tension as observed in the beams with bonded tendons. However, the use of unbonded tendons shifted the failure mode of the beams from tension controlled to compression controlled as the beams with unbonded tendons showed severe concrete crushing on the compression zone before the rupture of the tendons at the ultimate stage.

Regarding the type of joints, Saibabu et al. (2013) conducted an experimental program on PSBs prestressed with external steel tendons and found that the beams with epoxied joints showed higher cracking load and ultimate load compared to the beams with dry joints. This was due to the additional tensile strength of concrete and the high concentration of rotation and deflection at individual dry joints. However, both the beams achieved almost the same deflection at the failure. Meanwhile, other studies (Li et al. 2013b; Li et al. 2013a) found that beams with epoxied joints showed greater ductility compared to beams with dry joints. Le et al. (2018) and Le et al. (2019) found that the type of joint had an insignificant effect on the overall flexural response of the segmental concrete beams. Even though the beams with epoxied joints showed strengths about 3-8% higher than the one with dry joints, both the beams exhibited very similar load-deflection curves up to the ultimate stage. This was true for both the cases of the beams with bonded and unbonded CFRP tendons. It is worth mentioning that the effective prestress, f_{pe}, has a strong effect on the flexural behaviour of PSBs (Le et al. 2020). The two beams with unbonded tendons in Le et al. (2019) had different effective prestresses. Therefore, more tests are required on the effect of type of joints on the performance of PSBs with CFRP tendons.

Dry joints and epoxied joints exhibited different failure modes (Le et al. 2018; Le et al. 2019). Cracking of epoxied joints developed in the concrete adjacent to the segment interface. This cracking behaviour was brittle due to cracks in concrete when the

applied tensile stress exceeded its tensile strength. In contrast, opening of dry joints occurred at the segments' interfaces, which was less brittle therefore led to a smoother transition from the first stage of elastic behaviour to the second stage of non-linear behaviour of the beams. Similar observations were also observed in previous studies (Li et al. 2013b; Yuan et al. 2014) on PSBs externally prestressed with steel tendons. It is noted that after the epoxied joints opened (i.e. cracked), they performed similarly to the dry joints under the applied load. Both the beams with dry or cracked epoxied joints underwent various load cycles until they reached the ultimate stage (Saibabu et al. 2013; Le et al. 2018; Le et al. 2019).

The flexural behaviour of a beam with external tendons is different from that of a beam with internal unbonded tendons. This difference is mainly caused by the so-called secondary effect, i.e. the variation in the depth of the external tendon. Since the tendons are external to the concrete cross-section and are only attached to the concrete girder at deviators, insufficient number of deviators can result in a significant loss in the eccentricity of the tendons. This reduction in the tendons' eccentricity results in the decrease in the flexural efficiency (MacGregor 1989). The use of deviators along the span of a structure can effectively reduce this secondary effect. Tests conducted by Tan and Ng (1997) showed that a single deviator at the section of maximum deflection led to satisfactory service and ultimate load behaviour. Harajli et al. (1999) also confirmed the efficiency of the deviators in the external prestressing system. In addition, a single concentrated load produces a less significant secondary effect because it mobilizes lower post-elastic deflection compared to two-third point load or uniform load application. Jiang et al. (2016) tested segmental concrete beams and found that the beam with solely external tendons had the lowest flexural strength and deflection as compared to those with hybrid tendons. Yuan et al. (2013) also conducted tests on PSBs and concluded that the more internal bonded tendons were used, the higher the load-carrying capacity and better ductility.

In this study, CFRP tendons were the first time used for externally prestressing segmental concrete beams. Two deviators were used in the specimens to minimize the secondary effect as recommended by Harajli et al. (1999). Both dry and epoxied joints were used in the specimens. Segmental beams with external steel tendons were also tested for comparison. The main aim of the study is to investigate the possible use of CFRP tendons as an external prestressing solution for PSBs to mitigate the corrosion

problem, which is a great concern of PSBs with steel tendons.

4.2 Experimental program

Four large-scale T-shaped segmental concrete beams were built and tested in this experimental program to investigate the flexural behaviour of PSBs prestressed with external CFRP tendons. It is noted that all the four beams had the same dimensions and configurations as those in Chapter 2, except that external steel/CFRP tendons were used in the specimens instead of internal tendons. In addition, the specimens' fabrication, post-tensioning and testing set up are almost similar to those described in Chapter 2 and therefore they are not repeated herein except for the differences for the sake of brevity.

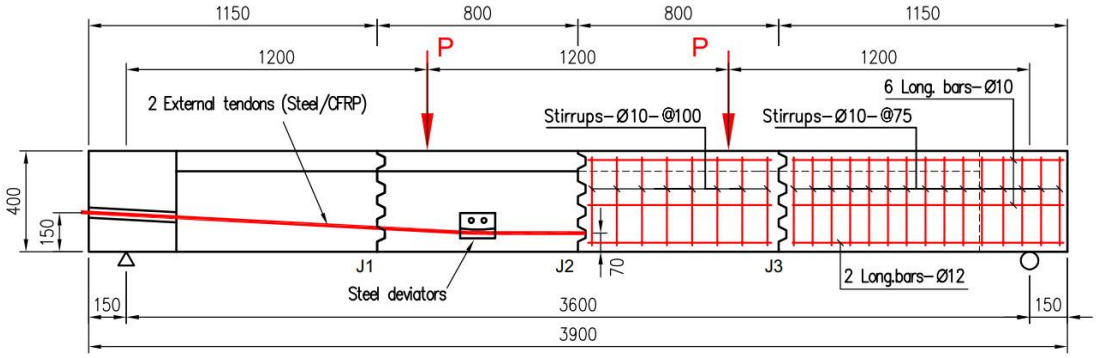

Figure 4-1: Configuration of the tested beams

Figure 4-1shows a typical configuration of the tested beams. Two steel/CFRP tendons were used as external tendons to connect the segments for each beam, using the post-tensioning technique. The tendons were attached to the middle segments by two steel deviators which consisted of 500 mm radius curved steel plates (Figure 4-2). The radius of the curved steel plates was selected based on study by Quayle (2005) to minimize the stress concentration in the tendons. The tendons were draped at 3^{o} angle from the deviators to the two ends. This draping angle was selected to minimize the harping effect, which occurs in the deviated FRP tendons as recommended by Wang et al. (2015). Table 4-1 summarises details of beams' configuration, in which Beams S-D and S-E contained steel tendons with dry/epoxied joints while Beams C-D and C-E had CFRP tendons with dry/epoxied joints. It is noted that letters "*S*" and "*C*" respectively stand for steel carbon tendons while the dry and epoxied joints were abbreviated by letters "*D*" and "*E*", respectively. Details of materials' properties are given in

Table 2-2 of Chapter 2. The beams were then tested under four-point cyclic loading up to failure. Figures 4-3 to 4-6 show procedures of fabrication of specimens, post-tensioning, and testing set up. More details were presented in Section 2.2 of Chapter 2.

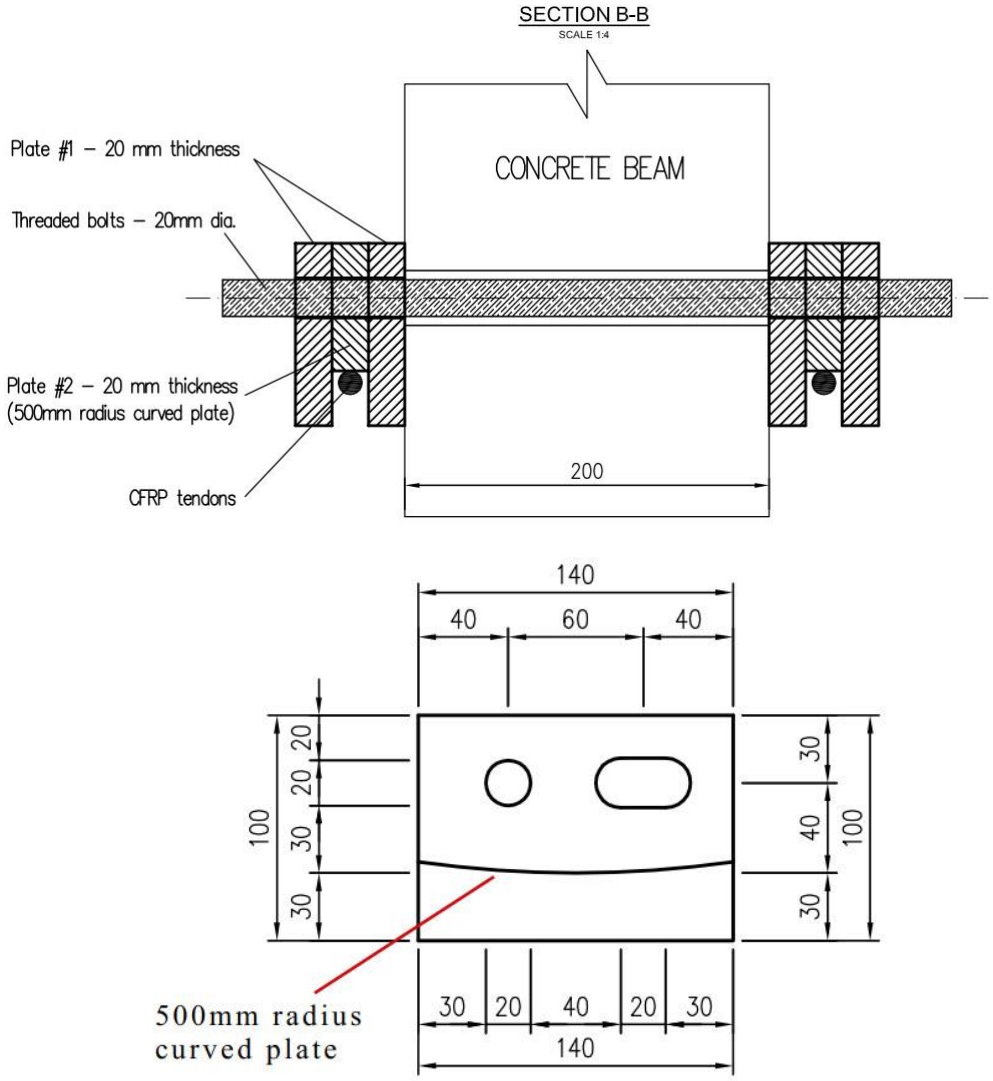

Figure 4-2: Details of Deviators

Table 4-1: Configuration of the tested beams

Specimen	Tendon type	Joint type	f'_c (MPa)	f_{pe} (MPa)	f_{pe}/f_{pu}	P_{pe} (kN)
S-D	2 steel tendons	Dry	41.5	1102	0.59	110
S-E	2 steel tendons	Epoxied	41.5	1071	0.58	107
C-D	2 CFRP tendons	Dry	41.5	1090	0.44	138
C-E	2 CFRP tendons	Epoxied	41.5	752	0.31	95

(a) formwork

(b) 1st concrete batch

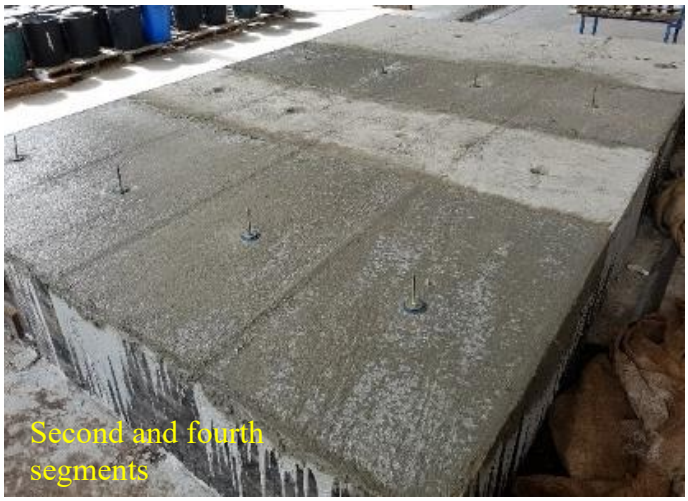

(c) 2nd concrete batch

Figure 4-3: Casting of specimens

Figure 4-4: Segments at completion

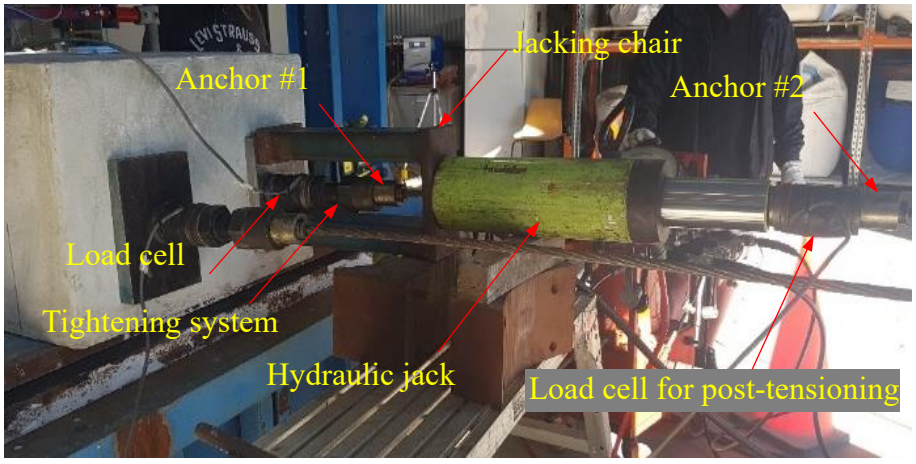

Figure 4-5: Typical post-tensioning set up using external tendons

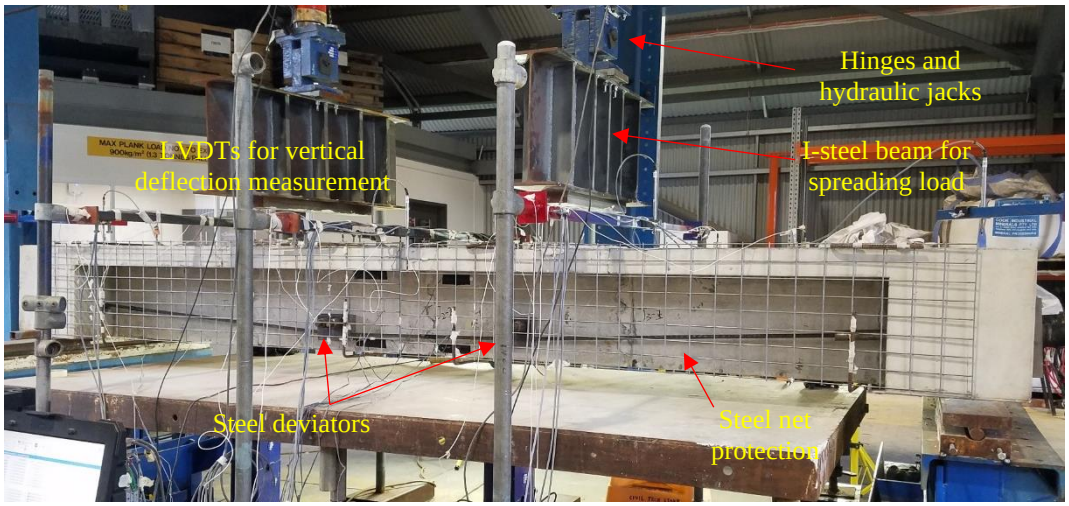

Figure 4-6: A typical testing set up

4.3 Experimental results and discussions

All the experimental results are given in Table 4-2, in which P_y, $\delta_{mid,y}$, $\Delta_{J,y}$, P_u, $\delta_{mid,u}$ and $\Delta_{J,u}$ are the applied loads, midspan deflections, and total openings of all joints of

the specimens at yield point and at the ultimate stage, respectively. It is noted that the definition of yield point, which was provided in Park (1989), was used here to determine the yield point for the beams with dry joints, i.e. Beams S-D and C-D, since no tensile cracking of concrete was observed (Figure 2-11). For Beams S-E and C-E with epoxied joints the yield point was taken at the cracking of concrete in tension. The failure modes of all the tested beams are shown in Figure 4-7 and Figure 4-8. Details of the structural behaviour and failure modes of the beams are discussed in the following sections.

Table 4-2: Tested results of all the beams

Specimen	Yield point			Ultimate			Failure mode
	P_y	$\delta_{mid,y}$	$\Delta_{J,y}$	P_u	$\delta_{mid,u}$	$\Delta_{J,u}$	
S-D	59.9	2.9	0.48	91	50.3	20.9	Tendon yielded and top concrete crushed
S-E	68.3	2.2	0.93	92	56.6	22.1	Tendon yielded and top concrete crushed
C-D	59.0	3.2	0.54	109	64.8	26.9	Top concrete crushed and CFRP tendons ruptured
C-E	40.0	2.0	0.38	114	96.9	39.8	Top concrete crushed

(a) Beam S-D

(b) Beam C-D

Figure 4-7: Failure modes of the beams with dry joints

(a) Beam S-E

(b) Beam C-E

Figure 4-8: Failure modes of the beams with epoxied joints

4.3.1 Beams prestressed with steel tendons

Figure 4-9 shows the load-deflection curves and corresponding envelops of Beams S-D and S-E prestressed with steel tendons and different types of joints. It is seen from the figure that except a difference in the cracking/opening load at the yield point, the two beams behaved very similarly up to failure. The load-deflection curves of the beams can be divided into three stages. In the first stage, the beams deformed linearly under the applied load up to the cracking/opening of the joints. The opening of the joints resulted in a sudden loss in the beams' stiffness as shown in the figure. In the second stage, the beams showed a non-linear behaviour until the tendons yielded, which also led to a further loss in the beams' stiffness. After that, in the third stage, the beams just gained marginal increases in the applied load and reached the maximum load onset of the failure of concrete in the compression zone, then the applied load started to decrease. In both the beams, the tendons yielded at displacements of about 36-38 mm, and the maximum loads were reached at a displacement of approximately 50 mm.

The failure of concrete and the tendons at the ultimate stage of the two beams were observed as follows. At the load of about 86-88 kN, there were some minor cracks in concrete on the extremely top fibre while the applied load kept increasing. Then the tendons yielded at the load of about 90 kN. After that, the beams reached their

maximum loads (91 kN for Beam S-D and 92 kN for Beam S-E) before the applied load started to decrease as mentioned earlier. The tests were stopped for safety reasons when the beams deflected at about 80 mm. It therefore can be deduced that the type of joint had an insignificant effect on the flexural response of PSBs prestressed with external steel tendons.

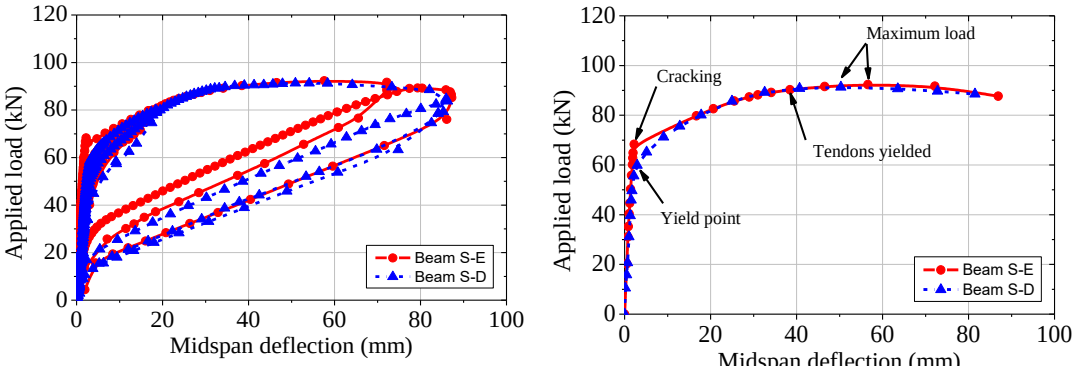

(a) Cyclic loads (b) Envelop curves

Figure 4-9: Load-deflection curves of the beams with steel tendons

The flexural behaviour of Beams S-D and S-E in this study was similar to that of the beam internally prestressed with steel tendons in the previous study by Le et al. (2018). Beam BS1 in Le et al. (2018)'s study had the same configuration with Beams S-D and S-E except that the internal unbonded steel tendons were used. The load-deflection curve of Beam BS1 in Le et al. (2018)'s can also be divided into three stages, in which the opening of joints and the yielding of steel tendons led the beam's stiffness to decrease significantly. However, the yielding point of the steel tendons was not defined in Le et al. (2018)'s study, instead the load-deflection curve of the beam was divided into two stages with one inflection point corresponding to the joints opening. The applied load and the corresponding deflection at the ultimate stage of Beam BS1 were 96 kN and 89.4 mm, respectively, which were higher than those of Beam S-D in this study, which were 91 kN and 50.3 mm (Table 4-2). This confirmed the reduction in the flexural strength and deflection due to the secondary effect in the beam prestressed with external tendons as presented in previous studies (MacGregor 1989; Harajli et al. 1999).

4.3.2 Beams prestressed with CFRP tendons

The load-deflection curves and the corresponding envelops of the beams prestressed with CFRP tendons with dry and epoxied joints are shown in Figure 4-10. One

objective of the tests on these two beams is to investigate the effect of the type of joints on the flexural behaviour of PSBs with external CFRP tendons. However, due to the challenges in the stressing work, Beam C-E had the effective prestress, f_{pe} lower than that of Beam C-D (Table 4-1) and thus it is difficult to directly compare the performance of these two beams. Le et al. (2020) found that increasing f_{pe} leads to increases in the opening load and maximum load. Beam C-E with a lower effective prestress showed a smaller cracking/opening load compared to that of Beam C-D as shown in Figure 4-10(b). However, Beam C-E gained higher maximum load and larger deflection at the ultimate stage compared to those of Beam C-D, which were different from the findings of Le et al. (2020) for which the beam with higher f_{pe} should have higher maximum load and deflection capacity. It is noted that Beams C-D and C-E in this study failed in tension, i.e. CFRP tendons ruptured, while the beams in Le et al. (2020)'s study failed in compression. As such, Le et al. (2020)'s findings were not applicable herein regarding the maximum load and deflection at the ultimate stage.

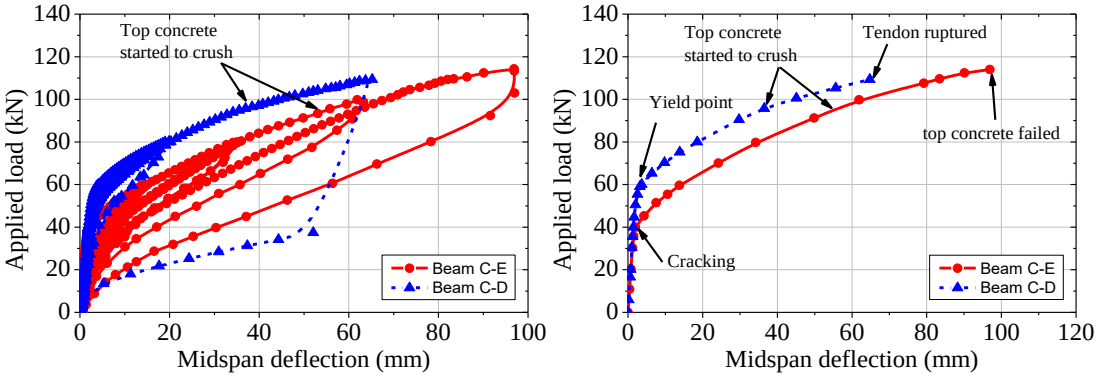

(a) Cyclic loads (b) Envelop curves

Figure 4-10: Load-deflection curves of the beams with CFRP tendons

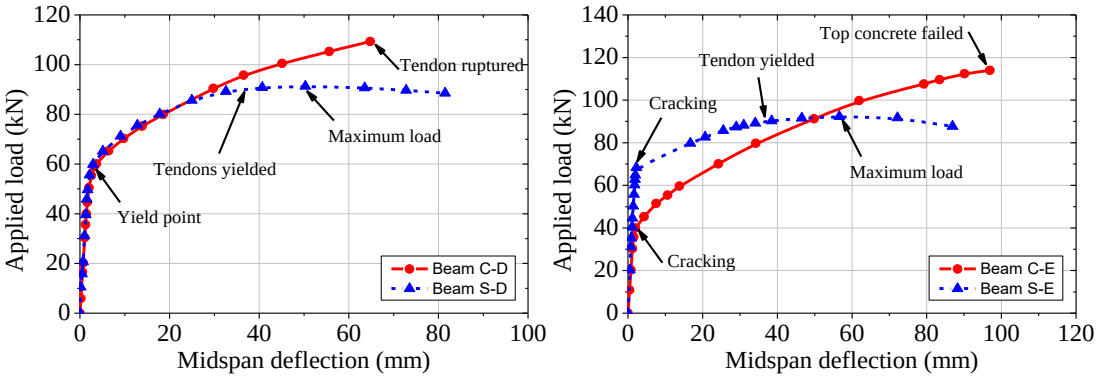

(a) dry joints (b) epoxied joints

Figure 4-11: Load-deflection curves: steel vs CFRP tendons

The load-deflection curves of the two beams can be divided into two stages (Figure

4-10b). In the first stage, the beams showed a linear behaviour up to the cracking/opening of the joints, which was very similar to those of the beams with steel tendons as clearly shown in Figure 4-11. The cracking/opening of the joints also resulted in a dramatic loss in the beams' stiffness. In the second stage, the beams also exhibited a non-linear behaviour up to the ultimate load, however, the levels of nonlinearity were different to those of beams with steel tendons. In the cases of Beams S-D and S-E, the beams' stiffness reduced dramatically when the steel tendons yielded as discussed previously leading the beams to the third stage of behaviour. Meanwhile, in the cases of Beams C-D and C-E, there were also reductions in the beams' stiffness when the applied loads were approximately at 94 kN (for Beam C-D) and 90 kN (for Beam C-E), for which the concrete on the top fibre of the beams started to crush (Figure 4-10a,b). However, the changes in the beams' stiffness due to the crushing of compressive concrete in Beams C-D and C-E were much less severe than those in Beams S-D and S-E due to the yielding of steel tendons (Figure 4-11**)**. This explains the reason why the load-deflection curves of Beams C-D and C-E were divided into two stages instead of three stages as observed in the cases of the beams with steel tendons.

The failure of Beam C-D was due to the rupture of CFRP tendons (Figure 4-7b). Crushing of the compressive concrete on the top fibre was also observed. However, this crushing of concrete had not resulted in a reduction in the applied load. The failure process was observed as follows. When the applied load was at about 94 kN as mentioned earlier, the concrete on the top fibre of the beam started to crush. The beams still resisted higher loads though and reached its maximum load at the rupture of CFRP tendons (Figure 4-10). In contrast, the failure of Beam C-E was due to the failure of concrete in compression. The concrete on the top fibre of the beam started to crush at the load of about 90 kN, but the beam still resisted higher loads (Figure 4-10). When the applied load was at about 112 kN-114 kN, severe damages were observed in the concrete on the top fibre as observed in Figure 4-8. At that time, continuous cracking sounds were also heard in the tendons. The test was then stopped for safety reason.

From the above analyses, it can state that CFRP tendons can be well used in the replacement of the steel tendons for the use in segmental concrete beams as an external prestressing material. All the tested beams showed good performances regarding the load-carrying capacity and ductility.

4.3.3 Joint opening

The opening of all the joints under the applied load for all the tested beams are plotted and shown in Figure 4-12. It is seen from the figure that the shape of the load and joint opening curves are similar to the load-deflection curves for all the tested beams as shown in Figure 4-9(b) and Figure 4-10(b). In the case of the beams with steel tendons, Beam S-E with epoxied joints had the cracking load of about 14% higher than that of Beam S-D with dry joints (Table 4-2). This was due to the additional tensile strength of the concrete in tension. A similar observation was observed in the study of Saibabu et al. (2013) as the beam with epoxied joints showed higher opening load than that of the beam with dry joints. After the epoxied joint cracked, Beam S-E behaved like Beam S-D with dry joints in the next load cycles (Figure 4-9a). Similar observations were observed in the beams with CFRP tendons. However, Beam C-E showed a smaller cracking load compared to that of Beam C-D due to the smaller effective prestress as discussed previously. After cracking, Beam C-E behaved like Beam C-D with dry joint and underwent many load cycles before the beams reached their ultimate stage by the rupture of CFRP tendons.

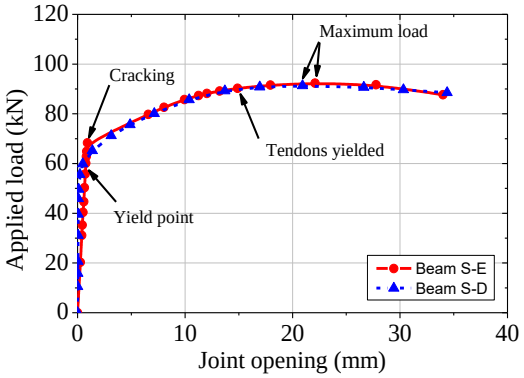

(a) Beams with steel tendons

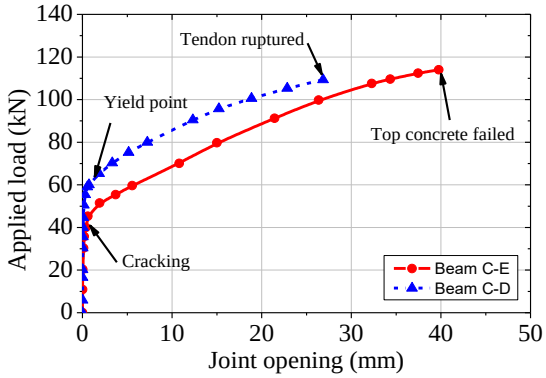

(b) Beams with CFRP tendons

Figure 4-12: Opening of joints

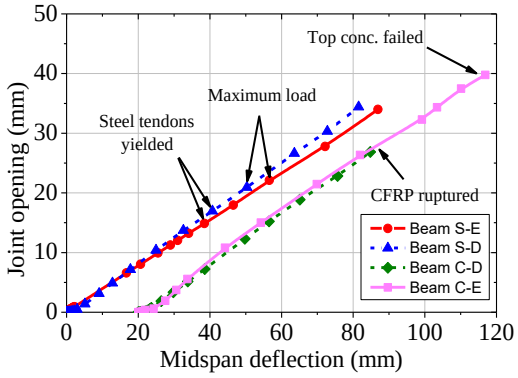

Figure 4-13: Joint opening vs deflection

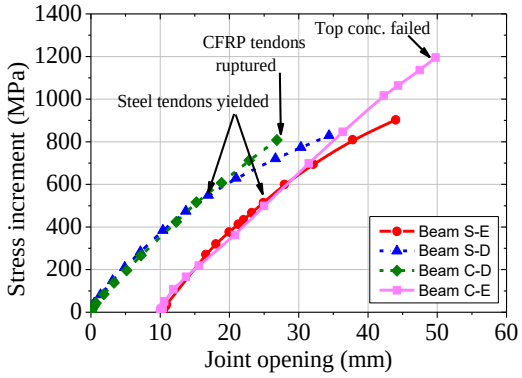

Figure 4-14: Joint pening vs stress increment

Although both the beams with epoxied joints behaved similarly to their counterparts with dry joints, the cracking behaviours of the epoxied joints and dry joints were different. The response of epoxied joints was brittle when the applied load reached its cracking resistance. The epoxied joint formed a vertical crack cutting all the shear keys' bases as shown in Figure 4-9(b) and Figure 4-10(b). In contrast, the dry joints did not show any cracks but it opened at the segment interface when the applied load reached the opening load. The gradual opening of the joint leads to the smoother change in the beams' stiffness compared to the beams with epoxied joints. It is worth mentioning that in all the four tested beams, the opening of the joints mainly concentrated on the middle joint, while the other two side joints almost remained closed under the applied load as also observed in the previous studies (Le et al. 2018; Le et al. 2019).

Figure 4-13 shows the relationships between the joint opening and the midspan deflection of all the tested beams. It is clearly seen from the figure that the opening of all the joints was almost linear to the midspan deflection up to the ultimate stage. This is true for all the beams with steel/CFRP tendons and dry/epoxied joints. Previous studies also observed this linear behaviour in segmental concrete beams with internal unbonded steel/CFRP tendons (Le et al. 2018; Le et al. 2019). The opening of joints was also plotted against the tendon stress increments and shown in Figure 4-14. It is observed that the opening of joints also exhibited an approximately linear relationship with the tendon stress increments for the case of the beams with CFRP tendons. Meanwhile, there was a nonlinear relationship between the opening of joints and the stress increments in the case of the beams with steel tendons. However, it is noted that before the yielding of the steel tendons, the opening of the joints was almost linear with the stress increment in the tendons. Therefore, a linear relationship between the opening of joints and the tendon stress increment can be assumed for the analysis and design of PSBs with external unbonded steel tendons since the point at which the prestressing steel yields is considered the ultimate stage in practice.

4.3.4 Stress development

The development of tendon stresses under the applied load of all the tested beams are shown in Figure 4-15. In the first stage of the applied load vs tendon stress relationship before the joints opening, the tendon stress increments in all the beams were very small. The tendon stresses of Beams S-D and S-E increased by 3.4% and 3.7% while

those of Beams C-D and C-E were 3.2% and 2.7%, respectively. After joints opened/cracked, the stress in the tendons started to increase at a much higher rate until the yielding of steel tendons or the rupture of CFRP tendons. The tendon stresses recorded at the maximum loads of Beams S-D and S-E were 1731 MPa and 1766 MPa, respectively, which were higher than the yielding stress and were 94% and 95% of their nominal ultimate strength (Table 4-3). In the case of the beams with CFRP tendons, the tendon stresses at the ultimate stage were quite low compared to their nominal breaking strength. Stresses in the CFRP tendons of Beams C-D and C-E at the rupture were 1898 MPa and 1949 MPa, corresponding to 77% and 79% of the nominal breaking strength, respectively. The stress reduction in the CFRP tendons at the rupture could be attributed to the bending effect of the beams and the harping effect of the CFRP tendons at the deviators. According to Wang et al. (2015), a harped angle of 3^{o} used in the tendons in this study could lead to a strength reduction of 10%. This requires special attention in the design of the deviator system when the external CFRP tendons are used to avoid significant loss and premature failure of the CFRP tendons. Particularly, shear stress on the CFRP tendons at the deviators might also cause a reduction in the rupture stress as discussed previously.

The relationships between the stress increment and the midspan deflection for all the beams are also plotted and shown in Figure 4-16. Since the opening of joints is linearly related to the midspan deflection, the relationships of the stress increment and the midspan deflection are similar to those of stress increment and the opening of joints as observed in Figure 4-14. In the case of the beams with CFRP tendons, the tendon stress increment was almost linear to the deflection under the applied load up to the ultimate stage. Meanwhile, in the beams with steel tendons, the stress in the tendons also increased almost linearly to the deflection up to the yielding of the steel tendons. After that, it showed a highly non-linear behaviour as shown in the figure. However, this stage of behaviour after the yielding of the tendons is not considered in the design of the beam. A beam with steel tendons is considered to reach its ultimate stage when the tendon yields. This linear relationship between the stress increments and the midspan deflection was also true in the case of internal unbonded steel/CFRP tendons as observed in the previous studies (Le et al. 2018; Le et al. 2019). This relationship will support the computation of stress increment in PSBs with internal/external unbonded CFRP tendons based on the beams' deflection, which has been used for predicting the

stress increment in the monolithic beams by other researchers (Harajili and Kanj 1992; He and Liu 2010).

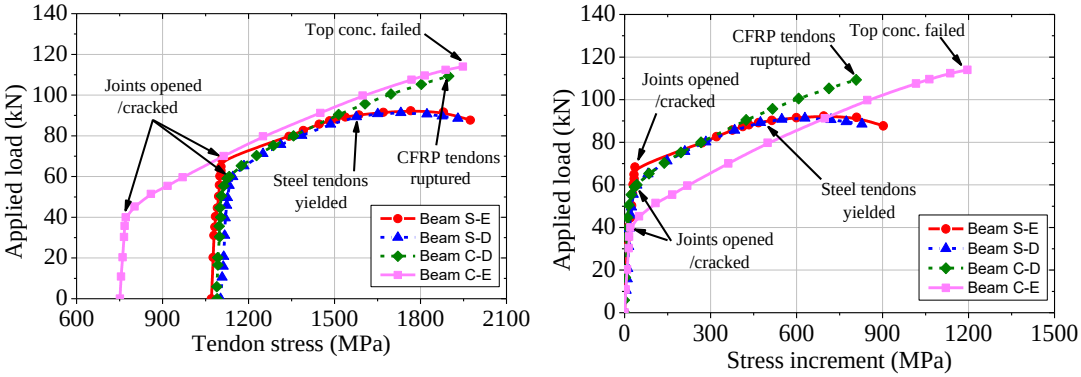

(a) Tendon stresses

(b) Tendon stress increment

Figure 4-15: Stress development in the tendons

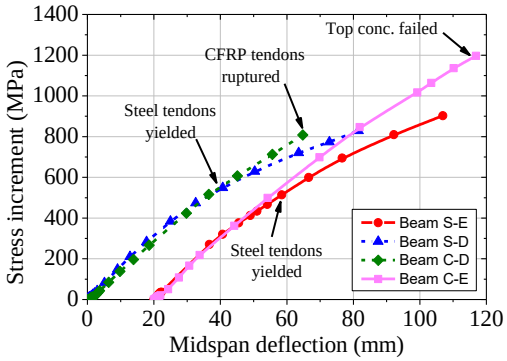

Figure 4-16: Tendon stress increment vs deflection

4.4 Theoretical considerations

4.4.1 Existing models for computation of unbonded tendon stress

In this section, several models for predicting the stress in the unbonded tendons are employed to calculate the tendon stress at the ultimate stage and are then compared with the experiment results. These models include the equations recommended by AASHTO LRFD (2012), ACI 318 (2015) and ACI 440.4R (2004). It is worth noting that amongst the examined models, only the one recommended by ACI 440.4R (2004) is for the computation of stress in the CFRP tendons. This model is, however, developed based on the analysis of monolithic concrete beams. The other models are for the monolithic beams with unbonded steel tendons. In other words, there has been no specific design model for predicting the stress in the tendons of segmental concrete beams with unbonded CFRP tendons. Symbols for the same parameters in different models are rewritten for convenience.

AASHTO LRFD (2012) recommended the following equation to calculate the stress in the unbonded tendons at the ultimate stage:

$$f_{ps} = f_{pe} + 6200\left(\frac{d_{ps} - c}{l_e}\right), MPa \tag{4.1}$$

In which, f_{ps} is the effective tendon stress; d_{ps} is the distance from extreme top fibre to centroid of prestressing tendons; c is the neutral axis depth of the section; $l_e = l_i/(1+[N/2])$, where l_i is the length of the tendon between anchorages and N is the number of support hinges required to form a mechanism crossed by the tendon.

ACI 318 (2015) adopted the following equation for predicting the stress in the unboned tendons, which is applicable to beams with $L/d_{ps} \leq 35$:

$$f_{ps} = f_{pe} + 69 + \frac{f_c^{'}}{100\rho_{ps}}, MPa \tag{4.2}$$

where ρ_{ps} is the prestressing reinforcement ratio.

ACI 440.4R (2004) recommended the following equation to predict the stress in CFRP tendons based on the work of Naaman et al. (2002):

$$f_{ps} = f_{pe} + \Omega_u E_{ps} \varepsilon_{cu}\left(\frac{d_{ps}}{c_u} - 1\right) \tag{4.3}$$

where E_{ps} is the tendon modulus of elasticity; ε_{cu} is the ultimate concrete compression strain which was taken as 0.003; c_u is the neutral axis depth at ultimate loading; and Ω_u is a strain reduction coefficient, $\Omega_u = 3/(L/d_{ps})$ for uniform or third-point loading, where L is the span length. It is noted that a limitation of 0.94 f_{py} is applied when using Eq. 4.3 to calculate the stress in the steel tendons as recommended by Naaman and Alkhairi (1991), where f_{py} is the yielding stress of steel tendons.

4.4.2 Results and discussion

The predicted results by all the models for tendon stresses and the strength of all the tested beams are given in Tables 4-3 to 4-5 and Figs. 4-17 to 4-19. It is noted that the experimental values of tendon stresses, stress increments and ultimate loads (f_{ps}, Δf_{ps}, and P_u) of Beams S-D and S-E are taken at where the steel tendons yielded for fair comparisons with the codes' predictions. It is seen that all the models predict well the

tendon stresses and ultimate loads of Beams S-D and S-E prestressed with steel tendons, although they show relatively large differences for the predictions of the tendon stress increments. ACI 318 (2015) and ACI 440.4R (2004) show an approximately 18% difference in the predictions of Δf_{ps} on average while both the models give only 6% and 7% difference on average in the predictions of f_{ps} and P_u, respectively (Tables 4-3 to 4-5). AASTHO LRFD (2012) yields slightly better predictions compared to the other models with a 9% difference in the prediction of Δf_{ps}, and 3% and 4% difference on average in the predictions of f_{ps} and P_u, respectively.

For the beams with CFRP tendons, the accuracy in the predictions of f_{ps} and P_u by these models varies. AASTHO LRFD (2012) and ACI 318 (2015) yield fairly good predictions of P_u for Beam C-D with dry joints, but highly underestimate P_u for Beam C-E with epoxied joints. In contrast, ACI 440.4R (2004) highly overestimates P_u of the two beams (Tables 4-3 to 4-5 and Figs. 4-17 to 4-19). AASTHO LRFD (2012) and ACI 318 (2015) underestimate f_{ps} of Beam C-D by 13% and 21% compared to the experimental results, but show close predictions of P_u with only 1% and 8% differences, respectively. For Beam C-E, the predictions of f_{ps} by AASTHO LRFD (2012) and ACI 318 (2015) differ by 36% and 41% compared to the experimental results. Those variations in the predictions of P_u by the two codes are 23% and 32%, respectively. Whereas, ACI 440.4R (2004) highly overestimates f_{ps} and P_u of Beam C-D by 13% and 29%, respectively. Those differences in the predictions of f_{ps} and P_u of Beam C-E by the guide are 3% and 13%, respectively.

Table 4-3: Theoretical predictions of f_{ps}

Specimen	$f_{ps.expt}$ (MPa)	$f_{ps}/f_{ps.expt}$			
		AASTHO LRFD	ACI 318	ACI 440	Modified ACI 440
S-D	1674	0.98	0.94	0.94	-
S-E	1674	0.96	0.93	0.94	-
C-D	1898	0.87	0.79	1.13	0.95
C-E	1949	0.66	0.59	1.03	0.83

Table 4-4: Theoretical predictions of Δf_{ps}

Specimen	$\Delta f_{ps.expt}$ (MPa)	$\Delta f_{ps}/\Delta f_{ps.expt}$			
		AASTHO LRFD	ACI 318	ACI 440	Modified ACI 440
S-D	572	0.93	0.84	0.82	-
S-E	603	0.89	0.80	0.83	-
C-D	808	0.70	0.49	1.29	0.88
C-E	1196	0.45	0.33	1.03	0.76

Table 4-5: Theoretical predictions of P_u

Specimen	$P_{u.expt}$ (kN)	$P_u/P_{u.expt}$			
		AASTHO LRFD	ACI 318	ACI 440	Modified ACI 440
S-D	90.8	0.97	0.94	0.93	-
S-E	90.3	0.95	0.92	0.94	-
C-D	109.3	1.01	0.92	1.29	1.10
C-E	114.1	0.77	0.68	1.13	0.95

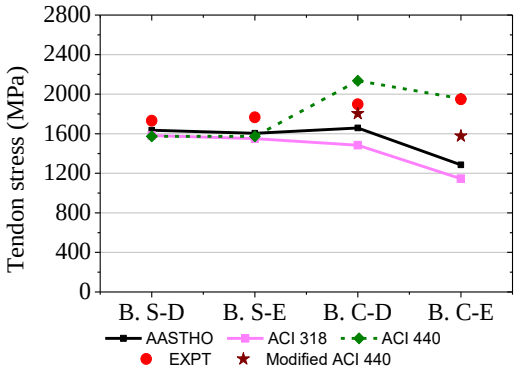

Figure 4-17: Predictions of f_{ps}

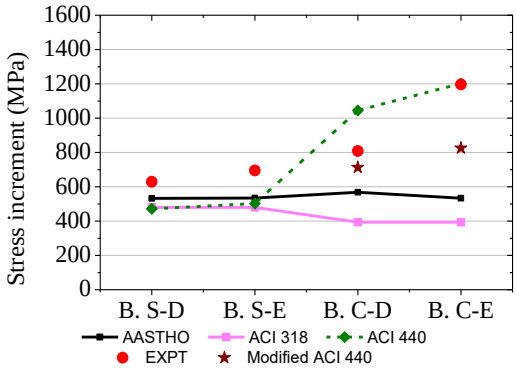

Figure 4-18: Predictions of Δf_{ps}

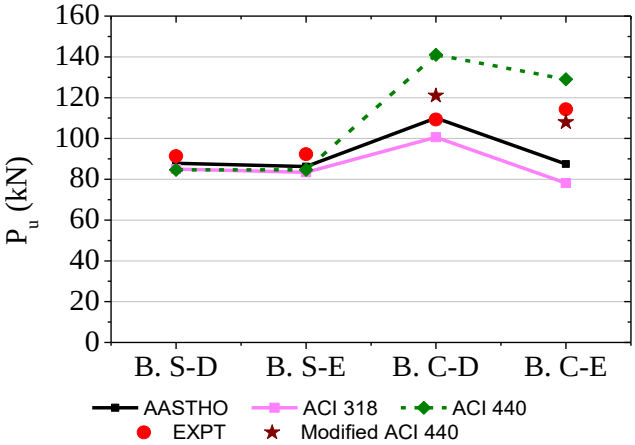

Figure 4-19: Predictions of P_u

It is noted that, among the examined models, only ACI 440.4R (2004) is used for

monolithic beams with CFRP tendons. Using it for segmental concrete beams considered in this study may lead to unconservative estimations as observed. As such, the strain reduction coefficient, Ω_u in Eq. 3 recommended by ACI 440.4R (2004) is modified to improve the predictions of f_{ps} and P_u in the cases of segmental concrete beams with CFRP tendons. Based on the experimental results conducted in this study, $\Omega_u = 1.7/(L_b/d_{ps})$ is suggested for the use in segmental concrete beams externally prestressed with CFRP tendons. The predicted results of f_{ps} and P_u obtained by the modified model are given in Tables 3-5 and Figs. 17-19. Although the modified model gives relatively large differences in the predictions of Δf_{ps}, it yields good predictions of P_u, with errors less than 10% for Beams C-D and C-E.

4.5 Conclusion

This chapter experimentally investigates the use of CFRP tendons as an external prestressing material on precast segmental concrete beams. Four large-scale segmental T-shaped concrete beams post-tensioned with both steel/CFRP tendons and different types of joints were cyclically tested under four-point loading up to failure. Main findings from the study are summarized as follows:

- CFRP tendons can be used in the replacement of steel tendons for the use in segmental concrete beams. All the beams with external CFRP tendons exhibited excellent load-carrying capacity and deflection at the ultimate stage.

- The beams with steel tendons failed by both the yielding of tendons and crushing of concrete on the compression zone, in which the yielding of steel tendons took place before the failure of the concrete. As such, the beams with steel tendons failed in a more ductile manner than that of beams with CFRP tendons. The beams with CFRP tendons failed by either rupture of the tendons or crushing of compression concrete, which were brittle and explosive.

- The type of joints had an insignificant effect on the overall flexural behaviour of the tested beams. Both the beams with epoxied and dry joints behaved similarly under the applied loads up to the ultimate stage, though the beams with epoxied joints showed larger cracking/opening loads.

- Even though all the tested beams showed non-linear behaviours after the joints opened/cracked, the levels of non-linearity between the beams with CFRP tendons

differed from the beams with steel tendons. In the beams with steel tendons, the yielding of the steel tendons resulted in significant losses in the beams' stiffness while in the beams with CFRP tendons the reduction in the beams' stiffness due to the crushing of compressive concrete were much less severe.

- In the case of the beams with CFRP tendons, the tendon stress increment was almost linearly related to the opening of the joints and the deflection of the beam throughout the whole loading stages. In the case of beams with steel tendons, this linear relationship was also valid up to the yielding of steel tendons. After that, the tendon stress increment showed a non-linear relationship with the opening of joints or the deflection of the beams.

- Steel tendons achieved very high stress values at the ultimate stage, which were about 95% of their ultimate tensile strength. In contrast, CFRP tendons ruptured at quite low stress levels, which were approximately 77% of its nominal breaking strength.

- All the codes examined in this study showed good predictions of f_{ps} and P_u for the beams with steel tendons. However, they encounter large scatter for the beams with CFRP tendons, which requires further investigations. A modification of the strain reduction coefficient, Ω_u in ACI 440.4R code yields better predictions of strength of PSBs with external CFRP tendons.

4.6 References

AASHTO (1999). *Guide Specifications for Design and Construction of Segmental Concrete Bridges: 2nd Ed with 2003 Interim Revis*, American Association of State Highway and Transportation Officials, Washington, DC.

AASHTO LRFD (2012). *Bridge Construction Specifications, 6th Edition, U.S. Units*, American Association of State Highway and Transportation Officials, Washington, DC.

ACI 318 (2015). *Building code requirements for structural concrete and commentary*, ACI 318-14, American Concrete Institute, Farmington Hills, MI.

ACI 440.4R (2004). *Prestressing concrete structures with FRP tendons (Reapproved 2011)*, American Concrete Institute, Farmington Hills, USA.

BS 8110 (1997). *Structural use of concrete*, British Standards Institution, London.

Dextra Group. "CFRP tendons." https://www.dextragroup.com/offices/dextra-building-products-limited.

Harajili, M., and Kanj, M. (1992). Ultimate flexural strength of concrete members prestressed with unbonded tendons. *Structural Journal*, 88(6), 663-674.

Harajli, M., Khairallah, N., and Nassif, H. (1999). Externally prestressed members: evaluation of second-order effects. *Journal of Structural Engineering*, 125(10), 1151-1161.

He, Z., and Liu, Z. (2010). Stresses in External and Internal Unbonded Tendons: Unified Methodology and Design Equations. *Journal of Structural Engineering*, 136(9), 1055-1065.

Jiang, H., Cao, Q., Liu, A., Wang, T., and Qiu, Y. (2016). Flexural behavior of precast concrete segmental beams with hybrid tendons and dry joints. *Construction and Building Materials*, 110, 1-7.

Le, T. D., Pham, T. M., and Hao, H. (2020). Numerical study on the Flexural Performance of Precast Segmental Concrete Beams with Unbonded Internal Steel Tendons. *Building and Construction Materials*, 248: 118362.

Le, T. D., Pham, T. M., Hao, H., and Hao, Y. (2018). Flexural behaviour of precast segmental concrete beams internally prestressed with unbonded CFRP tendons under four-point loading. *Engineering Structures*, 168(2018), 371-383.

Le, T. D., Pham, T. M., Hao, H., and Yuan, C. (2019). Performance of precast segmental concrete beams posttensioned with carbon fiber-reinforced polymer (CFRP) tendons. *Composite Structures*, 208, 56-69.

Li, G., Yang, D., and Lei, Y. (2013a). Combined shear and bending behavior of joints in precast concrete segmental beams with external tendons. *Journal of Bridge Engineering*, 18(10), 1042-1052.

Li, G., Zhang, C., and Niu, C. (2013b). Experimental study on shear behavior in negative moment regions of segmental externally prestressed concrete continuous beams. *Journal of Bridge Engineering*, 18(4), 328-338.

Lou, T., Lopes, S. M., and Lopes, A. V. (2016). Response of continuous concrete

beams internally prestressed with unbonded FRP and steel tendons. *Composite Structures*, 154(2016), 92-105.

MacGregor, R. J. G. (1989). Evaluation of strength and ductility of a three-span externally post-tensioned box girder bridge model. University of Texas at Austin.

Naaman, A. E., and Alkhairi, F. (1991). Stress at ultimate in unbonded prestressing tendons: Part 2—Proposed Methodology. *ACI Structural Journal*, 88(6), 683-692.

Naaman, A. E., Burns, N., French, C., Gamble, W. L., and Mattock, A. H. (2002). Stresses in unbonded prestressing tendons at ultimate: Recommendation. *Structural Journal*, 99(4), 518-529.

Park, R. (1989). Evaluation of ductility of structures and structural assemblages from laboratory testing. *Bulletin of the New Zealand national society for earthquake engineering*, 22(3), 155-166.

Pisani, M. A. (1998). A numerical survey on the behaviour of beams pre-stressed with FRP cables. *Construction and Building Materials*, 12(4), 221-232.

Saibabu, S., Srinivas, V., Sasmal, S., Lakshmanan, N., and Iyer, N. R. (2013). Performance evaluation of dry and epoxy jointed segmental prestressed box girders under monotonic and cyclic loading. *Construction and Building Materials*, 38, 931-940.

Sika Australia Sikadur-30. *https://aus.sika.com/*.

Tan, K.-H., and Ng, C.-K. (1997). Effects of deviators and tendon configuration on behavior of externally prestressed beams. *ACI Structural Journal*, 94(1), 13-22.

Tan, K. H., and Tjandra, R. A. (2007). Strengthening of RC continuous beams by external prestressing. *Journal of Structural Engineering*, 133(2), 195-204.

Wang, X., Shi, J., Wu, G., Yang, L., and Wu, Z. (2015). Effectiveness of basalt FRP tendons for strengthening of RC beams through the external prestressing technique. *Engineering Structures*, 101, 34-44.

Yuan, A., Dai, H., Sun, D., and Cai, J. (2013). Behaviors of segmental concrete box beams with internal tendons and external tendons under bending. *Engineering Structures*, 48, 623-634.

Yuan, A., He, Y., Dai, H., and Cheng, L. (2014). Experimental Study of Precast

Segmental Bridge Box Girders with External Unbonded and Internal Bonded Posttensioning under Monotonic Vertical Loading. *Journal of Bridge Engineering*, 20(4), 04014075.

Zhou, X., Mickleborough, N., and Li, Z. (2005). Shear strength of joints in precast concrete segmental bridges. *ACI Structural Journal*, 102(1), 3.

CHAPTER 5 NUMERICAL STUDY ON THE FLEXURAL PERFORMANCE OF PRECAST SEGMENTAL CONCRETE BEAMS WITH UNBONDED INTERNAL STEEL TENDONS[4]

Abstract

This chapter presents a numerical investigation of the flexural performance of precast segmental concrete beams (PSBs) with unbonded internal steel tendons. Numerical models developed in this study using ABAQUS software capture well the responses of the PSBs reported by previous studies. This is the first time a three-dimensional numerical model is built and successfully validated against experimental results of PSBs in the literature. Based on the verified numerical model, intensive simulations of performances of segmental beams with different parameters and various conditions, i.e. tension-controlled, compression-controlled and balanced sections, are carried out. Based on the numerical results, the flexural behaviour of PSBs under four-point loading is extensively discussed regarding the failure modes, joint opening, stress increment in the tendon and the stress transfer mechanism. A parametric study is also conducted and the results show that the effective prestress, prestressing steel reinforcement ratio, and span length-to-tendon depth ratio strongly affect the load-carrying capacity, ductility, tendon stress increment, joint opening and failure modes of PSBs with unbonded tendons, while the type of load, concrete strength and number of joints show insignificant effects on the flexural performance of the structure.

[4] This chapter is compiled from the following paper which was published in Building and Construction Materials:
Le, T. D., Pham, T. M., and Hao, H. (2020). Numerical study on the Flexural Performance of Precast Segmental Concrete Beams with Unbonded Internal Steel Tendons. *Building and Construction Materials*, 248: 118362.

5.1 Introduction

Precast segmental prestressed concrete beams (PSBs) have been increasingly used in many bridge construction projects around the world as this type of structure provides shorter construction time and better quality control. The use of unbonded tendons and dry joints are preferred for new segmental concrete bridge constructions since they enable fast installation and easy replacement in cases of deterioration. Since the analysis and design of structures with unbonded tendons are more complex due to the lack of bonding between the tendons and surrounding concrete, the current methods for prediction of deflection and the stress increment in the prestressing steel at the ultimate stage of PSBs with unbonded tendons are questionable (Yuan et al. 2014; Le et al. 2018; Le et al. 2019). Therefore, more comprehensive investigations are required for better understanding the performance of PSBs, and developing more reliable analysis, and design of such structures.

This chapter presents a numerical approach to simulate the flexural behaviour of PSBs with unbonded steel tendons using ABAQUS CAE (2014) commercial software. To the authors' best knowledge, this is the first time a three-dimensional numerical model is successfully developed and validated against experimental results of PSBs in the literature. The validated model is used to conduct intensive simulations of PSBs with different parameters. Based on the numerical results, influences of effective prestress, reinforcement ratio, span-to-depth ratio, concrete strength, joint number and load type on the performance of PSBs are thoroughly discussed.

5.2 Literature review

Even though this study focuses on the behaviour of PSBs, the effects of the investigated parameters on the performance of monolithic beams are also reviewed and discussed. In the following sections, the influences of various parameters on the structural behaviour of monolithic beams are presented first.

5.2.1 Effect of the span-to-depth ratios on the performance of PSBs

The effects of the span-to-depth ratios of monolithic beams, L/d_{ps}, were studied by several researchers. Harajli (1990) theoretically investigated the influence of span-to-depth ratio on the stress increment of beams with unbonded internal tendons. A wide range of L/d_{ps} was studied ranging from 5 to 50. It was found that increasing L/d_{ps} significantly decreased the stress increment, Δf_{ps}, at the ultimate stage. In addition, the

reduction in the stress increment with the increase in L/d_{ps} is directly related to the length of a plastic region in the member. As such, beams loaded with three-point loading encountered a higher reduction in Δf_{ps} with increasing L/d_{ps} as compared to beams loaded with four-point loading because the first one had a shorter plastic region than the second one. It is noted that the plastic hinge herein refers to the compressive concrete regions at and close to the loading points. On the other hand, Harajli and Kanj (1992) conducted an experimental investigation on beams with the range of L/d_{ps} between 8 and 20 and found that the load type (third-point or four-point loadings) and the L/d_{ps} ratio did not have significant effects on the stress increment at the ultimate stage, which contradicted earlier analytical studies by Harajli (1990). However, no explanations for this contradictory observation were provided by the authors. Tanchan (2003) conducted a numerical investigation and found that L/d_{ps} ratio greatly affected the ultimate moment capacity of the member while only a slight effect was observed for the change in Δf_{ps}. For instance, the ultimate moment capacity decreased by 50% for both four-point and three-point loadings when L/d_{ps} increased from 10 to 45. Meanwhile, Δf_{ps} slightly decreased by 9% for four-point loading and by 1% for three-point loading as the L/d_{ps} ratio increased from 10 to 35. Those values were 18% and 2% for the case of four-point loading and three-point loading respectively when the L/d_{ps} ratio increased from 35 to 45.

Meanwhile, there have been no studies on the effect of L/d_{ps} on the structural behaviour of segmental beams. Instead, the effect of shear span-to-depth ratio, a/h, on the shear resistance capacity of the structures has been studied by several researchers. Li et al. (2013b) conducted an experimental study on segmental simply-supported beams prestressed with external tendons under combined shear and bending forces and found that for the beams with the same type of joints, the shear resistance of joint decreased as a/h increased. When a/h changed from 1.5 to 3.5, the shear force in the joint plane at the ultimate stage reduced respectively by 45.4% and 42.8% for epoxied and dry joints although the ultimate moment capacity increased by 22.9% and 28.8%, respectively. Similar results were observed in the tests by Li et al. (2013a) on segmental concrete continuous beams with external tendons as the shear span ratio is inversely proportional to the shear resistance of the structure. The shear span ratio also showed an influence on the failure mode of the specimens. For the beams with epoxied joints which failed by compression shear, the larger is the shear span ratio, the less

number and sparse distribution of the shear compressive cracks are.

As can be seen from the above review that the effect of *a/h* on the shear behaviour of segmental beams has been reported in the literature while the effect of L/d_{ps} on the flexural behaviour of segmental beams has not been addressed yet. The understandings of this parameter on the failure mode, stress increment in the tendons, and joint opening are necessary to attain better predictions of the performance of segmental beams under flexural loading.

5.2.2 Influence of effective prestress on the performance of PSBs

The effective prestress in the tendons, f_{pe}, is one of the main factors that strongly affects the performance of prestressed concrete beams. In the case of monolithic beams with unbonded tendons, f_{pe} was found to affect the failure modes, crack patterns and plastic rotation capacity of the structure (Pannell 1969; Tam and Pannell 1976; Tan and Ng 1997). The beams with high f_{pe} behaved rather like a beam with bonded tendons, and formed a deep compression zone with considerable concrete distress, together with a number of cracks in the tension zone. On the other hand, the beams with low f_{pe} showed a quite shallow compression zone but exhibited a much greater capacity for plastic rotation before failure. The beams with low f_{pe} developed two or three widely spaced cracks and only one of which continued to widen under the applied loads. Tanchan (2003) conducted a numerical analysis on beams with unbonded tendons with span-to-depth ratios L/d_{ps} varying from 10-18.5 and observed that f_{pe} slightly affected the ultimate moment capacity M_u, but significantly affected the stress increment in the tendons, Δf_{ps}. As f_{pe} increased from 827 MPa to 1241 MPa, the ultimate moment capacity increased by 10% for both four-point loading and three-point loading while Δf_{ps} decreased considerably by 35%.

The effects of f_{pe} on the behaviour of PSBs were investigated in several studies (Turmo et al. 2005; Turmo et al. 2006b; Turmo et al. 2006c). The main conclusions can be summarized as follows: (1) f_{pe} directly impacts the joint opening load, at which the lower the f_{pe}, the lower the joint opening load; (2) f_{pe} shows no influence on the stiffness of the structure while joints are closed, but strongly affects the stiffness of the structure once the joints open, i.e. the higher the f_{pe}, the stiffer the structure; (3) the maximum deflection at failure is also affected by the prestressing force - the higher f_{pe}, the larger the deflection at failure; and (4) the increase in f_{pe} leads to the increases in

the load-carrying capacity of the structure. Turmo et al. (2005) also noted that a minor decrease in the actual prestressing can lead to a rapid loss of safety of the structure.

It is seen from the above review that studies have been conducted to investigate the effects of f_{pe} on the segmental beams' stiffness, join opening, strength and deflection capacity of the structure. However, it is noted that these studies were conducted on segmental beams with external tendons, no studies on segmental beams with unbonded internal tendons have been reported. Furthermore, the effects of f_{pe} on the flexural performance of segmental beams regarding failure modes, stress increment in the tendons, ultimate strength and deflection capacity for different failure modes such as tension-controlled or compression-controlled sections have not yet been reported in the previous studies, which will be addressed in this study.

5.2.3 Effect of amount of prestressing steel on the performance of PSBs

Amount of prestressing steel, A_{ps}, is another factor strongly affecting the strength and deflection capacity of the beams with unbonded tendons. In case of monolithic beams with unbonded tendons, it was found that as the area of prestressing steel increased, the ultimate strength capacity of the structure increased, but the deflection capacity decreased. In other words, the beam is less ductile with the increase of the area of the prestressing steel (Tao and Du 1985; Tanchan 2003; Lou et al. 2012; Lou et al. 2017). All the beams tested by Tao and Du (1985) with low values of combined reinforcement ratio were very ductile as they underwent large deflections of 90 to 120 mm (1/47 to 1/35 of the effective span) at failure while that for beams with higher values of combined reinforcement ratio was about 40 to 50 mm (1/105 to 1/93 of effective span). Moreover, the increment of stress in the tendons was also affected by A_{ps}. When A_{ps} increased from 161 mm^2 to 742 mm^2, Δf_{ps} considerably reduced by 35% as observed in the study by Tanchan (2003). Lou et al. (Lou et al. 2012; Lou et al. 2017) conducted a numerical study on beams prestressed with unbonded fibre-reinforced polymer (FRP) tendons and observed that the ultimate deflection decreased consistently with the increase of prestressing reinforcement ratio. Lou et al. (2016) examined the tendon stress increment with the variation of prestressing reinforcement ratio and found that the tendon stress increment at the ultimate stage decreased almost linearly as the reinforcement ratio increased.

In the case of segmental beams, to the authors' best knowledge the effect of A_{ps} on the

flexural performance of PSBs with unbonded tendons have not been reported yet. Instead, the effects of the use of hybrid tendons were investigated by several researchers. Yuan et al. (2013) experimentally investigated the behaviour of PSBs with combined external and internal tendons under bending, in which the internal tendons were bonded to concrete. The authors concluded that the tendon ratio between the internal and external tendons had a significant effect on the strength capacity and ductility of the structure. The more internal tendons were used, the higher load-carrying capacity and better ductility the beams achieved. This phenomenon is attributed to the fact that the bonding effect helps the beams with bonded tendons better mobilize the tendon strain and the use of internal tendons discarded the second-order effect occurring in the external tendons. These effects allowed the beams with more internal bonded tendons to achieve higher load-carrying capacity and deflection capacity. Therefore, the ratio between internal and external tendon not less than 1:1 was recommended by Yuan et al. (2013). This effect of tendon ratio is also valid for the case of segmental continuous concrete beams. Li et al. (2013a) conducted tests on segmental continuous beams and observed that the ultimate stresses in the external tendons in beams also having internal tendons were higher than those in beams having only external tendons. Jiang et al. (2016) studied simply supported segmental beams with hybrid tendons and also found that the use of hybrid tendons improved both the strength and ductility compared to beams with sole external tendons.

5.2.4 Effect of concrete strength on the performance of PSBs

The concrete strength, f'_c, considerably affects the ultimate strength capacity and ductility of monolithic concrete beams with unbonded tendons. Tao and Du (1985) tested monolithic beams with unbonded internal tendons and found that increasing f'_c led to increasing the tendon stress increment, strength, and deflection capacity of the beams. Similar results were observed in the study by Tanchan (2003). Furthermore, when f'_c increased, beams loaded under four-point loading exhibited greater increases in the ultimate moment capacity and stress increment in the tendons compared to the beams under three-point loading. When f'_c increased from 41 MPa to 82 MPa, the ultimate moment capacity was respectively increased by 10% for three-point loading and 15% for four-point loading, and Δf_{ps} was respectively increased by 20% for three-point loading and 40% for four-point loading (Tanchan 2003). To the authors' best knowledge, no studies on the effects of f'_c on the flexural behaviour of segmental

concrete beams with unbonded tendons have been reported in the literature.

5.2.5 Effect of joint's type, number, and location on the performance of PSBs

Joint type

The effect of joint type on the behaviour of segmental concrete beams has been well documented in the literature. It was found that segmental beams with epoxied joints obtained higher cracking load than beams with dry joints due to the additional tensile strength of concrete (MacGregor 1989; Saibabu et al. 2013). Loads at the first joint opening for the dry-joined specimen were about 27% less than those of the epoxy-joined specimens (Saibabu et al. 2013). Saibabu et al. (2013) also found that, in terms of the flexural strength, the maximum load and failure load of dry-joined specimens were 8.6% and 16.7% less than that of the epoxy-joined specimen, respectively. In terms of the shear strength, MacGregor (1989) found that the joint type had no effect on the shear strength of the segmental beams. Jiang et al. (2018), however, found that dry-joined specimens exhibited a lower shear strength capacity than the epoxied-joined specimens.

Regarding the rotation capacity and ductility, MacGregor (1989) found that the epoxy-joined beams showed a less rotation capacity than dry-joined beams. In the epoxy-joined beams, only a single joint or crack opened resulting in large rotations to be concentrated at a single location while several midspan joints opened causing rotations being distributed over several joints in the dry-joined beams. This redistribution of the rotations helped the dry-joined beams withstand larger cumulative rotations than epoxy-joined beams. This observation was also supported by experimental results presented in other studies (Le et al. 2018; Pham et al. 2018; Le et al. 2019). MacGregor (1989) also found that the use of epoxied joints did not provide any increase in the ductility of the segmental beams compared to the use of dry joints. This conclusion, however, is contrary to the results presented in recent studies on both simply-supported and continuous segmental beams (Li et al. 2013b; Li et al. 2013a), where beams with epoxied joints showed greater ductility compared to beams with dry joints.

Previous studies have observed that epoxied and dry joints exhibit different failure modes (Li et al. 2013b; Yuan et al. 2014; Le et al. 2018; Le et al. 2019). The failure of epoxied joints developed in the concrete adjacent to the segment interface. In contrast, the failure of dry joints took place at the interfaces (Li et al. 2013b; Yuan et al. 2014).

Similar observations were found in the previous studies (Le et al. 2018; Le et al. 2019) when testing segmental concrete beams with either dry and epoxied joints and prestressed with CFRP tendons. The response of epoxied joints was brittle and failed in a sudden manner when the applied load reached its cracking/opening load. However, after the epoxied joints opened, i.e. cracked, it exhibited similar behaviour to the dry joints under the applied load. Both the beams with dry and cracked epoxied joints underwent various load cycles until they reached the ultimate stage (Le et al. 2018; Le et al. 2019).

Joint number and joint location

The effect of the number of joints on the performance of segmental beams was examined in a limited number of studies. Jiang et al. (2016) found that the beam with two joints showed smaller flexural strength than the beam with seven joints. As observed in the tests, the flexural strength of the two-joint segmental beam with hybrid tendons was 12.8% less than that of the seven-segmental beam. This is due to a high concentration of rotation and deflection at individual joints in the two-segmental beams as explained by the authors. In addition, the two-joint segmental beams exhibited less deflection than the seven-joint segmented beam. Jiang et al. (2018) investigated the shear behaviour of PSBs with external tendons and found that with the increase in the number of joints, the shear strength and deflection of PSBs with external tendons increased. They observed that the stiffness of the segmental beams decreased when the number of joints increased, which caused the beam with a higher joint number to undergo larger deformation. In terms of joint's location, Li et al. (2013b) tested segmental beams with external tendons and found that the joint location had a significant influence on the joint bearing capacity, particularly when the load was applied to the immediate vicinity of the joints. For beams with the same joint types, the joint resistance reduced when the joint locates at or near the midspan.

It can be summarized from the above review that joint type was found to have a significant effect on the flexural and shear capacity of the segmental beam, i.e. epoxied joints increased the cracking load, ultimate flexural and shear strength of the segmental beam but limited the beam's rotation capacity. However, there is a controversy regarding the ductility as several researchers observed an increase in the beam's ductility while others did not. In terms of the number of joints, researchers found that

reducing the number of joints led to a lower flexural and shear strength capacity of the segmental beam, but increasing the number of joints led to the decrease in the beam's stiffness as concluded in the study by Jiang et al. (2018). In terms of joint's location, Li et al. (2013b) found that the joint resistance reduced when the joint approaches the beam's midspan. This study will further investigate the effect of a number of joints on the flexural behaviour of the segmental beams with unbonded internal tendons.

5.2.6 Effect of load type on the performance of PSBs

Previous studies showed that type of load, i.e. three-point or four-point loadings, had an insignificant effect on the flexural behaviour of monolithic beams with unbonded tendons (Harajli and Kanj 1992; Tanchan 2003). Harajli and Kanj (1992) conducted an extensive test program on concrete monolithic beams prestressed or partially prestressed with unbonded tendons. The beams were tested under three-point loading and four-point loading and the tested results showed that the type of load had an insignificant effect on the nominal flexural characteristics of the beams. Tanchan (2003) carried out a numerical study on monolithic beams prestressed with unbonded internal tendons and the results revealed that the change in the type of load had a minor change in the bending moment of the beams at the ultimate stage. However, Harajli et al. (1999) found that the beams under three-point loading tended to mobilize less deflection at the ultimate stage compared to beams under four-point loading because it developed smaller equivalent plastic hinge length at failure. Yuan et al. (2014) tested segmental beams with external tendons and observed that both the beams subjected to four-point loading and three-point loading had the same bending moments at the onset of joint opening but the latter beam exhibited a higher bending moment at the ultimate stage compared to the former one. No studies have been done to investigate the effect of loading types on the flexural behaviour of the segmental beams, except the previous study by Yuan et al. (2014). As such, further studies are necessary to obtain sufficient data in order to be able to quantitatively predict the behaviour of the segmental beams with unbonded tendons under different loading types.

5.2.7 Contribution of conventional steel reinforcements

For the segmental concrete beams, the longitudinal steel bars are cut-off at the joints' locations. As such, there is theoretically no contribution of longitudinal reinforcement to the tension force of the section. This was confirmed by previous studies, which were

conducted on segmental concrete beams with either steel or CFRP tendons with dry/epoxied joints (Le et al. 2018; Le et al. 2019). Similar conclusions were also reached by other studies (Yuan et al. 2014; Jiang et al. 2016) and confirmed that the longitudinal reinforcement contributed little to the flexural capacity of the segmental beams.

In terms of the contribution of the transverse steel reinforcement on the behaviour of PSBs, Turmo et al. (2006c) studied the shear behaviour of segmental beams with external tendons and found that the shear reinforcement had a minor contribution to the shear strength of the structure. After joint opening, the shear was resisted solely by the concrete on the top fibre, which was in compression. As such, no need to provide hangover steels for the shear transfer as concluded by the authors. Similar conclusions were given in recent studies (Li et al. 2013b; Jiang et al. 2016; Le et al. 2018) in which it was found that stirrups contributed little to the shear capacity of the structure because it is governed by weaker sections at the joints. Meanwhile, in the case of continuous segmental beams, Li et al. (2013a) observed that the contribution of stirrups is large than that in simply-supported beams. The contribution of stirrups to the shear strength was 14-21% of the total shear capacity.

5.3 Description of Finite Element Model

This section describes the use of ABAQUS CAE (2014) software to simulate the behaviour of segmental concrete beams internally prestressed with unbonded tendons. Two segmental concrete beams (Beams BS1 and BC1) reported in the study by Le et al. (2018) are simulated first to verify the accuracy of the numerical model. The two beams had T-section and were 400-mm in height and 3.9-m of overall length. Each beam consisted of four segments, which were made of reinforced concrete and had the length of 800 mm and 1150 mm, respectively. Two steel/CFRP tendons, which were internally unbonded to the concrete, were used to join these segments (Figure 5-1) More details of the beams' dimension, reinforcement, and material properties were presented in Section 2.2 of Chapter 2.

Three-dimensional solid finite elements are used to simulate the response of the different components of the finite element models. Eight-node linear brick, reduced integration hexahedral elements (C3D8R) are selected to model concrete elements, prestressing tendons, and supplementary elements including steel loading plates,

anchor blocks and steel plates at the two ends of the beam. Two-node linear 3-D truss elements (T3D2) are selected to simulate the conventional steel reinforcements (Figure 5-2).

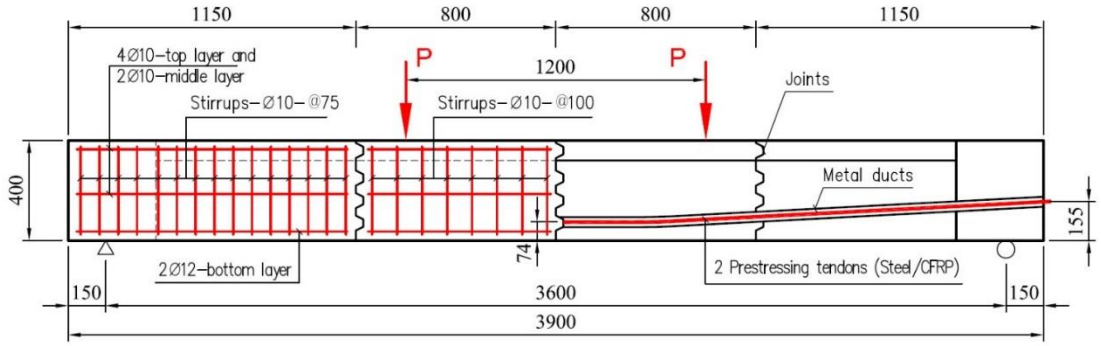

(a) Detailed dimensions of the tested beams in Le et al. (2018)

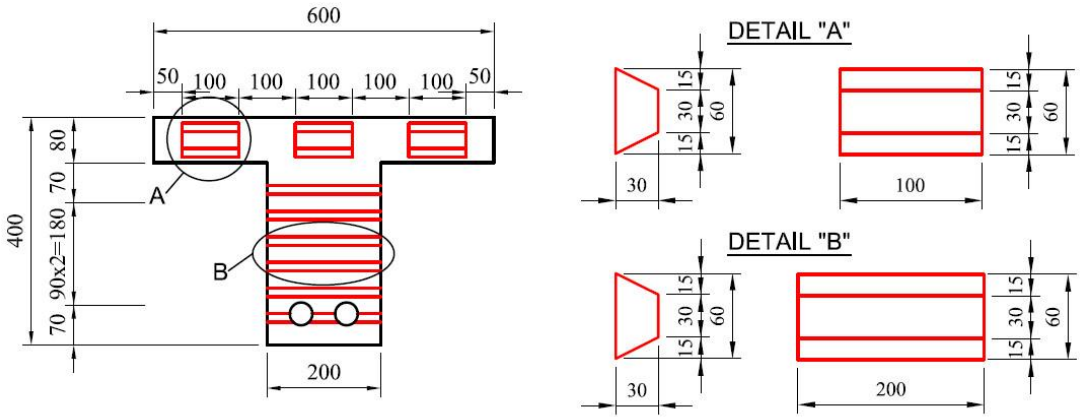

(b) Multiple shear-keyed joints

Figure 5-1: Details of beams used in validation (repeated Figures 2-1 and 2-2 of Chapter 2 for convenience)

5.3.1 Concrete material model

Concrete damage plasticity (CDP) model incorporated in ABAQUS CAE (2014) is used to model concrete elements. The CDP model is able to capture the elastic and plastic behaviours of concrete for damage characteristics in both compression and tension. It can be applied for concrete subjected to static and cyclic loadings.

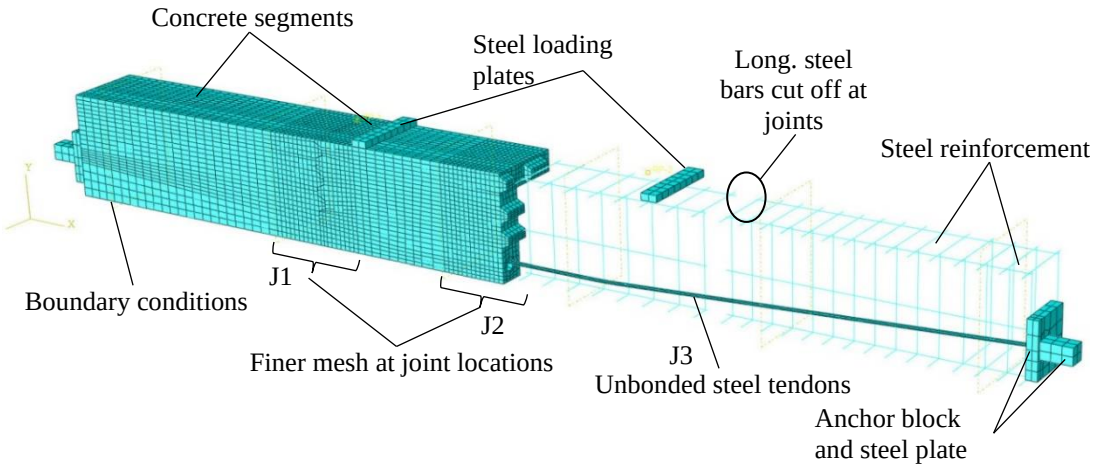

Figure 5-2: Components of the finite element model: symmetricity along beam's cross-section

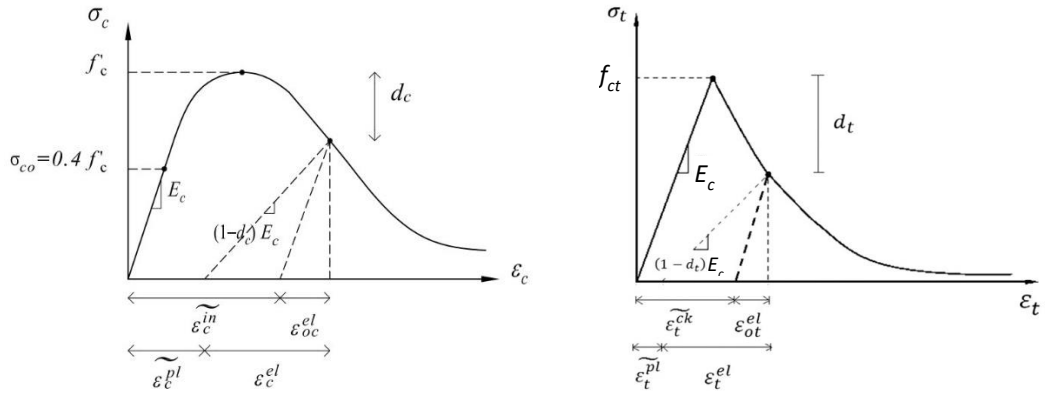

(a) Compression behaviour (b) Tension behaviour

Figure 5-3: CDP model for concrete (Abaqus 2014)

General parameters of the CDP model are given as follows (Yapar et al. 2015): dilation angle ψ, flow potential eccentricity e, and viscosity parameter μ, are equal to 30°, 0.1, and 0.001, respectively; the ratio of initial equibiaxial compressive yield stress to initial uniaxial compressive yield stress, σ_{b0}/σ_{c0} = 1.16; and the ratio of the second stress invariant on the tensile meridian to the compressive meridian, K_c = 0.667. These material parameters are also summarized and listed in Table 5-1.

The stress-strain curve proposed by Carreira and Chu (1985) is adopted in this study for concrete under compression. The relationship is expressed as follows:

$$\sigma_c = \frac{\beta\left(\varepsilon_c/\varepsilon_c^{'}\right) f_c^{'}}{\beta - 1 + \left(\varepsilon_c/\varepsilon_c^{'}\right)^{\beta}} \tag{5.1}$$

where f'_c and ε'_c are the compressive concrete strength (MPa) and its corresponding

strain; σ_c and ε_c are the stress and strain of concrete, respectively; β is a material parameter which depends on the shape of the stress-strain diagram. A detailed procedure to compute β is provided in Carreira and Chu (1985). It is noted that a linear stress-strain relationship is assumed up to 40% of the concrete maximum compressive strength in the ascending branch (Shamass et al. 2014) as shown in Figure 5-3.

Inelastic strain $\dot{\varepsilon}_c^{in}$ in Figure 5-3(a) is assigned in CDP model for the compression behaviour, $\dot{\varepsilon}_c^{in} = \varepsilon_c - \varepsilon_{oc}^{el}$, where E_c is the concrete modulus and $\sigma_{oc}{}^{el}$ is the concrete elastic strain in compression, $\varepsilon_{oc}^{el} = \frac{\sigma_c}{E_c}$. The compressive damage parameter d_c is also assigned in the CDP model. Birtel and Mark (2006) developed the following expression to compute d_c:

$$d_c = 1 - \frac{\sigma_c E_c^{-1}}{\varepsilon_c^{pl}\left(1/b_c - 1\right) + \sigma_c E_c^{-1}} \tag{5.2}$$

where ε_c^{pl} is the plastic strain, which is determined proportionally to the inelastic strain $\dot{\varepsilon}_c^{in}$ using a constant factor b_c, i.e., $\varepsilon_c^{pl} = b_c \dot{\varepsilon}_c^{in}$. The constant factor b_c is taken as 0.7 as proposed by Birtel and Mark (2006). In this study, concrete fails when it reaches the ultimate strain of 0.003 under compression.

The stress-strain relationship for concrete in tension is assumed to consist of a linear ascending part up to the cracking strength f_{ct} and a linear descending part to a total strain of approximately 10 times the strain at the tensile cracking ε_{ct} (Shamass et al. 2014). Similar to the concrete behaviour in compression, cracking strain $\dot{\varepsilon}_t^{ck}$ and tensile damage parameter d_t are used in the CDP model for the concrete in tension (Figure 5-3b). Cracking strain $\dot{\varepsilon}_t^{ck}$ is computed as $\dot{\varepsilon}_t^{ck} = \varepsilon_t - \varepsilon_{ot}^{el}$, in which $\varepsilon_{ot}^{el} = \frac{\sigma_t}{E_c}$, where ε_{ot}^{el} is the concrete elastic strain in tension. Tensile damage parameter d_t is calculated as follows:

$$d_t = 1 - \frac{\sigma_t E_c^{-1}}{\varepsilon_t^{pl}\left(1/b_t - 1\right) + \sigma_t E_c^{-1}} \tag{5.3}$$

In Eq. 5.3, ε_t^{pl} is the plastic tensile strain, $\varepsilon_t^{pl} = b_t \dot{\varepsilon}_t^{ck}$ and the parameter b_t is taken as 0.1 (Birtel and Mark 2006).

Table 5-1: Details material properties

Concrete	Compressive strength (MPa)	44
	Tensile strength (MPa)	2.65
	Elastic modulus E_c (GPa)	31.17
	Poisson's ratio	0.18
∅12 steel bars	Area (mm^2)	113
	Elastic modulus E_c (GPa)	200
	Yielding stress (MPa)	534
	Poisson's ratio	0.3
∅12 steel bars	Area (mm^2)	78.5
	Elastic modulus E_c (GPa)	200
	Yielding stress (MPa)	489
	Poisson's ratio	0.3
Steel tendons Grade 270	Area (mm^2)	78.5
	Elastic modulus E_c (GPa)	195
	Yielding stress (MPa)	1674
	Ultimate stress (MPa)	1860
	Poisson's ratio	0.3
CFRP tendons	Area (mm^2)	126.7
	Elastic modulus E_c (GPa)	145
	Yielding stress (MPa)	-
	Ultimate stress (MPa)	2450
	Shear strength (MPa)	262
	Poisson's ratio	0.27
CDP parameters	ψ	30°
	e	0.1
	σ_{b0}/σ_{c0}	1.16
	K_c	0.667
	μ	0.001

5.3.2 Reinforcement material model

The stress–strain curve proposed by Devalapura and Tadros (1992) is adopted in this study to model the prestressing steel as given in Eq. 5.4. For low-relaxation prestressing steel Grade 270, which was used in Le et al. (2018) and in this study, the constants *A*, *B*, *C*, *D* are taken as 887, 27613, 112.4 and 7.36, respectively.

$$f_{ps} = \varepsilon_{ps}\left[A + \frac{B}{\left\{1+\left(C\varepsilon_{ps}\right)^{D}\right\}^{1/D}}\right] \leq f_{pu} \tag{5.4}$$

For CFRP tendons, the isotropic elastic material model is chosen to model the tendons since CFRP tendons exhibit a linear stress-strain relationship up to the failure. The failure of the CFRP tendons is considered to occur when their nominal tensile strength f_{pu} (2450 MPa) is reached or when the shear stress in the tendon obtained from the simulation exceeds its nominal shear resistance. The nominal shear strength of the CFRP tendons is 262 MPa as reported in the previous studies (Le et al. 2018; Le et al. 2019).

An elastoplastic stress-strain material model is used for conventional steel reinforcements in both tension and compression (Xu et al. 2014). The longitudinal and transverse reinforcements are embedded into the concrete elements. Details of material properties are given in Table 5-1.

5.3.3 Contact mechanism

The surface-to-surface contact model incorporated in ABAQUS CAE (2014) is chosen to formulate the contacts between joint surfaces of the two adjacent segments (key-key contact), and the unbonded tendons vs the surrounding concrete (unbonded tendon-concrete contact). For the key-key contact, a friction coefficient of 0.7, which is based on previous experimental studies (Buyukozturk et al. 1990; Zhou et al. 2005), is selected to define the tangential behaviour while hard contact type is used to define the normal behaviour. The hard contact type allows surfaces to develop compression behaviour when they are in contact without penetration into each other and to separate in case of tension without tensile stress transferring through the interfacial interaction. For the unbonded tendon-concrete contact, frictionless is assumed between the tendon and the surrounding concrete to define the tangential behaviour and hard contact type

is used for the normal behaviour. Tie constraint contact type is used to model the contacts of steel loading plates to concrete, anchor blocks to steel end-plates, and steel end-plates to concrete.

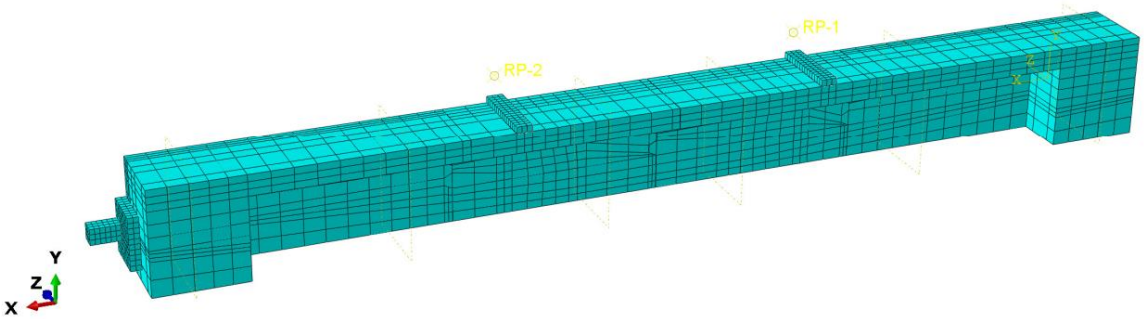

(a) 80 mm mesh size

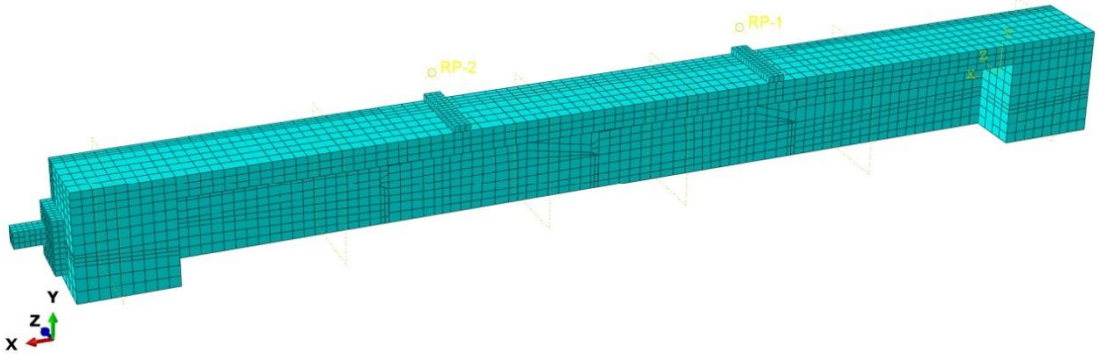

(b) 40 mm mesh size

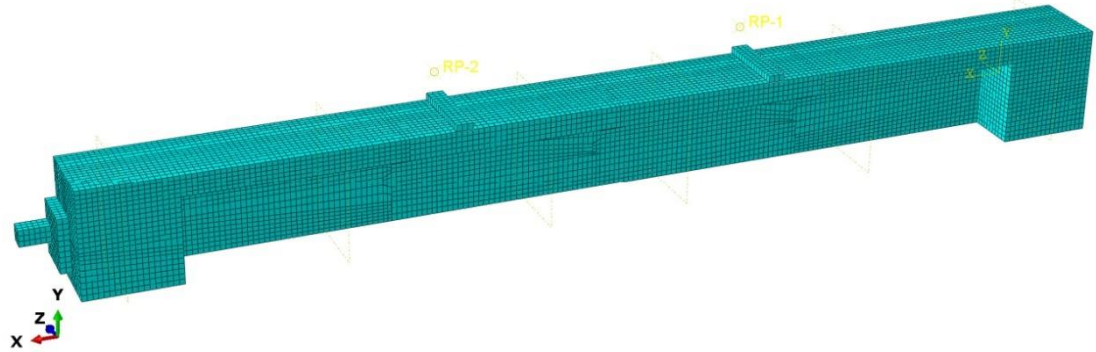

(c) 20 mm mesh size

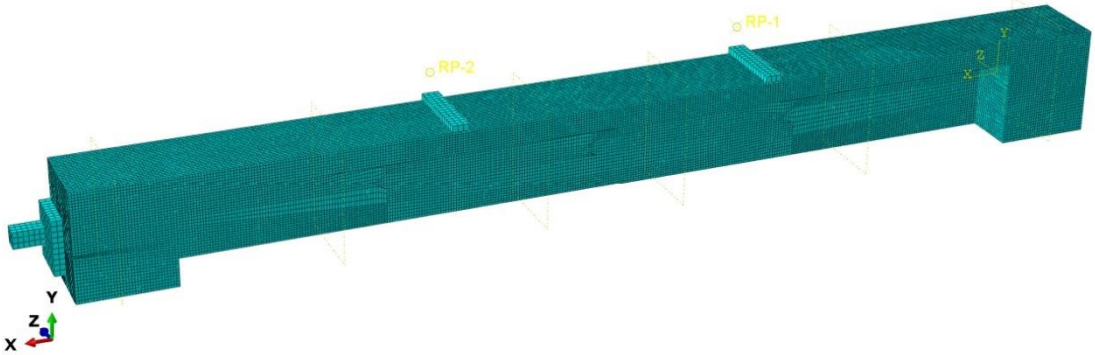

(d) 10 mm mesh size

Figure 5-4: Element mesh sizes used in convergence tests

5.3.4 Modelling procedure

The beam model is built symmetrically with regard to the beam's longitudinal axis at the centroid of the cross-section (Figure 5-2). For the concrete elements, the most critical areas occurred at joint locations where the cracking happened as observed in the experiment (Le et al. 2018; Le et al. 2019). A finer mesh with an element size of 20 mm, therefore, is applied for these areas compared to a courser mesh, with the element size of 40 mm for the other areas. The prestressing tendons and the conventional steel reinforcement are meshed with an element size of 20 mm. The remaining components including steel plates and anchors are meshed with an element size of 40 mm. It is noted that mesh convergence tests are carried out by halving the mesh size from 80 mm, 40 mm, 20 and 10 mm (Figure 5-4). The numerical results show that further reducing the mesh size under 40 mm does not considerably affect the results but requires a significantly high computation cost (Figure 5-5). Therefore, the mesh size of 20 mm close to the joints and 40 mm for other regions are used in this study. In total, the numerical model consists of 38,620 nodes and 30,013 elements including 27,093 solid elements and 2,920 truss elements.

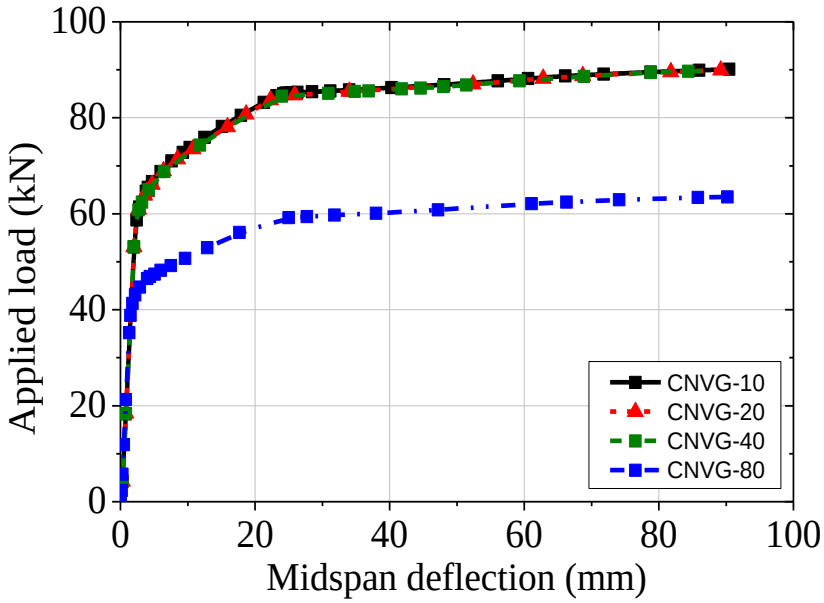

Figure 5-5: Convergence test results. Note: all the load-deflection curves were plotted up to a displacement of 89.9 mm to represent the experimental test result of Beam BS1

The prestressing effects in the model are specified using Predefined Fields function provided in ABAQUS CAE (2014). The effective prestress in the tendons f_{pe} after post-

tensioning is specified in the model to be equal to the values reported in the work by Le et al. (2018) for the tested beams. In the experiment, the applied load was exerted by two vertical hydraulic jacks placed symmetrically at one-third span length. Numerically, this is simulated by creating two boundary conditions vertically moving downward, which are also placed symmetrically at the one-third span length of the beam as shown in Figure 5-2.

5.3.5 Model validation

Experimental results are used to validate the numerical models in terms of the load-deflection responses and failure modes. As observed in Figure 5-6, the numerical models well capture the load-deflection responses of the tested beams by Le et al. (2018). For the case of Beams S1 with steel tendons, the test was stopped for safety reason at a very high loading level. At that point, the applied load was 96 kN and its corresponding mid-span deflection was 89.4 mm. In the numerical model, the applied load corresponding to the deflection of 89.4 mm is 91 kN, which differs by approximately -5.7% as compared to the experimental result (Figure 5-6a). In the case of Beam C1 with CFRP tendons, the numerical model also accurately predicts the applied load at the ultimate stage P_u. P_u obtained from the numerical model is approximately 115 kN, which is about 1.8% higher than the experimental result (113 kN). It is noted that the ultimate stage of Beam C1 is taken at a step where the shear stress obtained in the tendon exceeds its nominal shear resistance. At this step, the longitudinal tensile stress in the tendon is 1925 MPa, which has not reached its nominal tensile strength yet.

Failure modes of the tested beams are also well captured by the numerical models. As observed in the test of Le et al. (2018), both Beams S1 and C1 exhibited very similar concrete responses in the compression zone, i.e. concrete in the compression at the middle joint J2 crushed, whereas no damage was observed in the other joints (J1, J3). Numerical models capture the same failure modes as shown in Figure 5-6(b). In Figure 5-6(b), only a photo showing the failure mode of Beam S1 is provided for brevity. In the numerical model, concrete fails when it reaches the ultimate strain of 0.003 under compression. Yielding of steel tendons is also observed in the numerical model, which takes place before the crushing of the concrete. After that, the beam continues to deform under the applied load leading to the crushing of concrete on the top fibre when it reaches its ultimate strain as observed in the experiment. For Beam C1, the rupture

of the CFRP tendons is observed in the numerical model as also seen in the experimental test. The rupture of the CFRP tendons, which happens at the middle joint location, is due to the shear stress in the tendons generated by the applied load exceeded its nominal shear resistance. It is worth noting that the rupture of the CFRP tendons was observed in the experiment but the causes, i.e. by tensile or shear stress, were not clear. This numerical simulation has confirmed that shear stress primarily causes the rupture of the tendons.

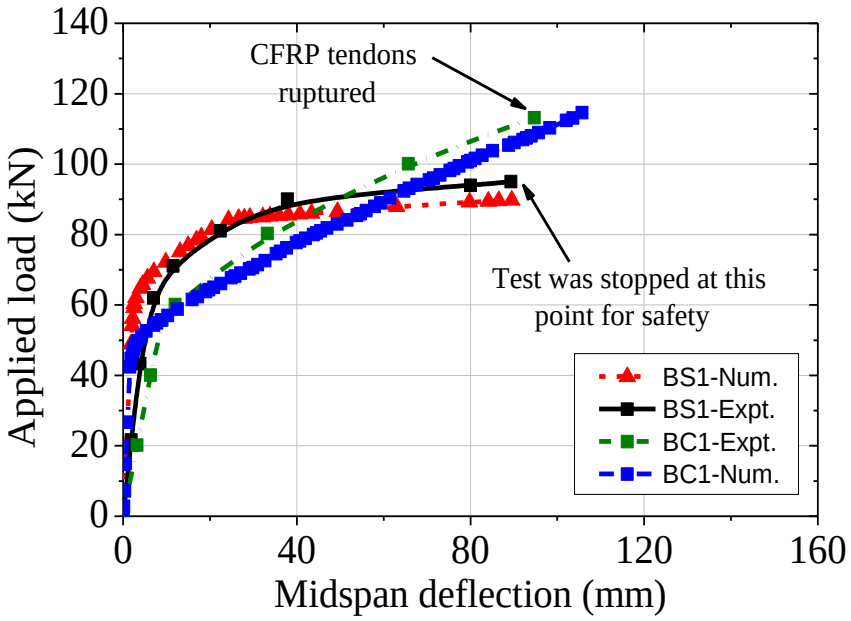

(a) Load-deflection curves

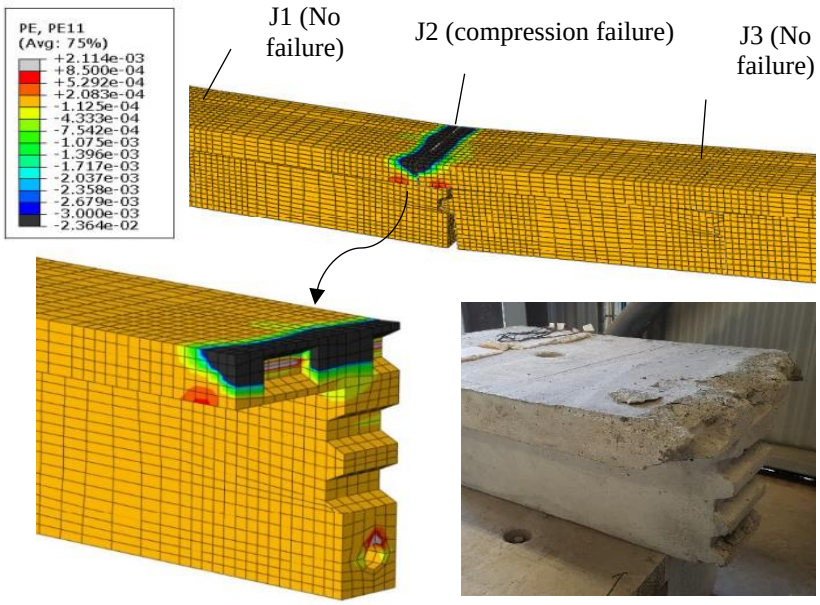

(b) Failure mode of Beam BS1

Figure 5-6: Numerical vs experiment results

From the above discussions, it is evident that the numerical model developed in this study is reliable and capable of simulating the behaviour of segmental concrete beams prestressed with unbonded internal tendons. In the next sections, intensive simulations are conducted using the validated model in this section to investigate the behaviour of PSBs with unbonded tendons under bending.

5.4 Flexural behaviour of segmental beams

5.4.1 Load-deflection curves: compression-controlled and tension controlled sections

Based on the calibrated models, various numerical models are built to investigate the load-deflection responses of PSBs with unbonded internal tendons. The beams' cross-section and conventional steel reinforcement configuration are maintained the same as the beam shown in Figure 5-2. All the beams are built with dry joints while different effective prestressing stress f_{pe}, amount of prestressing steel A_{ps}, concrete strength f'_c and span length to tendon depth ratio L/d_{ps} are investigated. All the beams are loaded under four-point loading as shown in Figure 5-2.

From the numerical results, there are two types of load-deflection responses for the PSBs with unbonded internal tendons (Figure 5-7a). Only the load-deflection curves of two beams are presented herein for brevity for which the curve of Beam SD25-118-069 represents a typical load-deflection curve of a beam failing in tension while the one of Beam SD25-284-02 represents a typical curve for a beam failing in compression. It is noted that Beam SD25-118-069 has the ratio of L/d_{ps} of 25, is prestressed with two 11.8-mm diameter tendons at an effective prestress ratio f_{pe}/f_{pu} of 0.69. Beam SD25-284-02 has the same beam's configuration and dimensions as of Beam SD25-118-069 except for the reinforcement ratio and effective prestress for which Beam SD25-284-02 comprises two 28.4-mm diameter tendons of f_{pe}/f_{pu} of 0.20. The load-deflection curves of these two beams are also generalized in Figure 5-7(b).

In the case of a tension-controlled section, the load-deflection curve of Beam SD25-118-069 is divided into two stages distinguished by a transition zone. In the first stage from Points 1 to 3, the beam exhibits a linear relationship between the applied load and deflection. Then, the middle joint starts to open at Point 3 creating a transition zone as observed in Figure 5-7(b). After that, the beam behaves nonlinearly up to failure in the second stage. The failure is due to the yielding of steel tendons starting

at Point 6, which occurs before the crushing of concrete in compression zone (Point 7).

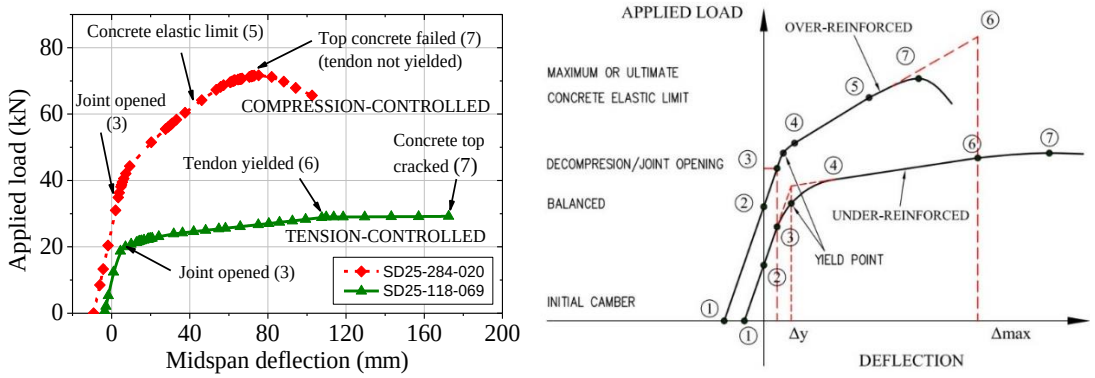

(a) Simulation (b) Generalized responses

Figure 5-7: Load-deflection curves

In the case of a compression-controlled section, Beam SD25-284-02 also exhibits two stages in the load-deflection curve with one inflection point. However, the failure of the beam is due to the crushing of concrete in compression (Point 7), which takes place before the yielding of tendons (Point 6) as observed in the figure. After the crushing of concrete, the beam does not show sufficient ductility but fails in a brittle manner, which is not desirable for structures from a ductility and safety viewpoint.

5.4.2 Joint opening and tendon stress increment

Figure 5-8 shows the opening of joints under the applied load. As can be seen from Figure 5-8(a) that for the beams investigated in this study all the joints open under the applied load at different opening rates. The opening concentrates in the middle joint J2 at midspan while the other joints show a much smaller magnitude of opening. The opening of Joints J1 (J3) of Beam SD25-118-069 (tension-controlled beam) remains constant after the tendon yields. This phenomenon is also observed in the experimental tests by Le et al. (2018) in which the two side joints J1 and J3 of Beams BS1 and BC1 almost remained at the same opening level after the tendons yielded. These two beams were under-reinforced as reported by the authors. Meanwhile, that for joint J1 (J3) of Beam SD25-284-02 gradually reduces when the concrete in the compression zone reaches its elastic limit as defined in Figure 5-3(a). It can be stated at this stage that the opening level of side joints (other than middle joint) depends on the level of the prestressing reinforcement ratio. However, to draw a final conclusion on the level of opening of the side joints and how they behave under the applied loads, it requires

further studies in which the effects of parameters including the number of joints, joints' locations, joint types and the location of loading points need to be investigated. The total opening of all the joints under the applied load for the two beams is shown in Figure 5-8(b). As seen from the figure the shape of the applied load-opening curves are similar to the applied load-deflection curves shown in Figure 5-7. The load causing joints to open in Beam SD25-118-069 is about 53% of the ultimate load and that value is about 48% for the case of Beam SD25-284-020.

The opening of the joints leads to a dramatic increase in the tendon stress as observed in Figure 5-9(a). Beam SD25-118-069 shows an almost constant stress increment rate until the yielding of the tendon. In contrast, the tendon in Beam SD25-284-020 shows a higher rate in the stress increment after the concrete elastic limit is reached until the ultimate stage. It is worth mentioning that the tendon stress starts to increase at the beginning of the applied load, but with a low rate. In Beam SD25-118-069, the stress in the tendon only increases by approximately 1.3% of the effective stress f_{pe} at the onset of the joint opening, while that for the tendon in Beam SD25-284-020 is approximately 9.8%. Therefore, it can be deduced from this observation that the change in the tendon stress at the opening of the joints is significantly influenced by the amount of the prestressing steel which classifies the beam's behaviour as compression control or tension control. In other words, the contribution of steel tendons at the onset of joint opening depends on the reinforcement ratio, which draws attention during the analysis and design of this type of structure. The results from the present study revealed that for the PSBs under four-point loading the ratio f_{psYP}/ f_{pe} shows an almost linear relationship with the reinforcement ratio, where f_{psYP} is the stress in the tendons at the yield point as defined in Figure 5-7b.

The relationship between the stress increment and the joint opening is plotted in Figure 5-9(b). For the case of the tension-controlled beam, the stress increment shows an approximately linear relationship with joint opening up to the yielding of tendons. Meanwhile, in the case of the compression-controlled beam, this linear relationship is maintained to the point where the concrete reaches its elastic limit. After that, a highly non-linear relationship is observed between the stress increment and joint opening up to the ultimate stage. Similar behaviours are observed for the relationship between the stress increment and midspan deflection as shown in Figure 5-10(b). Meanwhile, the joint opening shows an almost perfectly linear relationship to the midspan deflection

up to the ultimate stage as observed in Figure 5-10(a). This linear relationship is valid for both the two beams investigated.

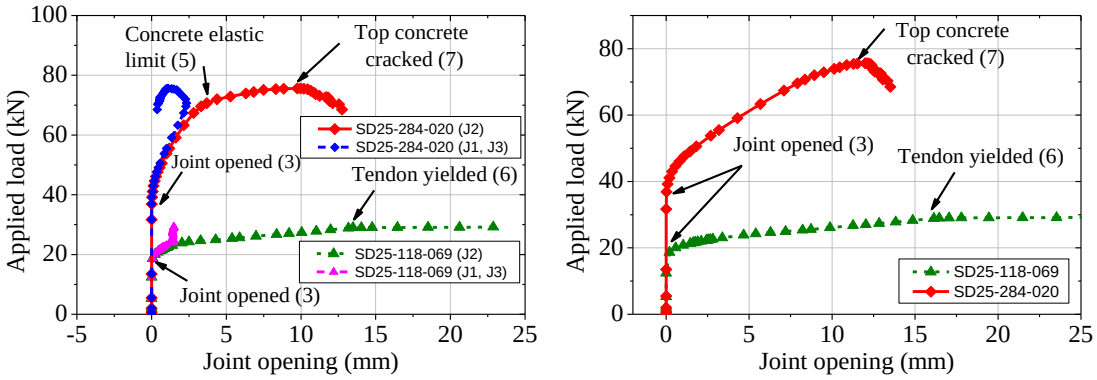

(a) each joint (b) total opening

Figure 5-8: Load vs joint opening curves (refer to Figure 5-2 for joints' locations)

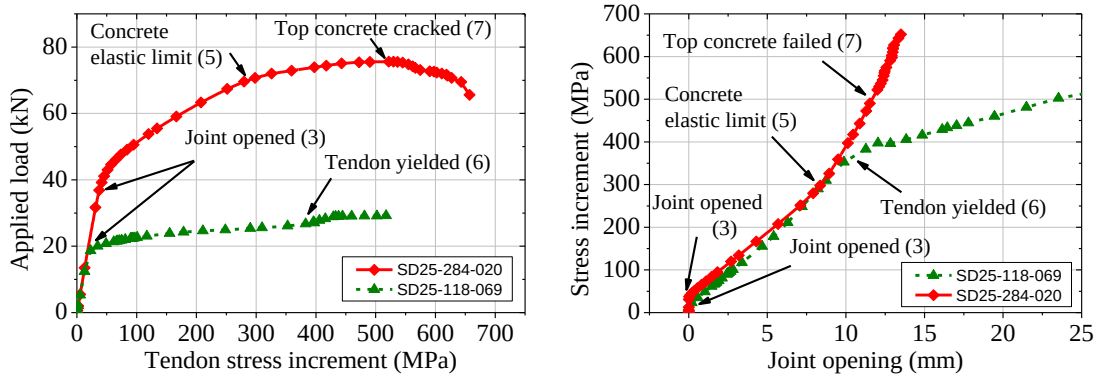

(a) Load vs stress increment (b) Stress increment vs total opening

Figure 5-9: Relations between applied load, stress increment and joint opening

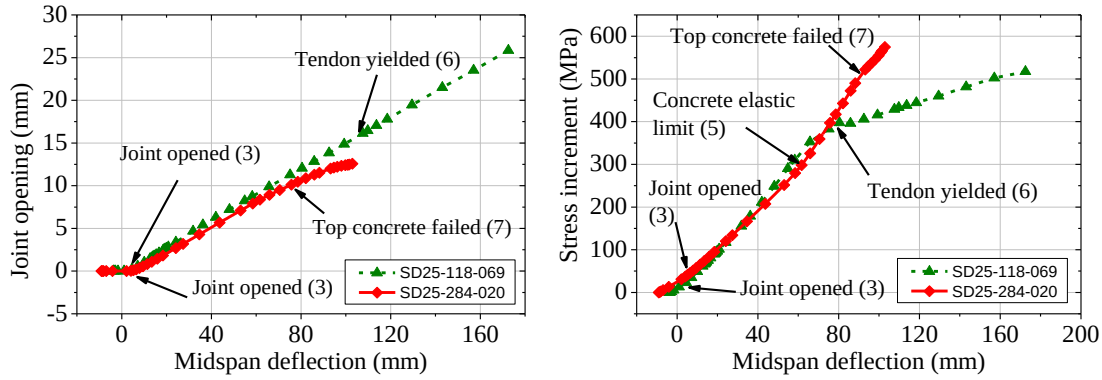

(a) Joint opening vs midspan deflection (b) Stress increment vs midspan deflection

Figure 5-10: Relations between joint opening, deflection and stress increment

5.4.3 Principle stresses contours in the beam

Figure 5-11 presents the principal compressive stresses contours in Beam SD25-118-069. Only compressive stresses of absolute values higher than 1.60 MPa are shown in the figure for a better visual examination. In the initial state (Figure 5-11a), most of the section's height is in compression due to the effect of prestressing, except for the top fibre which is in tension as a result of the eccentricity of the prestressing force. The inclination of the principal compressive stresses shows how the shear stresses are transferred across the web in the beam, which is clearly displayed in Figure 5-11(d) for the anchorage zones. Similar observations are observed for Beam SD25-284-020 as shown in Figure 5-12(a, d). After joints open there is a shift in the neutral axis as the top fibre of the section is in compression. As can be seen clearly in Figure 5-11(b) that the shear and bending moment are resisted by an arch, which is formed starting at the prestressing anchorages and developing towards the top compression zone at the midspan. Similar observations were obtained in the work of Turmo et al. (2005) on segmental concrete beams prestressed with external tendons as the authors found that the compression force is resisted by a concrete arch formed across all segments. In addition, it can be seen from Figure 5-11 and Figure 5-12 that the portion of the arch between the two loading points is narrower than the other portions and also the arch is narrower at the joint locations. Therefore, it can be deduced that the joint reduces the depth of the neutral axis. Figure 5-11(c) shows the field of principal compressive stresses at the ultimate stage, where the tendon yields in the case of Beam SD25-118-069. By comparing Figure 5-11(b) and Figure 5-11(c), it can be observed that the height of the compression zone of the section reduces. It means that the depth of the neutral axis reduces under the applied load as the neutral axis moves towards the top fibre. The change in the depth of the neutral axis from yield point to the ultimate stage is more significant in the case of Beam SD25-284-020 compared to that of Beam SD25-118-069 and at the ultimate stage, the neutral axis depth of Beam SD25-284-020 is greater than that of Beam SD25-118-069.

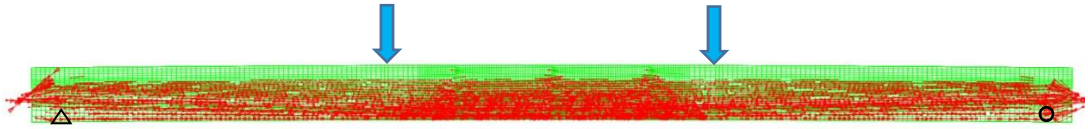

(a) Initial state (effect of f_{pe})

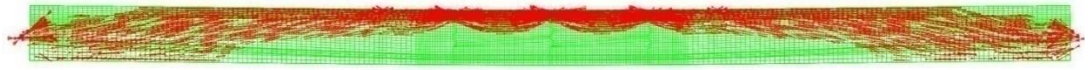

(b) At yield point

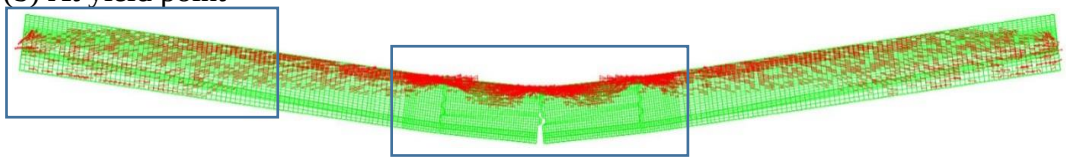

(c) At yielding of tendon

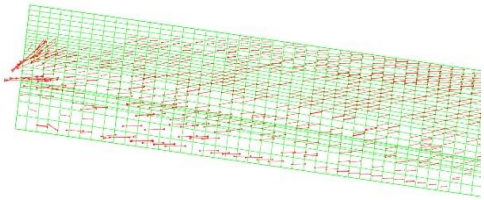

(d) End segment

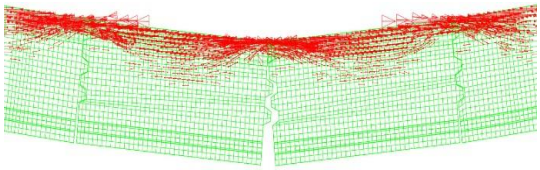

(e) Central segments

Figure 5-11: Beam SD25-118-069: principal compressive stress distributions

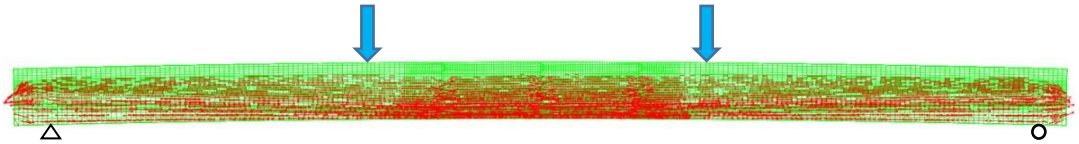

(a) Initial state (effect of f_{pe})

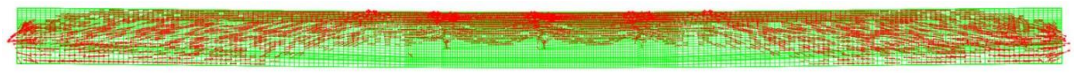

(b) At yield point

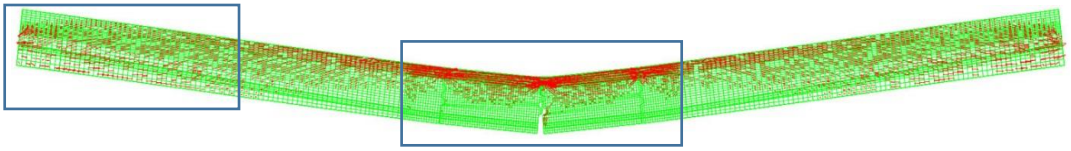

(c) At crushing of concrete in compression zone

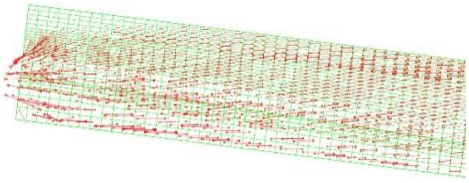

(d) End segment

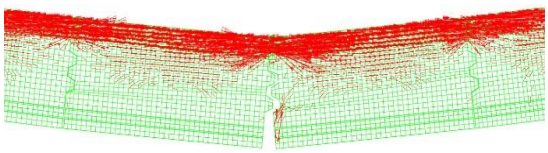

(e) Central segments

Figure 5-12: Beam SD25-284-020: principal compressive stress distributions

5.5 Parametric study

Various numerical models are built to investigate the effects of a number of parameters on the flexural performance of PSBs with dry joints and prestressed with unbonded internal steel tendons. All the beams have the same T-shaped cross-section, the configuration of conventional reinforcement as shown in Figure 5-1 and a ratio of L/d_{ps} of 25 except the beams in Section 5.5.3, where different values of L/d_{ps} are used. More details of the material properties defined in the models and beams' configuration for the parametric study are given in Tables 5-1 to 5-2.

Table 5-2: Beams' configuration for parametric study

Group	Specimen	f_{pe}/f_{pu}	ρ_{ps}	L/d_{ps}	f'_c	No. of joints	Load type
1	SD25-190-060	0.60					
(f_{pe})	SD25-190-074	0.74	0.64%	25	44	3	four-point loading
	SD25-190-081	0.81					
2	SD25-190-060		0.28%				
(A_{ps})	SD25-152-060	0.6	0.18%	25	44	3	four-point loading
	SD25-134-060		0.14%				
3	SD25-284-030			25			
(L/d_{ps})	SD35-284-030	0.3	0.64%	35	44	3	four-point loading
	SD45-284-030			45			
4	SD25-284-C34				34		
(f'_c)	SD25-284-C44	0.2	0.64%	25	44	3	four-point loading
	SD25-284-C54				54		
5	SD25-284-3J					3	
(No. of joints)	SD25-284-5J	0.3	0.64%	25	44	5	four-point loading
	SD25-284-9J					9	
6	SD25-284-4P						four-point loading
(Load type)	SD25-284-3P	0.3	0.64%	25	44	3	three-point loading

5.5.1 Influence of effective prestress, f_{pe}

In this section, three beams with different effective prestress levels are built to investigate the effect of f_{pe} (Table 5-2). It is found that f_{pe} strongly affects the flexural

performance of PSBs with unbonded tendons as the f_{pe} affects not only the load-carrying capacity and ductility of the segmental beams but also the failure modes of the structure. It is seen from Figure 5-13(a) that increasing f_{pe} leads to increases in the opening load and maximum load of the beam. As the ratio f_{pe}/f_{pu} increases from 0.60 to 0.74 and 0.81, the opening load increases respectively by approximately 27% and 34% while the maximum load increases by 20% and 22%, respectively.

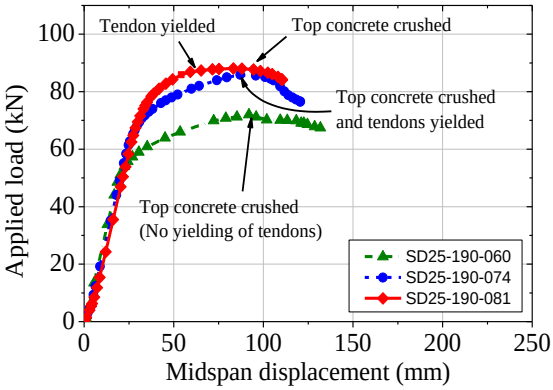

(a) Load vs deflection curves

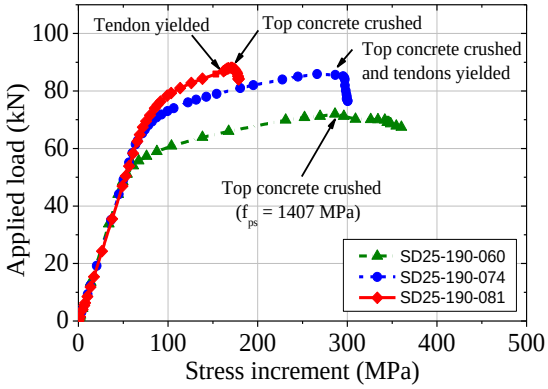

(b) Tendon stress increment

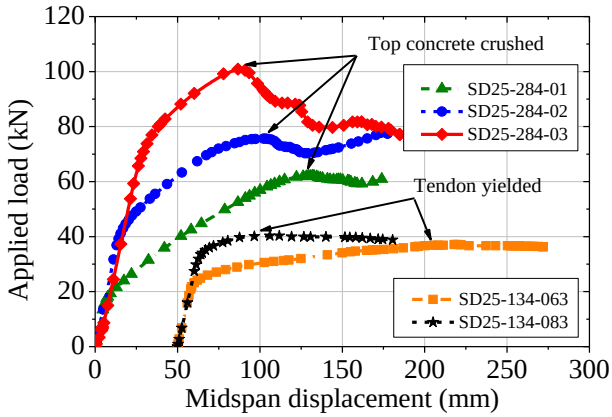

(c) Load vs deflection curves of Beams SD25-284 and SD25-134

Figure 5-13: Effect of f_{pe}

It is noted that the increase in the opening load is linearly proportional to the increase in f_{pe} but this correlation does not exist for the ultimate load. This is because the failure mode of Beam SD25-190-081 differs from the failure modes of Beam SD25-190-060 and Beam SD25-190-074. Beam SD25-190-081 with only 9% of allowable strain reserved in the tendons fails in tension while the other two beams, Beam SD25-190-060 and Beam SD25-190-074, fail in compression. This brings to another conclusion that the change in f_{pe} results in the change in the failure modes of PSBs. Beam SD25-190-060 with a ratio f_{pe}/f_{pu} of 0.60 fails in compression, for which the concrete in the

compression zone fails before the yielding of prestressing steel. The stress in the tendon is 1407 MPa when the top concrete crushes as can be seen from Figure 5-13(b). However, when f_{pe}/f_{pu} increases from 0.60 to 0.81, the failure mode shifts to tension-controlled as observed in Beam SD25-190-081, for which the yielding of the tendon takes place before the crushing of concrete in the compression zone (Figure 5-13a).

In addition, increasing f_{pe} significantly reduces the beam's deflection under the applied load. By comparing the load-deflection curves of Beam SD25-190-060 and SD25-190-074 (Figure 5-13a), which have the same failure mode, it can be seen that under the same level of the applied load, Beam SD25-190-074 clearly exhibits less deflection than Beam SD25-190-060 after the opening of joints. This draws attention in the design of the structure regarding the deflection limits in the serviceability limit state. It is worth mentioning that Beam SD25-190-074 with higher f_{pe} exhibits smaller deflection at the ultimate stage as compared to that of Beam SD25-190-060. This observation is contrary to the results from previous studies (Turmo et al. 2005; Turmo et al. 2006b) as they found that higher f_{pe} led to larger maximum deflection at failure of the beam. An effort has been made to verify this contradiction, in which beams with different prestressing reinforcement ratios and effective prestresses are built. The results are plotted in Figure 5-13(c) which clearly shows that increasing f_{pe} significantly reduces the beams' deflections at the ultimate stage. This decrease in the beams' deflections at the ultimate stage is valid for both the beams failing in compression and tension. As can be seen in the figure, Beam SD25-284-01 which fails in compression deforms 132 mm at the ultimate stage, while those for Beams SD25-284-02 and SD25-284-03 are 102 mm and 86 mm, respectively. In the case of tension-controlled failures, Beam SD25-134-063 undergoes 160 mm deflection at the ultimate stage, i.e. when tendon yields while that for Beam SD25-134-083 is 47 mm. The higher the f_{pe}, the less the workable stress reserved in the tendon. This less stress reservation in the tendon explains the decrease in the beam's deflection at the ultimate stage as observed in the beams showed in Figure 5-13(a and c).

5.5.2 Effect of amount of prestressing steel, A_{ps}

Three beams with different prestressing reinforcement ratios are considered in this section in order to investigate the effect of A_{ps} on the flexural behaviour of PSBs. All the beams have the same f_{pe}/f_{pu} ratio of 0.6 (Table 5-2). It is seen from Figure 5-14(a) that the change in A_{ps} leads to the change in the beam's failure modes. Beam SD25-

190-06 which is prestressed with two 190-mm diameter tendons fails in a compression-controlled manner. However, the failure mode shifts to tension-controlled when the beam is prestressed with two 134-mm tendons as observed in Beam SD25-134-06.

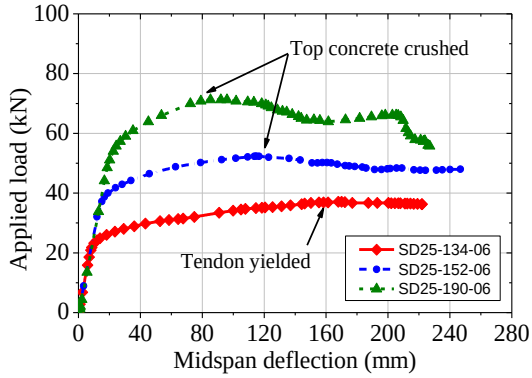

(a) Load vs deflection curve

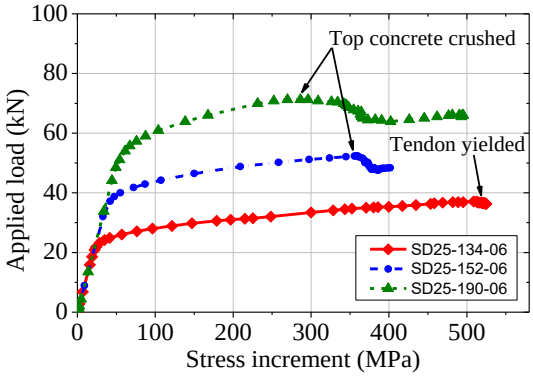

(b) Tendon stress increment

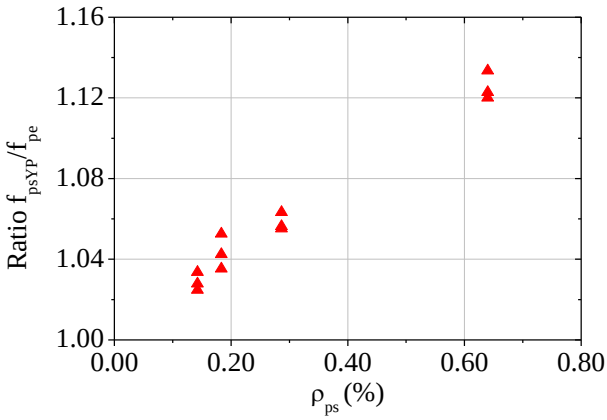

(c) stress increment at yield point

Figure 5-14: Effect of A_{ps}

The change in A_{ps} also affects the load-carrying capacity and stress increment in the tendons. As observed in Figure 5-14, increasing A_{ps} results in an increase in the opening load and maximum load-carrying capacity of the beam but decreases the stress increment in the tendon at the ultimate stage. When the reinforcement ratio increases from 0.14% (Beam SD25-134-06) to 0.28% (Beam SD25-190-06), the maximum load increases by 92% while the stress increment decreases by 44%. Since the stress increment in the tendon is generated by the deformation of the beam and it shows to be linearly related to the deflection of the beam as seen in Figure 5-10(b), this reduction in the tendon stress increment explains the reduction in the deflection capacity of the beam when A_{ps} increases. As observed in Figure 5-14(a), Beam SD25-134-060 deforms approximately 160 mm at the ultimate stage while those for Beam SD25-152-060 and SD25-190-060 are 118 mm and 85 mm, respectively. Similar conclusions

were made from previous studies on monolithic beams with internal unbonded tendons (Tao and Du 1985; Tanchan 2003) as the area of prestressing steel increased, the ultimate strength capacity of the structure increased, but the deflection capacity decreased.

The prestressing reinforcement ratio also affects the stress increment at the opening of the joints. The yield point (as defined in Figure 5-7b) is adopted in this study to represent the transition between the first stage of behaviour when the joints still close and the second stage when the joints open. Various numerical models with different values of f_{pe} and A_{ps} are built, in which f_{pe}/f_{pu} varies from 0.1 to 0.81 and ρ_{ps} varies from 0.10% to 0.64%. The concrete compressive stresses in the bottom fibre at the midspan, σ_c, due to f_{pe} are measured, which are in between 5.49 MPa and 29.80 MPa (σ_c/f'_c = 0.12 to 0.68). The relationship between the stress in the tendon at the yield point, f_{psYP} and the prestressing reinforcement ratio, ρ_{ps} is plotted in Figure 5-14(c). It is seen from the figure that there is an almost linear relationship between the ratio f_{psYP}/f_{pe} and the prestressing reinforcement ratio. In other words, increasing A_{ps} leads to an increase in the tendon stress increment at the yield point. As observed in Figure 5-14(c), when the prestressing reinforcement ratio is 0.14%, the stress increment in the tendon at the yield point is only about 2%. But, when the prestressing reinforcement ratio increases to 0.64%, an increase of about 12% is observed in the tendon stress. This observation deserves attention during the analysis and design of the structure for the calculation of cracking load, which is required for the calculation of the beam's deflection. Existing design codes (PCI 2004; AASHTO LRFD 2012; ACI 318 2015) recommend the use of the effective prestress f_{pe} for the calculation of the cracking load for the stress increment in the tendon at the cracking is small. However, it can be seen from this study that the stress increment in the tendon at cracking/opening is considerably larger than the effective prestress f_{pe} and the increment is related to the prestressing reinforcement ratio as observed in Figure 5-14(c). Therefore, the increase in the tendon stress at the yield point should be taken into consideration during the calculation of the cracking/opening load in order to yield a better prediction of the beam's deflection.

5.5.3 Effect of span-to-depth ratio, L/d_{ps}

Three beams with L/d_{ps} of 25, 35, and 45 are considered in this section to study the

effect of L/d_{ps} on the flexural capacity of PSBs. These three beams have the same cross-section, effective depth of the tendons and materials' properties except for the span length. More beams' details are given in Table 5-2. It is seen from Figure 5-15 that increasing L/d_{ps} ratio significantly reduces the load-carrying capacity of the beam at the yield point and at the ultimate stage. When L/d_{ps} increases from 25 to 35 and 45, the yielding load decreases by 38% and 65% and the maximum load decreases by 36% and 63%, respectively.

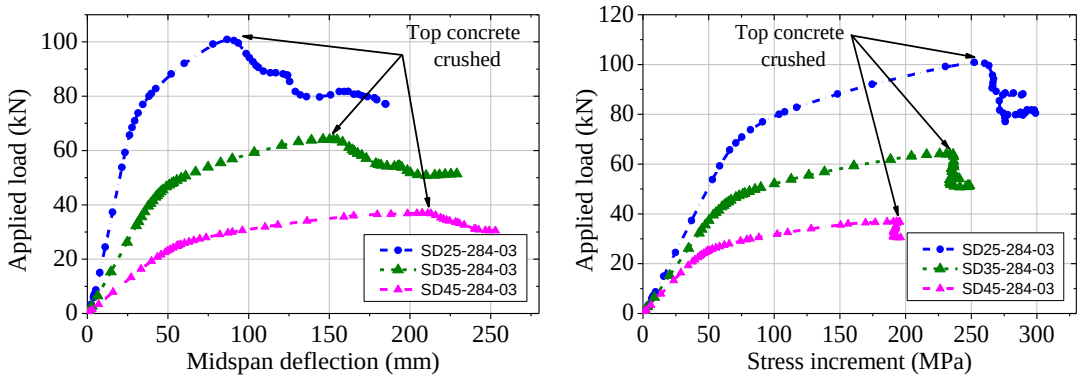

(a) Load vs deflection curve (b) Tendon stress increment

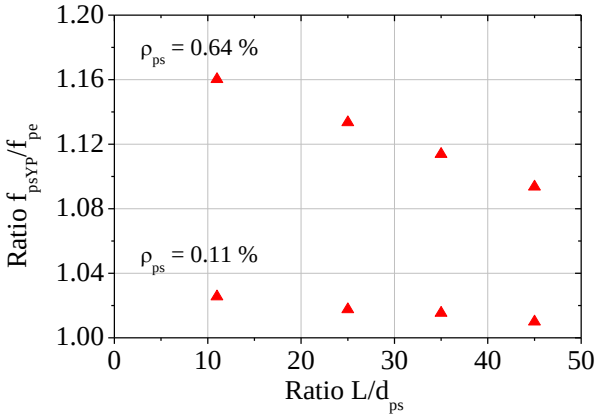

(c) tendon stress at yield point

Figure 5-15: Effect of L/d_{ps}

L/d_{ps} significantly affects the stress increment in the tendon. The tendon stress at the ultimate stage respectively decreases by 10% and 22% as L/d_{ps} increases from 25 to 35 and 45. This observation is similar to the findings by Harajli (1990) on monolithic beams with internal unbonded tendons, however, it differs from the results obtained by Tanchan (2003) and Harajli and Kanj (1992). Tanchan (2003) and Harajli and Kanj (1992) also conducted researches on monolithic beams with internal unbonded tendons and found that the change of L/d_{ps} did not lead to a significant change in the tendon stress increment. This study also found that the tendon stress at the yield point shows

an almost linear relationship with L/d_{ps} ratio as shown in Figure 5-15(c). As L/d_{ps} ratio increases the tendon stress at the yield point decreases and the level of this decrease is greater for the beams with higher prestressing reinforcement ratios.

5.5.4 Effect of load type

Two beams are built to investigate the effect of load type on the flexural behaviour of PSBs with unbonded tendons. The two beams have the ratio L/d_{ps} of 25, internally prestressed with two 28.4-mm diameter tendons at the effective prestress of f_{pe}/f_{pu} of 0.3. One beam is loaded under there-point loading at the midspan and the other under four-point loading placed symmetrically at one-third of the span (Table 5-2).

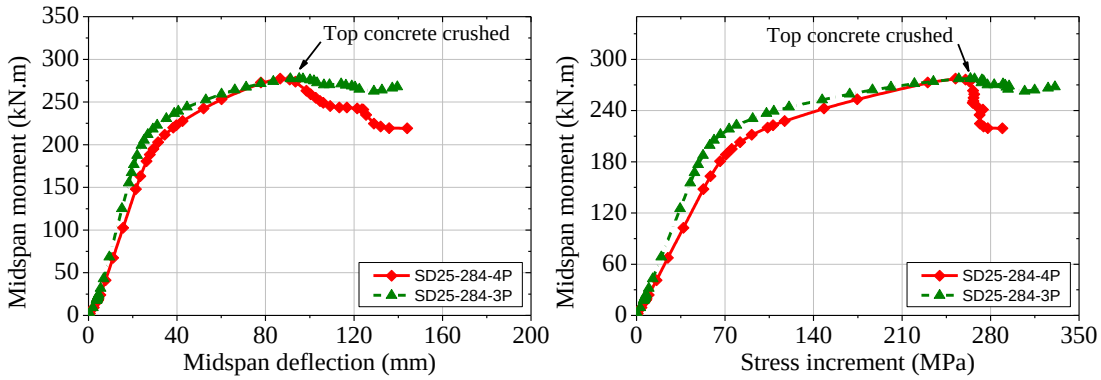

(a) Load vs deflection curve (b) Tendon stress increment

Figure 5-16: Effect of load type

Figure 5-16 shows the deflection and stress increment in the tendon of the two beams under the applied load. It is seen from the figure that the type of load has a minor effect on the flexural behaviour of the beams investigated in this study. Although the beam under three-point loading exhibits lower deflection and the stress increment in the tendon at the yield point (when joints opened as defined in Figure 5-7b), both the beams achieve almost the same bending moments, deflections and stress increments at the ultimate stage as shown in the figure. The bending moment, deflection and the tendon stress increment of Beam SD25-284-4P are respectively 278 kN.m, 86.6 mm, and 252 MPa while those values of Beam SD25-284-3P are 276 kNm, 95.2 mm, and 264 MPa, respectively. Yuan et al. (2014) also observed a reduction in the deflection and stress increment of the beam loaded under three-point loading, however, this beam showed a bending moment at the ultimate stage about 17% greater than the beam under four-point loading. It is worth mentioning that changing the load type also affects the distance between the loading points to the nearest joints, which shows a significant

influence on the beam performance. Therefore, the effect of load type in segmental beams is scenario-dependent and is associated with the influence of the distance between the loading point and the nearest joint.

5.5.5 Effect of concrete strength and number of joints

Three beams with different compressive concrete strengths are considered in this section. All the beams are prestressed with two 28.4-mm diameter tendons at the prestressing level f_{pe}/f_{pu} of 0.2 (Table 5-2).

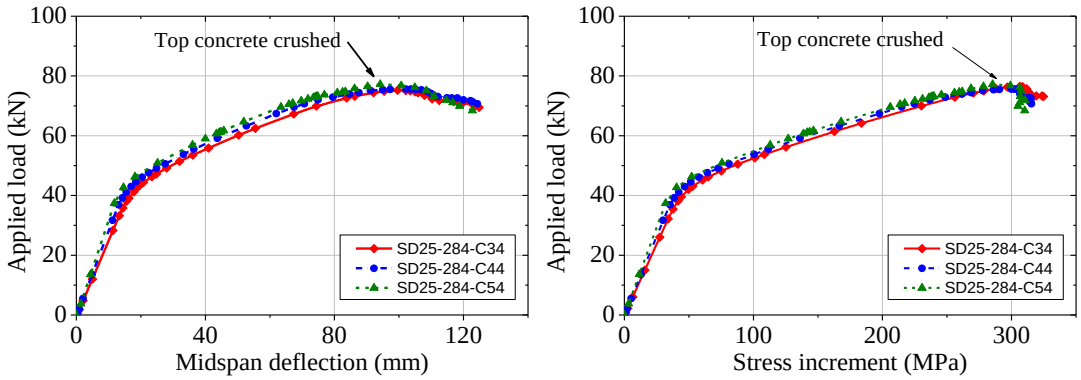

(a) Load vs deflection curve (b) Tendon stress increment

Figure 5-17: Effect of f'_c

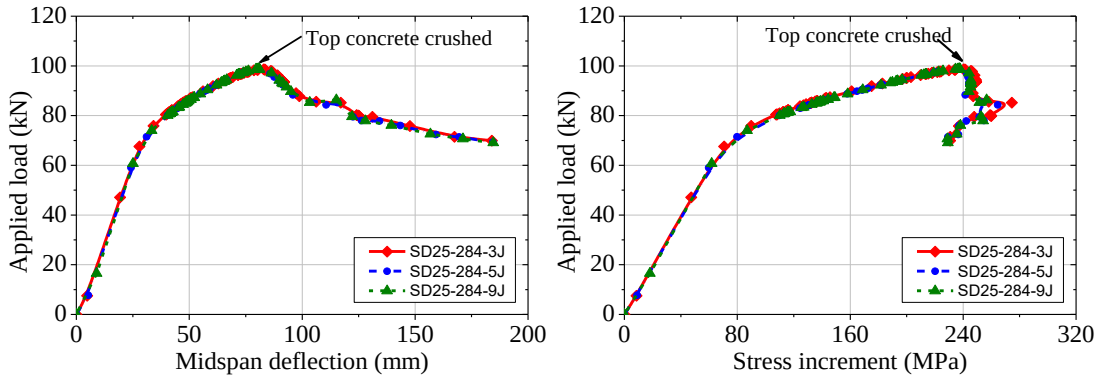

(a) Load vs deflection curve (b) Tendon stress increment

Figure 5-18: Effect of number of joints

It is seen from Figure 5-17 that the variation in the concrete strength does not lead to a considerable change in the beam's strength and ductility. All the three beams fail by crushing of concrete in the compression zone in the top fibre. When f_c' increases from 34 MPa to 54 MPa, the maximum load of the beam only increases by approximately 3%. Similarly, all the beams exhibit insignificant differences in the tendon stresses at the corresponding maximum load. This increment is small as compared to the results

of the monolithic beams where the previous studies found that the maximum loads increased with the increase in the concrete strength (Tanchan 2003). Tanchan (2003) used high-strength concrete; when the concrete strength was doubled from 41 MPa to 82 MPa a 15% increase in the ultimate load of the beam under four-point loading was achieved. In this study, the ultimate load of the segmental beam increased by 3% when the concrete strength increased by 59%. In terms of beam's stiffness, the beam with higher concrete strength exhibits slightly higher initial stiffness, which results in a slightly higher yield load. The applied load at yield point of Beam SD25-284-C54 is 42.7 kN, which is approximately 9% higher than that of Beam SD25-284-C34 which is 39.1 kN.

Regarding the effect of joints on the flexural behavior of segmental beams, previous study observed that the beam with lesser number of joints showed smaller flexural strength than the beam with more number of joints (Jiang et al. 2016). Test results showed that the flexural strength of the two-joint segmental beam was 12.8% less than that of the seven-segmental beam and the reason for this was due to the high concentration of rotation and deflection at individual joints in the two-segmental beams as explained by Jiang et al. (2016). However, this study finds different behaviour that the beams with different number of joints exhibit similar flexural strength and deflection responses under bending. Beams with different numbers of joints, i.e. 3, 5 and 9 joints, are built in this study, in which the beams are prestressed with unbonded tendons (Table 5-2) and are loaded under four-point loading. As observed in Figure 5-18, the number of joints has an insignificant effect on the behaviour of the structure under bending. All the specimens exhibit almost the same load-deflection responses and the tendon stress increments under the applied load. Since all the beams have the same cross-section, reinforcement and loading scheme except for the number of joints, the stiffness and the strength capacity of the beams depend only on the properties of the cross-section. The dry joints are used in the specimens in the numerical models, as such there is no contribution of concrete tensile strength to the tension resistance at any section of the beam. As a result, the load-carrying capacity of the beam at the midspan section will be the same for different beams with different numbers of joints. This explains the similar behavior of the beams as observed in Figure 5-18.

It is worth mentioning that in practice, the number of joints is likely to affect the

stiffness of the beam due to the imperfect condition of the contacts between joint's surfaces of the beam. As such, the more joints designed in the beam, the larger contact errors accumulated. These errors are likely to cause a reduction in the area of the concrete in the compression zone, which will cause the beam's stiffness to decrease. Whereas, perfect contact condition between the segment joints is obtained in the numerical models which therefore disregards the contact errors in the beams. Further experimental works are required to validate this observation for the effect of the number of joints on the stiffness of the segmental concrete beams.

5.6 Conclusion

The numerical models developed in this chapter using ABAQUS software capture well the responses of the segmental concrete beams reported in the literature. The verified numerical models are used to conduct intensive simulations of behaviour of segmental beams with different parameters for tension-controlled, compression-controlled and balanced sections. Flexural behaviour of PSBs with unbonded tendons in terms of failure modes, joint opening and stress increment in the prestressing tendons are discussed.

- It is found from the parametric study that effective prestress in the tendon strongly affects the load-carrying capacity, deflection and failure modes of concrete segmental beams. Beams with higher effective prestress exhibit greater load-carrying capacity but less deflection at the ultimate stage. With the same prestressing amount, the change in effective prestress can lead to the change in the failure modes from compression- or tension-controlled failures.

- Increasing the prestressing reinforcement ratio leads to the increase in the load-carrying capacity of the segmental beams, but decreases the beam's deflection. The stress increment in the tendon at the cracking/opening of the joint is found to be considerable in this study however it is not considered in the current design codes. 2% to 12% increase in the tendon stress at the cracking/opening is observed in this study and this stress increment is directly related to the area of prestressing steel.

- Increasing the span-to-depth ratio significantly reduces the load-carrying capacity of the beam and stress increment in the tendon, and the level of decrease in the tendon stress incensement is greater in the beam with a higher reinforcement ratio.

- The load type has an insignificant effect on the flexural behaviour of the beam, although the beam loaded with three-point loading registers lower deflection and stress increment in the tendon at the yield point of the structure compared to the beam loaded under four-point loading.
- Finally, the concrete strength and number of joints show insignificant effects on the flexural performance of the segmental beams in terms of the load-carrying capacity, deflection and failure mode.

5.7 References

AASHTO LRFD (2012). *Bridge Construction Specifications, 6th Edition, U.S. Units*, American Association of State Highway and Transportation Officials, Washington, DC.

ABAQUS CAE (2014). *Analysis user's manual, Version 6.14*, ABAQUS.

ACI 318 (2015). *Building code requirements for structural concrete and commentary*, ACI 318-14, American Concrete Institute, Farmington Hills, MI.

Birtel, V., and Mark, P. (2006). "Parameterised finite element modelling of RC beam shear failure." *Proc., ABAQUS Users' Conf.*, 95-108.

Buyukozturk, O., Bakhoum, M. M., and Michael Beattie, S. (1990). Shear behavior of joints in precast concrete segmental bridges. *Journal of Structural Engineering*, 116(12), 3380-3401.

Carreira, D. J., and Chu, K.-H. (1985). Stress-strain relationship for plain concrete in compression. *Journal Proceedings*, 82(6), 797-804.

Devalapura, R. K., and Tadros, M. K. (1992). Stress-strain modeling of 270 ksi low-relaxation prestressing strands. *PCI Journal*, 37(2), 100-105.

Harajli, M., Khairallah, N., and Nassif, H. (1999). Externally prestressed members: evaluation of second-order effects. *Journal of Structural Engineering*, 125(10), 1151-1161.

Harajli, M. H. (1990). Effect of span-depth ratio on the ultimate steel stress in unbonded prestressed concrete members. *ACI Structural Journal*, 87(3), 305-312.

Harajli, M. H., and Kanj, M. Y. (1992). Service Load Behavior of Concrete Members Prestressed with Unbonded Tendons. *Journal of Structural Engineering*, 118(9), 2569-2589.

Jiang, H., Cao, Q., Liu, A., Wang, T., and Qiu, Y. (2016). Flexural behavior of precast concrete segmental beams with hybrid tendons and dry joints. *Construction and*

Building Materials, 110, 1-7.

Jiang, H., Li, Y., Liu, A., Ma, Z. J., Chen, L., and Chen, Y. (2018). Shear Behavior of Precast Concrete Segmental Beams with External Tendons. *Journal of Bridge Engineering*, 23(8), 04018049.

Le, T. D., Pham, T. M., Hao, H., and Hao, Y. (2018). Flexural behaviour of precast segmental concrete beams internally prestressed with unbonded CFRP tendons under four-point loading. *Engineering Structures*, 168(2018), 371-383.

Le, T. D., Pham, T. M., Hao, H., and Yuan, C. (2019). Performance of precast segmental concrete beams posttensioned with carbon fiber-reinforced polymer (CFRP) tendons. *Composite Structures*, 208, 56-69.

Li, G., Yang, D., and Lei, Y. (2013a). Combined shear and bending behavior of joints in precast concrete segmental beams with external tendons. *Journal of Bridge Engineering*, 18(10), 1042-1052.

Li, G., Zhang, C., and Niu, C. (2013b). Experimental study on shear behavior in negative moment regions of segmental externally prestressed concrete continuous beams. *Journal of Bridge Engineering*, 18(4), 328-338.

Lou, T., Lopes, S. M. R., and Lopes, A. V. (2012). Numerical analysis of behaviour of concrete beams with external FRP tendons. *Construction and Building Materials*, 35, 970-978.

Lou, T., Lopes, S. M., and Lopes, A. V. (2016). Response of continuous concrete beams internally prestressed with unbonded FRP and steel tendons. *Composite Structures*, 154(2016), 92-105.

Lou, T., Liu, M., Lopes, S. M. R., and Lopes, A. V. (2017). Effect of bond on flexure of concrete beams prestressed with FRP tendons. *Composite Structures*, 173, 168-176.

MacGregor, R. J. G. (1989). Evaluation of strength and ductility of a three-span externally post-tensioned box girder bridge model. University of Texas at Austin.

Pannell, F. (1969). The ultimate moment of resistance of unbonded prestressed concrete beams. *Magazine of Concrete Research*, 21(66), 43-54.

PCI (2004). *Design Handbook*, 6th ed., Precast/Prestressed Concrete Institute, Chicago, IL.

Pham, T. M., Le, T. D., and Hao, H. (2018). Behaviour of Precast Segmental Concrete Beams Prestressed with CFRP Tendons. *Proc., 9th International Conference on Fibre-Reinforced Polymer (FRP) Composites in Civil Engineering (CICE 2018)*, 945-953.

Saibabu, S., Srinivas, V., Sasmal, S., Lakshmanan, N., and Iyer, N. R. (2013).

Performance evaluation of dry and epoxy jointed segmental prestressed box girders under monotonic and cyclic loading. *Construction and Building Materials*, 38, 931-940.

Shamass, R., Zhou, X., and Alfano, G. (2014). Finite-Element Analysis of Shear-Off Failure of Keyed Dry Joints in Precast Concrete Segmental Bridges. *Journal of Bridge Engineering*, 20(6), 04014084.

Tam, A., and Pannell, F. (1976). The ultimate moment of resistance of unbonded partially prestressed reinforced concrete beams. *Magazine of Concrete Research*, 28(97), 203-208.

Tan, K.-H., and Ng, C.-K. (1997). Effects of deviators and tendon configuration on behavior of externally prestressed beams. *ACI Structural Journal*, 94(1), 13-22.

Tanchan, P. (2003). Flexural behavior of high-strength concrete beams prestressed with unbonded tendons. Doctoral Dissertation, Rutgers University.

Tao, X., and Du, G. (1985). Ultimate stress of unbonded tendons in partially prestressed concrete beams. *PCI Journal*, 30(6), 72-91.

Turmo, J., Ramos, G., and Aparicio, A. C. (2005). FEM study on the structural behaviour of segmental concrete bridges with unbonded prestressing and dry joints: Simply supported bridges. *Engineering Structures*, 27(11), 1652-1661.

Turmo, J., Ramos, G., and Aparicio, Á. C. (2006a). Shear behavior of unbonded post-tensioned segmental beams with dry joints. *ACI Structural Journal*, 103(3), 409-417.

Turmo, J., Ramos, G., and Aparicio, A. C. (2006b). FEM modelling of unbonded post-tensioned segmental beams with dry joints. *Engineering Structures*, 28(13), 1852-1863.

Xu, X., Liu, Y., and He, J. (2014). Study on mechanical behavior of rubber-sleeved studs for steel and concrete composite structures. *Construction and Building Materials*, 53, 533-546.

Yapar, O., Basu, P. K., and Nordendale, N. (2015). Accurate finite element modeling of pretensioned prestressed concrete beams. *Engineering Structures*, 101(2015), 163-178.

Yuan, A., Dai, H., Sun, D., and Cai, J. (2013). Behaviors of segmental concrete box beams with internal tendons and external tendons under bending. *Engineering Structures*, 48, 623-634.

Yuan, A., He, Y., Dai, H., and Cheng, L. (2014). Experimental Study of Precast Segmental Bridge Box Girders with External Unbonded and Internal Bonded Posttensioning under Monotonic Vertical Loading. *Journal of Bridge Engineering*,

20(4), 04014075.

Zhou, X., Mickleborough, N., and Li, Z. (2005). Shear strength of joints in precast concrete segmental bridges. *ACI Structural Journal*, 102(1), 3.

CHAPTER 6 ANALYTICAL INVESTIGATION OF THE PERFORMANCE OF PRECAST SEGMENTAL CONCRETE BEAMS INTERNALLY PRESTRESSED WITH UNBONDED STEEL TENDONS[5]

Abstract

This chapter presents an analytical and a numerical approach to predict the flexural behaviour of precast segmental concrete beams (PSBs) with unbonded steel tendons. The analytical predictions match the experimental and numerical results very well, therefore can be adopted for design analysis. The numerical investigation on the flexural behaviour of PSBs with unbonded tendons is reported the first time in open literature. Based on the numerical results, the load-deflection responses of PSBs with unbonded steel tendons are generalized and presented for both tension-controlled and compression-controlled sections, and the results are compared with those from existing models for predicting the strength of PSBs at the ultimate stage. Naaman and Alkhairi (1991)'s model is found to capture very well the changes of tendon stress, f_{ps}, with respects to the changes of various studied parameters. However, it overestimates the strength of the structures even though the strain reduction coefficient, Ω_u, recommended by Naaman and Alkhairi (1991) for conservative predictions is used. As such, a new value of Ω_u is proposed for the application on PSBs with unbonded steel tendons. Finally, an empirical equation is developed to estimate the balanced reinforcement ratio of PSBs with unbonded steel tendons. The equation is validated with detailed numerical predictions.

[5] This chapter is compiled from the following paper which is under review:
Le, T. D., Pham, T. M., and Hao, H. (2019). Analytical Investigation of the Performance of Precast Segmental Concrete Beams Internally Prestressed with Unbonded Steel Tendons, (Under review).

6.1 Introduction

Precast segmental prestressed concrete beams (PSBs) have been increasingly used in many bridge projects around the world over the past four decades. Corrosion problems of the steel tendons at segment joints are a great concern of the use of PSBs, especially in places exposed to highly aggressive environmental conditions. The use of unbonded tendons, therefore, is a practical solution for structures in general and PSBs in particular as unbonded tendons enable fast installation and easy replacement in cases of deterioration. However, due to the lack of bonding between the tendons and surrounding concrete, the analysis of beams with unbonded tendons in terms of both the strength and deflection at the ultimate stage is more complex than those with bonded tendons (Naaman and Alkhairi 1991). As such, with the increase in the application of PSBs with unbonded tendons, closer examinations in the analysis and design of this type of structures are necessary. This chapter further investigates the flexural behaviour of PSBs prestressed with unbonded steel tendons under bending, in which the predictions of the load-carrying capacity and displacement at the ultimate stage are discussed. In addition, an analytical procedure for determining the balanced reinforcement ratio of precast segmental concrete beams with unbonded tendons is also developed.

6.2 Background

The prediction of the load-carrying capacity of PSBs with unbonded tendons at the ultimate stage in bending has been extensively studied by researchers and well documented in design standards (AASHTO 1999; AASHTO LRFD 2012). Meanwhile, very few studies have addressed the deflections of the structures at the ultimate stage. Existing codes (PCI 2004; AASHTO LRFD 2012; ACI 318 2015) only recommend methods to compute the instantaneous deflections of beams with bonded tendons by using either the effective moment of inertia or bilinear moment-deflection relationship approach. No detailed guidance is given for the calculation of deflections of the beams with unbonded tendons. Harajli and Kanj (1992) modified several approaches, which were reported in the literature for computing the deflections of bonded or partially bonded prestressed members for application to beams with unbonded tendons. From their study, the main problem lies in the computation of the moment of inertia of cracked section, I_{cr}. Harajli and Kanj (1992) assumed the area of the unbonded prestressing tendons to be $\Omega_{cr}A_{ps}$ and then I_{cr} is computed by using

cracked section analysis. In which, Ω_{cr} is a bond reduction coefficient in the elastic cracked state, which was defined earlier by Naaman (1990). However, the computation of an exact value of Ω_{cr} for different types of loading and tendon profiles is an extremely difficult task. Harajli and Kanj (1992) examined the variation of Ω_{cr} versus different ratios of the total applied moment to the cracking moment, M_a/M_{cr} and different ratios of the moment of inertia of cracked section to the gross section moment of inertia, I_{cr}/I_g and observed that Ω_{cr} does not differ significantly from its value before cracking. As a result, they assumed $\Omega_{cr} = \Omega$ and used this value in the cracked section analysis procedure. Ω is a bond reduction coefficient in the pre-cracking stage, which is developed by Naaman (1990) for different types of loading and tendon profiles.

Au et al. (2005) extended the use of coefficient λ proposed by Pannell (1969), which is the ratio of plastic hinge length to the neutral axis depth c at critical sections, to the cracked section analysis of unbonded partially prestressed concrete beams. They found that λ is not sensitive to the variation of combined reinforcement index until the yielding of non-prestressed steel and it can be taken as a constant. A cubic equation was established by the authors for the neutral axis depth resulting in the calculation of I_{cr}. However, the calculation procedure is tedious, and it is inconvenient for practical use to compute the deflections of partially unbonded prestressed concrete beams. Du et al. (2016) proposed a method to estimate the deflections of partially unbonded prestressed continuous beams. The main point of their method lies in converting the amount of prestressing unbonded tendons into an equivalent amount of non-prestressed reinforcing steel for the calculation of I_{cr}. This is based on their observation that the stress increment in the unbonded tendons was limited and relatively low. This stress increment was, therefore, neglected and only the effective prestress f_{pe} was considered in the analysis. The method proposed by Du et al. (2016) yields satisfactory predictions of deflection till the yielding of non-prestressed steel while the deflections afterwards till the ultimate stage was not considered in their calculation. In PSBs with unbonded tendons, there is almost no contribution of the conventional steel to the beam's strength capacity since the steel is cut-off at the segment joints. Also, previous experimental results showed that the stress increment in the unbonded tendons after the opening of joint is significant (Le et al. 2018). This method, therefore, cannot be applied for PSBs with unbonded tendons. From the above analyses it is noted that no any studies have been conducted on the computation of deflection of PSBs with

unbonded tendons at the ultimate stage.

In the meantime, the balanced reinforcement ratio of a PSB with unbonded tendons is another concern, which requires further investigations. To the authors' best knowledge, an estimation of the balanced reinforcement ratio for beams with unbonded tendons, ρ_b^u has not been reported in the open literature so far except the work recently done by Lee et al. (2017). Due to the absence of bonding between the prestressing tendons and the surrounding concrete as mentioned previously, the stress increment in the tendons depends on the deformation of the entire member rather than the analysis of a single section. As a result, the determination of ρ_b^u becomes more challenging for beams with unbonded tendons. Lee et al. (2017) developed an analytical model based on three equivalent curvature blocks for simply supported beams internally prestressed with unbonded carbon fibre-reinforced polymer (CFRP) tendons and then conducted parametric studies to evaluate the effects of various parameters on ρ_b^u. It was found that ρ_b^u is always smaller than that of a beam with bonded tendons, ρ_b^b and the ratio of ρ_b^u/ρ_b^b were shown to be between 0.43 and 0.83. However, the computation procedure for ρ_b^u is tedious and it is inconvenient for practical engineers to get the first estimation of the minimum amount of reinforcement required. In addition, this proposed procedure is applicable for monolithic beams only while there has been no such study for precast segmental beams.

Efforts have been expended for decades on the prediction of stress increment in the unbonded tendons, it is still questionable whether any of the proposed methods are consistent in all situations (Yuan et al. 2014). The accuracy of the prediction of stress increment in the unbonded tendons for PSBs was evaluated in the study by Yuan et al. (2014). It was found that all methods including Naaman and Alkhairi (1991), Harajli (2006), ACI 318 (2008) and AASHTO (1999) encounter considerable scatter in the predictions of tendon stress increment for PSBs with external tendons. The methods proposed by Du and Liu (2003) and He and Liu (2010) were then recommended by Yuan et al. (2014) for the computation of ultimate stress in the external tendons of segmental bridges. As far as the authors are aware, no any study has been done on the assessment of the accuracy of the existing equations in the literature on the prediction of tendon stress at the ultimate stage for PSBs with internally unbonded tendons.

Therefore, this study further investigates the flexural behaviour of PSBs internally

prestressed with unbonded steel tendons. Analytical procedures to predict the performance of PSBs are proposed, the analytical predictions are then verified against experimental and numerical results from previous studies. However, experimental studies in the literature do not always provide sufficient information on the wide range of important parameters, which may highly affect the behaviour of PSBs, such as the ratio of the span length to the depth of the tendons L/d_{ps}, the effective prestress in the tendons f_{pe}, the amount of prestressing reinforcement A_{ps}, and the strength of concrete f'_c. Therefore, a numerical study using ABAQUS CAE (2014) commercial software is conducted in this study to cover a wide range of such parameters. To the authors' best knowledge, this is the first time ever numerical investigations on the behaviour of segmental concrete beams with unbonded tendons under flexural loads are conducted.

Based on the numerical and analytical results, the load-deflection curves of PSBs under the applied loads and the prediction of tendon stress at the ultimate stage by existing models are carefully assessed. Moreover, an analytical procedure for the estimations of the instantaneous deflections and the balanced reinforcement ratio of precast segmental concrete beams are proposed.

6.3 Description of Finite Element Model

ABAQUS CAE (2014) software is used to simulate the behaviour of segmental concrete beams internally prestressed with unbonded tendons. Segmental concrete beams which were tested and presented in Chapter 2 are used to validate the numerical simulation. The validated finite element models are then used to generate further results to assist analytical analyses.

Two segmental concrete beams (Beams BS1 and BC1) in the study by Le et al. (2018) are simulated. The two beams had T-shaped cross-section of 400 mm height and 3.9 m overall length. Each beam comprised four segments which were made of reinforced concrete and had the lengths of 800 mm and 1150 mm. Beam S1 was post-tensioned with two unbonded steel tendons while two unbonded CFRP tendons were used in Beam C1. Details of the beams' dimensions, reinforcements and material properties were presented in Section 2.2 of Chapter 2.

To simulate the beams, three-dimensional solid finite elements are used to capture the response of the different components in the finite element models. Eight-node linear brick, reduced integration hexahedral elements (C3D8R) are selected to model the

concrete elements, prestressing steel tendons, and auxiliary elements such as steel loading plates, anchor blocks and steel plates at beams' ends. Two-node linear 3-D truss elements are selected to model the conventional steel reinforcement. Details of the material models, material properties, contact models, modelling procedure and model validation were given in Section 5.3 of Chapter 5.

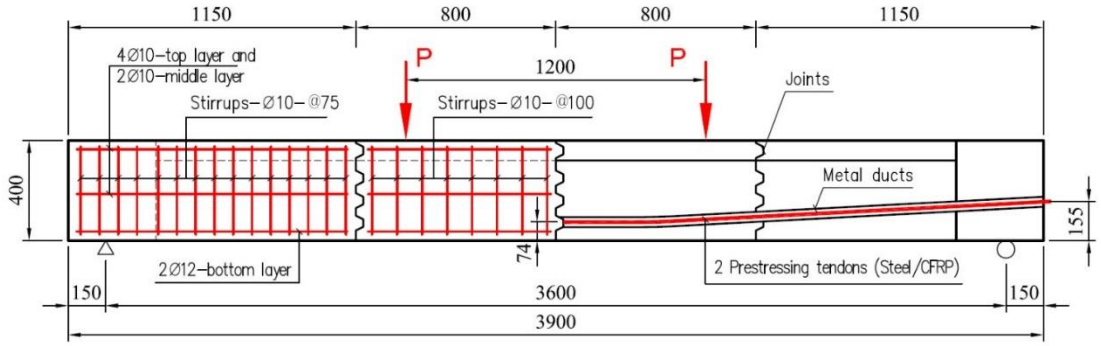

(a) Detailed dimensions of the tested beams in Le et al. (2018)

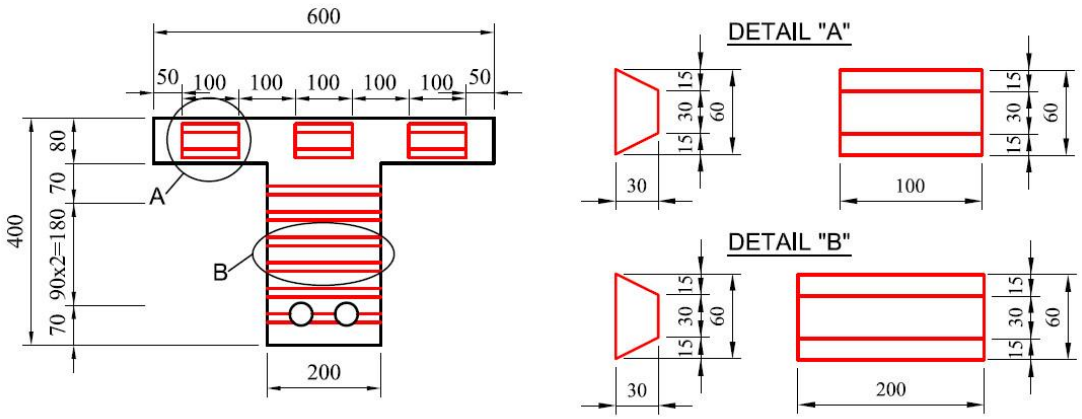

(b) Multiple shear-keyed joints

Figure 6-1: Details of beams used in validation (repeated Figures 5-1 of Chapter 5 for convenience)

6.4 Load-deflection curves

In this section, various numerical models are developed based on the validated models to investigate the load-deflection responses of PSBs with unbonded steel tendons under four-point loading. In all the developed models, the cross-section of the beams and the configuration of the conventional steel reinforcements are kept the same as the beam shown in Figure 6-1. However, different span length to tendon depth ratios L/d_{ps}, effective prestressing stress f_{pe}, area of prestressing tendons A_{ps}, and concrete strength

f'_c are considered in the models. The generalized load-deflection curve of segmental concrete beams has not been reported in the literature yet. This section thus generalizes the load-deflection responses of the segmental concrete beams. There are three conditions taken into consideration: tension-controlled sections, compression-controlled sections and balanced condition.

6.4.1 Tension-controlled sections

In this study, a section is defined as tension-controlled when the yielding of the prestressing steel takes place before crushing of the concrete in compression. The prestressing steel yields when it reaches its yielding stress of 1674 MPa for steel Grade 270. The failure of concrete occurs when its strain reaches 0.003. The balanced condition of the sections is discussed in the next section.

A typical load-deflection curve from the numerical simulation for a segmental concrete beam that fails in tension, Beam SD25-118-069, is plotted in Figure 6-2(a). A monolithic beam M025-118-069, which has the same configuration as Beam SD25-118-069 except the longitudinal steel bars are continuous along the beam's length, is also simulated and its load-deflection curve is plotted in the figure for comparison. The simulated beams in this study are labelled as follows: the first part includes letters, "SD" denotes segmental beams with dry joints or "MO" denotes monolithic beams, and a number which denotes the L/d_{ps} ratio; the second part indicates the tendon's diameter (each beam is prestressed with two tendons); and the last one denotes the f_{pe}/f_{pu} ratio. For example, Beam SD25-118-069 stands for the segmental beam with dry joints and L/d_{ps} = 25; having two steel tendons of 11.8 mm diameter; and each tendon is prestressed with an effective prestress equal to 0.69 of the ultimate stress, f_{pe}/f_{pu} = 0.69. With that amount of prestressing steel reinforcements (ρ_{ps}=0.11%), both the beams exhibit tension-controlled failures, i.e., the tendon yields before the crushing of the concrete in compression. As shown in Figure 6-2, the load-deflection curve of the segmental beam falls below the monolithic counterpart. The load-deflection curves of the two beams are generalized in Figure 6-2(b), which represents the load-deflection responses of segmental and monolithic beams with unbonded tendons in the case of tension-controlled failures.

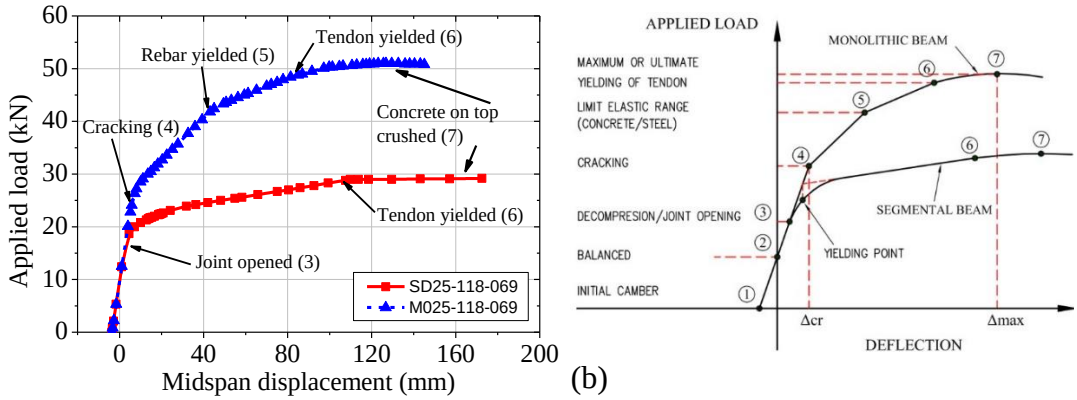

(a) (b)

Figure 6-2: Load-deflection curve of under-reinforced beams: (a) Simulation; (b) Generalized

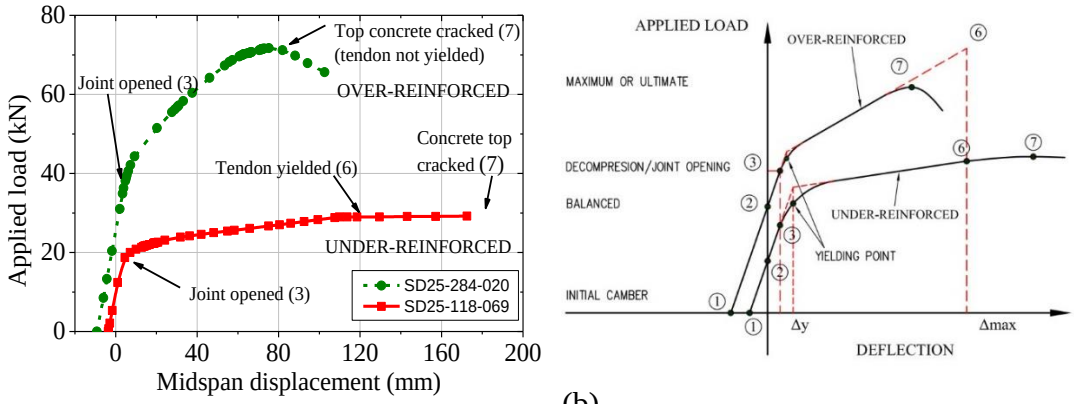

(a) (b)

Figure 6-3: Load-deflection curve of under- vs over-reinforced beams: (a) Simulation; (b) Generalized

The load-deflection curve of a monolithic beam with unbonded tendons was well described elsewhere (Alkhairi and Naaman 1993; Naaman 2004). Several particular states of behaviour are recited herein (Figure 6-2b). In the curve of the monolithic beam, Point 1 represents the initial camber due to the combined effects of the effective prestressing force and self-weight. Point 2 represents balanced stress state where the camber backs to zero (zero deflection) under the applied load, forming a uniform stress state in the section. Point 3 represents decompression or zero stress at the bottom fibre. Point 4 represents the onset of cracking in the concrete at the bottom fibre. In theory, a sudden change in the beam's stiffness occurs at this point (Point 4), however, the real behaviour may show a more gradual change in the beam's stiffness (Naaman and Alkhairi 1991), which is also observed in Figure 6-2(a). With the increase in the applied load, the stresses in the steel rebars and the concrete on the top fibre would increase until either material reaches its non-elastic characteristic, which is represented

by Point 5. Point 6 represents the yielding of steel tendons before the maximum loading capacity is reached at Point 7. Point 7 represents the ultimate loading capacity of the beams, which is characterized by the failure of the concrete in the top fibre.

This study proposes a generalized load-deflection curve for precast segmental beams. The first two points, Points 1 and 2, are to be the same with those of a monolithic beam. This is due to the effect of prestressing, which compresses the bottom fibre in compression resulting in the segmental beam to act like a monolithic beam before the opening of joints. As the load increases, the bottom fibre continues to decompress till it reaches the zero stress representing the onset of the opening of the joint, Point 3. This point corresponds to the decompression in the bottom fibre in the case of the monolithic beam. It is noted that if the tensile strength of the concrete is neglected in the analysis of the monolithic beam, Point 4 in the monolithic beam curve would represent the boundary between the cracked and uncracked section behaviour and would take the place of Point 3 (Naaman 2004). As such, if all parameters of the two beams are maintained the same, the load-deflection curves of a segmental beam with dry joints would fall under the curve of the corresponding monolithic beam due to the lost contribution of tensile strength in concrete and reinforcements as observed from the numerical results shown in Figure 6-2(a). The curve from Points 1 to 3 corresponds to the first stage of behaviour of a segmental beam, where the beam exhibits a linear relationship between the deflection and applied load. There is then a transition zone where the beam's stiffness reduces gradually due to the gradually opening of joints. After that, the beam deforms almost linearly in the second stage until the prestressing steel reaches its yielding strength, which is represented by Point 6. The absence of conventional steel and the less significant change in the compressive concrete stiffness for the case of under reinforced beams explain the approximately linear behaviour observed in the second stage. After Point 6, the beam still shows some increase in the applied load till the beam reaches its ultimate state by either rupture of prestressing tendons or compression failure of concrete at Point 7. It is worth noting that in order to be able to construct the load-deflection curve of the segmental beam, the transition zone is replaced by a yield point, which is shown in Figure 6-2(b) and Figure 6-3(b). The determination of the yield point will be discussed in next sections.

6.4.2 Compression-controlled sections

When the reinforcement ratio exceeds the balanced ratio, a segmental concrete beam

will fail as compression-controlled, which exhibits brittle behaviour as compared to tension-controlled beams (Figure 6-3a). Everything in Beam SD25-284-02 is the same as Beam SD25-118-069, except Beam SD25-284-02 is prestressed with two tendons of 28.4 mm diameter (ρ_{ps}=0. 64%). The tendons are tensioned with f_{pe}/f_{pu} ratio of 0.20 to ensure the stress in the concrete at the bottom fibre due to f_{pe} not exceed $0.6f'_c$ as recommended by AASHTO LRFD (2012). The load-deflection curves of these beams are generalized in Figure 6-3(b).

The distinguished states in the load-deflection curve of the over-reinforced beam are presented in Figure 6-3. In the first stage, the beam deforms linearly up to the decompression of the bottom fibre or the onset of joint opening which is represented by Point 3 as shown in Figure 6-3(b). Then, the beam's stiffness gradually reduces due to the opening of joint corresponding to the transition zone. In the second stage, the beam shows a non-linear relationship between the deflection and the applied load. This non-linear behaviour is due to the highly non-linear characteristics of concrete when the compressive failure is pronounced. Finally, the beam reaches its ultimate load-carrying capacity at Point 7 by the compression failure of the concrete, which takes place before the yielding of prestressing tendons. This type of failure is brittle and is not desirable for structures from a ductility and safety viewpoint.

6.5 Prediction of load-deflection curves

Bilinear moment-deflection relationship (bilinear method) recommended by PCI (2004) is adopted in this study to construct the load-deflection curves of segmental beams with unbonded tendons. The method is used to predict the deflection of PSBs up to the ultimate stage of the beams, i.e. to Point 6, yielding of the prestressing steel, in the case of tension-controlled sections or to Point 7, at which compression failure of concrete occurs, in the case of compression-controlled sections. However, the computation of deflections of the beams with unbonded tendons is far more complex than that of beams with bonded tendons because the strain compatibility at critical sections is not maintained (Naaman and Alkhairi 1991). As such, modifications are made in this study for the computation of the cracked moment of inertia, I_{cr}, and the applied load at yield point.

6.5.1 Bilinear method

In the bilinear method, the total deflection of a beam, Δ, is the sum of components Δ_1

due to the load leading to cracking, and Δ_2 due to the load increment from cracking to the ultimate. The gross moment of inertia of the concrete section, I_g, is used in the computation of Δ_1 while the moment of inertia of a cracked section, I_{cr}, is used for the computation of Δ_2. For segmental beams with dry joints, no cracking takes place in the tensile concrete at the bottom fibre. Therefore, the load resulting in Δ_1 is taken as the load leading to the yield point of the beam as shown in Figure 6-3(b), which is called yield load P_y. The determination of yield point is based on the definition of Park (1989), in which the yield point is where the projection of the intersection point of the two tangents corresponding to the two stages of the load-deflection curve at the transition zone (Figure 2-11). The selection of yield point in this approach to represent the change in the beam's stiffness is less conservative compared to the use of Point 3 for determination of P_y.

For the case of third-point loading, equations presented in Section 3.5.3 of Chapter 3 for computation of deflection can be expressed as follows:

$$\Delta_i = \frac{Pa}{24E_cI}\left(3L^2 - 4a^2\right) \tag{6.1}$$

thus,

$$\Delta_1 = \frac{P_1a}{24E_cI_g}\left(3L^2 - 4a^2\right) \tag{6.2}$$

$$\Delta_2 = \frac{P_2a}{24E_cI_{cr}}\left(3L^2 - 4a^2\right) \tag{6.3}$$

then, the total deflection Δ is computed as:

$$\Delta = \Delta_1 + \Delta_2 \tag{6.4}$$

where, P is the applied load; a is the distance from the centre of supports to the loading point, $a = L/3$ for the four-point loading; L is the span length; E_c is the concrete modulus of elasticity; I is the moment of inertia of the beam section; P_1 is the applied load leading to the yielding point, P_1 is taken as P_y; and P_2 is the load increment from P_y to the load at the ultimate stage, P_u, consequently $P_2 = P_u - P_y$. In this study, P_u is taken as the load at Point 7 for the case of over-reinforced beams where the compression failure of concrete occurs (Figure 6-3b). Meanwhile, in the case of under-

reinforced beams, P_u is taken as the load at Point 6 corresponding to the yielding of prestressing tendons.

6.5.2 Estimation of yield load

The proposed estimation of the yield load, P_y in this study is different from the computation procedure recommended by PCI (2004) because of the selection of yield point as the boundary between the first and second stage of beam's behaviour instead of using the cracking point, which is used in PCI (2004). The yield load can be determined from the following equations:

$$P_y = \frac{f_{cYP} I_g}{a\, y_{cb}} \tag{6.5}$$

$$f_{cYP} = \frac{f_{psYP} A_{ps}}{A_g} + \frac{f_{psYP} A_{ps} e_{ps}}{S_b} \tag{6.6}$$

where y_{cb} is the distance from extremely bottom fibre to the neutral axis of the concrete section; S_b is the section modulus, $S_b = I_g/y_{cb}$; A_g is the gross area of concrete section; A_{ps} is the cross-section area of prestressing tendons; e_{ps} is the eccentricity of the prestressing steel to the neutral axis; f_{cYP} is defined here as a "virtual" stress in the outmost tensile fibre of the concrete section corresponding to the stress in the tendon at yield point, f_{psYP};

In order to determine f_{psYP}, numerous numerical simulations are conducted. Table 6-1 gives the numerical results of stress values in tendons at the yield point. It is observed from the table that ratio f_{psYP} / f_{pe} is slightly affected by the variation of f_{pe} and f'_c. Hence, they are neglected in the analysis for simplicity. However, the ratio is significantly affected by the change of ρ_{ps} and L/d_{ps}. These effects of ρ_{ps} and L/d_{ps} on the ratio f_{psYP} / f_{pe} are plotted in Figure 6-4 for visualization. It is seen from the figure that ratio f_{psYP} / f_{pe} exhibits an almost perfectly linear relationship with ρ_{ps} and L/d_{ps}. Based on regression analysis, the following relation is obtained to calculate the stress in the tendon at the defined yield point:

$$\frac{f_{psYP}}{f_{pe}} = 18.9\rho_{ps} - 0.00113\, L/d_{ps} + 1.032 \tag{6.7}$$

The predicted values of f_{psYP} by Eq. 6.7 are also given in Table 6-1, which show very good agreements with the numerical results.

Table 6-1: Tendon stress at yield point

Variables	No.	Specimen	L/d_{ps}	ρ_{ps}	Effective	Yield point		f_{psYP}/f_{pe} by Eq.3	Diff. (%)
					f_{pe} (MPa)	f_{psYP} (MPa)	f_{psYP}/f_{pe}		
Group 1:	1	SD25-134-075	25	0.14%	1400	1439	1.03	1.03	0.27
A_{ps}	2	SD25-134-056	25	0.14%	1050	1076	1.02	1.03	0.58
f_{pe}	3	SD25-134-030	25	0.14%	566	585	1.03	1.03	-0.28
	4	SD25-152-075	25	0.18%	1368	1440	1.05	1.04	-1.35
	5	SD25-152-064	25	0.18%	1190	1232	1.04	1.04	0.30
	6	SD25-152-030	25	0.18%	566	590	1.04	1.04	-0.38
	7	SD25-190-081	25	0.29%	1368	1445	1.06	1.06	0.15
	8	SD25-190-050	25	0.29%	932	991	1.06	1.06	-0.51
	9	SD25-190-030	25	0.29%	616	650	1.06	1.06	0.25
	10	SD25-284-01	25	0.64%	175	196	1.12	1.12	0.42
	11	SD25-284-02	25	0.64%	342	384	1.12	1.12	0.17
	12	SD25-284-03	25	0.64%	547	620	1.13	1.12	-0.77
Group 2:	1	SD11-118-069	11	0.11%	1176	1206	1.03	1.04	1.46
A_{ps}	2	SD25-118-069	25	0.11%	1191	1212	1.02	1.02	0.70
L/d_{ps}	3	SD35-118-069	35	0.11%	1044	1060	1.02	1.01	-0.19
	4	SD45-118-069	45	0.11%	1018	1028	1.01	1.00	-0.79
	5	SD11-284-03	11	0.64%	443	514	1.16	1.14	-1.70
	6	SD25-284-03	25	0.64%	547	620	1.13	1.12	-0.77
	7	SD35-284-03	35	0.64%	527	587	1.11	1.11	-0.04
	8	SD45-284-03	45	0.64%	502	549	1.09	1.10	0.77
Group 3:	1	SD25-284-C34	25	0.64%	337	381	1.13	1.12	-0.52
f'_c	2	SD25-284-C44	25	0.64%	342	384	1.12	1.12	0.17
	3	SD25-284-C54	25	0.64%	348	384	1.10	1.12	1.93

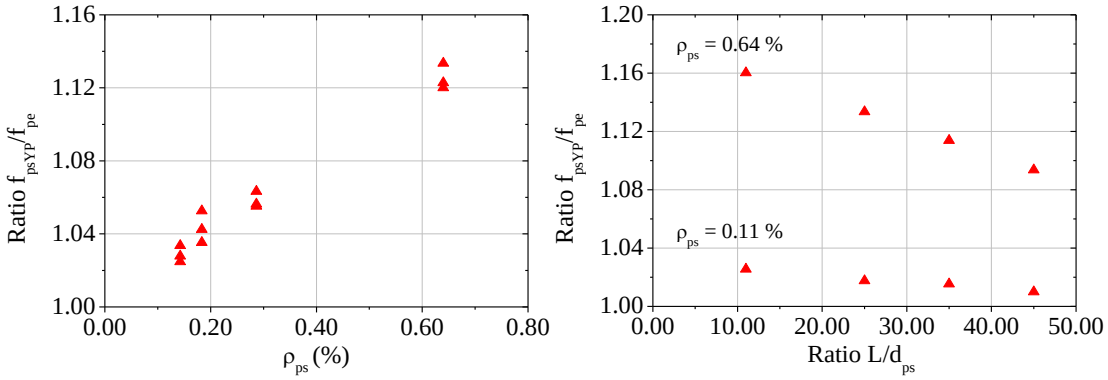

(a) (b)

Figure 6-4: Correlation of ratio f_{psYP}/f_{pe} with: (a) ρ_{ps} and f_{pe}; (b) ρ_{ps} and L/d_{ps}

6.5.3 Determination of I_{cr}

After joint opens, the segmental beam acts like a cracked beam. Therefore, the moment of inertia of the cracked section is used to compute the beam's deflection in the second stage. The moment of inertia of the cracked section is based on the cracked section analysis which is illustrated in Figure 6-5. The strain reduction coefficient, Ω_{cr}, proposed by Naaman and Alkhairi (1991) is employed in this analysis in order to convert the strain of unbonded tendons into the strain of bonded tendons. Consequently, previous analytical principles for beams with bonded tendons could be used.

From the cracked section analysis of a reinforced concrete beam, one important relationship between the steel stress, f_s, and the stress of the concrete at the level of the steel reinforcement, f_{ct}, is initiated as $f_s / f_{ct} = n$, in which n is the modulus ratio between steel and concrete. Relating this observation for the prestressed concrete, several relations are obtained as shown in Eqs. 6-8 and 6-9. It is noted that in these relations the decompression strain of concrete due to prestressing is disregarded since it is small compared to other items and the behaviour of concrete in tension is assumed to be linear as shown in Figure 5-3(b).

For a bonded tendon:

$$n = \frac{E_{ps}}{E_c} = \frac{E_{ps}\varepsilon_{ct}}{E_c\varepsilon_{ct}} = \frac{E_{ps}\Delta\varepsilon_{ps}^{bonded}}{E_c\varepsilon_{ct}} = \frac{\Delta f_{ps}^{bonded}}{f_{ct}} \tag{6.8}$$

For an unbonded tendon, n_{unb} is defined as follows:

$$n_{unb} = \frac{\Delta f_{ps}^{unbonded}}{f_{ct}} = \frac{\Omega_{cr}\Delta f_{ps}^{bonded}}{f_{ct}} = \Omega_{cr} n = \Omega_{cr}\frac{E_{ps}}{E_c} \tag{6.9}$$

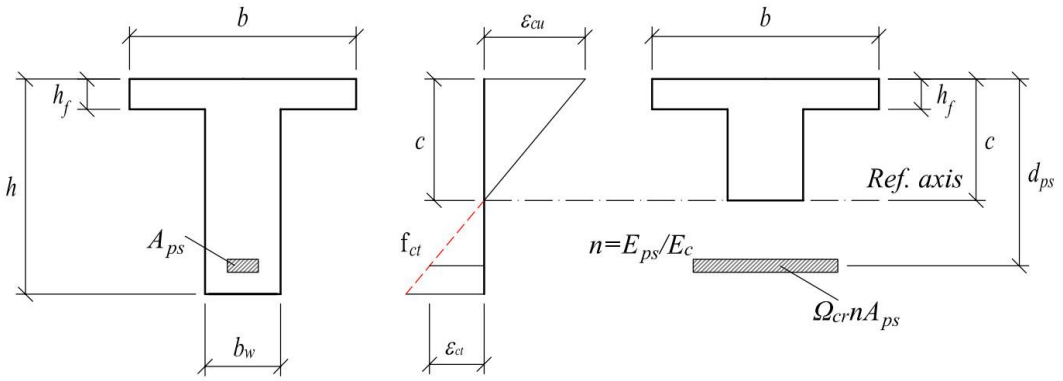

Figure 6-5: Transformed concrete section used in cracked section analysis

Consequently, the amount of unbonded prestressing tendons is assumed to be replaced by an equivalent amount of concrete, which is taken as $\Omega_{cr} nA_{ps}$. Taking the first moment of the cracked section area with respect to the reference axis (Figure 6-5), the neutral axis *c* for the case of T-sections can be determined from the following quadratic equation:

$$\frac{1}{2}b_w c^2 + \left[\frac{1}{2}(b-b_w)h_f + \Omega_{cr} nA_{ps}\right]c - \left[\frac{1}{2}(b-b_w)h_f^2 + \Omega_{cr} nA_{ps} d_{ps}\right] = 0 \tag{6.10}$$

$$c = \frac{\sqrt{D} - (b-b_w)h_f - \Omega_{cr} nA_{ps}}{b_w} \tag{6.11}$$

where,

$$D = (b-b_w)h_f\left[bh_f + 2\Omega_{cr} nA_{ps}\right] + 2\Omega_{cr} nA_{ps} b_w d_{ps} + \Omega_{cr}{}^2 n^2 A_{ps}^2 \tag{6.12}$$

then,

$$I_{cr} = \frac{1}{12}(b-b_w)h_f^3 + (b-b_w)h_f\left(c-h_f\right)^2 + \frac{1}{3}b_w c^3 + \Omega_{cr} nA_{ps}\left(d_{ps}-c\right)^2 \tag{6.13}$$

For rectangular sections, substitute $b = b_w$, and $\rho_{ps} = \dfrac{A_{ps}}{bd_{ps}}$ leading to:

$$D = \Omega_u{}^2 n^2 \rho_{ps}^2 + 2\Omega_{cr} n\rho_{ps} \tag{6.14}$$

$$c = \left(\sqrt{D} - \Omega_{cr} n \rho_{ps}\right) d_{ps} = k_1 d_{ps} \tag{6.15}$$

$$I_{cr} = \frac{1}{3} b \left(k_1 d_{ps}\right)^3 + \Omega_{cr} n A_{ps} \left(1 - k_1\right)^2 d_{ps}^2 \tag{6.16}$$

It is worth noting that Harajli and Kanj (1992) observed that Ω_{cr} in the post-cracking stage does not differ significantly from its value before cracking as mentioned previously. Since the primary concern is to simplify the cracked section analysis, they used $\Omega_{cr} = \Omega$ in their calculations. Ω is a bond reduction coefficient in the pre-cracking stage, which is provided in Naaman (1990) for different types of loading and different tendon profiles. $\Omega_{cr} = \Omega$ is also adopted in this study for the computation of I_{cr}. For the four-point loading and parabolic tendon profiles used in the specimens in this study, Ω is taken as $\Omega = \frac{44}{81} + \frac{10}{81}\frac{e_s}{e_m}$, where e_s and e_m are the tendon eccentricities at the support and at the midspan, respectively.

6.5.4 Analytical predictions

Figure 6-6 shows the prediction of the load-deflection curve of Beam S1, which was tested in the study of Le et al. (2018). A good agreement is observed between the analytical prediction and the experimental result. As mentioned previously, the calculation procedure presented above is to predict the load-deflection curve up to the yielding of the prestressing steel as shown in the figure. It is noted that the predicted curve exhibits a higher initial stiffness compared to the experimental result. This leads to a higher stiffness in the predicted curve in the second stage as compared to the experimental curve. This difference might be due to the imperfect testing conditions of Beam S1, i.e. the imperfect contact of the keyed joints between segments causing the reduction in the beam's initial stiffness, which in turn resulted in the variations between the experimental and predicted results as observed.

The load-deflection curves of various numerical models are shown in Figure 6-7. These numerical models simulate the behaviour of PSBs with different parameters including the variations in the ratio L/d_{ps} as shown in Figure 6-7(a), A_{ps} and f_{pe} as shown in Figure 6-7 (b and c), and the concrete strength f'_c as shown in Figure 6-7(d). It is seen clearly that the bilinear method presented above predicts very well the load-deflection responses from the numerical simulations of PSBs of different designs.

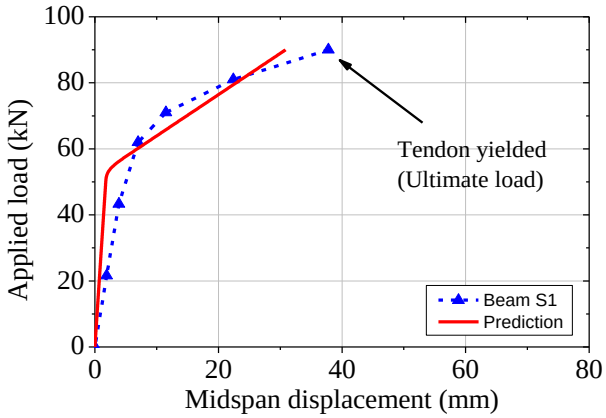

Figure 6-6: Prediction of load-deflection curve of Beam S1 tested by Le et al. (2018)

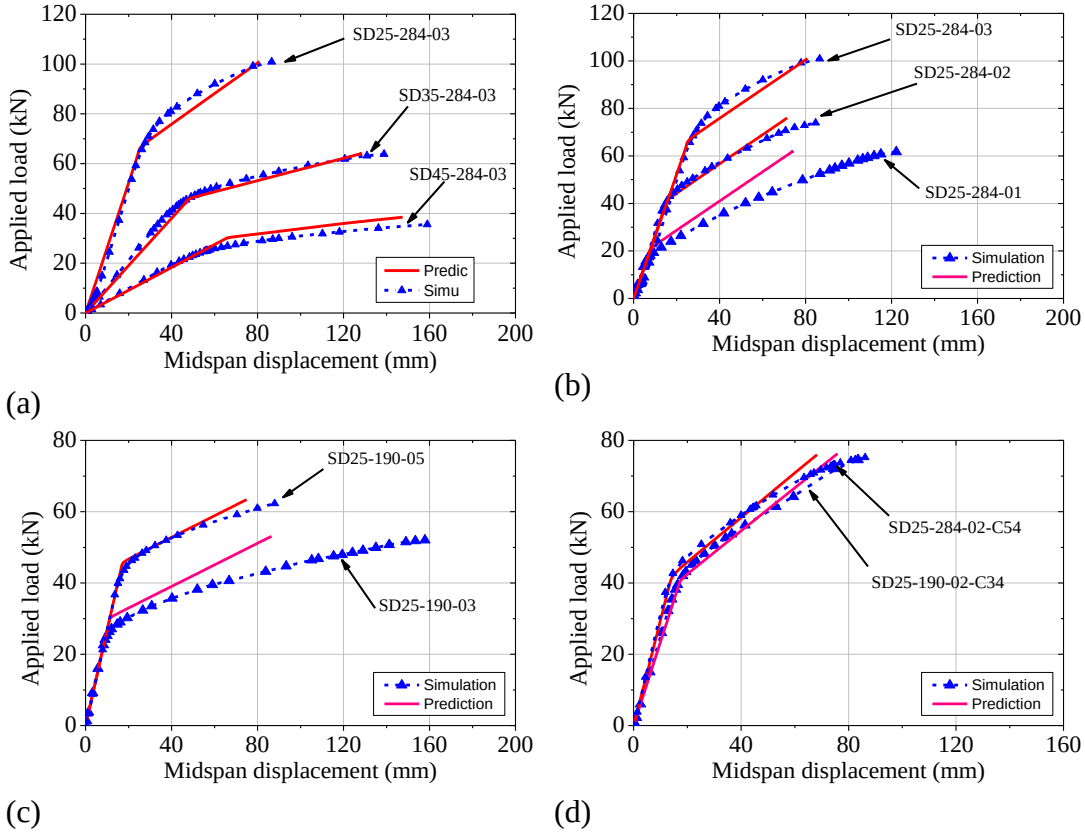

Figure 6-7: Load-deflection curve of beams with: (a) Variation in L/d_{ps} ratio ; (b) Variation of f_{pe}/f_{pu} ratio; (c) Variation in A_{ps} compared to Beams in Group (b); (d) Variation in f'_c

However, the presented procedure does not predict well the load-deflection curves of Beam SD25-284-01 (Figure 6-7b) and Beam SD25-190-03 (Figure 6-7c). It is noted that Beam SD25-284-01 is prestressed with f_{pe}/f_{pu} = 0.1, which generates a compressive stress of 7.4 MPa ($0.17f'_c$) in the concrete. Meanwhile, the compressive stress in concrete due to f_{pe} in Beam SD25-190-03 with f_{pe}/f_{pu} = 0.3 is 11.03 MPa, which is equal to $0.25f'_c$. When the ratio f_{pe}/f_{pu} is increased in these two beams, that

leads to the higher compressive stress in the concrete due to f_{pe}, the accuracy in the predictions of the load-deflection curves for these beams is greatly improved as observed in Figure 6-7 (b and c). In fact, large variations are also observed in the prediction of tendon stresses for these beams by existing models as presented later in the next sections. These large variations in the prediction of tendon stresses are the reason for the considerable variations in the prediction of load-deflection responses for these beams. This is because the strain reduction factor Ω_{cr}, which represents the strain correlation between an unbonded tendon and a bonded tendon, is used in the calculation of load-deflection responses by the above presented procedure. From the analysis in this study, which will be presented later, it is suggested that f_{pe} leading to compressive stresses in the concrete not lesser than $0.27f'_c$ should be maintained in order to gain accurate predictions of load-deflection responses of the segmental beams.

6.6 Balanced condition

6.6.1 Without considering self-weight of beam's components

Balanced condition is defined as a state at which the tension reinforcement reaches its yield strength while the concrete in compression reaches its assumed ultimate strain of 0.003. The reinforcement ratio, ρ corresponds to this balanced strain condition is called balanced reinforcement ratio, ρ_b. From the strain compatibility and force equilibrium (Figure 6-8), the following equation is obtained to compute ρ_b for beams with bonded tendons:

$$\rho_b = 0.85\beta_1 \frac{f_c^{'}}{f_{py}} \frac{\varepsilon_{cu}}{\varepsilon_{cu} + \Delta\varepsilon_{py}^{bonded} - \varepsilon_{ce}} \tag{6.17}$$

where f'_c is the compressive concrete strength; β_1 is the stress-block factor for concrete; f_{py} is the yield strength of prestressing steel; $\Delta\varepsilon_{py}^{bonded}$ is the strain increment in the tendon from effective prestress strain $\varepsilon_{pe}^{bonded}$ to the yield strain ε_{py}; ε_{cu} is the assumed ultimate strain of concrete, which is taken as 0.003; ε_{ce} is the strain in concrete at level of prestressing steel due to f_{pe}; other terms are defined in Figure 6-8. Since ε_{ce} is very small compared to the other terms (Naaman and Alkhairi 1991), it is neglected in this analysis for simplification leading to the following expression for ρ_b:

$$\rho_b = 0.85\beta_1 \frac{f_c^{'}}{f_{py}} \frac{\varepsilon_{cu}}{\varepsilon_{cu} + \Delta\varepsilon_{ps}^{bonded}} \tag{6.18}$$

Eq. 6.18 is only valid for beams with bonded tendons when the strain compatibility exists. Due to the lack of strain compatibility between the tendon and the surrounding concrete in the case of beams with unbonded tendons, Eq. 6.18 cannot be directly applied for beams with unbonded tendons. Therefore, the strain reduction factor Ω_u, which was proposed by Naaman and Alkhairi (1991) is employed herein to relate the strain in the unbonded tendons to the strain of equivalent bonded tendons that makes the possible use of Eq. 6.18 for beams with unbonded tendons.

According to Naaman and Alkhairi (1991), the strain increment in the unbonded tendon, $\Delta\varepsilon_u$, is related to the strain increment of a bonded tendon, $\Delta\varepsilon_u^{bonded}$ as follows:

$$\Delta\varepsilon_u^{bonded} = \frac{\Delta\varepsilon_u}{\Omega_u} \tag{6.19}$$

Substituting Eq. 6.19 into Eq. 6.18 and setting the strain increment in the unbonded tendon when it reaches its yield strength at the balanced condition, $\Delta\varepsilon_u = \varepsilon_{py} - \varepsilon_{pe}$, Eq. 6.18 can be expressed as follows:

$$\rho_b = 0.85\beta_1 \frac{f_c^{'}}{f_{py}} \frac{\varepsilon_{cu}}{\varepsilon_{cu} + \dfrac{\varepsilon_{py} - \varepsilon_{pe}}{\Omega_u}} \tag{6.20}$$

6.6.2 Considering self-weight of beam's components

Practically, the effects of self-weight and prestressing will simultaneously act on a structure. In this analysis, these effects are considered as separate loads and are applied on structures in sequence. As such, there are three individual loads applied on the beam as follows: the prestressing effect is applied at first, following by the self-weight of the beam and then the external load (four-point loading) is applied up to the ultimate stage of the structure.

Due to the effect of self-weight, the prestressing steel is further tensioned to an extra amount before being subjected to the external loads. It means the initial state of the prestressing steel before applying the external loads is changed. The tensile strain of

concrete in the top fibre due to prestressing is reduced while the concrete in the bottom fibre decompresses. The strain states of concrete in the top and bottom fibres to be in compression or tension depend on the level of prestressing and the effect of self-weight. As such, there are two cases to be considered in the analysis. In the first case, stress in the concrete at the bottom fibre at the level of prestressing steel due to self-weight (absolute value), σ_{cSW}^{bot} is smaller than the stress in the concrete in the bottom fibre due to prestressing, σ_{cfpe}^{bot} as shown in Figure 6-9(a). The second case is when σ_{cSW}^{bot} (absolute value) is greater than σ_{cfpe}^{bot} as shown in Figure 6-9(b).

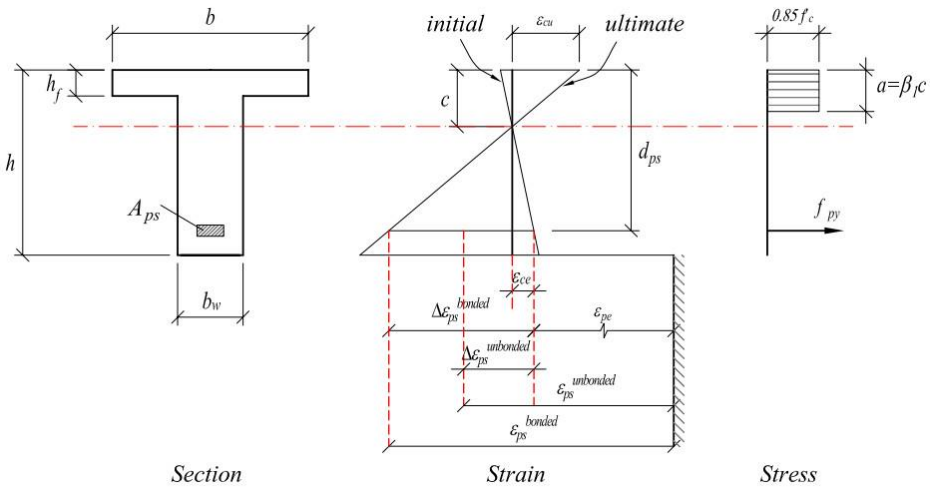

Figure 6-8: Strain condition at balanced condition without self-weight

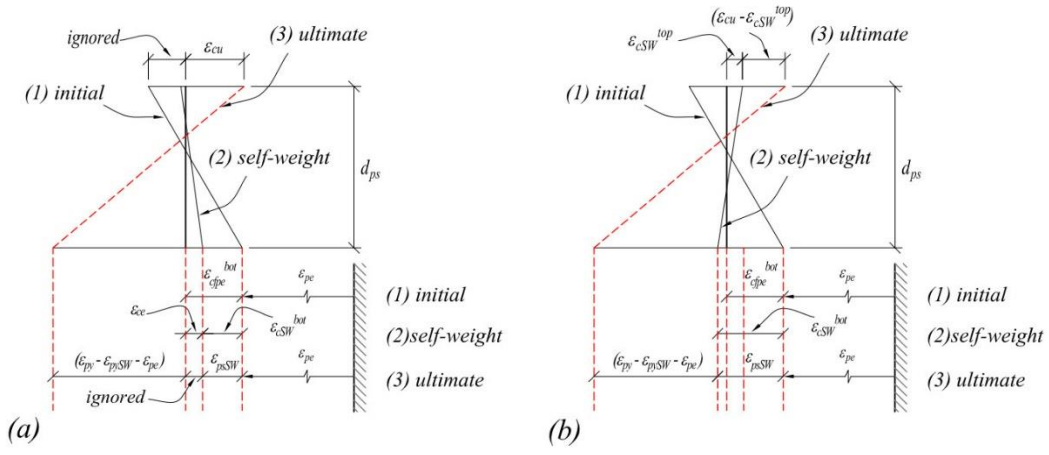

Figure 6-9: Strain conditions at balanced condition considering self-weight

The following assumptions are used in the analyses in this section: (1) the self-weight of the beam's components is uniformly distributed along the member's axis; (2) before the opening of joints, the beams section remains plane under bending; and (3) when

tensile concrete is considered, linear behaviour is assumed for its tensile behaviour.

In the first case, when $\sigma_{cSW}^{bot} < \sigma_{cfpe}^{bot}$, the concrete in the bottom fibre is still in compression, while the concrete in the top fibre is in tension. In other words, the beam exhibits a camber after the effects of prestressing and self-weight. In this study, dry joints are used in the specimens. Therefore, the tensile strain is ignored for the concrete in the top fibre. If bonded tendons are used, the strain in the tendons is equal to the strain in the concrete at its level. But when unbonded tendons are used, the strain in the tendons due to self-weight, ε_{psSW} can be correlated to the strain in the concrete at its level, ε_{cSW}^{bot} as below:

$$\varepsilon_{psSW} = \frac{\varepsilon_{cSW}^{bot}}{\Omega} \tag{6.21}$$

where Ω is the strain reduction factor in the pre-cracking stage developed by Naaman and Alkhairi (1991). For the four-point loading and parabolic tendon profiles used in the specimens in this study, Ω is taken as $\Omega = \frac{44}{81} + \frac{10}{81}\frac{e_s}{e_m}$. For other loading types and tendon profiles refers to Naaman and Alkhairi (1991).

Based on Eq. 6.20, the following expression is derived for the balanced ratio of segmental concrete beams when the self-weight is taken into account:

$$\rho_b = 0.85\beta_1 \frac{f_c^{'}}{f_{py}} \frac{\varepsilon_{cu}}{\varepsilon_{cu} + \frac{1}{\Omega_u}\left(\varepsilon_{py} - \varepsilon_{pe} - \varepsilon_{psSW}\right)} \tag{6.22}$$

or,

$$\rho_b = 0.85\beta_1 \frac{f_c^{'}}{f_{py}} \frac{\varepsilon_{cu}}{\varepsilon_{cu} + \frac{1}{\Omega_u}\left(\varepsilon_{py} - \varepsilon_{pe} - \frac{1}{\Omega}\varepsilon_{cSW}^{bot}\right)} \tag{6.23}$$

The strain in the concrete at the prestressing level, ε_{cSW}^{bot} in Eq. 6.23 is computed as follows by assuming the self-weight is uniformly distributed over the beams' length:

$$\varepsilon_{cSW}^{bot} = \frac{\sigma_{cSW}^{bot}}{E_c} = \frac{M_{SW}}{E_c I_g} y_{bps} = \frac{wL^2}{8E_c I_g} y_{bps} \tag{6.24}$$

where M_{SW} is the moment due to self-weight; y_{bps} is the distance from the prestressing tendon to the neutral axis of the beam's gross section; w is the unit weight of the beam, which is taken as the weight of the beam's components divided by the beam length; L is the span length.

Substituting Eq. 6.24 into Eq. 6.23 and replacing strain values of prestressing steel by their stress values, the following expression is finally obtained to compute the balanced ratio of the segmental concrete beams with unbonded tendons, when the self-weight is taken into account:

$$\rho_b = 0.85\beta_1 \frac{f_c^{'}}{f_{py}} \frac{\varepsilon_{cu}}{\varepsilon_{cu} + \frac{1}{\Omega_u}\left(\frac{f_{py} - f_{pe}}{E_{ps}} - \frac{1}{\Omega}\frac{wL^2 y_{bps}}{8E_c I_g}\right)} \tag{6.25}$$

It is noted that for segmental beams with unbonded steel tendons, the strain reduction factor Ω_u in Eq. 6.25 is taken as $\Omega_u = 2.4/(L/d_{ps})$. Since this value of Ω_u shows the best correlation between the predicted and the numerical values for the strain in the unbonded tendons at ultimate stage. Details of the determination of Ω_u for PSBs with unbonded steel tendons will be discussed in next sections. It is noted that Eq. 6.25 is mathematically derived from the section analysis, it therefore can be applied for the case of a beam with CFRP tendons. If so, same values of Ω provided in Naaman and Alkhairi (1991) can be used in Eq. 6.25 since Ω is a material independent coefficient and is mathematically obtained from given loading types and tendon profiles. Only the coefficient Ω_u requires modification for the case of CFRP tendons for which $\Omega_u = 2.1/(L/d_{ps})$ can be used for the case of beams with internal unbonded CFRP tendons as suggested by Le et al. (2018).

In the second case, when $\sigma_{cSW}^{bot} > \sigma_{cfpe}^{bot}$, the concrete in the bottom fibre is in tension. This tensile strain in the concrete in the bottom fibre is ignored since the dry joints are considered. The strain in the prestressing tendon due to self-weight is computed the same as the above. Meanwhile, the concrete in the top fibre is in compression. In other words, the beam exhibits an initial deflection due to the effects of prestressing and self-weight as shown in Figure 6-9(b). When this compressive strain in the concrete in the top fibre is considered, Eq. 6.23 derived previously is rewritten as follows:

$$\rho_b = 0.85\beta_1 \frac{f_c^{'}}{f_{py}} \frac{\left(\varepsilon_{cu} - \varepsilon_{cSW}^{top}\right)}{\left(\varepsilon_{cu} - \varepsilon_{cSW}^{top}\right) + \frac{1}{\Omega_u}\left(\varepsilon_{py} - \varepsilon_{pe} - \frac{1}{\Omega}\varepsilon_{cSW}^{bot}\right)} \tag{6.26}$$

In Eq. 6.26, ε_{cSW}^{top} is the compressive strain in the concrete in the extreme top fibre. Similarly, ε_{cSW}^{top} is calculated as follows:

$$\varepsilon_{cSW}^{top} = \frac{wL^2 y_{t,cr}}{8E_c I_g} \tag{6.27}$$

where $y_{t,cr}$ is the distance from the extreme top fibre to the neutral axis of the cracked section. Then, the following equation is obtained for balanced ratio when $\sigma_{cSW}^{bot} > \sigma_{cfpe}^{bot}$:

$$\rho_b = 0.85\beta_1 \frac{f_c^{'}}{f_{py}} \frac{\left(\varepsilon_{cu} - \frac{wL^2 y_{t,cr}}{8E_c I_g}\right)}{\left(\varepsilon_{cu} - \frac{wL^2 y_{t,cr}}{8E_c I_g}\right) + \frac{1}{\Omega_u}\left(\frac{f_{py} - f_{pe}}{E_{ps}} - \frac{1}{\Omega}\frac{wL^2 y_{bps}}{8E_c I_g}\right)} \tag{6.28}$$

However, in practice the concrete in the bottom fibre of a segmental beam is designed to be in compression with the aim of creating an initial camber in the beam. This initial compression in the concrete at the bottom fibre also prevents the prestressing steel from exposed to harsh environments. As such, Eq. 6.28 does not have practical use.

6.6.3 Evaluation of analytical predictions

To evaluate the accuracy of Eq. 6.25 for the estimation of ρ_b, two beam configurations with unbonded tendons and different reinforcement ratios ρ are simulated and analysed. The detailed beams' configurations are given in Table 6-2. Beams SD25-190 are configured with two tendons of 19.0 mm diameter while Beams SD25-152 are configured with two 15.2-mm-diameter tendons. These beams are prestressed with three different effective prestress values as shown in the table. According to Eq. 6.25, Specimens SD25-190-074 and SD25-152-064 will fail in the balanced condition, i.e. both concrete in compression crushes and tendon yields at the ultimate stage since $\rho_{ps} = \rho_b$ as shown in Table 6-2. Beams SD25-190-083 and SD25-152-75 will fail in tension-controlled mode since $\rho_{ps} < \rho_b$ while Beams SD25-190-065 and SD25-152-

050 will fail in compression-controlled mode since $\rho_{ps} > \rho_b$. Very good agreements in the failure modes of these beams are observed as compared to the numerical results as shown in Figs. 6-10 and 6-11. As observed in Figure 6-10, in Beam SD25-190-083 the tendons reached its yielding stress before the occurrence of concrete compression failure. In contrast, concrete in compression side in Beam SD25-190-065 crushes but no yielding of prestressing steel is observed. Meanwhile, both concrete in compression crushing and tendon yielding are observed in Beam SD25-190-074 at the ultimate stage. Similar observations in the failure modes of Beams SD25-152 are also observed in Figure 6-11, which agrees well with the analytical predictions.

Table 6-2: Balanced reinforcement ratio

Specimen	f_{pe}/f_{pu}	ρ_{ps}	ρ_b by Eq. 6.25		Prediction	Simulation
SD25-190-083	0.83	0.26%	0.61%	$\rho_{ps} < \rho_b$	Tension-controlled	Tension-controlled
SD25-190-074	0.74	0.26%	0.29%	$\rho_{ps} = \rho_b$	Balanced condition	Balanced condition
SD25-190-065	0.65	0.26%	0.19%	$\rho_{ps} > \rho_b$	Compression-controlled	Compression-controlled
SD25-152-075	0.80	0.18%	0.45%	$\rho_{ps} < \rho_b$	Tension-controlled	Tension-controlled
SD25-152-064	0.64	0.18%	0.18%	$\rho_{ps} = \rho_b$	Balanced condition	Balanced condition
SD25-152-050	0.50	0.18%	0.09%	$\rho_{ps} > \rho_b$	Compression-controlled	Compression-controlled

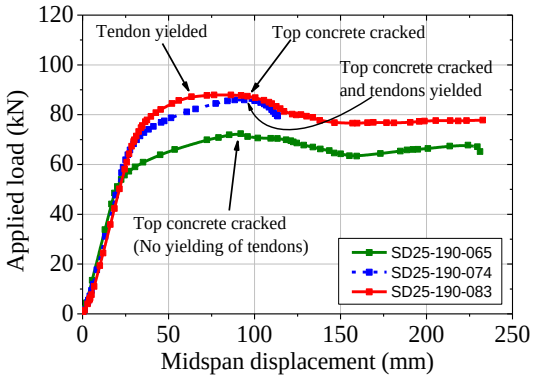

Figure 6-10: Load-deflection curve of SD25-190 specimens

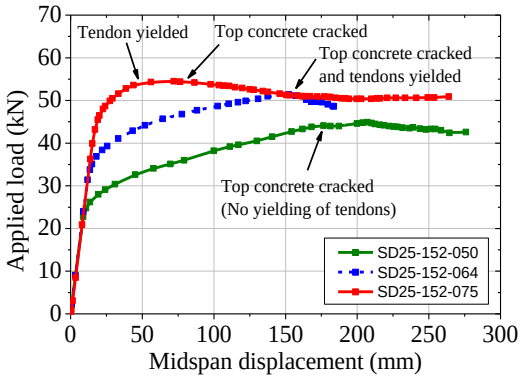

Figure 6-11: Load-deflection curve of SD25-152 specimens

6.7 Evaluation of prediction of strength by existing models

This section evaluates the accuracy of existing models for predicting the ultimate strength capacities of PSBs with unbonded tendons. The examined models include equations for predicting f_{ps} recommended by AASHTO (1999), ACI 318 (2015) and Naaman and Alkhairi (1991). Various simulation models are built and analysed, which

take into consideration the effects of four main parameters on the strength capacities of PSBs under four-point bending. These parameters include the ratio of span length to tendon depth L/d_{ps}, the effective prestressing stress f_{pe}, the area of prestressing tendons A_{ps}, and the concrete strength f'_c. All the beams in the models have the same section geometry as shown in Figure 6-1. The details of the beams' configuration are given in Table 6-3.

Table 6-3: Beams' configuration for strength evaluation

Group	Specimen	L/d_{ps}	f_{pe}/f_{pu}	ρ_{ps}	f'_c
1	SD11-284-03	11			
(L/d_{ps})	SD15-284-03	15			
	SD25-284-03	25	0.3	0.00640	44
	SD35-284-03	35			
	SD45-284-03	45			
2	SD25-284-01		0.1		
(f_{pe})	SD25-284-02	25	0.2	0.00640	44
	SD25-284-03		0.3		
3	SD25-284-03			0.00640	
(A_{ps})	SD25-190-03	25	0.3	0.00286	44
	SD25-152-03			0.00183	
4	SD25-284-C34				34
(f'_c)	SD25-284-C44	25	0.2	0.00640	44
	SD25-284-C54				54

6.7.1 Existing models for prediction of f_{ps}

AASHTO (1999) adopted the following equation, which is explained in Roberts-Wollmann et al. (2005) to compute the stress in the unbonded tendons of PSBs:

$$f_{ps} = f_{pe} + 6200\left(\frac{d_{ps} - c}{l_e}\right), MPa \tag{6.29}$$

where f_{pe} is the effective tensile stress of the tendons, $l_e = l_i/(1+[N/2])$, in which l_i is the length of the tendon between anchorages, and N is the number of support hinges required to form a mechanism crossed by the tendon. For a simply supported beam, l_e is equal to the span length L. Eq. 6.29 is also recommended by AASHTO LRFD (2012).

ACI 318 (2015) recommended the following equation, which is based on the research performed by Mattock et al. (1971):

$$f_{ps} = f_{pe} + 69 + \frac{f_c^{'}}{100\rho_{ps}}, MPa \tag{6.30}$$

where ρ_{ps} is the prestressing reinforcement ratio. This equation is applicable to beams with $L/d_{ps} \leq 35$ as recommended by the code.

Naaman and Alkhairi (1991) developed the following equation to predict the stress in the unbonded tendons at the ultimate stage.

$$f_{ps} = f_{pe} + \Omega_u E_{ps} \varepsilon_{cu} \left(\frac{d_{ps}}{c_u} - 1 \right) \tag{6.31}$$

where E_{ps} is the tendon modulus of elasticity, ε_{cu} is the ultimate concrete compression strain which is taken as 0.003; and Ω_u is a strain reduction coefficient. For conservative predictions, Naaman and Alkhairi (1991) recommended $\Omega_u = 3.0/(L/d_{ps})$ for uniform or four-point loading, where L is the span length. This value of Ω_u is used in the present study in order to have fair comparisons between results predicted by the examined models.

Strain compatibility analysis is then used for the computation of the flexural resistances of the beams. To evaluate the accuracy of these existing models for PSBs with internal unbonded tendons, comparisons between the analytical results by the models and the numerical results are made, which are presented in terms of mean value and standard deviation (SD). The comparison results are shown in Figure 6-12 to Figure 6-14.

6.7.2 Comparisons between prediction and numerical results

It is seen from Figure 6-12(a,b) that the two examined codes yield relatively good predictions of f_{ps} at the ultimate stage. All the predicted results are conservative since they are smaller than the corresponding numerical results. However, AASHTO (1999)'s equation yields better predictions than those of ACI 318 (2015). The mean value of the ratio predicted/simulated f_{ps} by AASHTO (1999) is 0.82 with the corresponding SD value is 0.14 while that value for ACI 318 (2015) is 0.71 with SD of 0.12. All the codes reflect relatively good trends in the change of f_{ps} with respects

to the change of the studied parameters, including L/d_{ps}, f_{pe}, and f'_c, but do not capture well f_{ps} when A_{ps} varies. This will be further discussed in the following section. Similar observations are seen in the predictions of Δf_{ps} by the examined codes as shown in Figure 6-13(a,b). AASHTO (1999)'s model gives better predictions of Δf_{ps} compared to the model recommended by ACI 318 (2015).

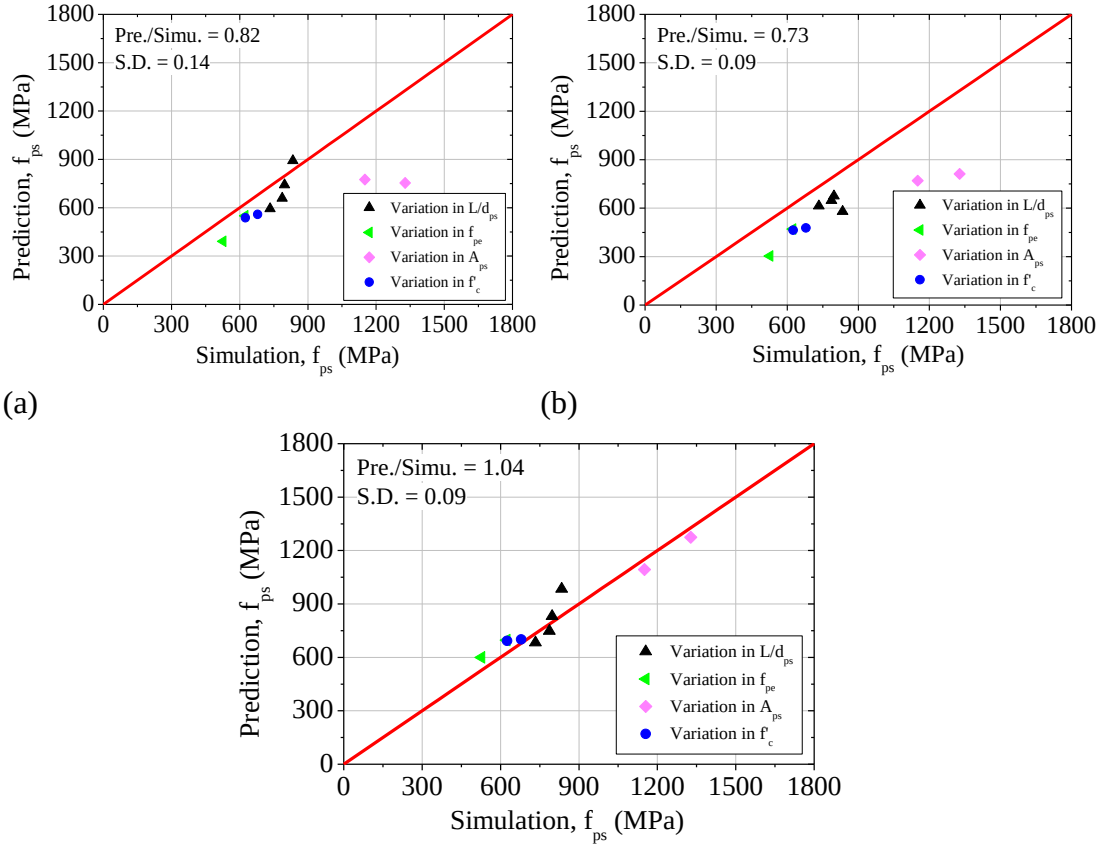

Figure 6-12: Prediction of f_{ps} by: (a) AASHTO (1999); (b) ACI 318 (2015); (c) Naaman and Alkhairi (1991)

As a consequence, AASHTO (1999)'s model gives more accurate predictions of P_u at the ultimate stage compared to ACI 318 (2015)'s model (Figure 6-14a,b). The mean value of the predicted to simulated results of P_u is 0.84 with SD of 0.13 while that value for ACI 318 (2015) is 0.75 with SD of 0.08. All the two codes give conservative predictions of P_u for all the beams, except for the case of Beam SD11-284-03, where AASHTO (1999)'s model slightly over-predict P_u by about 7% compared to numerical results. It is noted that Specimen SD11-284-03 has the ratio of L/d_{ps} equal to 11, which the span length is the shortest considered in this study.

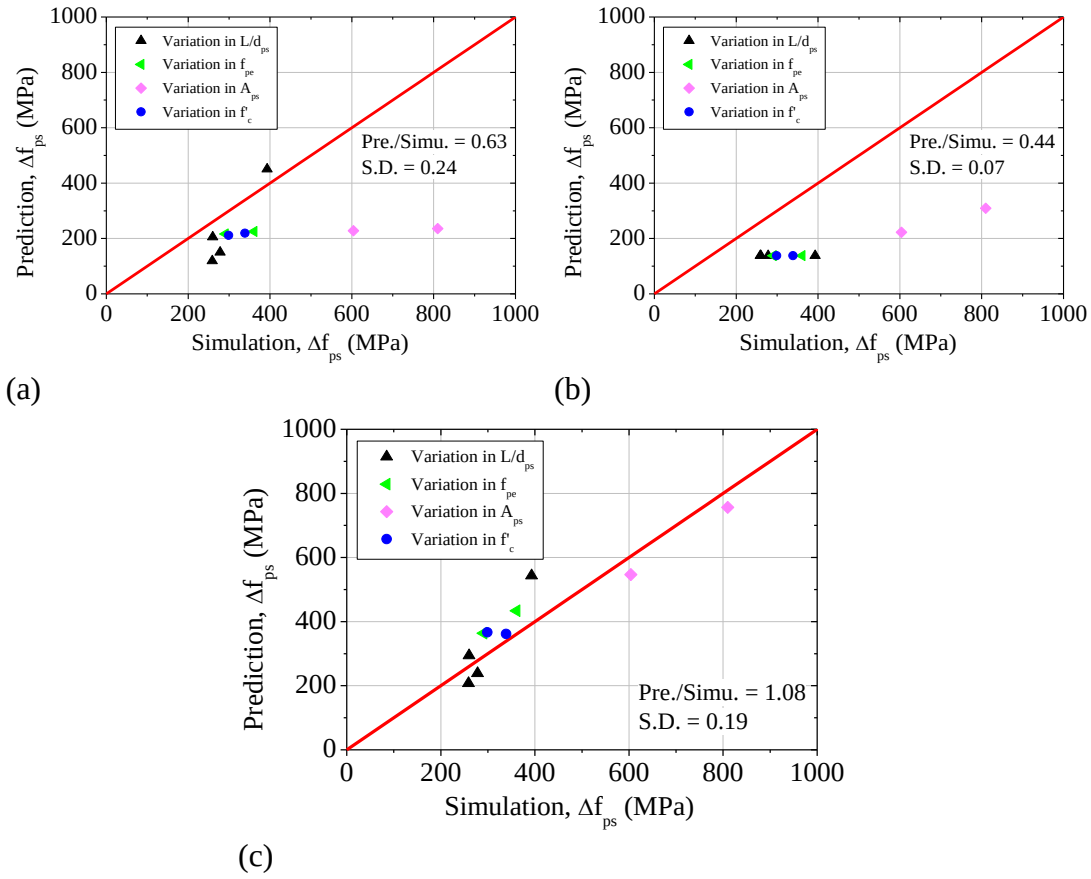

Figure 6-13: Prediction of Δf_{ps} by: (a) AASHTO (1999); (b) ACI 318 (2015); (c) Naaman and Alkhairi (1991)

Meanwhile, the model developed by Naaman and Alkhairi (1991) captures very well the changes of f_{ps} with respects to the changes of all the studied parameters as observed in Figure 6-12(c). However, it overestimates Δf_{ps}, hence f_{ps} at the ultimate stage. The mean value of the ratio between the predicted and simulated results of Δf_{ps} is 1.08 with SD of 0.19 (Figure 6-13c) while that value for the ratio between the predicted and simulated results of f_{ps} is 1.04 with SD of 0.09 (Figure 6-12c). As a result, the model over-estimates P_u at the ultimate stage as shown in Figure 6-14(c). The mean value of the ratio between the predicted and simulated results of P_u is 1.06 with SD of 0.09. It is worth noting that the value of the strain reduction factor $\Omega_u = 3.0/(L/d_{ps})$ is used in this analysis. This value of Ω_u is for conservative predictions of f_{ps} recommended by Naaman and Alkhairi (1991) and is based on the analyses of monolithic beams with unbonded tendons. Since segmental beams with dry joints are investigated in this study, Naaman and Alkhairi (1991)'s model over-estimates f_{ps}, hence P_u at the ultimate stage as observed.

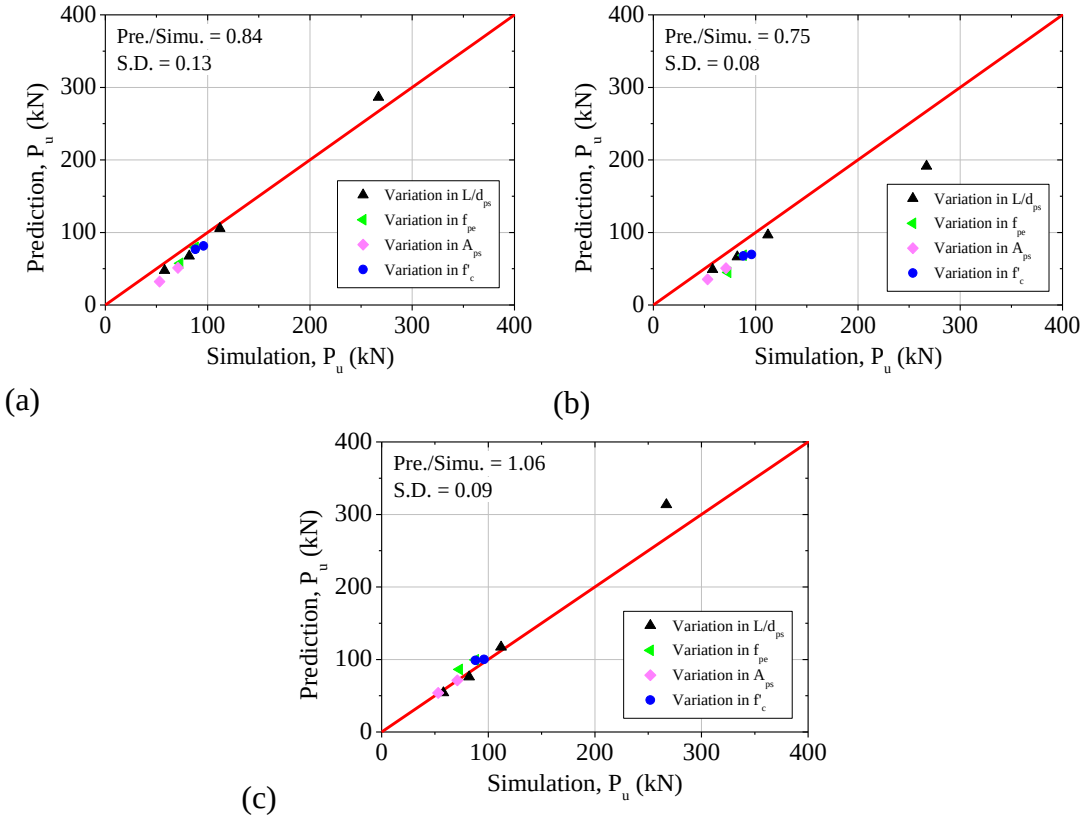

Figure 6-14: Prediction of P_u by: (a) AASHTO (1999); (b) ACI 318-14 (2015); (c) Naaman and Alkhairi (1991)

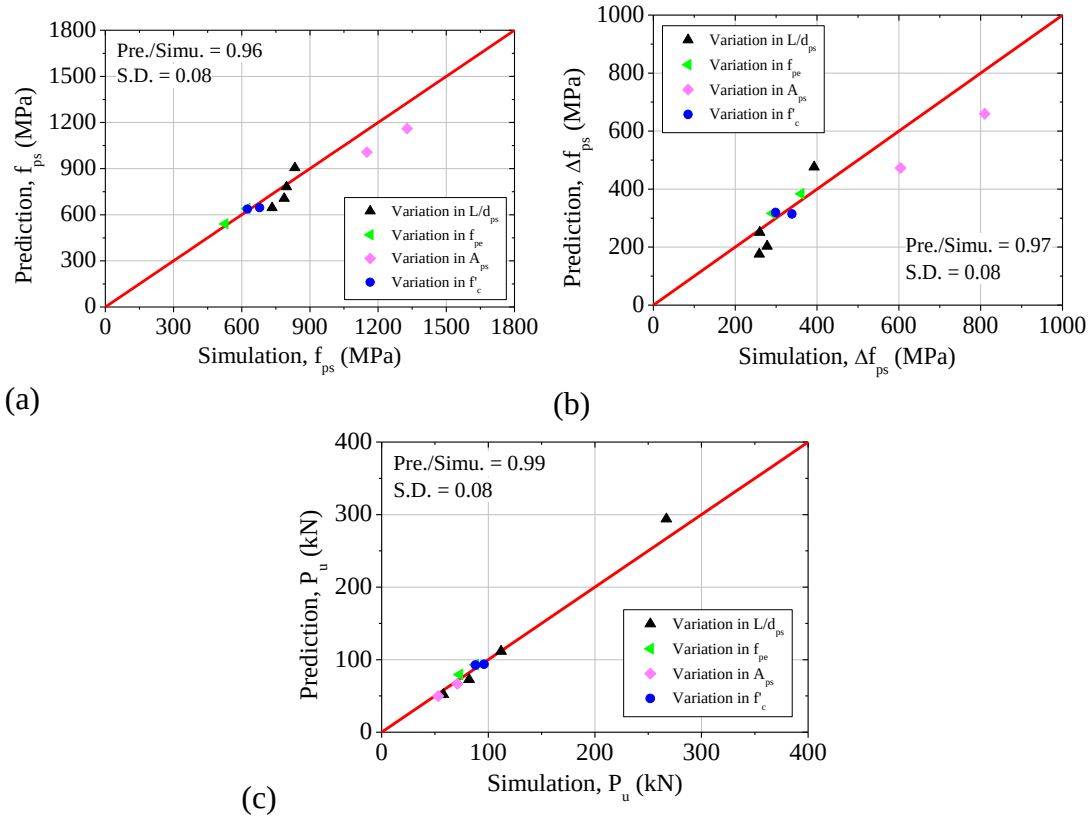

Figure 6-15: Performance of Naaman and Alkhairi (1991) modified by this study for the prediction of: (a) f_{ps}; (b) Δf_{ps}; (c) P_u

It is suggested to use the numerical results to determine the value of Ω_u which will lead to the best correlation between the numerical observations and predicted values of f_{ps} at the ultimate stage. The specimens modelled in this study focus on the variation in the four parameters (Table 6-3). Their span length to tendon depth L/d_{ps} ratio ranges from 11 to 45, the area of prestressing tendons A_{ps} and the effective prestress vary in a range to generate the concrete stress in compression due to f_{pe} ranging from $0.16f'_c$ to $0.54f'_c$, and three values of concrete strength (34 MPa, 44 MPa, and 54 MPa) are used. All the beams are subjected to four-point loading. The value $\Omega_u = 2.4/(L/d_{ps})$ shows the best correlation between the numerical and analytical results for f_{ps} , Δf_{ps} , *and* P_u as shown in Figure 6-15. All the mean values of the predicted to simulated results and their SD values are greatly improved as seen in the figure. This value of $\Omega_u = 2.4/(L/d_{ps})$ is used for the analyses of the load-deflection responses and the balanced condition of PSBs with unbonded tendons presented in the previous sections.

6.7.3 Correlation of A_{ps} and f_{pe} on the effectiveness of codes' predictions

As discussed previously, all the three examined codes do not predict well the f_{ps} and the corresponding P_u when varying A_{ps}. This happens to Specimen SD25-152-03, which is prestressed with two 15.2-mm diameter tendons (ω_{ps} = 0.183%) at an effective prestress f_{pe} equal $0.3f_{pu}$. This low effective prestress value might be the reason of the ineffectiveness of the codes' predictions.

An effort is made by the authors to verify this by further simulating the behaviour of the beam with various values of effective prestress f_{pe}. It is observed from Table 6-4 that the changes in f_{pe} highly affect the accuracy of all the codes' model in the prediction of f_{ps} and P_u of the specimens. The higher the f_{pe} is, the more accurate the codes' models predict. To unify the combined effect of A_{ps} and f_{pe}, compressive concrete stress at the bottom fibre, σ_c due to f_{pe} are determined and are also provided in Table 6-4. It is seen that when σ_c is greater than 11.88 MPa ($0.27f'_c$), the differences between the predicted results and the corresponding numerical values are less than 17%, i.e. ratio of Pre./Simu. of P_u is greater than 0.83 as shown in Table 6-4 and Figure 6-16.

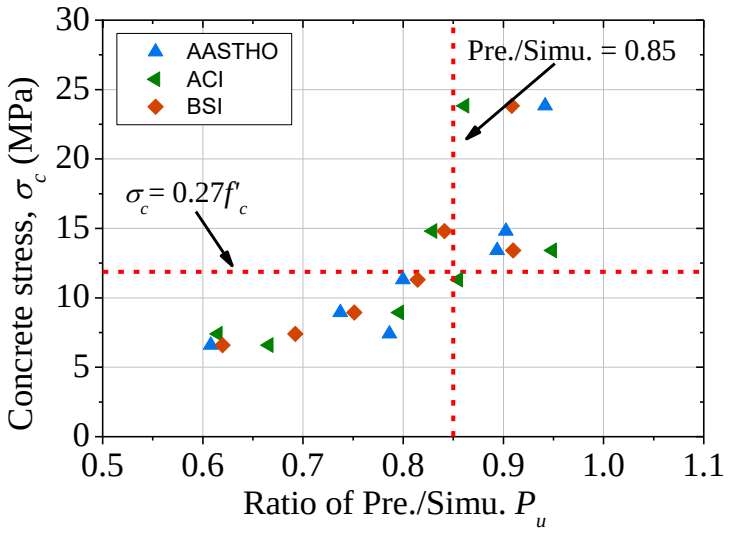

Figure 6-16: Value of compressive concrete stress σ_c

Table 6-4: Codes' strength predictions under the changes of A_{ps} and f_{pe}

Specimen	ρ_{ps}	f_{pe}/f_{ps}	$\sigma_c^{(*)}$	f_{pe}	f_{ps}			P_u		
					Simu.	Pre.	Pre./Simu.	Simu.	Pre.	Pre./Simu.
by AASTHO (1999)										
SD25-284-01	0.638%	0.09	7.4	166	527	391	0.74	73	57	0.79
SD25-284-02	0.638%	0.18	14.8	333	624	549	0.88	88	79	0.90
SD25-284-03	0.638%	0.29	23.8	537	797	742	0.93	112	105	0.94
SD25-152-03	0.183%	0.28	6.6	518	1328	754	0.57	53	32	0.61
SD25-152-04	0.183%	0.38	8.9	703	1322	936	0.71	54	40	0.74
SD25-152-05	0.183%	0.48	11.3	884	1513	1114	0.74	59	47	0.80
SD25-152-06	0.183%	0.57	13.4	1066	1509	1293	0.86	61	55	0.89
by ACI 318 (2015)										
SD25-284-01	0.638%	0.09	7.4	166	527	304	0.58	73	45	0.62
SD25-284-02	0.638%	0.18	14.8	333	624	479	0.77	88	73	0.83
SD25-284-03	0.638%	0.29	23.8	537	797	675	0.85	112	96	0.86
SD25-152-03	0.183%	0.28	6.6	518	1328	827	0.62	53	35	0.67
SD25-152-04	0.183%	0.38	8.9	703	1322	1012	0.77	54	43	0.80
SD25-152-05	0.183%	0.48	11.3	884	1513	1193	0.79	59	50	0.86
SD25-152-06	0.183%	0.57	13.4	1066	1509	1375	0.91	61	58	0.95

ACI 318 (2015) limits the use of Eq. 6.30 for members prestressed with unbonded tendons if $f_{pe} \geq 0.5f_{pu}$. Meanwhile, no limitations of minimum value of f_{pe} are specified by AASHTO (1999). ACI 318 (2015) and AASHTO LRFD (2012) limit the maximum of compressive concrete stress under the service limit state ($0.6f'_c$ by ACI 318 (2015) or $0.6\phi_w f'_c$ by AASHTO LRFD (2012)). However, no recommendations on the minimum value of compressive concrete stress due to f_{pe} are given. It is found from

this study that when the compressive stress in the concrete stress due to f_{pe} not less than $0.27f'_c$ is maintained, the predictions of beams' strength at the ultimate stage by the examined codes show a good agreement with the numerical results, which are less than 17% variations. When these criteria are applied, the mean values of Pre./Simu. of f_{ps} and P_u are greatly improved, i.e. for AASHTO (1999), these ratios are 0.87 with SD of 0.10 for f_{ps}, and 0.88 with SD of 0.09 for P_u; for ACI 318 (2015), those are 0.75 with SD of 0.09 for f_{ps}, and 0.76 with SD of 0.08 for P_u, respectively. When the compressive stress in the concrete due to f_{pe} is below that criteria, large deviations are observed in the predictions of beams' strength by the codes compared to the numerical results and therefore requires further investigations to improve the codes' accuracy.

6.8 Conclusion

This chapter proposes an analytical procedure to predict the flexural behaviour of precast segmental concrete beams (PSBs) internally prestressed with unbonded steel tendons. ABAQUS commercial software, for the first time, is successfully used in the study to simulate the behaviour of PSBs. Main findings are summarized as follows:

- The developed numerical models captured well the responses of the segmental concrete beams tested in a previous study. The verified numerical model was used to conduct intensive simulations of PSBs with different parameters for tension-controlled, compression-controlled and balanced sections.

- An analytical procedure was proposed to predict the load-deflection curves of PSBs with unbonded steel tendons. Its accuracy was confirmed with the numerical results.

- An empirical equation was developed and validated with numerical simulations to estimate the balanced reinforcement ratio of PSBs with unbonded tendons. This equation can be applied for both the PSBs with unbonded steel or CFRP tendons. It was found that the effective prestress in the tendons, f_{pe} greatly affected the balanced condition of PSBs with unbonded steel/CFRP tendons.

- Among the examined codes, AASHTO (1999) was found to yield the most accurate predictions of the strength of PSBs with unbonded steel tendons at the ultimate stage. Naaman and Alkhairi (1991)'s model captured very well the changes of f_{ps} with respects to the changes of all the studied parameters. However,

it overestimated f_{ps}, hence P_u at the ultimate stage. Based on the numerical results, a new value of Ω_u was proposed for PSBs with unbonded steel tendons.

- It is recommended that the prestressing steel should be stressed to achieve f_{pe} that leads to the initial compressive stress in the concrete not lesser than $0.27f'_c$ in order to gain high accurate predictions of both strength and deflection at the ultimate stage by existing models for the PSBs with unbonded steel tendons.

6.9 References

AASHTO (1999). *Guide Specifications for Design and Construction of Segmental Concrete Bridges: 2nd Ed with 2003 Interim Revis*, American Association of State Highway and Transportation Officials, Washington, DC.

AASHTO LRFD (2017). "Bridge Design Specifications, 8th Edition (LRFD-8)." American Association of State Highway and Transportation Officials, Washington, DC.

ACI 318 (2015). "Building code requirements for structural concrete and commentary (ACI 318-14)." American Concrete Institute, Farmington Hills, MI.

ACI 318 (2019). "Building Code Requirements for Structural Concrete and Commentary (ACI 318-19)." American Concrete Institute, Farmington Hills, MI.

ACI 440.4R (2004). "Prestressing concrete structures with FRP tendons (Reapproved 2011)." American Concrete Institute, Farmington Hills, USA.

AS 1012.8.1 (2014). "Methods of testing concrete - Method 8.1: Method for making and curing concrete—Compression and indirect tensile test specimens." *Standards Australia International Ltd., NSW*.

AS 1012.9 (2014). "Methods of testing concrete - Method 9: Compressive strength tests— Concrete, mortar and grout specimens." *Standards Australia International Ltd., NSW*.

AS 1391 (2007). "Metallic materials - Tensile testing at ambient temperature (Reconfirmed 2017)/Amdt 1-2012." *Standards Australia Limited, NSW*

ASTM D7205-06 (2016). "Standard test method for tensile properties of fiber reinforced polymer matrix composite bars." ASTM International, United States.

Dextra Group "CFRP tendons." https://www.dextragroup.com/offices/dextra-building-products-limited.

Hadi, M. N. S., and Le, T. D. (2014). "Behaviour of hollow core square reinforced concrete columns wrapped with CFRP with different fibre orientations." *Constr. Build. Mater.*, 50, 62-73.

Harajili, M., and Kanj, M. (1992). "Ultimate flexural strength of concrete members

prestressed with unbonded tendons." *Struct. J.*, 88(6), 663-674.

Harajli, M., Khairallah, N., and Nassif, H. (1999). "Externally prestressed members: evaluation of second-order effects." *J. Struct. Eng.*, 125(10), 1151-1161.

He, Z., and Liu, Z. (2010). "Stresses in External and Internal Unbonded Tendons: Unified Methodology and Design Equations." *J. Struct. Eng.*, 136(9), 1055-1065.

Jiang, H., Cao, Q., Liu, A., Wang, T., and Qiu, Y. (2016). "Flexural behavior of precast concrete segmental beams with hybrid tendons and dry joints." *Constr. Build. Mater.*, 110, 1-7.

Le, T. D., Pham, T. M., and Hao, H. (2020). "Numerical study on the Flexural Performance of Precast Segmental Concrete Beams with Unbonded Internal Steel Tendons." *Constr. Build. Mater.*, (Revision Submitted).

Le, T. D., Pham, T. M., Hao, H., and Hao, Y. (2018). "Flexural behaviour of precast segmental concrete beams internally prestressed with unbonded CFRP tendons under four-point loading." *Eng. Struct.*, 168(2018), 371-383.

Li, G., Yang, D., and Lei, Y. (2013a). "Combined shear and bending behavior of joints in precast concrete segmental beams with external tendons." *J. Bridge Eng.*, 18(10), 1042-1052.

Li, G., Zhang, C., and Niu, C. (2013b). "Experimental study on shear behavior in negative moment regions of segmental externally prestressed concrete continuous beams." *J. Bridge Eng.*, 18(4), 328-338.

Lou, T., Lopes, S. M., and Lopes, A. V. (2016). "Response of continuous concrete beams internally prestressed with unbonded FRP and steel tendons." *Compos. Struct.*, 154(2016), 92-105.

MacGregor, R. J. G. (1989). "Evaluation of strength and ductility of a three-span externally post-tensioned box girder bridge model." University of Texas at Austin.

Naaman, A. E., and Alkhairi, F. (1991). "Stress at ultimate in unbonded prestressing tendons: Part 2—Proposed Methodology." *ACI Struct. J.*, 88(6), 683-692.

Naaman, A. E., Burns, N., French, C., Gamble, W. L., and Mattock, A. H. (2002). "Stresses in unbonded prestressing tendons at ultimate: Recommendation." *Struct. J.*, 99(4), 518-529.

Park, R. (1989). "Evaluation of ductility of structures and structural assemblages from laboratory testing." *Bull. N. Z. Natl. Soc. Earthq. Eng.*, 22(3), 155-166.

Pisani, M. A. (1998). "A numerical survey on the behaviour of beams pre-stressed with FRP cables." *Constr. Build. Mater.*, 12(4), 221-232.

Saibabu, S., Srinivas, V., Sasmal, S., Lakshmanan, N., and Iyer, N. R. (2013). "Performance evaluation of dry and epoxy jointed segmental prestressed box girders under monotonic and cyclic loading." *Constr. Build. Mater.*, 38, 931-940.

Sika Australia "Sikadur-30." *https://aus.sika.com/*.

Tan, K.-H., and Ng, C.-K. (1997). "Effects of deviators and tendon configuration on behavior of externally prestressed beams." *ACI Struct. J.*, 94(1), 13-22.

Tan, K. H., and Tjandra, R. A. (2007). "Strengthening of RC continuous beams by external prestressing." *J. Struct. Eng.*, 133(2), 195-204.

Wang, X., Shi, J., Wu, G., Yang, L., and Wu, Z. (2015). "Effectiveness of basalt FRP tendons for strengthening of RC beams through the external prestressing technique." *Eng. Struct.*, 101, 34-44.

Yuan, A., Dai, H., Sun, D., and Cai, J. (2013). "Behaviors of segmental concrete box beams with internal tendons and external tendons under bending." *Eng. Struct.*, 48, 623-634.

Yuan, A., He, Y., Dai, H., and Cheng, L. (2014). "Experimental Study of Precast Segmental Bridge Box Girders with External Unbonded and Internal Bonded Posttensioning under Monotonic Vertical Loading." *J. Bridge Eng.*, 20(4), 04014075.

Zhou, X., Mickleborough, N., and Li, Z. (2005). "Shear strength of joints in precast concrete segmental bridges." *ACI Struct. J.*, 102(1), 3.

CHAPTER 7 CONCLUSIONS AND RECOMMENDATIONS

Precast segmental prestressed concrete girder bridges have gained rapid acceptance in bridge construction around the world as this type of structure not only allows speeding up the construction but also improvs the quality control. However, corrosion of steel reinforcement is always a great concern, and this has long been recognized as a major and costly maintenance issue for concrete bridge which could potentially increases the structure's lifecycle costs. This study investigated the use of CFRP tendons for PSBs in the replacement of traditional steel tendons. Both internal/external and bonded/unbonded CFRP tendons were used in the specimens. The experimental test results revealed excellent load-carrying capacity and deflection of all the beams, therefore, confirm the feasibility of the use of CFRP tendons in PSBs.

Precast segmental concrete beams with external FRP tendons are strongly believed to become a future trend of prestressed bridge construction as this combination incorporates the advantages of the segmental construction process, external prestressing technology and superior properties of FRP materials. The use of external CFRP tendons and segmental structures will facilitate repair or maintenance work in the event of damage of concrete segments or tendons due to traffic collisions or ageing. Although more expensive initially, the potential reduction in maintenance costs associated with the use of noncorrosive FRPs may eventually make the FRPs being the least expensive option for bridge construction as indicated in recent studies (Eamon et al. 2012; Yang et al. 2020). With the continuous improvements in the manufacturing process, both the price and properties of CFRP tendons such as fire resistance would be improved, which will further promote the use of FRPs in the construction industry. This study is the first attempt applying CFRP tendons for prestressed segmental concrete beams.

This study focuses on the short-term behaviour of segmental concrete beams prestressed with CFRP tendons. Two series of experimental tests on large-scaled segmental concrete beams were conducted in the experimental program. In the first test series, all the beams were prestressed with internal unbonded/bonded tendons while external tendons were used in the specimens in the second test series. Different testing parameters including types of joints (dry/epoxied), bonding conditions (bonded/unbonded), and tendon profiles (internal/external) were considered. Both

analytical analysis and numerical studies were then carried out to investigate the flexural behaviour of the PSBs with unbonded steel/CFRP tendons. The following sections describe key findings from the study and recommendations for future studies.

7.1 Key findings

The key findings from this study are summarised as below:

The use of CFRP tendons on segmental concrete beams

- All the tested beams with either internal or external CFRP tendons exhibited excellent load-carrying capacity and ductility. It is, therefore, concluded that CFRP tendons can be well used to replace steel tendons in PSBs to tackle the corrosion problems.
- Bonding condition of the tendons greatly affected the flexural behaviour of the segmental beams. Beams with bonded tendons showed higher strength and stiffness and larger crack mobilization while the use of unbonded tendons allowed the beams to achieve much greater ductility and fail in a less explosive manner at the ultimate stage.
- The type of joints had an insignificant effect on the overall flexural behaviour of the tested beams. Both the beams with epoxied and dry joints behaved similarly under the applied loads up to the ultimate stage, though the beams with epoxied joints showed slightly higher cracking/opening loads.
- Due to the secondary effect, the beams with external tendons showed smaller load-carrying capacity and deflection at the ultimate stage compared to the beams with internal tendons.

Behaviour of the beams with CFRP vs steel tendons

- Both the beams with steel or CFRP tendons exhibited non-linear behaviours after the joints opened/cracked. However, the levels of non-linearity of these beams were different. The yielding of the steel tendons resulted in a significant reduction in the beams' stiffness leading to considerably higher levels of non-linearity compared to the beams with CFRP tendons.
- Meanwhile, the beams with bonded CFRP tendons still showed an almost linear relationship between the deflection and the applied load after the joint opening

until the failure of the tendons.

- The yielding of steel tendons led to more ductile failure than in the case with CFRP tendons. The failure of the beams with CFRP tendons, of which the CFRP tendons ruptured was brittle and explosive. Thus, it is recommended that the beams with CFRP tendons should be designed to fail in compression controlled to prevent this type of brittle and explosive failures.

Relationships between deflection, joint opening and stress increment

- In the beams with unbonded tendons, the opening of joints was almost linear to the midspan deflection of the beams up to the ultimate stage. This linear relationship is true for both the beams with either steel tendons or CFRP tendons, internal or external tendons. But it does not exist for the beams with bonded tendons.

- In the case of the beams with unbonded internal/external CFRP tendons, the tendon stress increment was almost linearly related to the opening of the joints and the deflection of the beam until failure.

- In the case of the beams with unbonded internal/external steel tendons, this linear relationship was also valid up to the yielding of steel tendons. Afterward, the tendon stress increment showed a non-linear relationship with the opening of joints or the deflection of the beams.

Stress in the steel/CFRP tendons at the ultimate stage

- Unbonded steel tendons achieved very high stress values at the ultimate stage, which almost reached its ultimate tensile strength (~95%). This is true for both the beams with internal or external steel tendons.

- Similarly, bonded CFRP tendons almost reached its nominal tensile strength at the rupture (~93%). However, this was not the case for unbonded CFRP tendons which ruptured at a relatively low stress levels compared to its ultimate strength.

- The average stress in the internal unbonded CFRP tendons of the beams tested in this study was approximately 70% of the breaking strength while that for external CFRP tendons was 77%. The reduction in the tendon stress at ultimate loading is governed by the loading type, harping effect and the joint opening, which require attention during the design process.

Prediction of stress in the unbonded tendons

- All the examined existing models in this study including AASHTO (1999), ACI 318 (2015), ACI 440.4R (2004), BS 8110 (1997) predicted well stress in the unbonded steel tendons but not for the CFRP tendons at the ultimate stage.
- For the case of internal unbonded CFRP tendons, AASHTO (1999) and BS 8110 (1997) equations underestimated f_{ps} by about 22% to 28% compared with the experimental results. ACI 318 (2015) showed 31% to 38% differences, whereas ACI 440.4R (2004) overestimated f_{ps} by 18% to 19% compared to experimental results.
- For the case of external CFRP tendons, AASHTO (1999) and BS 8110 (1997) equations also underestimated f_{ps} by about 12% to 34% compared with the experimental results. ACI 318 (2015) showed higher conservative predictions with the errors of 21% to 42%. Again, ACI 440.4R (2004) overestimated f_{ps} by 3% to 13% compared to experimental results.
- Appropriate modifications of the strain reduction coefficient, Ω_u, in ACI 440.4R (2004) were suggested for segmental concrete beams with unbonded internal and external CFRP tendons, which yielded better predictions of the stress in the tendons at the ultimate stage.

Prediction of deflection of PSBs with unbonded tendons

- A new analytical procedure for predicting the deflections of PSBs with unbonded tendons is developed.
- The procedure consists of a new empirical equation to calculate the stress increment in the tendon at joint opening (or yield point) for which the opening load and consequently the deflection of the beams in the first stage of elastic behaviour is calculated, and a modification in the calculation of the moment of inertia of a cracked section for the better prediction of deflection of the beams in the second stage of non-linear behaviour.
- The procedure is applicable for both the PSBs with internal unbonded steel/CFRP tendons.

Estimation of balanced conditions of PSBs with unbonded tendons

- A closed-form equation to estimate the balanced reinforcement ratio of PSBs with unbonded tendons is proposed. The equation accounts for the effects of the effective prestress and the self-weight of the structure.
- This equation can be applied for both the PSBs with internal unbonded steel/CFRP tendons.

Conclusion related to the parametric study

- The numerical models developed in this study using ABAQUS software capture well the responses of the segmental concrete beams reported in the literature. The verified models were used to conduct intensive simulations for better understandings of flexural behaviour of PSBs with unbonded tendons regarding the failure modes, joint opening and stress increment in the prestressing tendons. The numerical results were also used to validate the analytical predictions.
- It is found from the parametric study that the effective prestress in tendons significantly affects the load-carrying capacity, deflection and failure modes of concrete segmental beams. With the same cross-section of prestressing materials, a change in effective prestress can lead to a change in the failure modes from compression- or tension-controlled failures.
- The prestressing reinforcement ratio and span-to-depth ratio strongly affect the load-carrying capacity and deflection of the beams. The type of load has an insignificant effect on the flexural behaviour of the beam, although the beam loaded with three-point loading registers slightly lower deflection and stress increment in the tendon at the joint opening (yield point) compared to the beam loaded under four-point loading.
- Finally, the numerical results showed that the concrete strength and number of joints had insignificant effects on the flexural performance of the segmental beams in regards to the load-carrying capacity, ductility and failure mode.

7.2 Recommendations for future studies

The following possible areas are recommended for future research:

- This is the first study on the use of FRP tendons for segmental concrete beams. Due to the limitations of time and budget, many other important parameters cannot

be covered in this study. These parameters can be studied through numerical simulations; however, experimental results are necessary to validate numerical results. As such, further experimental works are needed to extend the understandings of the flexural response of PSBs with FRP tendons. These parameters can be the span-to-depth ratio, effective prestress, amount of FRP tendons, concrete strength, FRP materials (Carbon, Glass, Aramid or Basalt fibres), type of loading (three-point/four-point loading), and different cross-section shapes and sizes.

- When the external tendons are used, harping angles of the tendons need due care for which further studies are required. The use of hybrid tendons, i.e. the combination of internal and external tendons, or the steel tendons and FRP tendons are also highly recommended for further studies.

- Shear behaviour of PSBs with FRP tendons is another topic worth studying. Since FRP tendons are weak in shear, vertical sliding of the segments may cause serious damage to the tendons leading to premature failure of the tendons. Therefore, it is important to investigate the shear behaviour of PSBs with CFRP tendons before their practical applications.

- These studies on the flexural and shear behaviours can be extended to the continuous segmental spans. This will enable studying the effect of loading one or more spans on the stress in unbonded/bonded FRP tendons.

- Fire resistance of CFRP tendons is also a factor to be considered. As such, it is worthy investigating the behavior of CFRP-prestressed segmental concrete beams under elevated temperatures. Lifecyle cost of using CFRPs for prestressed segmental concrete beams is also required further studies.

- Long-term behaviour of PSBs prestressed with CFRP tendons is also a topic that requires further investigations before their practical application on this type of structure.

- Due to the asymmetry of the transverse and longitudinal mechanical properties of the CFRP tendons, segmental concrete beams especially the joints are potentially more critical when subjected to transverse loads such as blast and impact loads.

BIBLIOGRAPHY DISCLAIMER

Every reasonable effort has been made to acknowledge the owners of copyright material. I would be pleased to hear from any copyright owner who has been omitted or incorrectly acknowledged.

APPENDIX I

STATEMENTS OF THE CO-AUTHORS

To whom it may concern

I, Duy Tan Le, conducted literature review, experimental testings, analysis of experimental results and written the manuscript of the paper titled “Flexural behaviour of precast segmental concrete beams internally prestressed with unbonded CFRP tendons under four-point loading”, which was revised and edited by the second and third co-authors. The fourth co-author helped in procuring the testing materials and fixtures.

_____

I, as a Co-author, endorse that this level of contribution by the candidate indicated above is appropriate.

(Prof. Hong Hao) _____

(Dr. Thong Pham) _____

(Prof. Yifei Hao) _____

To whom it may concern

I, Duy Tan Le, conducted literature review, experimental testings, analysis of experimental results, theoretical analysis and written the manuscript of the paper titled "Performance of precast segmental concrete beams posttensioned with carbon fibre-reinforced polymer (CFRP) tendons", which was revised and edited by the second and third co-authors. The fourth co-author helped in conducting experimental tests.

_____

I, as a Co-author, endorse that this level of contribution by the candidate indicated above is appropriate.

(Prof. Hong Hao) _____

(Dr. Thong Pham) _____

(Mr. Cheng Yuan) _____

To whom it may concern

I, Duy Tan Le, conducted literature review, experimental testings, analysis of experimental results and written the manuscript of the paper titled “Behaviour of Precast Segmental Concrete Beams Prestressed with External Steel/Carbon Fibre-Reinforced Polymer (CFRP) Tendons”, which was revised and edited by the second and third co-authors. The fourth co-author helped in conducting experimental tests.

_____

I, as a Co-author, endorse that this level of contribution by the candidate indicated above is appropriate.

(Prof. Hong Hao) _____

(Dr. Thong Pham) _____

(Ms. Han Li) _____

To whom it may concern

I, Duy Tan Le, conducted literature review, analytical analysis, numerical analysis and written the manuscripts of the following papers, which were all revised and edited by the co-authors:

1) Numerical study on the Flexural Performance of Precast Segmental Concrete Beams with Unbonded Internal Steel Tendons
2) Analytical Investigation of the Performance of Precast Segmental Concrete Beams Internally Prestressed with Unbonded Steel Tendons

_____

I, as a Co-author, endorse that this level of contribution by the candidate indicated above is appropriate.

(Prof. Hong Hao) _____

(Dr. Thong Pham) _____

APPENDIX II

COPYRIGHT CLEARANCE

Flexural behaviour of precast segmental concrete beams internally prestressed with unbonded CFRP tendons under four-point loading

Author: Tan D. Le,Thong M. Pham,Hong Hao,Yifei Hao
Publication: Engineering Structures
Publisher: Elsevier
Date: 1 August 2018

Performance of precast segmental concrete beams posttensioned with carbon fiber-reinforced polymer (CFRP) tendons

Author: Tan D. Le,Thong M. Pham,Hong Hao,Cheng Yuan
Publication: Composite Structures
Publisher: Elsevier
Date: 15 January 2019